University of Wollongong

Research Online

University of Wollongong Thesis Collection 2017+

University of Wollongong Thesis Collections

2019

Behaviour of Self-Compacting Concrete Columns Reinforced Longitudinally with Steel Tubes

Faez Ahmed Mohammed Alhussainy
University of Wollongong

Follow this and additional works at: https://ro.uow.edu.au/theses1

University of Wollongong

Copyright Warning

You may print or download ONE copy of this document for the purpose of your own research or study. The University does not authorise you to copy, communicate or otherwise make available electronically to any other person any copyright material contained on this site.

You are reminded of the following: This work is copyright. Apart from any use permitted under the Copyright Act 1968, no part of this work may be reproduced by any process, nor may any other exclusive right be exercised, without the permission of the author. Copyright owners are entitled to take legal action against persons who infringe their copyright. A reproduction of material that is protected by copyright may be a copyright infringement. A court may impose penalties and award damages in relation to offences and infringements relating to copyright material. Higher penalties may apply, and higher damages may be awarded, for offences and infringements involving the conversion of material into digital or electronic form.

Unless otherwise indicated, the views expressed in this thesis are those of the author and do not necessarily represent the views of the University of Wollongong.

Recommended Citation

Alhussainy, Faez Ahmed Mohammed, Behaviour of Self-Compacting Concrete Columns Reinforced Longitudinally with Steel Tubes, Doctor of Philosophy (Integrated) thesis, School of Civil, Mining and Environmental Engineering, University of Wollongong, 2019. https://ro.uow.edu.au/theses1/544

Research Online is the open access institutional repository for the University of Wollongong. For further information contact the UOW Library: research-pubs@uow.edu.au

School of Civil, Mining and Environmental Engineering

Behaviour of Self-Compacting Concrete Columns Reinforced Longitudinally with Steel Tubes

A thesis submitted in fulfilment

of the requirements for the award of the degree of

DOCTOR OF PHILOSOPHY-INTEGRATED

By

Faez Ahmed Mohammed Alhussainy

2019

THESIS DECLARATION

I, Faez Ahmed Mohammed Alhussainy, hereby declare that this thesis, submitted in fulfilment of the requirements for the award of Doctor of Philosophy, in the School of Civil, Mining and Environmental Engineering, University of Wollongong, Australia, is wholly my own work unless otherwise referenced or acknowledged. The document has not been submitted for qualification at any other academic institution.

Faez Ahmed Mohammed Alhussainy

May 2019

ACKNOWLEDGMENTS

First and foremost, I have to thank and praise our God, who provided me physical and mental ability to carry out the present research.

I would like to express my gratitude to my supervisors, Associate Professor Muhammad N.S. Hadi and Associate Professor M. Neaz Sheikh, for their invaluable support, patience and encouragement throughout the duration of my PhD study. Their comments, constructive criticism and inspiration during the preparation of this thesis are highly appreciated.

I want to thank the University of Wollongong (UOW), Australia for accepting me as a PhD student. I also acknowledge the financial support from the Iraqi Government (The Higher Committee for Education Development-HCED) for sponsoring my study at the University of Wollongong.

I would also like to acknowledge Messrs Alan Grant, Ritchie McLean, Duncan Best, Richard Gasser, Fernando Escribano and Cameron Neilson and the other technical staff at the University of Wollongong, Australia. The technical assistance during my experimental work is highly appreciated.

Finally, and most importantly, I would like to thank my lovely wife Kawther, sons Ali and Mohammed, daughters Fatimah and Zainab, parents, brothers and sisters for their love, continuous support and motivation during all stages of my PhD study.

LIST OF PUBLICATIONS

Journal papers

1. Hadi MNS, **Alhussainy F**, Sheikh MN. (2017). "Behavior of self-compacting concrete columns reinforced longitudinally with steel tubes." *Journal of Structural Engineering ASCE*, 143(6), 1-14.

2. **Alhussainy F**, Sheikh MN, Hadi MNS. (2018). "Behaviour of small-diameter self-compacting concrete-filled steel tubes." *Magazine of Concrete Research*,70(16), 811-821.

3. **Alhussainy F**, Sheikh MN, Hadi MNS. (2017). "Behaviour of small diameter steel tubes under axial compression." *Structures Journal*, 11, 155-163.

4. **Alhussainy F**, Hasan HA, Sheikh MN, Hadi MNS. (2019). "A new method for direct tensile testing of concrete." *Journal of Testing and Evaluation*, 47(2), 704-718.

5. **Alhussainy F**, Hasan HA, Rogic S, Sheikh MN, Hadi MNS. (2016). "Direct tensile testing of self-compacting concrete." *Construction and Building Materials*, 112, 903-906.

6. **Alhussainy F**, Sheikh MN, Hadi MNS. (2018) "Axial load-axial deformation behavior of SCC columns reinforced with steel tubes." *Structures Journal*, 15, 259-269.

7. **Alhussainy F**, Sheikh MN, Hadi MNS. (2019) "P-M interactions of self-consolidating concrete columns reinforced with steel tubes." *ACI Structural Journal*, 116(3), 1-13. doi: 10.14359/51714473

Conference papers

1. Hasan HA, **Alhussainy F**, Sheikh MN and Hadi MNS. (2016). "Direct tensile test of high strength concrete with and without steel fibres." In: Proceedings, the 24th Australian Conference on the Mechanics of Structures and Materials (ACMSM24), 6-9 December, Perth, Australia, 487-492.

2. **Alhussainy F**, Sheikh MN and Hadi MNS. (2017). "Ultimate capacity estimate of self-compacting concrete-filled small diameter steel tubes under axial load." In: Proceedings, the 1st International Conference on Structural Engineering Research (iCSER 2017), 20-22 November, Sydney, Australia, 155-160.

3. **Alhussainy F**, Sheikh MN and Hadi MNS. (2017). "Ductility of self-compacting concrete columns reinforced longitudinally with steel tubes under axial compression." In: Proceedings, the First MoHESR and HCED Iraqi Scholars Conference in Australasia, 5-6 December, Melbourne, Australia, 11-17.

CONTRIBUTION OF OTHERS

The research works presented in this thesis were primarily carried out by the PhD candidate, which mainly include but not limited to reviewing the literature, conducting experimental works, interpreting experimental results, developing analytical models and writing manuscripts. All journal papers and conference papers were written by the PhD candidate with his supervisors. Contributions of others are described below.

Mr Hayder Alaa Hasan (PhD candidate) and Mr Sime Rogic (undergraduate student) contributed in carrying out the experimental work for the following article.

Alhussainy F, Hasan HA, Rogic S, Sheikh MN, Hadi MNS. (2016). "Direct tensile testing of self-compacting concrete." *Construction and Building Materials*, 112, 903-906.

In addition, Mr Hayder Alaa Hasan (PhD candidate) helped in defining the objectives and carrying out experimental work for the following article.

Alhussainy F, Hasan HA, Sheikh MN, Hadi MNS. (2017). "A new method for direct tensile testing of concrete." *Journal of Testing and Evaluation*, 47(2), 704-718.

ABSTRACT

Performance of concrete columns has been significantly improved by using composite material systems such as encased sections and concrete filled steel tubes. Different combinations of encased sections and steel sections have been widely studied. Steel sections and concrete have been used to construct composite columns with different cross-sections. The composite columns are usually constructed of normal vibrated concrete. Recently, self-compacting concrete (SCC) is also used in the construction of the composite columns. The synergies between steel and SCC in composite columns provide better performance in terms of high strength, stiffness, ductility, as well as fire and seismic resistance. This study proposes two innovative concepts: a new method to determine the stress-strain behaviour of SCC under direct uniaxial tension and a new method of reinforcing SCC columns by using longitudinal small-diameter steel tubes instead of reinforcing steel bars.

For the stress-strain behaviour of SCC under direct uniaxial tension, special steel claws were designed, built and installed at both ends of 100 × 100 × 500 mm SCC specimens. These claws were used to transfer the applied tensile forces to the specimens. The cross-section of the specimens was reduced in the middle to ensure that failure would occur in the middle of the specimen. The test results showed that there was no slippage or fracture at the ends of any of the tested specimens. Also, the failure occurred in the middle of specimens, as expected. The direct tensile testing method developed in this study was also used for different types of concrete including normal strength concrete (NSC), high-strength concrete (HSC) and steel fibre reinforced high-strength concrete (SFHSC). The developed method provided rational and reliable results for the direct tensile strength of the SCC, NSC, HSC and SFHSC using a simple and effective testing technique.

The second aim of this study was to propose a new method of reinforcing SCC columns by using longitudinal small-diameter steel tubes instead of reinforcing steel bars. A total of 20 SCC specimens with 240 mm diameter and 800 mm height were cast and tested. Four specimens were reinforced with normal steel bars (reference specimens) and the remaining 16 specimens with steel tubes. All specimens contained steel helices with a pitch of either 50 mm or 75 mm. Deformed steel bars of 16 mm diameter were used as longitudinal reinforcement in the four reference specimens. Steel tubes of 33.7 mm outside diameter with 2 mm wall thickness (ST33.7) and steel tubes of 26.9 mm outside diameter with 2.6 mm wall thickness (ST26.9) were used as longitudinal reinforcement in the remaining 16 specimens. The specimens were divided into five groups with four specimens in each group. From each group, one specimen was tested under concentric axial load, one under 25 mm eccentric axial load, one under 50 mm eccentric axial load and one under flexural load. Although the nominal yield tensile strength of steel bar was 150 and 250 MPa greater than the nominal yield tensile strength of steel tubes ST33.7 and ST26.9, respectively, the test results revealed that the steel tube reinforced SCC (STR SCC) specimens achieved ultimate load similar to reference specimens. Ductility of concentrically loaded STR SCC specimens was higher than the ductility of the reference specimen.

In addition to the experimental programs, the analytical axial load-axial deformation responses and axial load-bending moment interactions of the STR SCC columns were calculated based on the stress-strain responses of the longitudinal steel tubes, unconfined concrete cover, confined concrete core and confined concrete inside the steel tube. The influences of different parameters including the compressive strength of SCC, tensile strength of steel tube, wall thickness of steel tube and pitch of steel helix

were also investigated. The analytical and experimental results of STR SCC columns showed good agreements.

TABLE OF CONTENTS

LIST OF FIGURES

LIST OF TABLES

CHAPTER 1: INTRODUCTION

1.1 Overview

Solid steel bars are the dominant forms of reinforcement in concrete structural members such as beams, slabs and columns. Reinforced concrete (RC) columns traditionally use solid steel bars as longitudinal and transverse reinforcement. Recently, steel sections have been used in reinforcing composite columns (Espinos et al. 2016; Skalomenos et al. 2016; Liu et al. 2017). Composite columns consist of steel sections and concrete with two main types of configurations: encased steel section columns and concrete-filled steel tube (CFT) columns (Shanmugam and Lakshmi 2001). Composite columns are generally used in high-rise buildings due to their high axial load capacity, ductility as well as fire and seismic resistance (Rodrigues et al. 2015; Patel et al. 2015). To increase the ductility and confinement of composite columns, circular steel tube sections are used in constructing CFT columns (Schneider 1998).

In this study, small-diameter circular steel tube sections were used as longitudinal reinforcement for RC columns (Figure 1.1). For the same cross-sectional area of a solid steel bar and a circular steel tube, the radius of gyration of the circular steel tube is higher than the radius of gyration of the solid steel bar. Hence, the bending stiffness of the steel tube is higher than the bending stiffness of the steel bar. Filling these steel tubes with concrete can further increase the yield and ultimate strength as well as the ductility of the steel tube columns under axial compression (Alhussainy et al. 2017). This is because the concrete inside the steel tube delays the local buckling and converts the failure mode of the steel tube wall from inward to outward buckling (AISC 2010). Since the diameter of these steel tubes is quite small, concrete with high flowability is

required to completely fill the steel tubes without segregation. The self-compacting concrete (SCC) is considered a suitable option and has been used for constructing the columns in this study.

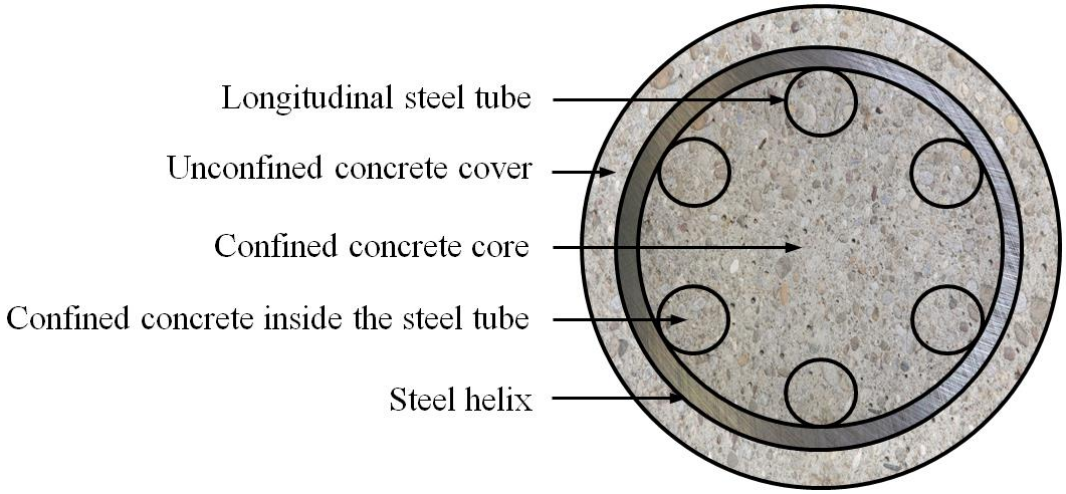

Figure 1.1: Schematic of the SCC column reinforced with steel tubes

The SCC can be used in complex forms and members that contain congestion of reinforcement, without needing vibration, as it is able to compact under its own weight (EFNARC 2002). The SCC offers a rapid rate of concrete placement, with faster construction times and ease of flow around congested reinforcement. The fluidity and segregation resistance of SCC ensures a high level of homogeneity, minimal concrete voids and uniform concrete strength, providing the potential for a superior level of finish and durability to the structure. The SCC is very suitable for CFT columns due to the rheological properties of the SCC (Han and Yao 2004). The essential characteristics of SCC are as follows (Heirman et al. 2008; Shen et al. 2014):

- Filling ability: fresh concrete is able to flow easily through unrestricted formwork or/and reinforcement.

- Passing ability: fresh concrete is able to flow through narrow opening or congested reinforcement without obstacle or segregation.
- Segregation resistance: fresh concrete is able to remain uniform in combination.

The mechanical properties of SCC such as compressive strength, flexural strength, splitting tensile strength, modulus of elasticity, ductility and toughness have been extensively studied (Sahmaran et al. 2006; Domone 2007; Khatib 2008; Filho et al. 2010). However, only a few studies investigated the direct tensile stress-strain behaviour of the SCC. This is mainly attributed to the difficult test setup and the proper execution of the experiments. Perfect alignment, secondary flexure, slippage and high stress-concentration at the ends of specimen due to gripping are considered the main factors that affect the direct tensile testing of the concrete (Wee et al. 2000; Mier and Vliet 2002; Swaddiwudhipong et al. 2003; Choi et al. 2014; Roziere et al. 2015). Hence, the direct tensile strength is usually calculated based on the test results obtained from splitting tensile strength or flexural strength using suitable conversion factors. However, it was reported that these conversion factors might not be applicable for SCC (Desnerck et al. 2014).

Based on the aforementioned discussion, this study proposes two concepts: one concept is a new method to determine the stress-strain behaviour of SCC under direct uniaxial tension and the other concept is a new method of reinforcing SCC columns by using longitudinal small-diameter steel tubes in lieu of steel reinforcing bars. This study also aims to investigate experimentally and analytically the behaviour of SCC specimens reinforced with steel tubes under axial concentric, 25 mm eccentric and 50 mm eccentric and flexural loads.

1.2 Research Significance

This study presents a new method to determine the stress-strain behaviour of the SCC and different types of concrete including normal strength concrete (NSC), high-strength concrete (HSC) and steel fibre reinforced high-strength concrete (SFHSC) under direct uniaxial tension. Review of literature showed that previous methods suffered several technical deficiencies including non-uniform fracture plane, stress concentration and slippage at the end of the specimens and flexural loads due to the imperfect alignment of the specimen during testing. The developed method provided rational and reliable results for the direct tensile strength of the SCC, NSC, HSC and SFHSC using a simple and effective testing technique.

This study also presents a new method for reinforcing concrete columns. Review of literature showed that reinforcing steel bars used in traditional concrete columns are usually solid in cross-sectional area. In the present study, small-diameter steel tubes instead of solid steel bars are used as longitudinal reinforcement for SCC columns. Beside, this study presents a simplified analytical model for the axial load-bending moment interactions of SCC columns reinforced with steel tubes. The analytical model takes into account the contributions of the steel tubes, unconfined concrete cover, confined concrete core and confined concrete inside the steel tube. The predictions of the developed analytical model have been found to be in good agreement with the experimental investigation results.

1.3 Aims and Objectives

The main aim of this study is to investigate the behaviour of columns reinforced with small-diameter steel tubes filled with SCC (STR SCC column). This study provides a

basis for using steel tubes instead of the conventional steel reinforcing bars as a new method for reinforcing concrete columns. It also reveals the problems associated with the use of plain steel tubes as longitudinal reinforcement in STR SCC column specimens under eccentric loads because of the slip of steel tubes in concrete. The main objectives are as follows:

- Investigate the properties of the SCC in fresh state. The SCC is used in casting columns as well as the small-diameter steel tubes. Hence, mix design for concrete needs to be satisfied by the SCC requirements.

- Investigate the direct tensile stress-strain behaviour of SCC and bond behaviour between the SCC and steel tubes.

- Investigate the performance of small-diameter steel tubes under axial compression.
- Investigate the performance of small-diameter SCC filled steel tubes under axial compression.
- Investigate the behaviour of SCC columns reinforced longitudinally with small-diameter steel tubes under concentric, eccentric and flexural loads.
- Develop an analytical model to predict the axial load-bending moment interactions of SCC columns reinforced with steel tubes. The analytical model takes into account the contributions of the steel tubes, unconfined concrete cover, confined concrete core and confined concrete inside the steel tube.
- Conduct a parametric study to investigate the influences of the compressive strength of SCC, tensile strength of the steel tube, the wall thickness of the steel tube and pitch of the steel helix on the axial load-bending moment interactions of SCC columns reinforced with steel tubes.

1.4 Thesis Outline

Based on the aims and objectives listed above, the combined experimental and theoretical studies in the present thesis are covered in nine chapters, details of each chapter are summarised below:

Chapter one presents an overview of using steel tubes and SCC in composite columns, advantages of the composite columns and SCC, and mechanical properties of SCC. It also discusses the significance and objectives of this study.

Chapter two presents a new method for the direct tensile strength of the SCC. The mechanical properties of SCC including compressive strength, splitting strength, flexural strength, compressive stress-strain behaviour and modulus of elasticity are also presented.

Based on the new method for the direct tensile strength of the SCC proposed in Chapter two, Chapter three used the developed method to determine the direct tensile strength of different types of concrete including normal strength concrete (NSC), high-strength concrete (HSC) and steel fibre reinforced high-strength concrete (SFHSC). Chapter three also presents the properties of SCC in fresh state and hardened state. The fresh SCC properties conform to the specifications according to American Society for Testing and Materials (ASTM methods). The hardened state including direct tensile strength and mechanical properties of the SCC are compared with direct tensile strength and mechanical properties of the NSC, HSC and SFHSC.

Chapter four investigates the performance of small-diameter steel tubes under axial compression. Galvanized and cold-formed steel tubes were used in this study, in order to specify which type of the steel tube is to be used in the experimental program.

Chapter five investigates the performance of small-diameter SCC filled steel tubes under axial compression.

Chapter six introduces the experimental program that includes twenty SCC columns reinforced with longitudinal steel tubes. Testing of materials, fabrication of columns and testing of columns are presented.

Chapters seven and eight present two simplified analytical models for the axial load-axial deformation behaviour and axial load-bending moment interactions of SCC columns reinforced with steel tubes, respectively. The analytical model takes into account the contributions of the steel tubes, unconfined concrete cover, confined concrete core and confined concrete inside the steel tube. The analytical results were compared to the experimental results from the Chapter six.

Chapter nine summarises the conclusions derived from experimental and analytical studies and provides recommendations for future research studies.

References

AISC. (2010). "Specification for structural steel buildings." *ANSI/AISC 360-10*, Chicago.

Alhussainy, F., Sheikh, M. N., and Hadi, M. N. S. (2017). "Behaviour of small-diameter self-compacting concrete-filled steel tubes." *Magazine of Concrete Research*. http://dx.doi.org/10.1680/jmacr.16.00531

Choi, S., Yang, K., Sim, J., and Choi, B. (2014). "Direct tensile strength of lightweight concrete with different specimen depths and aggregate sizes." *Construction and Building Materials*, 63, 132–141.

Desnerck, P., Boel, V., Craeye, B., and Itterbeeck, P. V. (2014). "Mechanical properties of self-compacting concrete." in K Khayat and G De Schutter (eds.), State-of-the-Art Report of RILEM Technical Committee 228-MPS, Springer, pp.15-71.

Domone, P. (2007). "A review of the hardened mechanical properties of self-compacting concrete." *Cement and Concrete Composites*, 29(1), 1-12.

EFNARC (European Federation of Specialist Construction Chemicals and Concrete Systems). (2002). "Specification and guidelines for self-compacting concrete." Norflolk, U.K., 1-32.

Espinos, A., Romero, M. L., and Lam, D. (2016). "Fire performance of innovative steel-concrete composite columns using high strength steels." *Thin-Walled Structures*, 106, 113-128.

Filho, F. M. A., Barragán, B. E., Casas, J. R., and El Debs, A. L. H. C. (2010). "Hardened properties of self-compacting concrete - A statistical approach." *Construction and Building Materials*, 24(9), 1608-1615.

Han, L.-H., and Yao, G.-H. (2004). "Experimental behaviour of thin-walled hollow structural steel (HSS) columns filled with self-consolidating concrete (SCC)." *Thin-Walled Structures*, 42(9), 1357-1377.

Heirman, G., Vandewalle, L., Gemert, D. V., Boel, V., Audenaert, K., Schutter G. D., Desmet, B., and Vantomme, J. (2008). "Time-dependent deformations of limestone powder type self-compacting concrete." *Engineering Structures*, 30(10), 2945-2956.

Khatib, J. M. (2008). "Performance of self-compacting concrete containing fly ash." *Construction and Building Materials*, 22, 1963-1971.

Liu, S.-W., Chan, T.-M., Chan, S.-L., and So, D. K.-L. (2017). "Direct analysis of high-strength concrete-filled-tubular columns with circular & octagonal sections." *Journal of Constructional Steel Research*, 129, 301-314.

Patel, V. I., Liang, Q. Q., and Hadi, M. N. S. "Nonlinear Analysis of Concrete-Filled Steel Tubular Columns, first ed.", Scholars' Press, Germany, 2015.

Rodrigues, J. P. C., Correia, A. J. M., and Pires, T. A. C. (2015). "Behaviour of composite columns made of totally encased steel sections in fire." *Journal of Constructional Steel Research*, 105, 97-106.

Roziere, E., Cortas, R., and Loukili, A. (2015). "Tensile behaviour of early age concrete: New methods of investigation." *Cement and Concrete Composites*, 55, 153-161.

Sahmaran, M., Christianto, H. A., and Yaman, I. O. (2006). "The effect of chemical admixtures and mineral additives on the properties of self-compacting mortars." *Cement and Concrete Composites*, 28(5), 432-440.

Schneider, S. P. (1998). "Axially loaded concrete-filled steel tubes." *Journal of Structural Engineering ASCE*, 124(10), 1125-1138.

Shanmugam, N. E., and Lakshmi, B. (2001). "State of the art report on steel-concrete composite columns." *Journal of Constructional Steel Research*, 57(10), 1041-1080.

Shena, L., Jovein, H. B., and Li, M. (2014). "Measuring static stability and robustness of self-consolidating concrete using modified Segregation Probe." *Construction and Building Materials*, 70, 210-216.

Skalomenos, K. A., Hayashi, K., Nishi, R., Inamasu, H., and Nakashima, M. (2016). "Experimental behavior of concrete-filled steel tube columns using ultrahigh-strength steel." *Journal of Structural Engineering*, 142(9), 1-13.

Swaddiwudhipong, S., Lu, H., and Wee, T. (2003). "Direct tension test and tensile strain capacity of concrete at early age." *Cement and Concrete Research*, 33(12), 2077-2084.

Van Mier, J., and Van Vliet, M. (2002). "Uniaxial tension test for the determination of fracture parameters of concrete: State of the art." *Engineering Fracture Mechanics*, 69(2), 235-247.

Wee, T., Lu, H., and Swaddiwudhipong, S. (2000). "Tensile strain capacity of concrete under various states of stress." *Magazine of Concrete Research*, 52(3), 185-193.

CHAPTER 2: DIRECT TENSILE TESTING OF SELF-COMPACTING CONCRETE

Summary

This chapter focuses on the mechanical properties of self-compacting concrete (SCC). The mechanical properties of SCC including compressive strength, splitting tensile strength, flexural strength, compressive stress-strain behaviour and modulus of elasticity were investigated. A new method for the direct tensile strength of SCC is proposed in this chapter. The direct tensile strength of the specimens was found to be lower than the splitting tensile strength and flexural strength. The developed procedure for the direct tensile strength to the SCC was found to be effective and efficient. The developed method is used in the next chapter (Chapter 3) to determine the direct tensile strength of different types of concrete including normal strength concrete (NSC), high-strength concrete (HSC) and steel fibre reinforced high-strength concrete (SFHSC).

Citation

This chapter has been published in the Construction and Building Materials with the following citation:

Alhussainy F, Hasan HA, Rogic S, Sheikh MN, Hadi MNS. (2016). "Direct tensile testing of self-compacting concrete." *Construction and Building Materials*, 112, 903-906.

Abstract

This study explores a new procedure to determine the stress-strain behaviour of Self-Compacting Concrete (SCC) under direct uniaxial tension. Special steel claws were designed, built and installed at both ends of $100 \times 100 \times 500$ mm SCC specimens. These claws were used to transfer the applied tensile forces to the specimens. The cross-section of the specimens was reduced in the middle to ensure that failure would occur in the middle. The specimens were tested at 28 days for direct tensile stress-strain behaviour as well as for compressive, splitting and flexural strengths. The test results showed that there was no slippage or fracture at the ends of any of the specimens. Also, the failure occurred in the middle of specimens, as expected. The direct tensile strength of the specimens was found to be lower than the splitting and flexural strengths.

Keywords: Self-compacting concrete; uniaxial tension; stress-strain behaviour; strain rate; direct tensile testing.

2.1 Introduction

The mechanical properties of Self-Compacting Concrete (SCC) have been extensively studied over past few years (Persson 2001; Holschemacher and Klug 2002; Holschemacher 2004; EFNARC 2005; Domone 2007). However, only few studies investigated the direct tensile stress-strain behaviour of the SCC. This is mainly attributed to the difficult test setup and the proper execution of the experiments. Perfect alignment, secondary flexure, slippage and high stress-concentration at the ends of specimen due to gripping are considered the main factors that affect the direct tensile testing of the concrete (Wee et al. 2000; Mier and Vliet 2002; Swaddiwudhipong et al.

2003; Choi et al. 2014; Roziere et al. 2015). Accordingly, the direct tensile strength is usually calculated based on the test results obtained from splitting tensile strength or flexural strength using conversion factors. However, it was reported that these conversion factors might not be applicable for SCC (Desnerck et al. 2014). Understanding the direct tensile stress-strain behaviour of the SCC is significantly important, as it affects the deflections, cracking, shear and bonding behaviours of reinforced concrete elements constructed with SCC. This paper proposes a new test setup to determine the direct tensile testing of the SCC.

2.2 Description of Experimental Program

The mix proportion of the Self-Compacting Concrete (SCC) used in this study is shown in Table 2.1. The standard mechanical properties including compressive strength, splitting tensile strength, flexural strength (modulus of rupture) and modulus of elasticity under compression as well as the uniaxial direct tensile strength of the SCC were determined. The compressive strength of the concrete was determined by testing three cylinders of 100 mm in diameter and 200 mm in height according to AS 1012.9 (AS 1012.9 2014). The indirect tensile strength (Brazil or splitting test) of the SCC was obtained by testing three cylinders of 150 in diameter and 300 mm in height according to AS 1012.10 (AS 1012.10 2000). The flexural strength (modulus of rupture) of the specimens was determined by testing three $100 \times 100 \times 500$ mm prisms under four point loading according to AS 1012.11 (AS 1012.11 2000). The concrete modulus of elasticity under compression was obtained by testing three cylinders of 150 in diameter and 300 mm in height according to AS 1012.17 (AS 1012.17 1997). The direct tensile testing of the SCC specimens was carried out according to the procedure developed in this study, which has been fully explained below.

Table 2.1: Mix proportion of the SCC used in this study

Material	Quantity
Cement	280 kg/m^3
Fly ash	120 kg/m^3
Slag	50 kg/m^3
Fine aggregate	950 kg/m^3
Coarse aggregate	780 kg/m^3
Water	182 kg/m^3
High Range Water Reducer	3.375 l/m^3
Water/Powder ratio	0.4/1 m^3

2.3 Direct Tensile Test Setup and Loading

Wooden boxes of 100 × 100 mm in cross-section and 500 mm in length were used as formwork for the specimens. Two gripping claws were embedded in both ends of the box which extend 125 mm in the specimen, as shown in Figure 2.1.

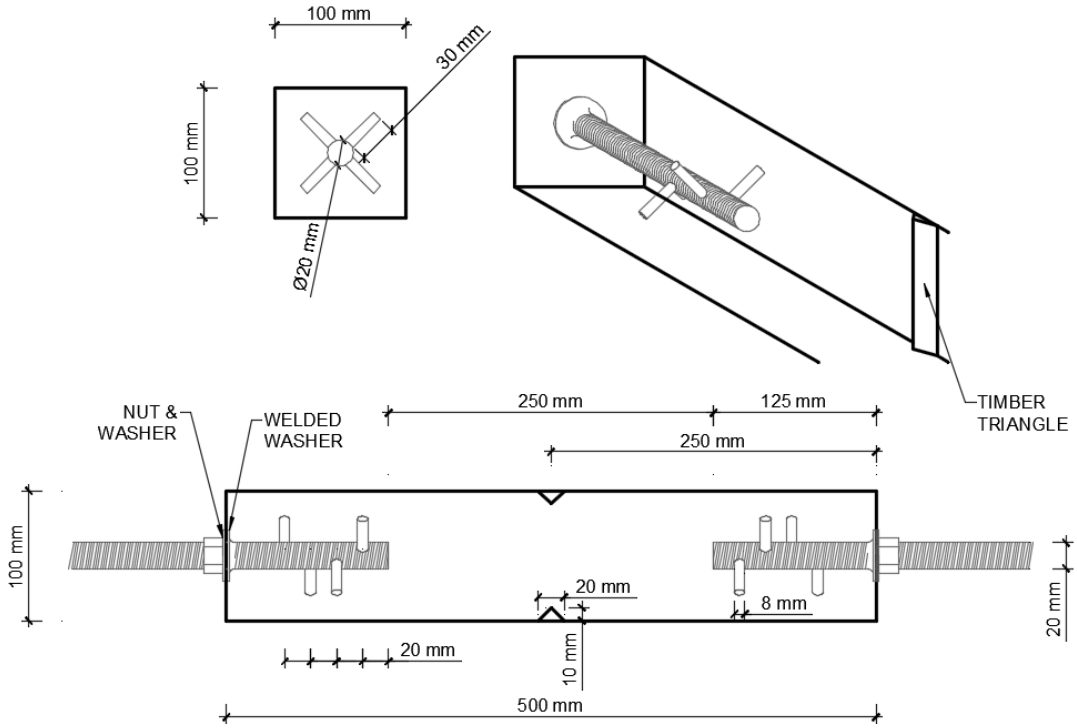

Figure 2.1: Details of direct tensile testing of SCC specimen

The claws were made from 20 mm diameter threaded rod which had four 8 mm diameter pins welded at 90 degrees with spacing of 20 mm, as shown in Figure 2.2. In order to keep the claws level and aligned within the formwork, a washer was welded to the threaded rod inside the box, whilst a nut and a washer were used on the outside to dismantle the box formwork. To induce failure in the middle of the specimen, two pieces of timber triangles with a base of 20 mm and a height of 10 mm were glued inside the wooden box vertically at the middle on the opposite sides, as shown in Figures 2.1 and 2.3. In order to test the specimens, the universal Instron testing machine at the School of Civil, Mining and Environmental Engineering, University of Wollongong, was used.

Figure 2.2: The claw designed for direct tensile testing of SCC specimen

Figure 2.3: Completed formwork for the casting of the SCC specimens

To successfully apply axial tensile loading in the specimen, two universal joints were designed to hold the ends of specimens by the machine. The universal joint allows movement of the specimen at both ends in order to align the specimen vertically between the jaws of the machine, as shown in Figure 2.4. Also, the joints overcome any defects in misalignment of the claws during the casting of the specimen. One of the universal joint ends had a diameter suitable for the gripping jaws of the testing machine, whilst the other end had a welded nut which could be screwed onto the test specimen claws. The developed universal joints were used for all the specimens. To ensure adequate safety, the lower half of the specimen was lightly held in place using a strap to prevent the sudden fall after failure.

Figure 2.4: Universal joints designed for direct tensile testing of SCC specimen

Displacement controlled tensile loading have a significant influence on the overall stress-strain behaviour of the specimen. Yan and Lin (2006) observed that the peak strain within a sample increased with the increase in the loading rate. The increase in the applied strain rate also affects the tensile stress, Young's modulus, Poisson's ratio and ultimate strain. In this study, strain rate of $6 \times 10^{-6}\varepsilon/s$ was used to test the specimens. This rate is within the range of strain rates applied by Yan and Lin (2006) and Chen et al. (2013). To measure the strain within each specimen, two 120 mm long strain gauges were attached in the middle on the opposite flat sides.

2.4 Results

As predicted, failure of all specimens occurred in the middle where the cross section was reduced by 20%, as shown in Figure 2.5. Reduction of the cross-sectional area of the specimens resulted in increasing the stress in the middle of the specimens, which induced a consistent failure in the middle. The reduction of the cross-section also prevented the failure to occur at undesirable locations along the length of the specimen. No concrete cracking occurred at either end of the specimens, as the designed claws

created a strong and evenly distributed bond between the claws and the concrete. In combination with the universal joints, proper alignments were achieved avoiding end crushing and slippage.

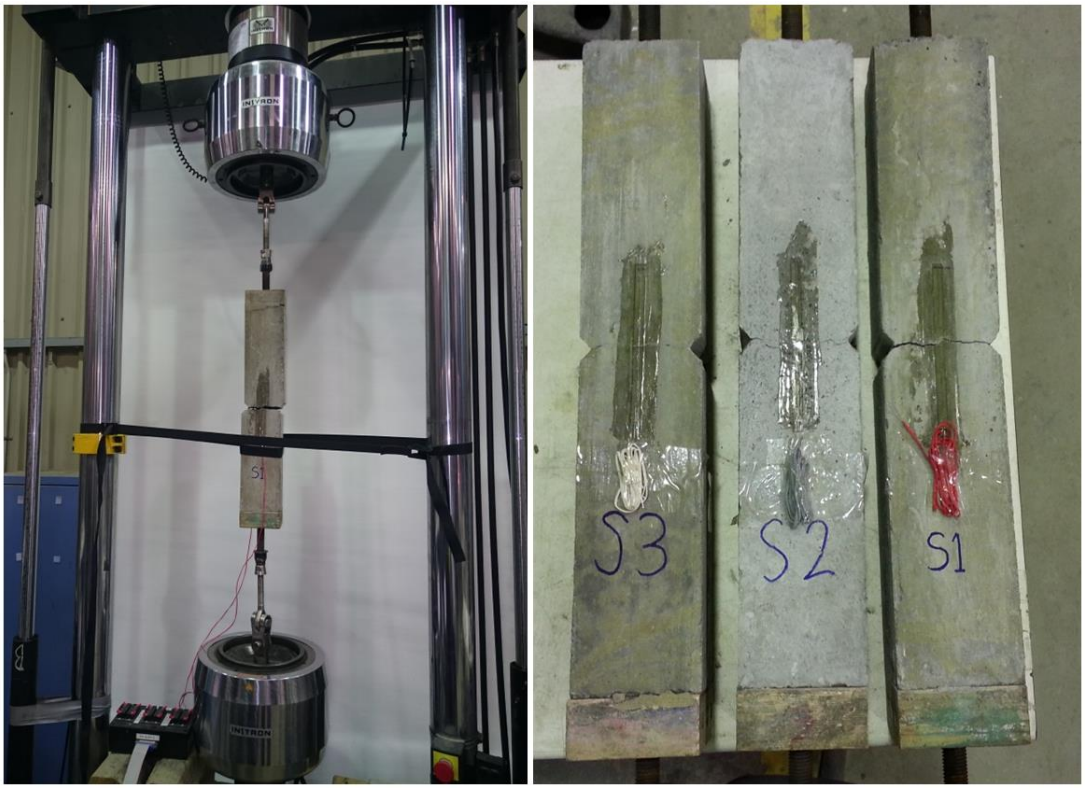

Figure 2.5: Failure mode of specimens

Table 2 summarises the mechanical properties of the SCC obtained from standard tests and direct tensile tests. Three specimens were tested to observe the direct tensile stress-strain behaviour of the SCC, as shown in Figure 2.6. The difference between the maximum and minimum values of the direct tensile strength of the SCC specimens was 5.8%. It was observed that the direct tensile strength of the SCC is less than the flexural strength (modulus of rupture) and splitting tensile strengths. The average direct tensile strength of the SCC was found to be 3.5 MPa, while the average flexural strength and splitting tensile strength were found to be 6.5 MPa and 3.8 MPa, respectively. The

lower value of the direct tensile strength compared to the splitting and flexural strengths was similar to the observation reported in Wee et al. (2000) for normal strength concrete.

Table 2.2: Summary of testing results for SCC

Type of test	Standard tests	Specimens			Average result
		S1	S2	S3	
Compressive strength (28 days)	AS 1012.9 (2014)	56.5	57	-	57 MPa
Indirect tensile strength (Brazil or splitting test)	AS 1012.10 (2000)	3.7	3.78	3.87	3.8 MPa
Flexural strength (modulus of rupture)	AS1012.11 (2000)	6	6.39	7.1	6.5 MPa
Modulus of elasticity (compressive stress-strain test)	AS 1012.17 (1997)	29.5	30	31	30 GPa
Modulus of elasticity (direct tensile stress-strain test)	Procedure developed in this study	19.5	20.4	21	20 GPa
Direct tensile strength	Procedure developed in this study	3.4	3.49	3.6	3.5 MPa

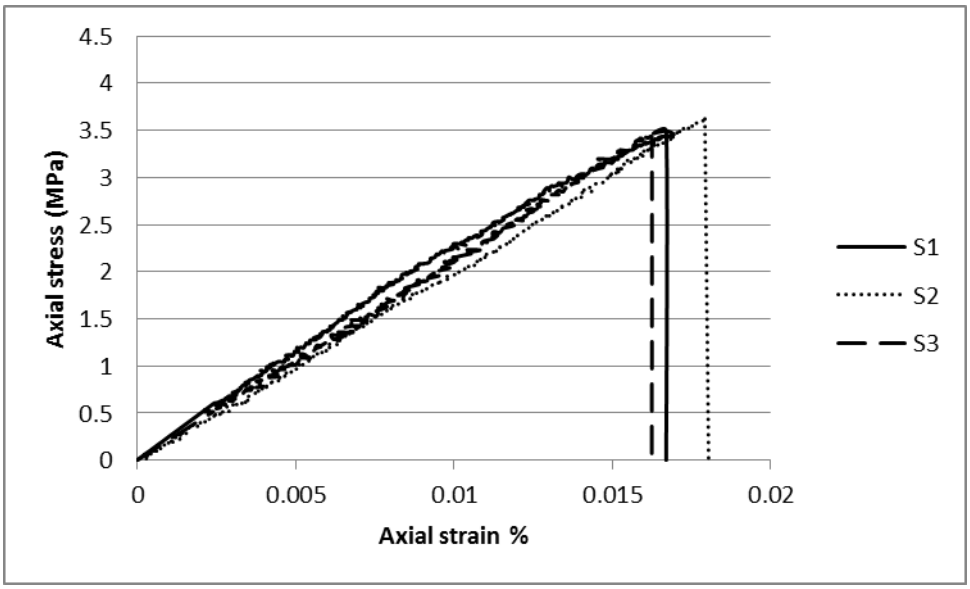

Figure 2.6: Direct tensile stress-strain behaviour of the SCC specimens

The direct tensile strength of the SCC specimens tested based on the designed and developed test setup was approximately equal to 90 percent of the splitting tensile strength, which is consistent with AS 3600 (AS 3600 2009) and EC 2 (2004). The

average result of the direct tensile strength was also compared with the model in CEB-FIB (2010). The experimental direct tensile strength of the SCC was within the limits specified in the CEB-FIB (2010). The predicted value of the direct tensile strength according to CEB-FIB (2010) was found to be only 0.5 MPa higher than the experimental value. It is noted that the main objective of this paper is to develop a test procedure to determine the stress-strain behaviour of the SCC under direct uniaxial tension. The development of correlation equations for the direct tensile strength of different types of SCC is beyond the scope of this paper.

The modulus of elasticity of the SCC was calculated using the slope of direct tensile stress-strain curves, Figure 2.6. The average modulus of elasticity in direct tension was found to be 20 GPa, which was equal to the two-thirds of the modulus of elasticity in compression. The average maximum direct tensile load carried by the specimens was 28 kN with corresponding axial deformation of 1.24 mm, as shown in Figure 2.7.

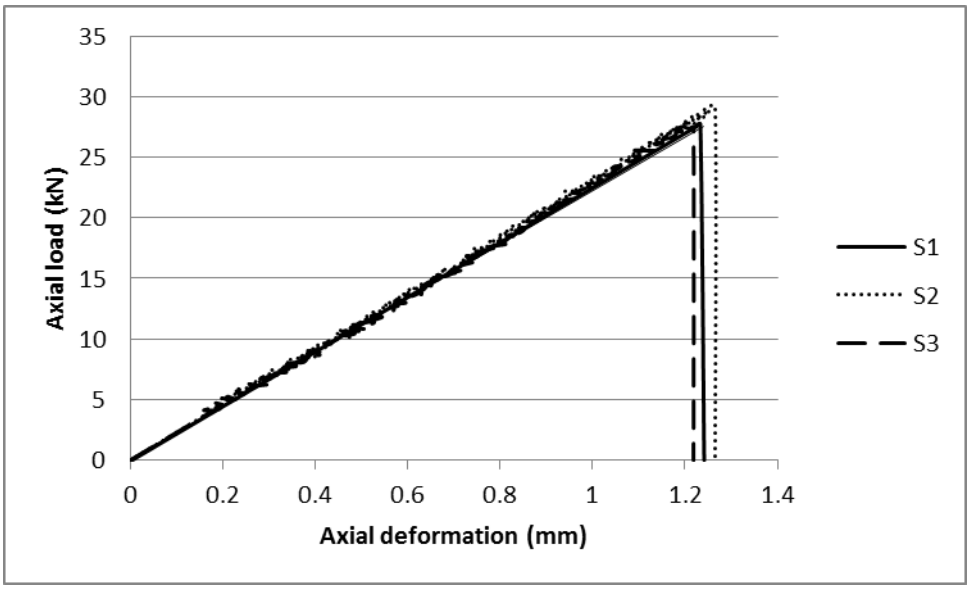

Figure 2.7: Axial load-axial deformation behaviour of the SCC specimens under uniaxial tension

2.5 Conclusions

The following conclusions can be drawn from the results of the experimental program carried out in this study on the direct tensile testing of the Self-Compacting Concrete (SCC). First, the designed and developed experimental setup was adequate in ensuring that specimens failed in the middle where the cross-sectional area was reduced by 20%. Second, due to adequate gripping, slippage and flexural induced cracking did not occur during loading. Third, the average direct tensile strength of the SCC was found to be less than the average flexural strength (modulus of rupture) and splitting tensile strength. Similarly, the modulus of elasticity in direct tension was found to be two-thirds of the modulus of elasticity in compression. Finally, the developed procedure for applying direct tensile strength to the SCC was found to be effective and efficient. Further research is needed to apply the developed procedure to determine the direct tensile strength of other types of concrete.

References

AS (Australian Standard). (2009). "Concrete structure." *AS 3600-2009*, Sydney, NSW, Australia.

AS (Australian Standards). (1997). "Methods of testing concrete – Method 17: Determination of the static chord modulus of elasticity and Poisson's ratio of concrete specimens." *AS 1012.17-1997*, Sydney, NSW, Australia.

AS (Australian Standards). (2000a), "Methods of testing concrete – Method 10: determination of indirect tensile strength of concrete cylinders ('Brazil' or splitting test)." *AS 1012.10-2000*, Sydney, NSW, Australia.

AS (Australian Standards). (2000b). "Methods of testing concrete – Method 11: determination of the modulus of rupture." *AS 1012.11-2000,* Sydney, NSW, Australia.

AS (Australian Standards). (2014). "Methods of testing concrete – Method 9: determination of the compressive strength of concrete specimens." *AS 1012.9-2014*, Sydney, NSW, Australia.

Aslani, F., and Nejadi, S. (2012). "Mechanical properties of conventional and self-compacting concrete: An analytical study." *Construction and Building Materials*, 36, 330-347.

CEB-FIB (2010). Bulletin 55-Model Code 2010-First completed draft, CEB-FIP, 1, p. 292.

Chen, X., Wu, S., Zhou, J., Chen, Y., and Qin, A. (2013). "Effect of testing method and strain rate on stress-strain behavior of concrete." *Journal of Materials in Civil Engineering*, 25(11), 1752-1761.

Choi, S., Yang, K., Sim, J., and Choi, B. (2014). "Direct tensile strength of lightweight concrete with different specimen depths and aggregate sizes." *Construction and Building Materials*, 63, 132–141.

Desnerck, P., Boel, V., Craeye, B., and Itterbeeck, P. V. (2014). "Mechanical properties of self-compacting concrete." in K Khayat and G De Schutter (eds.), State-of-the-Art Report of RILEM Technical Committee 228-MPS, Springer, pp.15-71.

Domone, P. (2007). "A review of the hardened mechanical properties of self-compacting concrete." *Cement and Concrete Composites*, 29(1), 1-12.

EC 2 (Eurocode). (2004). "Design of concrete structures." European Committee for Standardization, *EN 1992-1-1: Part 1-1*, p.225.

EFNARC (European Federation of Specialist Construction Chemicals and Concrete Systems). (2005). "The European guidelines for self-compacting concrete specification, production and use." Farnham, U.K., 1-63.

Holschemacher, K. (2004). "Hardened material properties of self-compacting concrete." *Journal of Civil Engineering and Management*, 10(4), 261-266.

Holschemacher, K. and Klug, Y. (2002). "A database for the evaluation of hardened properties of SCC." *Lacer*, 7, 123-134.

Persson, B. (2001). "A comparison between mechanical properties of self-compacting concrete and the corresponding properties of normal concrete." *Cement and Concrete Research*, 31(2), 193-198.

Roziere, E., Cortas, R., and Loukili, A. (2015). "Tensile behaviour of early age concrete: New methods of investigation." *Cement and Concrete Composites*, 55, 153-161.

Swaddiwudhipong, S., Lu, H., and Wee, T. (2003). "Direct tension test and tensile strain capacity of concrete at early age." *Cement and Concrete Research*, 33(12), 2077-2084.

Van Mier, J., and Van Vliet, M. (2002). "Uniaxial tension test for the determination of fracture parameters of concrete: State of the art." *Engineering Fracture Mechanics*, 69(2), 235-247.

Wee, T., Lu, H., and Swaddiwudhipong, S. (2000). "Tensile strain capacity of concrete under various states of stress." *Magazine of Concrete Research*, 52(3), 185-193.

Yan, D., and Lin, G. (2006). "Dynamic properties of concrete in direct tension." *Cement and Concrete Research*, 36, 1371–1378.

CHAPTER 3: A NEW METHOD FOR DIRECT TENSILE TESTING OF CONCRETE

Summary

Chapter three extends the procedure of the direct tensile test developed for self-compacting concrete (SCC) in Chapter two to other types of concrete. Based on the developed method for the direct tensile strength of the SCC, this chapter determines the direct tensile strength of normal strength concrete (NSC), high-strength concrete (HSC) and steel fibre reinforced high-strength concrete (SFHSC). This chapter presents a description of the previous investigations on the direct tensile strength of concrete. Besides, the properties of SCC in fresh state and hardened state were investigated. The fresh SCC properties conform to the specifications of the American Society for Testing and Materials (ASTM methods). The direct tensile strength and mechanical properties of SCC were compared with the direct tensile strength and mechanical properties of NSC, HSC and SFHSC.

Citation

This chapter has been published in the Journal of Testing and Evaluation with the following citation:

Alhussainy F, Hasan HA, Sheikh MN, Hadi MNS. (2017). "A new method for direct tensile testing of concrete." *Journal of Testing and Evaluation, ASTM International*, Accepted: 5 Sept 2017.

Abstract

Different testing methods were used in previous studies to measure the direct tensile strength of concrete. However, these methods experienced several major deficiencies such as stress concentration at the end of the specimens due to inadequate gripping and loading eccentricity and non-uniform fracture plane due to difficulties in aligning and centring the specimens during testing. This study presents the details of a new method of testing concrete under uniaxial tension. The method was developed to overcome the difficulties associated with testing methods adopted in the previous research studies. A full description of the wooden moulds used in casting the specimens and the loading arrangements including the end grips, universal joints and frame in which the specimens were tested under uniaxial tension are presented. As expected, all the tested specimens were fractured at the middle where the cross-sectional area was reduced by 20%. Also, no crushing failure or slippage was observed at the ends of the tested specimens.

Keywords: Direct tensile testing; concrete; uniaxial tension; stress-strain behaviour; strain rate.

3.1 Introduction

Tensile strength is one of the critical properties of concrete, because it influences the cracking, bonding and shear behaviours of reinforced concrete members. Many research studies attempted to use direct tensile, indirect tensile (splitting tensile) and flexural testing methods to investigate the properties of concrete under tension. However, it was reported that the direct tensile testing method provides more reliable and rational uniaxial tensile strength of concrete compared to the splitting tensile and flexural testing methods (Swaddiwudhipong et al. 2003; Choi et al. 2014).

The correlations between the direct tensile strength and the compressive, flexural and splitting tensile strength were investigated in several research studies. Wee et al. (200) carried out an experimental study to investigate the tensile strength of concrete. It was found that the tensile strength of the concrete was about 5.5-8.5% of the compressive strength of concrete. It was also found that the tensile strength of concrete obtained from the direct tensile testing was two-thirds of the flexural strength of the concrete. Swaddiwudhipong et al. (2003) studied the tensile behaviour of concrete at early ages. It was found that with curing age the direct tensile strength of the concrete increases at a lower rate compared to the compressive strength. Wu et al. (2012) conducted experimental investigations on the tensile strength of the concrete under static and intermediate strain rate using three different testing methods: direct tensile, splitting tensile and flexural testing methods. It was reported that specimens tested under flexural loads obtained greater tensile strength than the specimens tested under direct tensile and splitting tensile loads. Choi et al. (2014) performed a direct tensile testing on lightweight concrete specimens with different dimensions (lateral depth) and aggregate sizes. It was reported that the effect of the size of the tested specimens on the direct tensile strength of the concrete became greater with a decrease in the unit weight of the concrete. Also, it was observed that the effect of the aggregate interlocking capacity on the tensile strength of the concrete slightly increased with an increase in the lateral depth of the tested specimen. The influence of the end grips of the specimens on the tensile strength of concrete was investigated in Li et al. (1993), Wille et al. (2014) and Zijl et al. (2016). It was reported that rotational and non-rotational end conditions influence the crack formation and strain distribution in the cross-section of the tested specimens (2007).

Different methods were adopted to determine the direct tensile strength of the concrete in the previous studies. Based on the techniques used in gripping the specimen in the testing machine, four main direct tensile testing methods were identified: direct tensile test using truncated cone concrete samples (1968), direct tensile testing using embedded steel bars (1989), direct tensile testing by gluing gripping technique (1994) and direct tensile test by means of lateral gripping (1997). However, the above methods suffered several technical deficiencies including non-uniform fracture plane, stress concentration and slippage at the end of the specimens and flexural loads due to the imperfect alignment of the specimen during testing. As a result of the aforementioned problems associated with direct tensile testing methods, the tensile strength of the concrete has been mainly measured using the splitting tensile testing method and flexural testing method.

In this study, a new direct tensile testing method was designed, based on the embedded bar method, considering the following requirements:

1. The testing arrangements need to be suitable for different types of concrete;
2. The tensile load must be perfectly axial in order to obtain a uniform stress across the specimen section;
3. The end grips need to be simple and easy to fix to avoid the stress concentration and the failure due to fracture at the ends of the specimens;
4. The strain-measurement system has to be steady during the test; and
5. The cost of preparing the specimens should not be high.

The feasibility of using the developed method in testing concrete samples under uniaxial tension was assessed through testing different types of concrete samples: normal-strength concrete (NSC), high-strength concrete (HSC), self-consolidating concrete (SCC) and steel fibre reinforced high-strength concrete (SFHSC) having compressive strengths ranging between 39 and 93 MPa. The developed method of preparing and testing the concrete specimens makes the direct tensile testing of the concrete more reliable and cost-effective.

3.2 Description of the Developed Direct Tensile Testing Method

3.2.1 Formwork and Embedded Threaded Rod

Moulds of 100 mm × 100 mm in cross-section and 500 mm in length made from non-absorbing wood were used as formwork for the tested specimens (Figure 3.1). The cross-section of each specimen was reduced at the middle to 80 mm × 100 mm in order to induce the failure to occur in the middle of the tested specimen. The reduced cross-section at the middle of each specimen was achieved by gluing two timber prisms vertically at the middle of the inner faces of the 100 × 500 mm (long) sides of the wooden moulds. The timber prisms were 100 mm long having a triangular cross-section with a base of 20 mm and a height of 10 mm (Figure 3.1).

A couple of threaded steel rods were embedded at the ends of each specimen to be used as grips for the specimens. The embedded threaded steel rods were 20 mm in diameter and 200 mm in length and were embedded inside the specimen for a distance of 125 mm (Figure 3.1). In order to reduce the stress concentration at the ends of the tested specimens and to increase the bond between the embedded threaded steel rods and the concrete, four steel pins of 8 mm in diameter and 30 mm in length were welded at each

threaded rod. The steel pins were spaced at 20 mm from the tip of the threaded steel rod (located inside the tested specimens) and the steel pins were welded in a way that the angles between the steel pins were 90 degree (Figure 3.1). In order to align the embedded threaded steel rods in the centre of the tested specimens, two holes of 20 mm diameter were drilled in the 100 × 100 mm sides (ends) of the wooden molds. Besides, a washer was welded to the threaded rod from the inside of the wooden moulds and a nut and a washer were used on the outside to fix the threaded steel rods to the ends of the wooden moulds. The nuts and the washers further ensured a perfect alignment of the embedded threaded steel rods within the wooden moulds (Figure 3.1). The completed formwork with the embedded threaded steel rods of the tested specimens is shown in Figure 3.2.

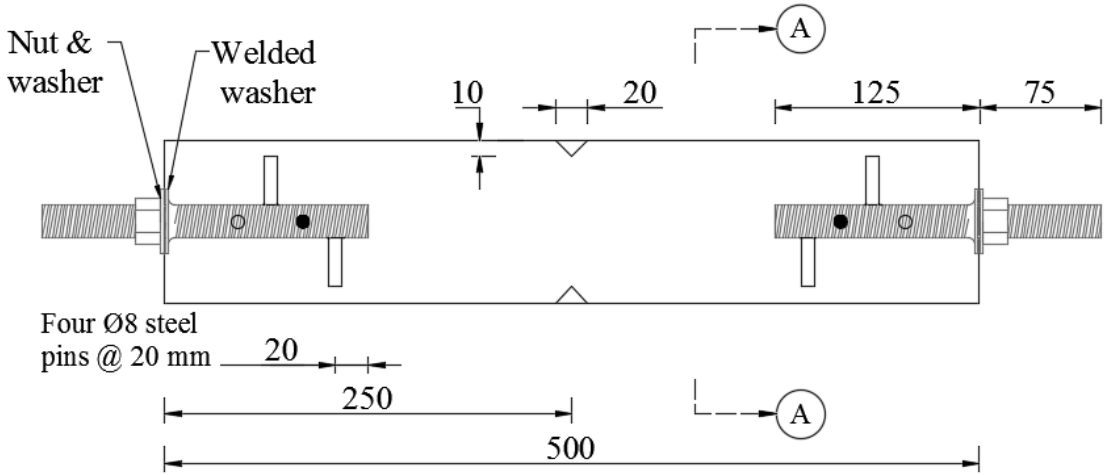

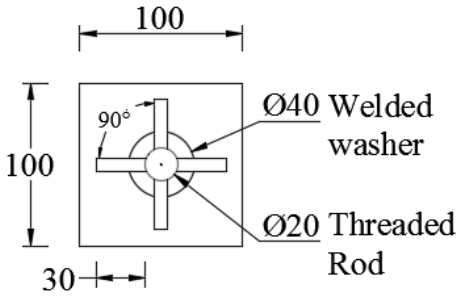

Section A-A

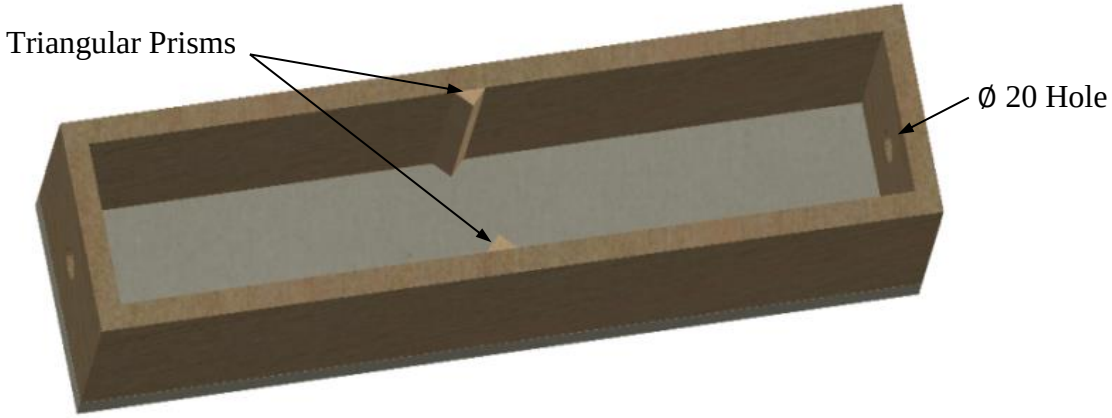

Wooden Mould

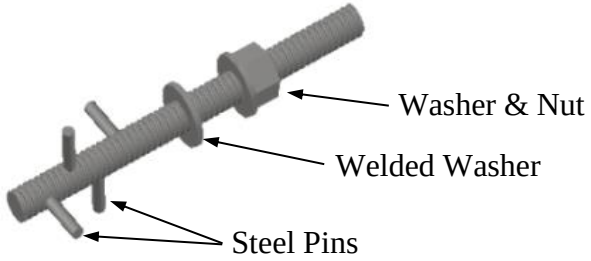

Embedded Threaded
Steel Rod

* All dimensions are in mm

Figure 3.1: Wooden mould and embedded threaded steel rod

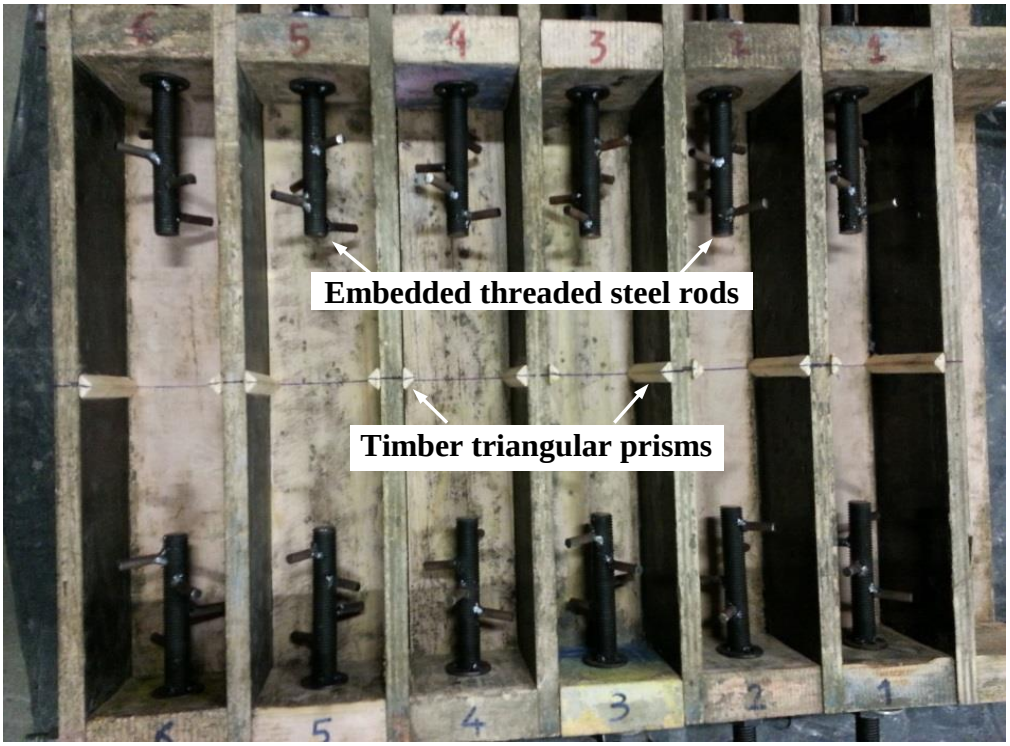

Figure 3.2: Completed formwork with the embedded threaded steel rods of the tested specimens

3.2.2 Universal Joints

The tested specimens were mounted to the testing machine using a couple of reusable universal steel joints manufactured at the University of Wollongong, Australia. The schematic of the universal joints is presented in Figure 3.3. Each universal joint consisted of two main parts: eye terminal and toggle terminal. One end of the eye terminal of each universal joint had a Ø30 mm steel rod to be gripped by using the jaw of the 500 kN Instron testing machine, whereas the other end had a Ø18 mm hole. The toggle terminal of each universal joint consisted of two main components: clevis holder and clevis. One end of the clevis holder had a Ø18 mm hole and the other end was fabricated to hold the clevis. Also, the clevis of the toggle terminal had two different ends: one end had a fixed pin to be held by using the clevis holder and the other end had a Ø16 mm threaded rod.

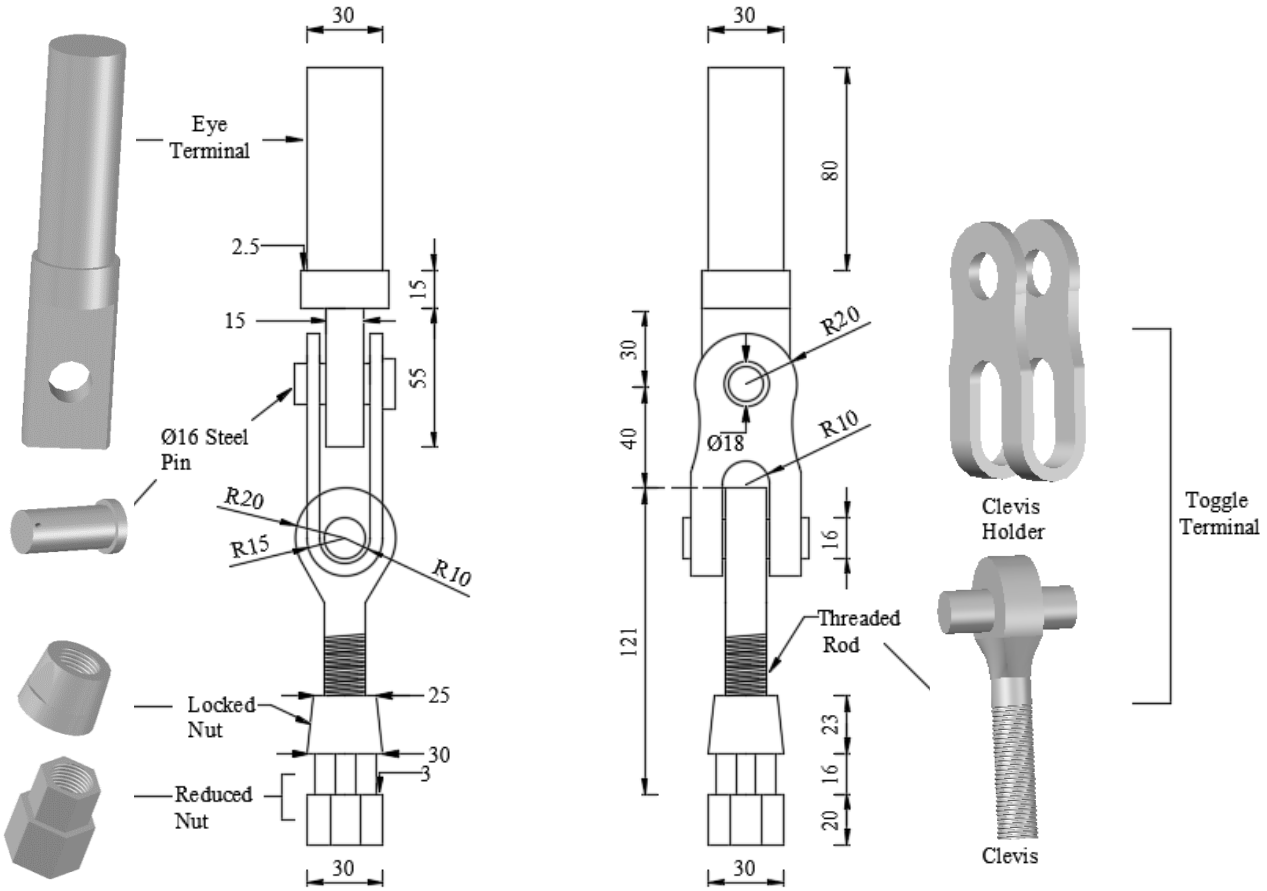

Figure 3.3: Schematic of the universal joint

The eye terminal and the toggle terminal of each universal joint were connected to each other thorough Ø18 mm holes using a Ø16 mm steel pin (Figure 3.3). For each universal joint, the threaded rod end of the clevis was screwed onto the threaded steel rod embedded in the end of the specimen using a Ø20 mm to Ø16 mm reduced nut. In order to avoid any loose connection in the reduced nut, a locked nut was used to hold the reduced nut firm during the test. The universal joints were used to avoid any bending moments that might be experienced by the specimens during testing as a result of an eccentricity in the applied load. This is because the universal joints allowed movement at both ends of each tested specimen (Figure 3.4), which ensured a perfect alignment for the specimen between the jaws of the Instron testing machine. Moreover, the universal joints overcame any defects in misalignment of the threaded steel rods that might occur during the casting of the specimen.

3.2.3 Strain Rate and Strain Measurement

Concrete is considered a sensitive material to the applied strain rate. Considerable efforts have been dedicated in the previous research studies to investigate the effect of the strain rate on the tensile properties of the concrete under uniaxial tension. Körmeling and Reinhardt (1987) studied the effect of strain rate on the fracture energy and the tensile strength of concrete specimens with and without steel fibres. It was observed that using high strain rates in testing the specimens resulted in a substantial increase in the fracture energy and the tensile strength of the plain and the steel fibre reinforced concrete specimens. Yan and Lin (2006) carried out an experimental investigation on the strain rate dependent response of the concrete in tension. Strain rate of $10^{-5}\ \varepsilon/s$ to $10^{-0.3}\ \varepsilon/s$ was used in testing the concrete specimens. It was observed that the strain rate influenced the direct tensile strength of the concrete more than it

influenced the modulus of elasticity. Chen et al. (2013) investigated the effect of four different strain rates ($10^{-6}\,\varepsilon/s$, $10^{-5}\,\varepsilon/s$, $10^{-4}\,\varepsilon/s$, $10^{-3}\,\varepsilon/s$) on the direct tensile strength of the concrete. It was found that the peak stresses decrease with the decrease in the strain rate. In this study, the strain rate used in testing all the specimens was $6 \times 10^{-6}\,\varepsilon/s$, which is considered within the intermediate strain rates suitable for testing of concrete under uniaxial tension (Chen et al. 2013).

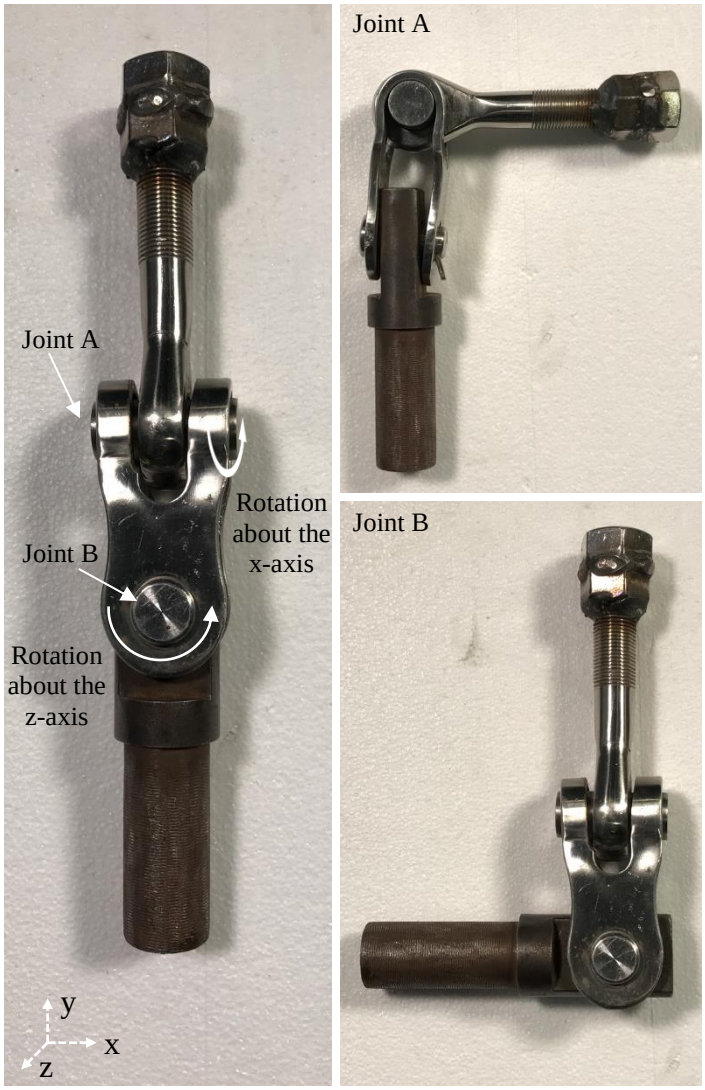

Each universal joint provides two degrees of freedom: rotation about the x-axis (Joint A) and rotation about the z-axis (Joint B)

Figure 3.4: Universal joint designed for direct tensile testing of all specimens

Concrete strain gauges with a length ranging between 30 mm to 120 mm were used in the previous research studies to measure the axial tension strain in the tested specimens [Swaddiwudhipong et al. 2003; Wu et al. 2012; Reinhardt et al. 1986). Short strain gauges are considered more susceptible to several forms of measurement errors especially error caused by the open cracks distributed along the face of the monitored material where those strain gauges attached. Hence, strain gauges with a long sensor length are need for inhomogeneous materials such as concrete (Glisic 2011). In this study, two concrete strain gauges of 120 mm length were attached at the middle of long non-notched sides of the tested specimens to measure the axial tension strain during the tests (Figure 3.5).

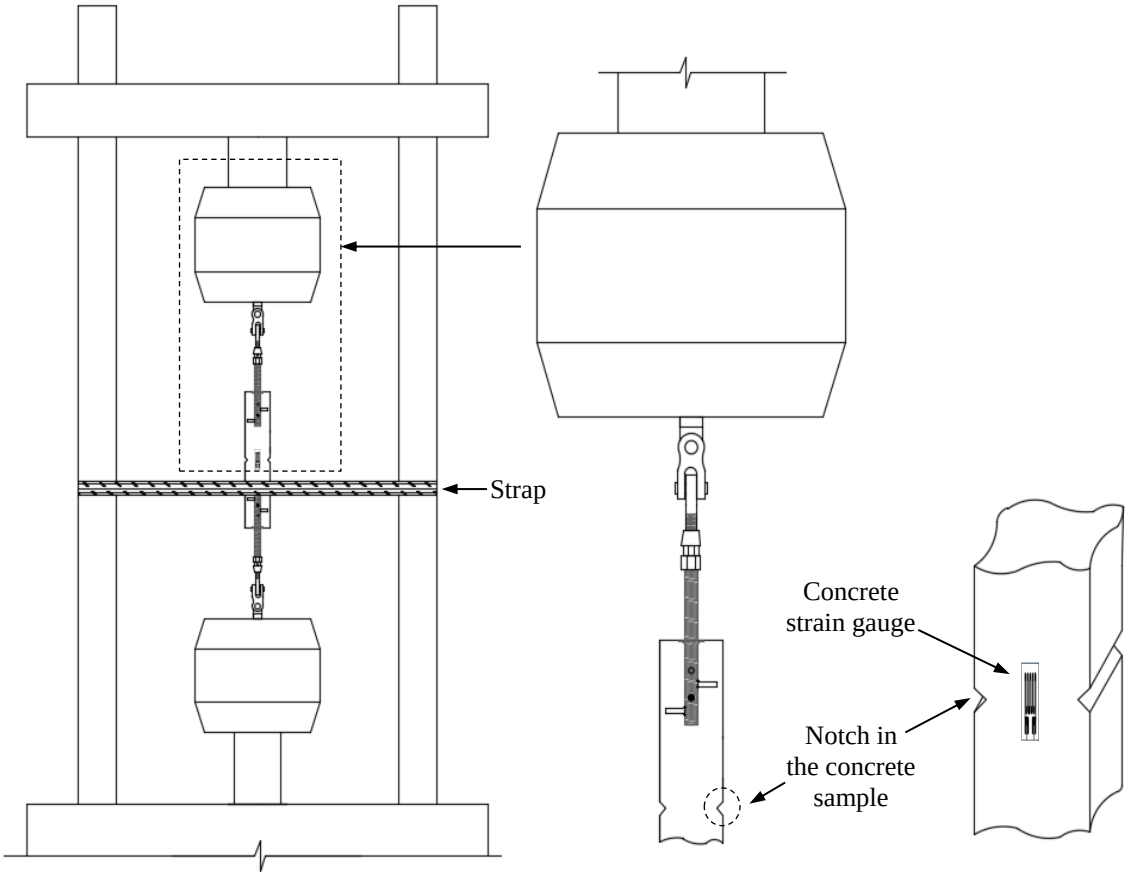

Figure 3.5: Schematic setup of the tested specimen

3.3 Specimen Preparation and Testing Setup

A total of 12 concrete specimens were cast and tested under uniaxial tension in order to validate the direct tensile testing method developed in this study. Four different types of concrete were used in casting the tested specimens: normal-strength concrete (NSC); high-strength concrete (HSC), self-consolidating concrete (SCC) and steel fibre reinforced high-strength concrete (SFHSC). Three specimens (S1, S2 and S3) were tested for each type of concrete. The ready mixes of NSC, HSC and SCC were provided by a local concrete company. The mix proportions of the NSC, HSC and SCC mixes are presented in Table 3.1. The SFHSC was prepared using a small lab concrete mixer having the maximum volume capacity of 0.2 m^3. The HSC ready mix, provided by a local company, was firstly placed in the lab mixer and then brass coated steel fibres with 1% by volume were added gradually inside the HSC mix. The steel fibres were straight in shape with 0.2 mm diameter and 13 mm length (aspect ratio = 65) having maximum tensile strength of 2500 MPa (Hasan et al. 2017). The maximum size of the aggregate used in the NSC, HSC, SCC and SFHSC was 10 mm. For NSC, HSC and SFHSC specimens, the concrete was placed into the formwork in two stages. After each stage, concrete was vibrated using an electrical concrete vibrator. No vibration was needed for the SCC specimens.

The properties of fresh SCC were tested according to ASTM C1610-14 (ASTM 2014d); ASTM C1611-14 (ASTM 2014c) and ASTM C1621-14 (ASTM 2014b); and the results were found to be satisfactory. The standard mechanical properties including compressive strength, splitting tensile strength, flexural strength, direct tensile strength and the modulus of elasticity of the NSC, HSC, SCC and SFHSC were determined. The compressive strengths of the concrete were determined by testing three 100 mm × 200

mm cylinder-specimens according to ASTM C39 (ASTM 2016a). The splitting tensile strengths of the concrete were determined by testing three 150 mm × 300 mm cylinder-specimens according and ASTM C496 (ASTM 2011). The flexural strengths of the concrete were determined by testing three 100 × 100 × 500 mm beam-specimens with third-point loading according to ASTM C78 (ASTM 2016b). The direct tensile strength and the modulus of elasticity of the concrete in tension were determined from the tensile stress-strain behaviour of three specimens tested by using the direct tensile testing method developed in this study. The modulus of elasticity of the concrete in compression was determined from the slope of the stress-strain behaviour obtained from testing three 150 mm × 300 mm cylinder-specimens under axial compression according to ASTM C469 (ASTM 2014a).

The universal Instron testing machine at the laboratory of School of Civil, Mining and Environmental Engineering, University of Wollongong, Australia was used in testing the specimens under uniaxial tension. First, the universal joints were fixed to the embedded threaded steel rods of the tested specimen. Afterwards, the specimens were mounted to the Instron testing machine. During the tests, a strap was used to slightly hold the lower part of tested specimens in order to avoid any sudden fall of any part of the specimen during the fracture of the specimen (Figure 3.5). Figure 3.6 shows a typical testing setup of the tested specimens.

Table 3.1: Mix proportions of the concrete used in this study

Mix	Cement (kg/m^3)	Fly ash (kg/m^3)	Slag (kg/m^3)	Silica fume (kg/m^3)	Sand (kg/m^3)	Coarse aggregate (kg/m^3)	Water (kg/m^3)	HRWR [a] (l/m^3)	Steel fibre content (%)
Normal-strength concrete	350	-	-	-	850	1000	185	-	---
High-strength concrete	576	64	-	30	540	990	197	6	---
Steel fibre high-strength concrete	576	64	-	30	540	990	197	6	1
Self-consolidating concrete	280	120	50	-	950	780	182	3.4	---

[a] HRWR: High range water reducer

Figure 3.6: Typical test setup for direct tensile testing of concrete

3.4 Results and Discussion

3.4.1 Failure Modes

All the tested specimens fractured once the specimens reached their maximum tensile strength. The fracture occurred in the middle of each specimen where the cross-sectional area of the specimens was reduced by 20%. Figure 3.7 shows the failure modes of the tested specimens. The reduced cross-sectional area in the middle of the specimens prevented the fracture to occur at undesirable locations along the length of the specimens. Furthermore, the reduced cross-sectional area contributed in concentrating the stresses in the middle of the specimens resulting in a uniform fracture plane at this location. None of the tested specimens experienced either a slippage or a crushing failure at the ends, which was an indication that the embedded threaded steel rods provided a strong and evenly distributed bond with the surrounding concrete. Moreover, no secondary flexural-related failure was observed, confirming that proper alignment was provided by the universal joints.

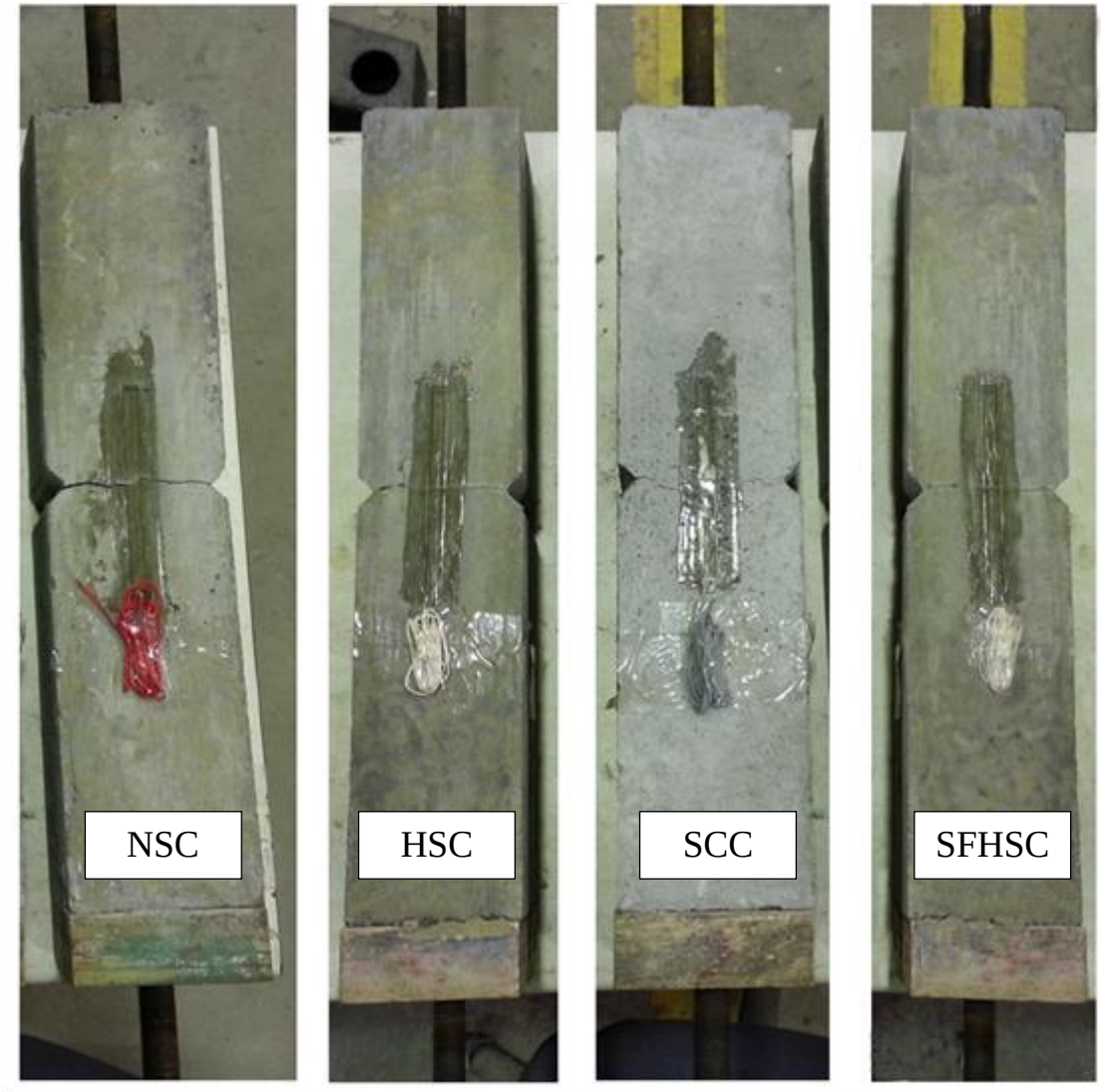

Figure 3.7: Failure modes of the tested specimens: (a) NSC, (b) HSC, (c) SCC and (d) SFHSC

3.4.2 Stress-Strain Behaviour of Tested Specimens

In this study, the axial tensile stress for the tested specimens was determined from dividing the axial tensile load recorded by the load cell of the Instron testing machine by the reduced cross-sectional area (80 × 100 mm) of the specimens. Two strain gauges were attached at the middle of long non-notched sides of each tested specimen to

measure the axial tensile strain. Figure 3.8 presents the elastic phase of the stress-strain behaviour of the SCC specimen (S1), in which the axial strains were recorded by the two strain gauges attached on both sides of the SCC specimen (S1). Since the strain gauges were not able to provide accurate readings after the specimens were fractured in the middle (notched zone), especially for SFHSC specimens, the stress-strain behaviours of the specimens were drawn, based on strain gauge readings, until the fracture occurred. Afterwards, the axial strains were calculated by dividing the axial deformation captured by the Instron testing machine by the overall length of the tested specimens in order to draw the post-fracture behaviour of the tested specimens. It is noted that the proposed testing configuration in a servo-hydraulic testing system with closed loop may reasonably capture the post-cracking stress-strain behaviour of the concrete.

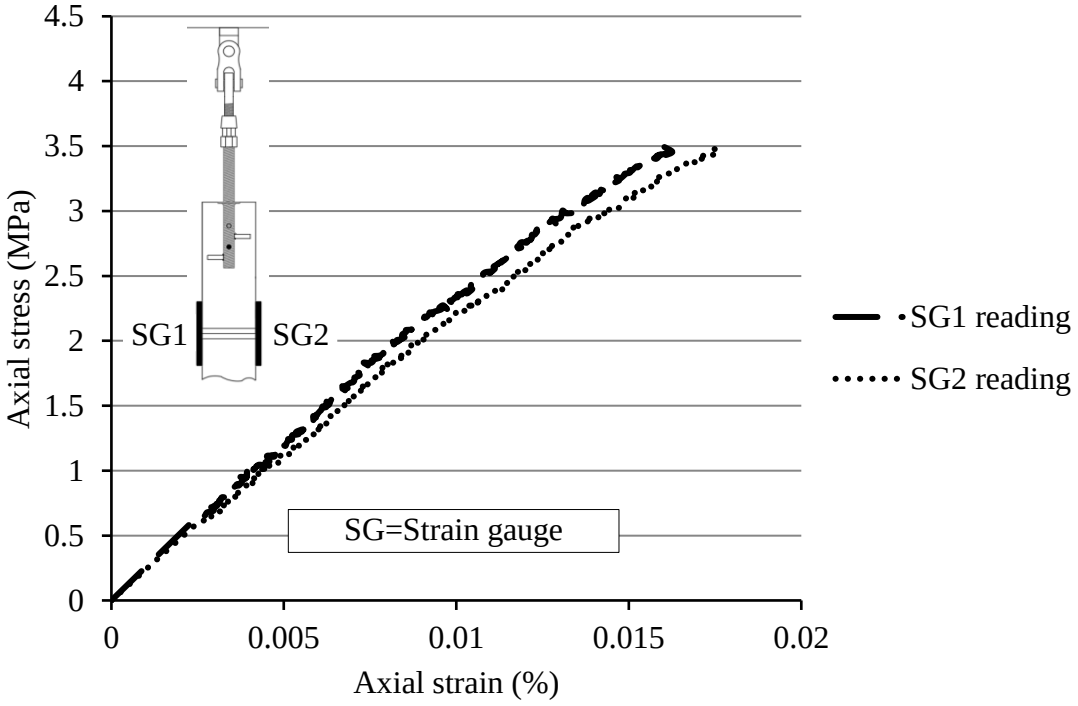

Figure 3.8: Elastic phase of the stress-strain behaviour of the SCC specimen (S1)

Figure 3.9 shows the stress-strain behaviour of the tested specimens under uniaxial tension. All the tested specimens experienced an almost linear stress-strain behaviour up to the peak stress. Similar observations were reported in Ref. (Chen et al. 2013; Wille et al. 2014). After the peak stress, the NSC, HSC and SCC specimens (plain concrete) failed immediately once they reached their peak tensile stresses. The immediate failure of the plain concrete specimens under uniaxial tension was attributed to the complete fracture failure exhibited by the tested specimens in the middle. As expected, the fracture failure occurred at the weakest section (notched zone) of the tested specimens. On the other hand, the failure of the SFHSC specimen started with a partial crack in the middle of the specimens which resulted in a drop of about 50% of the peak tensile stress followed by a gradual reduction in the stress-strain behaviour until failure. Similar stress-strain behaviour was reported for SFHSC in Ref. (Körmeling and Reinhardt 1987; Wille et al. 2014; Mobasher et al. 2014).

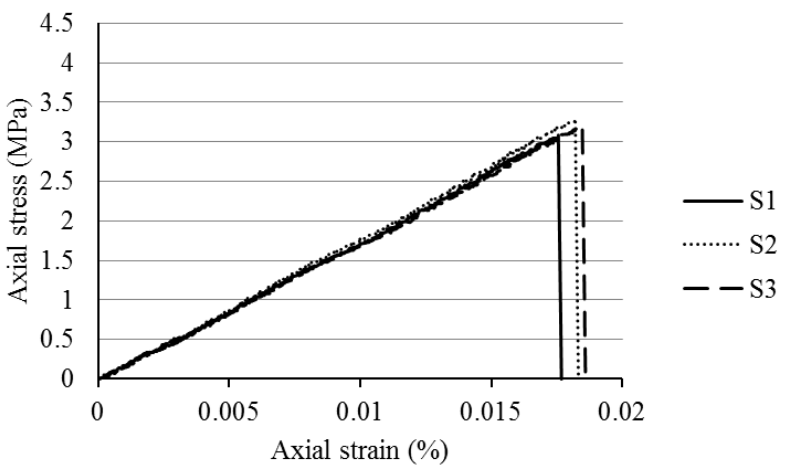

(a) Normal-strength concrete (NSC)

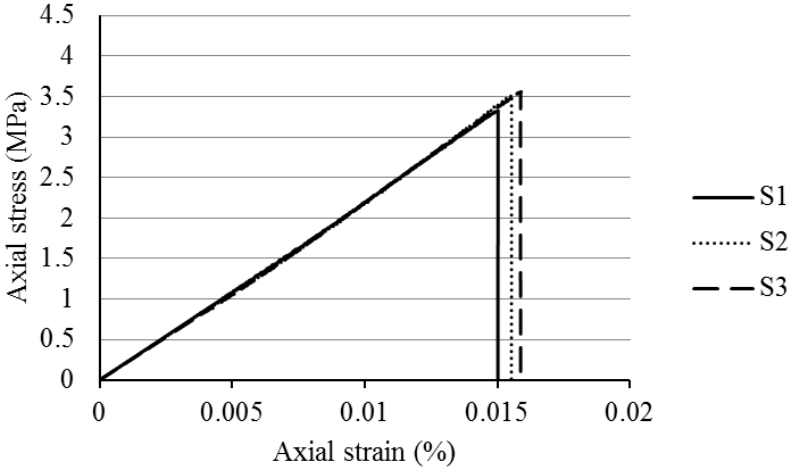

(b) High-strength concrete (HSC)

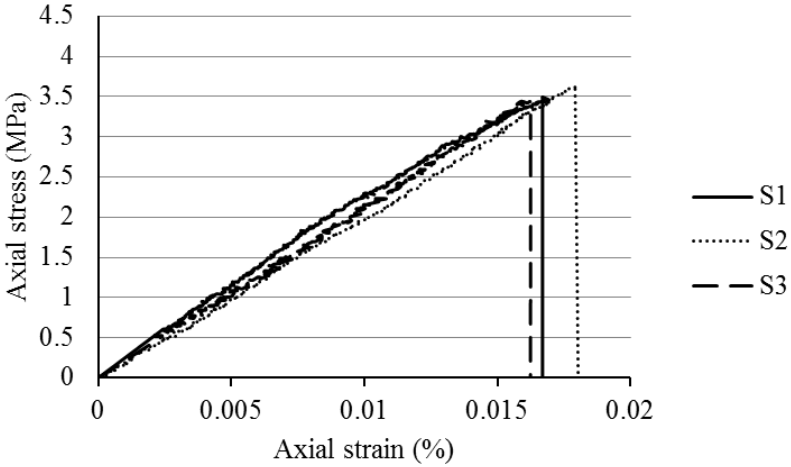

(c) Self-consolidating concrete (SCC)

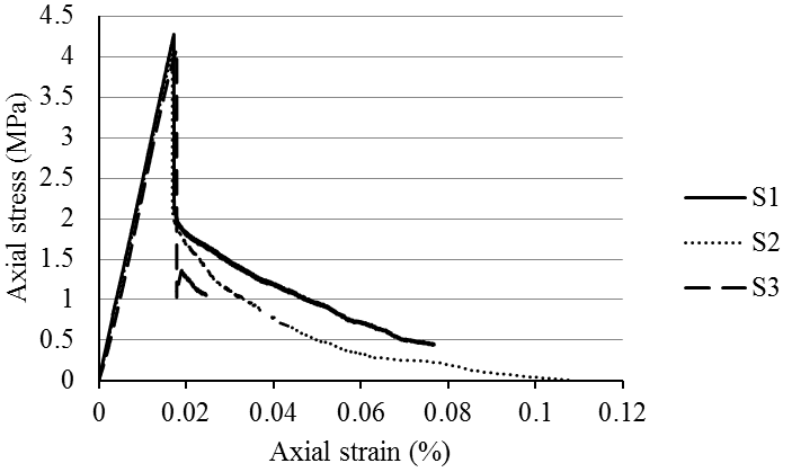

(d) Steel fibre reinforced high-strength concrete (SFHSC)

Figure 3.9: Uniaxial tensile stress-strain behaviour: (a) NSC, (b) HSC, (c) SCC and (d) SFHSC

3.4.3 Comparison of the Test Results

The experimentally obtained values of direct tensile strengths for NSC, HSC, SCC, and SFHSC were evaluated in order to assess the precision of the developed direct tensile testing method. Table 3.2 summarizes the mechanical properties of NSC, HSC, SCC and SFHSC including the compressive strength, splitting tensile strength, flexural strength, direct tensile strength and the modulus of elasticity.

The modulus of elasticity of the NSC, HSC, SCC and SFHSC was determined from the slope of the stress-strain behaviour of the specimens in tension and compression as mentioned earlier. It was observed that the modulus of elasticity of the NSC, HSC, SCC and SFHSC in tension was about 73%, 55%, 67% and 57% of the modulus of elasticity of the NSC, HSC, SCC and SFHSC in compression, respectively.

The compressive, splitting and the flexural strengths were obtained using standard concrete tests (ASTM 2016a; ASTM 2011; ASTM 2016b), whereas the direct tensile strength of the concrete was obtained using the testing method developed in this study. The average direct tensile strength for the NSC, HSC, SCC and SFHSC obtained using the developed direct tensile testing method were found to be 3.19, 3.5, 3.5 and 4.1 MPa, respectively. The average direct tensile strengths of the tested specimens were found to be less than the corresponding average splitting tensile and flexural strengths. The average direct tensile strength of NSC, HSC, SCC and SFHSC specimens were found to be 10%, 33%, 8% and 36% less than the average splitting tensile strengths of NSC, HSC, SCC and SFHSC, respectively.

Table 3.2: Test results for NSC, HSC, SCC and SFHSC specimens

Type of test	Standard tests	Tested specimens for different types of concrete															
		Normal-strength concrete (NSC)				High-strength concrete (HSC)				Self-consolidating concrete (SCC)				Steel fibre high-strength concrete (SFHSC)			
		S1	S2	S3	Ave	S1	S2	S3	Ave	S1	S2	S3	Ave	S1	S2	S3	Ave
Compressive strength (MPa)	ASTM C39-2016a	39	38.5	39.5	39	82.8	86.6	85.5	85	56.5	57	-	57	92.3	94.7	91.2	93
Splitting tensile strength (MPa)	ASTM C496-2011	3.56	3.65	3.42	3.54	5.4	5.3	4.8	5.2	3.7	3.78	3.87	3.8	6.8	6.2	6.1	6.4
Flexural strength (MPa)	ASTM C78-2016b	4.2	4.37	4.31	4.3	6.2	6.8	6.1	6.0	6.0	6.39	7.1	6.5	6.9	6.8	7.2	6.9
Direct tensile strength (MPa)	Developed method	3.08	3.29	3.2	3.19	3.6	3.3	3.5	3.5	3.4	3.49	3.6	3.5	4.1	4.0	4.3	4.1
Modulus of elasticity (compression) (GPa)	ASTM C469-2014a	30.5	31	30	30.5	40.5	39.3	38.5	39	29.5	30	31	30	42	39.8	41	41
Modulus of elasticity (direct tension) (GPa)	Developed method	21	22.4	23.5	22.3	21.4	21.8	21.6	21.6	19.5	20.4	21	20	21.9	23.5	24.7	23.4

In addition, The average direct tensile strength of NSC, HSC, SCC and SFHSC specimens were found to be 26%, 42%, 46% and 41% less than the average flexural strengths of NSC, HSC, SCC and SFHSC, respectively. The difference between the direct tensile strength and the tensile strengths obtained from the splitting tensile and flexural strengths might be attributed to the distribution of tensile stresses at the failure plane.

The average direct tensile strength of the NSC specimen was equal to 90% of the splitting tensile strength, which is consistent with AS 3600 (AS 2009) and EC 2 (2004). Similarly, the average direct tensile strength of the SCC specimens was approximately equal to 90% of the splitting tensile strength (Alhussainy et al. 2016). In addition, the average direct tensile strength of the HSC and SFHSC, obtained using the developed direct tensile testing method, were found to be close to the direct tensile strengths reported in the previous studies (Körmeling and Reinhardt 1987; Marzouk and Chen 1995; Ren et al. 2008; Hasan et al. 2016).

According to AS 3600 (AS 2009), the direct tensile strength of the concrete is calculated as 60% of the flexural strength of the concrete. The average direct tensile strength of NSC, HSC, SCC and SFHSC, obtained using the developed direct tensile testing method, were compared to that calculated from flexural strength according to AS 3600 (AS 2009). The ratio of the calculated to the experimental results of the direct tensile strength for NSC, HSC, SCC and SFHSC specimens were found to be 0.8, 1.0, 1.1 and 1.0, respectively.

The previous testing procedures for concrete under uniaxial tension were complicated. Besides, a considerable number of the experimental data reported in some previous research studies for the direct tensile strength of concrete were found to be unreliable due to the technical complicacies related to the testing procedure. However, the direct tensile testing method developed in this study provides rational and reliable results for the direct tensile strength of the NSC, SCC, HSC and SFHSC using a simple and an effective testing technique.

3.5 Conclusions

1. The developed direct tensile testing method was found to be efficient in ensuring that the fracture occurred in the middle of each specimen where the cross-sectional area was reduced by 20%.
2. Due to the use of an adequate gripping technique (embedded threaded steel rods), none of the tested specimens experienced slippage or crushing failure at the ends.
3. Due to the proper alignment provided by the universal joints, no secondary flexural-related failure occurred in the tested specimens.
4. The average direct tensile strengths of the tested specimens were found to be less than the average flexural strength and splitting tensile strength.
5. All tested specimens showed linear stress-strain behaviours under uniaxial tension almost up to the peak stress. The NSC, HSC and SCC specimens (plain concrete) failed immediately once the tensile stress peak was reached. However, the failure of the SFHSC specimen started with a partial crack in the middle of the specimens which resulted in a drop in the tensile peak stress by about 50%.

6. The developed procedure provided rational and reliable results for the direct tensile strength of the NSC, SCC, HSC and SFHSC using a simple and an effective testing technique.

Acknowledgment

The authors express special thanks to the technical officers at the High Bay Laboratories of the University of Wollongong, Australia, especially Mr. Ritchie McLean and Mr. Duncan Best, for their help in conducting the experimental programme of this study. Also, the first and second authors would like to acknowledge the Iraqi Government for the support of their PhD scholarship.

References

Alhussainy, F., Hasan, H. A., Rogic, S., Sheikh, M. N., and Hadi, M.N.S. (2016). "Direct tensile testing of Self-Compacting Concrete." *Construction and Building Materials*, 112, 903-906.

AS (Australian Standard). (2009). "Concrete structure." *AS 3600-2009*, Sydney, NSW, Australia.

ASTM. (2011). "Standard test method for splitting tensile strength of cylindrical concrete specimens." *ASTM C496/C496M-11*, West Conshohocken, PA.

ASTM. (2014a). "Standard test method for static modulus of elasticity and Poisson's ratio of concrete in compression." *ASTMC469/C469M-14*, West Conshohocken, PA.

ASTM. (2014b). "Standard test method for passing ability of self-consolidating concrete by J-ring." *ASTM C1621/C1621M-14*, West Conshohocken, PA.

ASTM. (2014c). "Standard test method for slump flow of self-consolidating concrete." *ASTM C1611/C1611M-14*, West Conshohocken, PA.

ASTM. (2014d). "Standard test method for static segregation of self-consolidating concrete using column technique." *ASTM C1610/C1610M-14*, West Conshohocken, PA.

ASTM. (2016a). "Standard test method for compressive strength of cylindrical concrete specimens." *ASTM C39/C39M-16b*, West Conshohocken, PA.

ASTM. (2016b). "Standard test method for flexural strength of concrete (using simple beam with third-point loading)." *ASTM C78/C78M-16*, West Conshohocken, PA.

Baishya, M. C., Cook, R. L., and Kelly, M. T. (1997). "Testing of polymer injection material." *Concrete International*, 19(4), 48-51.

Chen, X., Wu, S., Zhou, J., Chen, Y., and Qin, A. (2013). "Effect of testing method and strain rate on stress-strain behavior of concrete." *Journal of Materials in Civil Engineering*, 25(11), 1752-1761.

Choi, S., Yang, K., Sim, J., and Choi, B. (2014). "Direct tensile strength of lightweight concrete with different specimen depths and aggregate sizes." *Construction and Building Materials*, 63, 132–141.

EC 2 (Eurocode). (2004). "Design of Concrete Structures." European Committee for Standardization, *EN 1992-1-1: Part 1-1*, p.225.

Elvery, R. H., and Haroun, W. A. (1968). "A direct tensile test for concrete under long- or short-term loading." *Magazine of Concrete Research*, 20(63), 111-116.

Glisic, B. (2011). "Influence of the gauge length on the accuracy of long-gauge sensors employed in monitoring of prismatic beams." *Measurement Science and Technology*, 22(3), 035206.

Hasan, H. A., Alhussainy, F., Sheikh, M. N., and Hadi, M. N. S. (2016). "Direct tensile test of high strength concrete with and without steel fibres." *Mechanics of Structures and Materials: Advancements and Challenges*, 487-492.

Hasan, H. A., Sheikh, M. N., and Hadi, M. N. (2017). "Performance evaluation of high strength concrete and steel fibre high strength concrete columns reinforced with GFRP bars and helices." *Construction and Building Materials*, 134, 297-310.

Körmeling, H. A., and Reinhardt, H. W. (1987). "Strain rate effects on steel fibre concrete in uniaxial tension." *The International Journal of Cement Composites and Lightweight Concrete*, 9(4), 197-204.

Li, Z., Kulkarni, S. M., and Shah, S. P. (1993). "New test method for obtaining softening response of unnotched concrete specimen under uniaxial tension." *Experimental Mechanics*, 33(3), 181-188.

Marzouk, H., and Chen, Z. (1995). "Fracture energy and tension properties of high-strength concrete." *Journal of Materials in Civil Engineering*, 7(2), 108-116.

Mechtcherine, V. (2007). "Testing behaviour of strain hardening cement-based composites in tension – summary of recent research." In: RILEM-Symposium on high-performance fibre reinforced cementitious composites, RILEM PRO 53, 13–22.

Mobasher, B., Bakhshi, M., and Barsby, C. (2014). "Back calculation of residual tensile strength of regular and high performance fiber reinforced concrete from flexural tests." *Construction and Building Materials*, 70, 243–253.

Reinhardt, H. W., Cornelissen, H. A. W., and Hordijk, D. A. (1986). "Tensile tests and failure analysis of concrete." *Journal of Structural Engineering*, 112(11), 2462-2477.

Ren, X. D., Yang, W. Z., Zhou, Y., and Li, J. (2008). "Behavior of high-performance concrete under uniaxial and biaxial loading." *ACI materials journal*, 105(6), 548-557.

Swaddiwudhipong, S., Lu, H., and Wee, T. (2003). "Direct tension test and tensile strain capacity of concrete at early age." *Cement and Concrete Research*, 33(12), 2077-2084.

Ueda, M., Hasebe, N., Sato, M., and Okuda, H. (1994). "Fracture mechanism of plain concrete under uniaxial tension." *Concrete Library of the JSCE*, No. 24, 31-45.

Wee, T., Lu, H., and Swaddiwudhipong, S. (2000). "Tensile strain capacity of concrete under various states of stress." *Magazine of Concrete Research*, 52(3), 185-193.

Wille, K., El-Tawil, S., and Naaman, A. E. (2014). "Properties of strain hardening ultra high performance fiber reinforced concrete (UHP-FRC) under direct tensile loading." *Cement and Concrete Composites*, 48, 53-66.

Wu, S., Chen, X., and Zhou, J. (2012). "Tensile strength of concrete under static and intermediate strain rates: Correlated results from different testing methods." *Nuclear Engineering and Design*, 250, 173-183.

Xie, N., and Liu, W. (1989). "Determining tensile properties of mass concrete by direct tensile test." *ACI Materials Journal*, 86(3), 214-219.

Yan, D., and Lin, G. (2006). "Dynamic properties of concrete in direct tension." *Cement and Concrete Research*, 36(7), 1371-1378.

Zijl, G. P. A. G., Slowik, V., Filho, R. D. T., Wittmann, F. H., and Mihashi, H. (2016). "Comparative testing of crack formation in strain-hardening cement-based composites (SHCC)." *Materials and Structures*, 49(4), 1175-1189.

CHAPTER 4: BEHAVIOUR OF SMALL DIAMETER STEEL TUBES UNDER AXIAL COMPRESSION

Summary

This chapter presents the behaviour of small diameter steel tubes under axial compression. The effect of unsupported length to the outside diameter (L/D) ratio on the axial compressive behaviour of small diameter steel tubes was investigated. Galvanized and cold-formed steel tube specimens with L/D ratio of 2 to 12 were tested. The details of the experimental study including the design of experiments, preparation and testing, failure modes and behaviour of the specimens under concentric axial load were presented in this chapter. The results of this study are used in explaining the buckling behaviour of self-compacting concrete columns reinforced with small diameter steel tubes.

In order to compare the behaviour of unfilled small diameter steel tubes with the behaviour of concrete-filled small diameter steel tubes under axial compression, the next chapter (Chapter 5) experimentally explores the behaviour of small diameter self-compacting concrete-filled steel tubes under axial compression.

Citation

This chapter has been published in the Structures Journal with the following citation:

Alhussainy F, Sheikh MN, Hadi MNS. (2017). "Behaviour of Small Diameter Steel Tubes Under Axial Compression." *Structures Journal*, 11, 155-163.

Abstract

Small diameter steel tubes are used in many civil engineering applications. Recently, the behaviour of concrete columns reinforced with small diameter steel tubes was experimentally and analytically investigated. This study explores the effect of unsupported length to the outside diameter (L/D) ratio on the axial compressive behaviour of small diameter steel tubes, which has not yet been adequately investigated. Galvanized and cold-formed steel tube specimens with L/D ratio of 2 to 12 were tested. It was observed that for specimens with L/D ratio of 2 and 4, the compressive failure occurred due to local elephant's foot buckling. However, the compressive failure mode changed to global buckling for specimens with L/D ratio ≥ 6. The ultimate compressive strength was found to be lower than the ultimate tensile strength for specimens with L/D ratio ≥ 6.

Keywords: Steel tube; axial tension; axial compression; length to outside diameter ratio; stress-strain behaviour.

4.1 Introduction

Steel tubes are widely used in different structural applications and are subjected to different types of loading (An et al. 2015; Zheng et al. 2016). Circular steel tubes are used for the construction of concrete filled steel tube columns and double skin columns, as the steel tube provides a uniform hoop stress (Schneider 1998). Recently, Hadi et al. (2017) used small diameter steel tubes (33.7 mm and 26.9 mm) in lieu of solid steel bars as the main reinforcement in circular reinforced concrete columns. The innovative use of small diameter steel tubes in reinforcing concrete columns was found to be significantly effective, considering the axial load carrying capacity and ductility of the

reinforced concrete columns (Hadi et al. 2017). Small diameter steel tubes are also used in the construction of garage sheds, covered walkways, and pedestrian bridges. The radius of gyration (r) of a steel tube section is significantly higher than the radius of gyration of a solid steel section with similar cross-sectional area. Hence, the slenderness ratio (L/r ratio, where L is the length of the tube and r is the radius of gyration) of the steel tube section is much lower than the slenderness ratio of solid steel sections. The lower L/r ratio of the steel tube results in a higher axial load carrying capacity compared to axial load carrying capacity of solid steel section with the same effective length. In addition, a decrease in the L/r ratio of the steel tube increases the axial load carrying capacity of the tube (Rasmussen and Hancock 1993). The failure modes (local buckling and global buckling) of steel tubes are influenced by the diameter to thickness (D/t) ratio and length to diameter (L/D) ratio. The D/t ratio influences the local buckling and the L/D ratio influences the global buckling. Steel tubes with larger D and smaller t tend to be more sensitive to local buckling, while steel tubes with larger L and smaller D tend to be more sensitive to global buckling.

Design standards specify limits on the D/t ratio to prevent local buckling of steel tubes (European Standard Eurocode 4 2004; American Standard ANSI/AISC 360-10 2010; Canadian Standard CAN/CSA S16-09 2009). Zhao (2000) investigated very high strength circular tubes (ultimate tensile strength = 1500 MPa, outside diameter ranged from 31.97 mm to 38.31 mm and thickness ranged from 1.53 mm to 1.99 mm) under axial compression with different D/t ratio and compared the compressive strength with tensile strength. It was found that an increase in the D/t ratio reduced the section capacity (= tensile yield stress × cross-section area) due to the local buckling of the steel tubes. Sohal and Chen (1987) reported that the local buckling influenced the maximum

compressive strength of steel tubes with D/t ratio ≥ 36. Teng and Hu (2007) observed that the failure mode of steel tubes with small D/t ratio was outward buckling around the circumference. This local buckling failure occurred at one end of the steel tube, which is commonly known as the elephant's foot buckling. Only a limited number of studies, however, investigated the behaviour of steel tubes (mostly outside diameter larger than 500 mm) under axial compression with different L/D ratios of 0.5, 1.0, 2.36 and 3.0 (Murray 1997).

The L/D ratio of steel tubes is an important parameter, as it significantly influences the stability and global buckling of steel tubes. Steel tubes with a large L/D ratio causes global buckling before any significant yielding in the steel tube. For solid steel bars, the ultimate strength and ductility under axial compression decrease with the increase in the L/D ratio (Mau and El-Mabsout 1990). Hence, in the structural applications, to avoid global buckling of steel bars, the L/D ratio is kept limited to 6 (Mau and El-Mabsout 1990; Bayrak and Sheikh 2001; Bae et al. 2005), for which the behaviour under axial tension and compression is similar. The effect of increased L/D ratio on the stability of steel tubes is significantly important, especially when the D/t ratio is not critical for local buckling. Although the design standards (Eurocode 4-1-1 2004; Canadian Standards Association 2009; American Institute of Steel Construction 2010) specify factors to reduce the axial compression capacity of steel tubes with large L/D ratio, the design standards are not specifically intended for the small diameter of steel tubes. The Eurocode 4-1-2 (2005) specifies a minimum diameter of 160 mm for steel tubes, while the other design standards do not specify the limits for the minimum diameter of steel tubes. When the small diameter steel tube is used, the effect of L/D ratio on the reduction of the axial load carrying capacity and ductility becomes more significant.

Steel tube with a large L/D ratio may not reach the plastic axial compressive strength and may fail due to global buckling. However, the investigation on effect of L/D ratio on the behaviour of small diameter steel tubes under axial compression is very limited.

This study explores the effect of L/D ratio on the behaviour of galvanized and cold-formed small diameter steel tubes under axial compression. The failure modes of small diameter steel tubes with different L/D ratios were investigated. The behaviour of full section steel tubes under axial tension was also investigated to compare the behaviour of small diameter steel tubes under axial tension and compression.

4.2 Experimental Program

The experimental program contained two different types of steel tubes: galvanized steel tube and cold-formed steel tube. Galvanized and cold-formed steel tubes were chosen as they are commonly used in Australia. Cold-formed steel tubes are extensively used due to their high yield stress (Davies 2000). Galvanized steel tubes are also commonly used in structures in coastal areas to avoid damage and deterioration due to corrosion (AS 2309-2008). For cold-formed steel tube specimens, the outside diameter was 26.9 mm and the wall thickness was 2 mm. For cold-formed steel tube specimens, the outside diameter was 33.7 mm and the wall thickness was 2.6 mm. The nominal tensile strength of both galvanized and cold-formed steel tube was 350 MPa. For tension tests, three specimens were tested for each type of tube. The behaviour of steel tubes under axial compression depends on the unsupported length to outside diameters (L/D) ratio. In the experimental program, galvanized and cold formed steel tube specimens with L/D ratio of 2, 4, 6, 8, 10, and 12 were tested to include a wide range of L/D ratios of the small

diameter steel tubes used in various structural engineering applications. It is noted that, for the structural use of steel bars, similar range of L/D ratios were investigated (Mau and El-Mabsout 1990; Bayrak and Sheikh 2001; Bae et al. 2005). For each L/D ratio, three specimens were tested. A total of 42 steel tube specimens were tested, including 6 specimens under axial tension and 36 specimens under axial compression.

The specimen labels in Tables 4.1- 4.3 contain three parts. In the first part of the specimen label, the letters G and C refer to galvanized steel tube and cold-formed steel tube, respectively. In the second part of the specimen label, the letter T refers to the specimens tested under axial tension and the letter C refers to the specimens tested under axial compression. The number associated with letter C represents L/D ratio. The third part of the specimen label refers to the test specimen number, as three specimens were tested from each group. For example, Specimen G-C12-1 refers to galvanized steel tube specimen tested under axial compression with L/D ratio of 12 and the specimen is the first of the three tested specimens.

4.3 Instrumentation and Testing

A 500 kN universal testing machine in the High Bay laboratory at the University of Wollongong, Australia was used to conduct the tests for all specimens. For tension tests, different wedge grips of the machine jaw were used based on the outside diameters of the steel tube specimens. Tensile testing of steel tubes was conducted according to ASTM A370 (ASTM 2014). Full-size steel tube section was used to conduct the tensile test. The lengths of the galvanized and cold-formed steel tube specimens tested under axial tension were 302 mm and 324 mm, respectively. The gripping length at each end

of the steel tube specimen was 80 mm. To avoid the crushing at the ends of the tube due to gripping, two metal plugs fabricated from solid steel were inserted in both ends of the tube specimen. Figure 4.1 shows the schematic of the metal plugs for galvanized and cold-formed steel tubes. The gauge length of steel tube specimens tested under axial tension was 50 mm. The gauge length is the unfilled tube distance between the two metal plugs inside the steel tube (ASTM A370-2014). Flat grips were used for the compression test, as shown in Figure 4.2. The ends of steel tube specimen were milled for flat surfaces. The deformation was captured by the Instron testing machine. All specimens were tested under displacement controlled load applications at the rate of 1 mm/min.

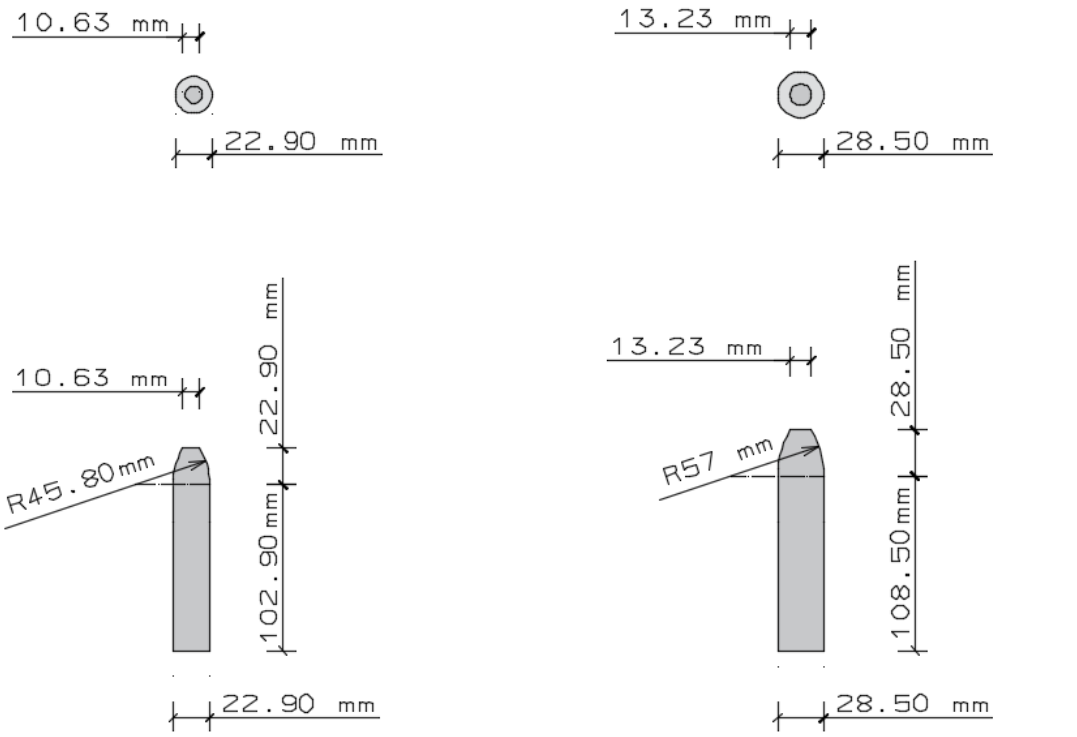

(a) Galvanized steel tube plug (b) Cold-formed steel tube plug

Figure 4.1: Metal plugs: (a) galvanized steel tube plug; and (b) cold-formed steel tube plug

Figure 4.2: Testing of specimen under axial compression

4.4 Results of Steel Tube Tensile Tests

Test results of galvanized and cold-formed steel tube specimens under axial tension have been reported in Table 4.1. Figure 4.3 shows the stress-strain behaviour of galvanized and cold-formed steel tube specimens under axial tension. It was observed from the stress-strain behaviour of the tested specimens that the galvanized steel tube specimens experienced well-defined yield points and also experienced plastic strain hardening after yield plateau. The cold-formed steel tube specimens did not show clearly defined yield points. Hence, yield stresses were calculated based on 0.2% proof stress (AISI 1996). The average ultimate strength to yield stress ratio for galvanized and cold-formed tube specimens was slightly greater than 1.08, which conforms the ductility requirement specified in AISI (1996). The average yield stress of the cold-formed steel tube specimens was 11% higher than the average yield stress of galvanized steel tube specimens. The average ultimate strength of cold-formed steel tube specimens was 14% higher than the average ultimate strength of galvanized steel tube specimens.

Table 4.1: Test results of galvanized and cold-formed steel tube specimens under axial tension

Specimen	Yield[a] stress (MPa)	Strain[a] corresponding to yield stress (%)	Ultimate strength (MPa)	Strain corresponding to ultimate strength (%)	Young's modulus (GPa)
G-T-1	408	0.27	440	5.7	190
G-T-2	411	0.27	448	5.53	210
G-T-3	410	0.29	441	5.51	185
Average (G-T)	410	0.28	443	5.58	195
C-T-1	450	0.65	501	3.27	180
C-T-2	455	0.66	505	3.72	190
C-T-3	460	0.67	511	3.41	195
Average (C-T)	455	0.66	506	3.47	190

[a] Yield stress and yield strain of C-T specimens were calculated based on 0.2% proof stress.

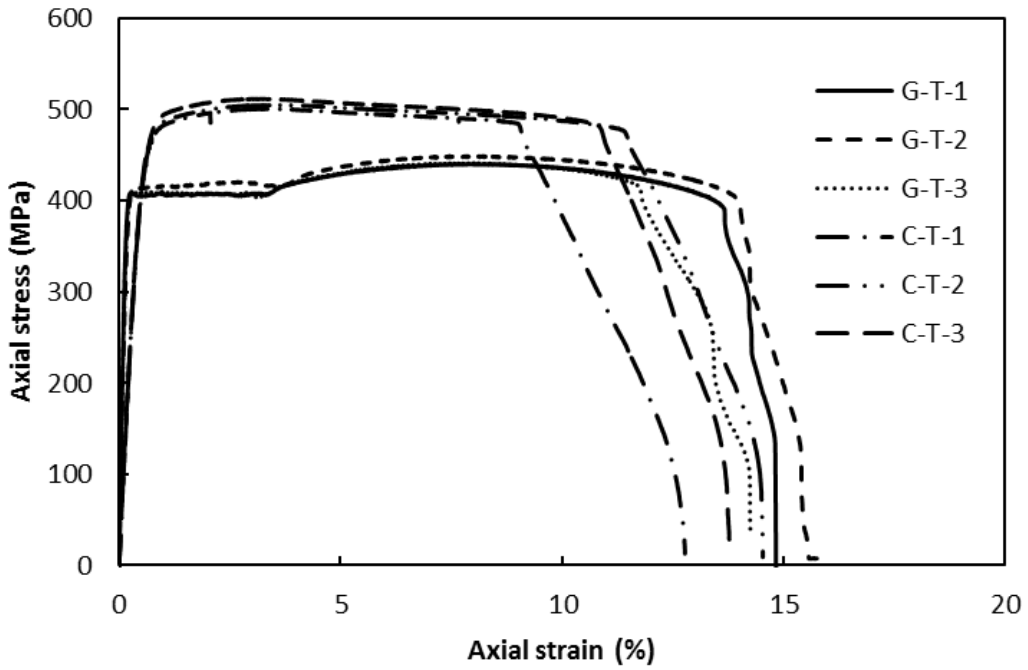

Figure 4.3: Stress-strain behaviour of galvanized and cold-formed steel tube specimens under axial tension

Figure 4.4 shows the typical failure modes of full-section tensile tests for the galvanized and cold-formed steel tube specimens. The failure modes of galvanized and cold-formed steel tubes were characterized by wall tearing of the tubes at the mid-height of the specimens. The planes of wall tearing in the galvanized steel tube specimens were slightly inclined. However, the planes of wall tearing in the cold-formed steel tube specimens were horizontal. The horizontal plane of wall tearing in the cold-formed steel tube was also observed in Jiao and Zhao (2001).

(a) Galvanized steel tube (b) Cold-formed steel tube

Figure 4.4: Typical failure modes of specimens under axial tension: (a) galvanized steel tube; and (b) cold-formed steel tube

4.5 General Behaviour of Steel Tubes under Axial Compression

The inelastic buckling behaviour of the steel tubes under compression was found to be significantly influenced by the L/D ratio of the tube specimens (Figure 4.5). Two failure modes were observed for galvanized and cold-formed steel tubes depending on the L/D ratio of the specimens. The first type of failure mode was local buckling (elephant's foot buckling) which occurred in a ring shape at one end of the steel tube. The second type of failure mode was global buckling which occurred along the entire length of the tube. Global buckling of the tubes occurred with insignificant local buckling at the ends of the

tube specimen. After the ultimate load, global buckling failure was observed to occur as a bend in a sharp angle near the mid-height of the tube.

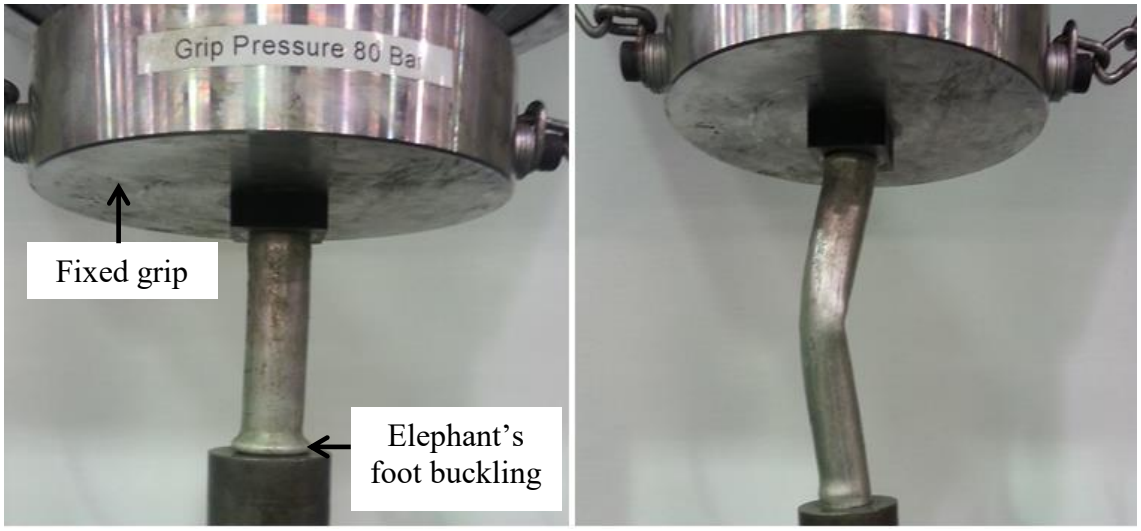

(a) Galvanized steel tube specimen with L/D=4

(b) Galvanized steel tube specimen with L/D=8

Figure 4.5: Failure modes of galvanized steel tube specimens: (a) local buckling; and (b) global buckling

4.6 Effect of L/D Ratio on the Compression Behaviour of Steel Tubes

4.6.1 Galvanized Steel Tube

Test results of galvanized steel tube specimen under axial compression are reported in Table 4.2. The stress-strain behaviour of the galvanized steel tube specimens tested under axial compression is shown in Figure 4.6. For each L/D ratio, three galvanized steel tube specimens were tested. It was observed that the three tested specimens for each L/D ratio experienced similar stress-strain behaviours. Hence, the axial load-axial deformation behaviour of one of the three tested specimens (the first specimen) for each L/D ratio is shown in Figure 4.7 for ease of comparison. The initial slopes of stress-

strain curves of steel tube specimens tested under axial compression were corrected according to the procedure outlined in Perea et al. (2013) and Gustafson et al. (1997).

Table 4.2: Test results of galvanized steel tube specimens under axial compression

Specimen	Yield stress (MPa)	Strain corresponding to yield stress (%)	Ultimate strength (MPa)	Strain corresponding to ultimate strength (%)
G-C2-1	410	0.78	492	7.21
G-C2-2	410	0.77	489	7.04
G-C2-3	416	0.80	492	7.15
Average (G-C2)	412	0.78	491	7.14
G-C4-1	410	0.78	491	6.06
G-C4-2	410	0.70	487	6.10
G-C4-3	412	0.77	476	6.2
Average (G-C4)	411	0.75	485	6.12
G-C6-1	411	0.73	434	3.59
G-C6-2	412	0.71	434	3.62
G-C6-3	410	0.68	433	3.64
Average (G-C6)	411	0.71	434	3.62
G-C8-1	-	-	426	0.69
G-C8-2	-	-	426	0.7
G-C8-3	-	-	426	0.5
Average (G-C8)	-	-	426	0.63
G-C10-1	-	-	426	0.39
G-C10-2	-	-	426	0.45
G-C10-3	-	-	425	0.47
Average (G-C10)	-	-	426	0.44
G-C12-1	-	-	424	0.40
G-C12-2	-	-	423	0.38
G-C12-3	-	-	424	0.41
Average (G-C12)	-	-	424	0.40

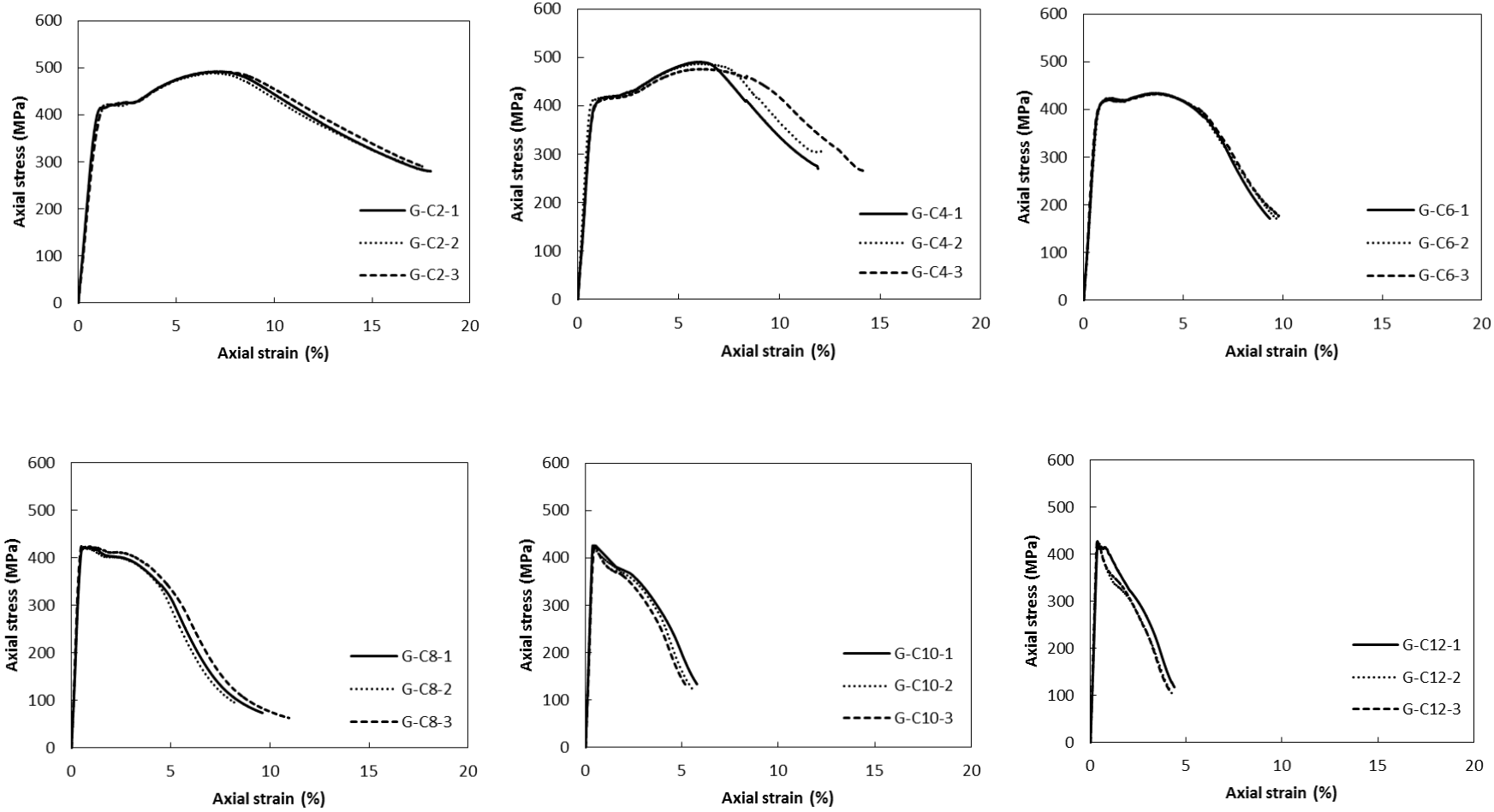

Figure 4.6: Galvanized steel tube specimens with different L/D ratios under axial compression

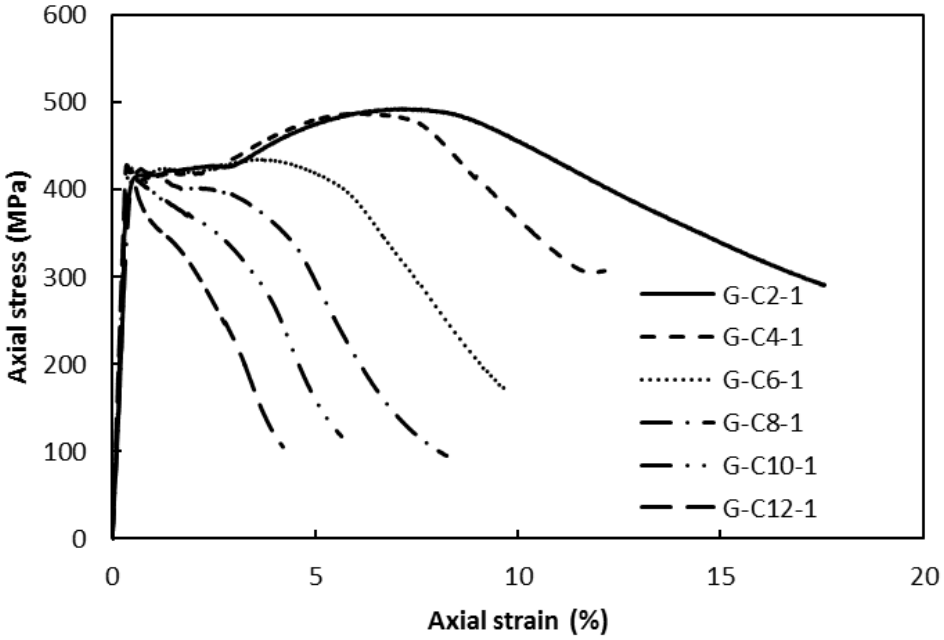

Figure 4.7: Stress-strain behaviour of galvanized steel tube specimens under axial compression

The galvanized tube specimens with L/D ratio ≤ 6 showed two peak stresses: yield stress and ultimate strength. Galvanized steel tube specimens with L/D ratio of 8 to12 showed one peak stress which is considered ultimate strength in this study. The yield compressive stress was slightly larger than the yield tensile stress for specimens with L/D ratio ≤ 6. The ultimate compressive strengths for specimens with L/D ratio of 2 and 4 were larger than the respective ultimate tensile strengths by about 9.8% and 8.7%, respectively. For specimens with L/D ratio of 6, the ultimate compressive strength was 2% less than the ultimate tensile strength. The ultimate compressive strength of the galvanized steel tube specimen was 5.3% larger than the compressive yield stress for the L/D ratio of 8.

Increasing the L/D ratio of galvanized steel tube specimens from 2 to 6 decreased the ultimate compressive strength and corresponding strain by 11.6% and 49.3%, respectively. However, no reduction in the compressive yield stress of the galvanized steel was observed for the specimens with L/D ratio $\leq$ 6. The average ultimate compressive strength to yield compressive stress ratio of the galvanized tube specimens was greater than 1.08 for specimens with L/D ratio of 2 and 4.

Figure 4.7 shows that for specimens with L/D ratio of 8 to 12, the strain hardening of the galvanized steel tube did not occur. Only one peak stress was observed for the specimens with L/D ratio of 8 to 12. The stress-strain curve of galvanized steel tube changed from strain hardening to strain softening for L/D ratio of 8 to 12. In addition, it was observed that the compressive failure mode of steel tube changed from local elephant's foot buckling to global buckling at L/D ratio of 6. Compressive failure in galvanized steel tube specimens with L/D ratio of 2 and 4 occurred due to local elephant's foot buckling. After the yield stress, the stress-strain behaviour of the steel tubes exhibited strain hardening due to further reduction in effective length, which occurred from the initiation of the elephant's foot buckling. For the specimen with L/D ratio of 6, galvanized steel tubes underwent yielding before insignificant local buckling at ends. Afterwards, global buckling took place and resulted in the failure of the steel tubes. For specimens with L/D ratio of 8 to 12, the compressive failure was observed to be more rapid due to the global buckling of the steel tube. Figure 4.8 shows the typical failure modes of galvanized steel tube specimens.

L/D=2 L/D=4 L/D=6 L/D=8 L/D=10 L/D=12

Figure 4.8: Typical failure modes of galvanized steel tube specimens

4.6.2 Cold-Formed Steel Tube

Test results of cold-formed steel tube specimens under axial compression are reported in Table 4.3. The stress-strain behaviour of cold-formed steel tube specimens tested under axial compression is shown in Figure 4.9. For each L/D ratio, three cold-formed steel tube specimens were tested. It was observed that the three tested specimens for each L/D ratio experienced similar stress-strain behaviours. Hence, the axial load-axial deformation behaviour of one of the three tested specimens (the first specimen) for each L/D ratio is shown in Figure 4.10. The stress-strain behaviour of the cold-formed steel tubes under axial compression showed no clear yield points. Therefore, the yield stresses of the cold-formed steel tubes were calculated by using 0.2% proof stress [20]. For the specimens with L/D ratio of 2, the yield compressive stress was slightly larger than the yield tensile stress. However, the yield compressive stress was 5.5% less than the yield tensile stress for specimens with L/D ratio of 4. The ultimate compressive strengths for specimens with L/D ratio of 2 and 4 were larger than the respective

ultimate tensile strengths by about 9.6% and 2.3%, respectively. For specimens with L/D ratio of 6, the ultimate compressive strength was less than the ultimate tensile strength by only 3%.

Table 4.3: Test results of cold-formed steel tube specimens under axial compression

Specimen	Yield[a] stress (MPa)	Strain[a] corresponding to yield stress (%)	Ultimate strength (MPa)	Strain corresponding to ultimate strength (%)
C-C2-1	458	1.4	562	6.63
C-C2-2	460	1.86	557	6.25
C-C2-3	455	1.52	560	6.42
Average (C-C2)	458	1.59	560	6.43
C-C4-1	430	1.17	515	4.51
C-C4-2	430	0.96	521	4.52
C-C4-3	429	1.01	518	4.49
Average (C-C4)	430	1.05	518	4.51
C-C6-1	420	0.87	483	2.45
C-C6-2	421	0.86	495	2.61
C-C6-3	420	0.68	496	2.64
Average (C-C6)	420	0.80	491	2.57
C-C8-1	418	0.64	452	1.51
C-C8-2	421	0.65	459	1.67
C-C8-3	419	0.65	457	1.55
Average (C-C8)	419	0.65	456	1.58
C-C10-1	413	0.64	438	1.22
C-C10-2	413	0.59	439	1.12
C-C10-3	411	0.55	439	1.12
Average (C-C10)	412	0.59	439	1.15
C-C12-1	405	0.57	412	0.73
C-C12-2	406	0.58	408	0.76
C-C12-3	405	0.57	413	0.88
Average (C-C12)	405	0.57	411	0.79

[a] Yield stress and yield strain were calculated based on 0.2% proof stress.

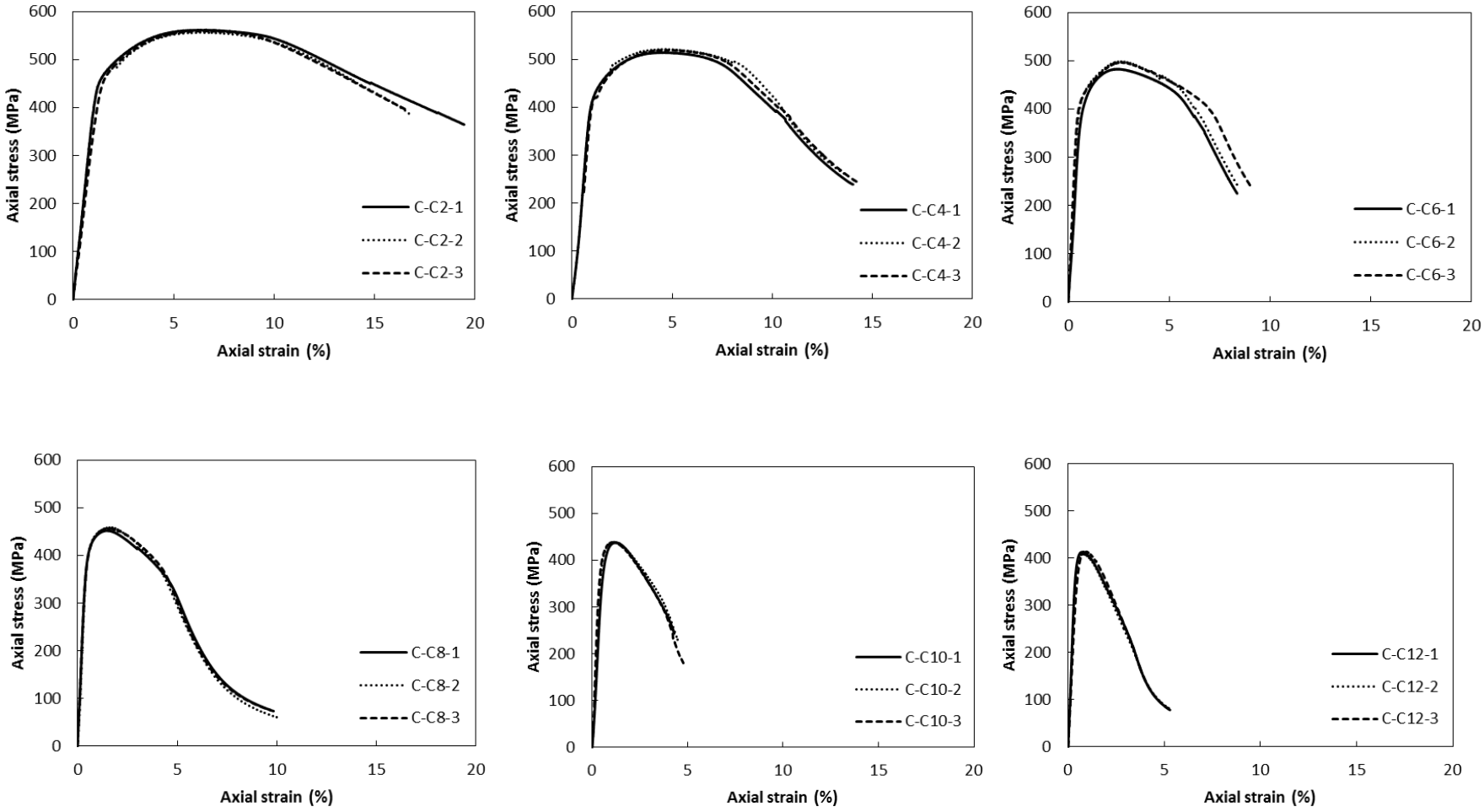

Figure 4.9: Cold-formed steel tube specimens with different L/D ratios under axial compression

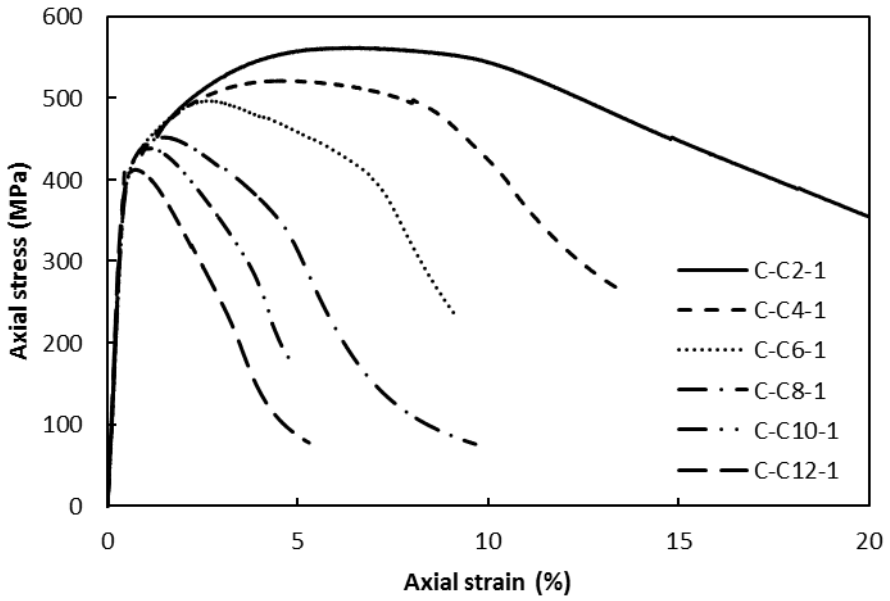

Figure 4.10: Stress-strain behaviour of cold-formed steel tube specimens under axial compression

Increasing the L/D ratio of the cold-formed steel tube specimens from 2 to 12 decreased the ultimate compressive strength and corresponding strain by 26.6% and 87.7%, respectively. When, the L/D ratio increased from 2 to 10, the yield compressive stress decreased by 10%. For specimens with L/D ratio of 2, the ultimate compressive strength was 18% larger than the yield compressive stress. This percentage reduced to only 6% for specimens with L/D ratio of 10. The average ultimate compressive strength to yield compressive stress ratio of cold-formed tube specimens was greater than 1.08 for specimens with L/D ratio of 8 and below. The initial slope of stress-strain behaviour in the cold-formed steel tube specimens with L/D ratio ≥ 6 was steeper than the initial slope of specimens with L/D ratio of 2 and 4.

The compressive failure modes of cold-formed and galvanized steel tubes were similar. For specimens with L/D ratio of 2 and 4, the compressive failure of cold-formed steel

tube specimens occurred due to the local elephant's foot buckling. After the yield stress, strain hardening occurred due to further reduction in the effective length, which occurred from the initiation of the elephant's foot buckling. For the L/D ratio of 6, cold-formed steel tube specimens underwent yielding before insignificant local buckling at ends followed by the global buckling of the entire tube specimens. Although the cold-formed steel tube specimens exhibited no clear yield point unlike galvanized steel tube specimens, the stress-strain behaviour of cold-formed steel tube specimens exhibited a rapid decrease in the stress with strain after the ultimate strength for L/D ratio of 8 to 12. Figure 4.11 shows the typical failure modes of cold-formed steel tube specimens.

Figure 4.11: Typical failure modes of cold-formed steel tube specimens

In general, to avoid global buckling of galvanized and cold-formed steel tubes in the structural applications, the L/D ratio needs to be less than 6. It is noted that for the use of small diameter steel tubes in reinforcing concrete columns, the effect of infill concrete together with the confinement provided by the surrounding concrete needs to be adequately investigated. Such investigations are considered beyond the scope of this paper and are considered part of the future research investigations by the authors.

4.7 Conclusion

Based on the experimental investigation presented in this study, the following conclusions and observations can be drawn:

1. The behaviour of galvanized and cold-formed small diameter steel tubes under axial compression is significantly influenced by the L/D ratio. For the L/D ratio of 2 and 4, the compressive failure in the steel tube specimens occurred due to local elephant's foot buckling. For the L/D ratio ≥ 6, the compressive failure modes of galvanized and cold-formed steel tube specimens changed from local elephant's foot buckling to global buckling. In structural applications, steel tubes with $L/D < 6$ should be used to prevent global buckling and to increase the ductility.

2. The stress-strain behaviour of galvanized steel tube specimens with L/D ratio ≤ 6 exhibited strain hardening after the yield stress. It is noted that the cold-formed steel tube specimens exhibited no clear yield point under axial tension and also under axial compression. However, the ultimate compressive strength of cold-formed steel tube specimen was higher than the yield compressive stress for specimens with L/D ratio of 10 and below.

3. The average ultimate compressive strength to yield compressive stress ratios of galvanized tube specimens were greater than 1.08 for the specimens with L/D ratio ≤ 4. The average ultimate compressive strength to yield compressive stress ratios of cold-formed tube specimens were greater than 1.08 for the specimens with L/D ratio ≤ 8.

4. The yield compressive stress was slightly larger than the yield tensile stress for galvanized steel tube specimens with L/D ratio ≤ 6. The yield compressive stress was slightly larger than the yield tensile stress for cold-formed steel tube specimens with L/D ratio of 2. The ultimate compressive strength of galvanized and cold-formed steel tube was found to be less than the ultimate tensile strength for specimens with L/D ratio ≥ 6.

Acknowledgment

The authors express special thanks to the technical officers at the High Bay Laboratories of the University of Wollongong, Australia, especially Mr. Ritchie McLean and Mr. Duncan Best, for their help in conducting the experimental program of this study. Also, the first author would like to acknowledge the Iraqi Government for the support of his PhD scholarship.

References

AISC. (2010). "Specification for structural steel buildings." *ANSI/AISC 360-10*, Chicago.

AISI. (1996). "Specification for the design of cold-formed steel structural members." Washington, DC, USA, American Iron and Steel Institute (AISI).

An, Y. F., Han, L. H., Roeder, C. (2015). "Performance of concrete-encased CFST box stub columns under axial compression." *Structures Journal*, 3, 211-226.

AS (Australian Standard). (2008). "Durability of galvanized and electrogalvanized zinc coatings for the protection of steel in structural applications-Atmospheric." *AS 2309-2008*, Sydney, NSW, Australia.

ASTM. (2014a). "Standard test method and definition for mechanical testing of steel products." *ASTM A370-14*, West Conshohocken, PA.

Bae, S., Mieses, A. M., and Bayrak, O. (2005). "Inelastic buckling of reinforcing bars." *Journal of Structural Engineering ASCE*, 131(2), 314-321.

Bayrak, O., and Sheikh, S. A. (2001). "Plastic hinge analysis." *Journal of Structural Engineering ASCE*, 127(9), 1092-1100.

CSA (Canadian Standards Association). (2009). "Limit states design of steel structures." *CAN/CSA-S16-09*, Mississauga, Canada.

Davies, J. M. (2000) "Recent research advances in cold-formed steel structures." *Journal of Constructional Steel Research*, 55, 267-288.

EC 2 (Eurocode). (2004). "Design of composite steel and concrete structures-Part 1-1: General rules and rules for buildings." Brussels, *EN 1994-1-1*.

EC 2 (Eurocode). (2005). "Design of composite steel and concrete structures-Part 1-2: General rules- structural fire design." Brussels, *EN 1994-1-2*.

Gustafson, T. W., Panda, P. C., Song, G., and Raj, R. (1997). "Influence of microstructural scale on plastic flow behavior of metal matrix composites." *Acta Materialia*, 45(4), 1633-1643.

Hadi, M. N. S., Alhussainy, F., and Sheikh, N. M. (2017). "Behavior of self-compacting concrete columns reinforced longitudinal with steel tubes." *Journal of Structural Engineering ASCE*, 143(6):1-14.

Jiao, H., and Zhao, X. L. (2001). "Material ductility of very high strength (VHS) circular steel tubes in tension." *Thin-Walled Structures*, 39, 887-906.

Mau, S. T., and El-Mabsout, M. (1990). "Inelastic buckling of reinforcing bars." *Journal of Engineering Mechanics ASCE*, 87(6), 671-677.

Murray, D. W. (1997) "Local buckling, strain localization, wrinkling and postbuckling response of line pipe." *Engineering Structures*, 19 (5), 360-371.

Perea, T., Leon, R. T., Denavit, M. D., and Hajjar, J. F. "Problems in determining the buckling loads of slender full-scale concrete-filled tube specimens." International Conference on Composite Construction in Steel and Concrete VII, ASCE; 2013.

Rasmussen, K. J. R., and Hancock, G. J. (1993). "Design of cold-formed stainless steel tubular members. I: Columns." *Journal of Structural Engineering ASCE*, 119(8), 2349-2367.

Schneider, S. P. (1998). "Axially loaded concrete-filled steel tubes." *Journal of Structural Engineering ASCE*, 124(10), 1125-1138.

Sohal, I. S., and Chen, W. F. (1987). "Local buckling and sectional behavior of fabricated tubes." *Journal of Structural Engineering ASCE*, 113(3), 519-533.

Teng, J. G., and Hu, Y. M. (2007). "Behaviour of FRP-jacketed circular steel tubes and cylindrical shells under axial compression." *Construction and Building Materials*, 21, 827-838.

Zhao, X. L. (2000). "Section capacity of very high strength (VHS) circular tubes under compression." *Thin-Walled Structures*, 37, 223-240.

Zheng, B., Shu, G., Xin, L., Yang, R., and Jiang, Q. (2016). "Study on the bending capacity of cold-formed stainless steel hollow sections." *Structures Journal*, 8, 63-74.

CHAPTER 5: BEHAVIOUR OF SMALL-DIAMETER SELF-COMPACTING CONCRETE-FILLED STEEL TUBES

Summary

Based on the test results of the preliminary experiments presented in Chapter four, this chapter experimentally explores the effect of length to diameter (L/D) ratio on the axial load capacity of small-diameter self-compacting concrete-filled cold-formed steel tube (SCFT) specimens. The SCFT specimens with L/D ratio of 2 to 14 were tested. Two different cold-formed steel tubes were used in the construction of the SCFT specimens. The details of the experimental study including the design of experiments, preparation and testing, failure modes and behaviour of the SCFT specimens under concentric axial load were presented in this chapter. Also, the experimental results of SCFT specimens were compared with the estimate from ANSI/AISC 360-10 (2010). The equations used for calculating the capacity of small-diameter steel tubes filled with and without the SCC were used in the analytical model in Chapters seven and eight.

Following the outcome of this chapter, the next chapter (Chapter 6) explains the experimental program for SCC columns reinforced with steel tubes as a new system of reinforcing concrete columns.

Citation

This chapter has been published in the Magazine of Concrete Research with the following citation:

Alhussainy F, Sheikh MN, Hadi MNS. (2017). "Behaviour of small-diameter self-compacting concrete-filled steel tubes." *Magazine of Concrete Research*, 70(16), 811-821.

Abstract

This study explores the effect of length to diameter (L/D) ratio on the axial load capacity of small-diameter self-compacting concrete-filled steel tube (SCFT) specimens. The SCFT specimens with L/D ratio of 2 to 14 were tested. Two different cold-formed steel tubes with diameters of 26.9 and 33.7 mm were used in the construction of the SCFT specimens. The behaviour of the SCFT specimens was compared with the unfiled steel tube (UT) specimens. The axial load capacity of SCFT specimens was found to be higher than the axial load capacity of UT specimens. The compressive failure of SCFT and UT specimens with a ratio of 2 and 4 occurred due to local buckling and with L/D ratio ≥ 6 occurred due to global buckling. However, the self-compacting concrete inside steel tubes improved the ductility and the post-peak axial load-axial deformation response of SCFT specimens compared to the UT specimens.

Keywords: Fresh concrete; workability; stress

Notation

A_c Cross section area of the concrete
A_s Cross section area of the steel tube
C_3 Coefficient of concrete effective stiffness
D Outside diameter of steel tube
E_c Modulus of elasticity of the concrete
E_s Modulus of elasticity of the steel tube
EI_e Effective flexural stiffness
f_c' Concrete compressive strength
f_y Steel yield stress
I_c Second moment of area of the concrete
I_s Second moment of area of the steel tube

k_e Member effective length factor

L Column length

N_c Nominal member capacity

N_{cd} Design member capacity

N_e Euler elastic buckling capacity

N_{exp} Average ultimate load capacity of two self-compacting concrete-filled steel tube specimens

N_o Squashing capacity of the cross-section

t Wall thickness of the steel tube

α_1 Reduction factor for the filling concrete

$\emptyset_{co}$ Partial safety factor for a composite column capacity

5.1 Introduction

Concrete-filled steel tubes (CFTs), constructed by filling steel tubes with concrete, are widely used as a structural members. The behaviour of CFTs is fundamentally different from the behaviour of unfilled steel tubes (UTs). The presence of the concrete infill changes the buckling mode of steel tube specimens from inward buckling to outward buckling (AISC, 2010). In addition, the change of buckling mode is not only evident in the cross-section but is also evident along the length of the member (AISC, 2010). CFTs have the following advantages.

- Yield load carrying capacity of a CFT is higher owing to the delay in the buckling of the steel tube in the elastic range (Lai and Ho, 2016).
- CFTs provide excellent resistance to seismic and impact loads (Shanmugam and Lakshmi, 2001).
- The strain concentrations of CFTs are reduced by spreading the localized buckling over the length of the CFT (Elchalakani et al., 2001).

- The failure of CFTs is not as rapid as UTs because the inward buckling failure mechanism is eliminated by the infill concrete (AISC, 2010; Zeghiche and Chaoui, 2005).
- The post-buckling behaviour of CFTs is more ductile than UTs owing to an increase in the wavelength of the bulking response (Ellobody et al., 2006).
- The fire resistance of CFTs is higher than that of UTs (Huo et al., 2014).
- In CFTs, the steel tube acts as permanent formwork.
- The circular steel tube section significantly increases the confinement of the concrete core owing to uniform membrane pressure (Schneider, 1998).

Due to the above mentioned advantages, CFTs have been widely used as columns for bridges and high-rise buildings (Fam et al., 2004; Giakomelis and Lam, 2004; Lai and Ho, 2015). The CFT is also used as chords in truss bridges (Han et al., 2011) and as ribs in transmission towers (Han et al., 2012). Han and An (2014) used composite columns consisting of an inner CFT and an outer layer of reinforced concrete. Recently, Hadi et al. (2017) proposed to use small-diameter CFTs for reinforcing concrete columns. The innovative use of the CFTs for reinforcing concrete column was found to be equally effectives, especially considering the axial load capacity and the ductility of the columns (Hadi et al., 2017). However, the axial load carrying capacity and the ductility of the CFT-reinforced concrete columns depends significantly on the behaviour of the CFTs under axial compression. The CFTs can be effectively used as structural members where small-diameter steel tubes are required. The concrete-filled small-diameter steel tubes can also be used in the construction of garage sheds, covered walkways, and pedestrian bridges to increase the axial load capacity and to reduce the vibration of the total structure.

In a CFT, the confinement provided by the steel tube is initiated by the expansion of concrete due to microcracking under axial load. The increase in load-resisting capacity is mostly observed in circular short CFT columns. However, when the length to outside diameter (L/D) ratio is high, the CFT columns tend to buckle before providing any confinement to the expanding concrete core. Knowles and Park (1969) reported that the CFT columns with L/D ratio $\geq$ 12 did not exhibit any significant confinement effect. Gupta et al. (2007) tested 72 CFT specimens (340 mm in length) with two different grades of concrete (nominal concrete compressive strength of 30 and 40 MPa) in steel tubes with outside diameters of 47.28, 89.32 and 112.56 mm and thicknesses of 1.87, 2.74 and 2.89 mm, respectively. Normal vibrated concrete (NVC) and self-compacting concrete (SCC) were used to fill the steel tubes. The SCC mix was produced by using three different percentages of fly ash (15, 20 and 25%). Gupta et al. (2007) reported that CFT specimens with 47.28 mm outside diameter failed by Euler bucking (global buckling) and CFT specimens with outside diameters of 89.32 mm and 112.56 mm failed by local buckling. However, Gupta et al. (2007) did not investigate the influence of different L/D ratios on the axial load capacity of the CFT specimens under axial compression. It was reported that the confinement effect decreased with an increase in the concrete strength for smaller L/D ratios. De Oliveira et al. (2009) tested 16 CFT columns (114.3 mm outside diameter and 3.35 mm wall thickness) with different grades of concrete (nominal concrete compressive strength of 32.7, 58.7, 88.8 and 105.5 MPa) and different L/D ratios (3, 5, 7 and 10). It was reported that the axial load capacity of CFT columns increased with the increase in the compressive strength of the concrete core and decreased with the increase in the L/D ratio of the specimen. Muciaccia et al. (2011) tested 24 CFT columns (139.6 mm outside diameter and 4 mm wall thickness) with different types of concrete (NVC, SCC and expansive SCC) and L/D ratios

ranging from 9 to 33 under 25 mm eccentric axial load. It was found that the influence of the L/D ratio and the failure mode of tested specimens were similar to previous findings of the CFT columns filled with NVC. Additionally, the use of SCC instead of NVC did not affect the design of CFT.

The behaviour of steel tubes filled with concrete has been extensively studied and included in major design standards, such as American Standard ANSI/AISC 360-10 (AISC 2010), Eurocode 4 (BSI, 2005) and the Canadian Standard CAN/CSA S16-09 (CSA 2009). A large number of studies were carried out on medium-scale specimens with an outside diameter between 100 mm and 200 mm using concrete of varying compressive strengths. However, only a limited number of research studies were conducted on the behaviour of small-diameter CFTs. In this paper, steel tubes with small diameters were used as CFTs. Since the diameter of the steel tubes is very small, the ability of concrete to flow and consolidate without segregation is highly critical. Therefore, concrete with high flowability is required to completely fill the tube without segregation. SCC is considered to be a suitable option; it is able to compact under its own weight without requiring any vibration. Besides the requirement for no vibration, the SCC is chosen due to its good rheological performance, constructional enhancement, environmental advantage and economic benefit (Aslani, 2015; Badry et al., 2016; Chamani et al., 2014; EFNARC, 2005). The present study investigates the influence of L/D ratio on the axial load capacity of small-diameter SCC-filled steel tube (SCFT) specimens under axial compression. For specimens with L/D ratio of 2 to 14, the compressive failure of SCFT specimens was compared with the compressive failure of the UT specimens. The influence of outside diameter to thickness (D/t) ratio of steel tubes on the behaviour of SCFT specimens was also investigated. Moreover,

experimental axial load capacities of SCFT specimens with different L/D ratios were compared with the estimates from American Standard ANSI/AISC 360-10 (AISC 2010).

5.2 Experimental Program

Two different types of cold-formed steel tubes were used to construct SCFT specimens. The first cold-formed steel tube had an outside diameter of 26.9 mm, wall thickness of 2.6 mm and a nominal tensile strength of 250 MPa. The second cold-formed steel tube had an outside diameter of 33.7 mm, a wall thickness of 2 mm and a nominal tensile strength of 350 MPa. The cold-formed steel tube specimens were divided into two groups: SCFT specimens and UT specimens. The behaviour of specimens under axial compression depends largely on the unsupported length to outside diameters (L/D) ratio. In the experimental program, two specimens of each L/D ratio of 2, 4, 6, 8, 10, 12 and 14 were tested under axial compression. Three specimens of each type of UT were also tested under axial tension. A total of 62 specimens were tested, which included 56 specimens under axial compression and 6 specimens under axial tension.

A SCC mix with a maximum aggregate size of 10 mm was used in casting the SCFT specimens. The SCC was prepared according to EFNARC (2002). Several concrete mixes were investigated to achieve SCC. The mix proportion of the SCC used in this study is shown in Table 5.1. The properties of fresh concrete were tested according to ASTM C1610-14 (ASTM, 2014b); ASTM C1611-14 (ASTM, 2014c) and ASTM C1621-14 (ASTM, 2014d). For the water/powder ratio of 0.4, column segregation test (ASTM, 2014b), slump flow test (ASTM, 2014c) and J-ring test (ASTM, 2014d) results were found to be satisfactory. The compressive strength of the SCC was determined by

testing three cylinders of 100 mm diameter and 200 mm height according to AS 1012.9-14 (SA, 2014). The average 28 d compressive strength of the SCC was 57 MPa. The formwork was constructed to keep both the top and bottom of the steel tube specimens in a fixed plumb position, as shown in Figure 5.1. Steel tube specimens were fixed to a non-absorbing plywood base plate. The SCC mix was poured in the steel tube specimens without any vibration or compaction.

Table 5.1: Mix proportion of the SCC used in this study

Material	Quantity
Cement	280 kg/m^3
Fly ash	120 kg/m^3
Slag	50 kg/m^3
Fine aggregate	950 kg/m^3
Coarse aggregate	780 kg/m^3
Water	182 kg/m^3
High range water reducer	3.375 l/m^3
Water/Powder ratio	0.4

Figure 5.1: Construction of formwork

The label for the specimen groups consist of one part and the labels for the specimens consist of three parts; these are listed in Tables 5.2–5.5. There are four groups of specimens. The Groups UT26.9 and UT33.7 refer to UTs with 26.9 mm and 33.7 mm outside diameters, respectively. The Groups SCFT26.9 and SCFT33.7 refer to SCFTs with 26.9 mm and 33.7 mm outside diameters, respectively. The first part of the specimen label represents the group name. In the second part of the specimen label, the letter ‘T’ refers to the specimens tested under axial tension, and the letter ‘C’ refers to the specimens tested under axial compression. The number associated with letter ‘C’

represents L/D ratio. The third part of the specimen label refers to the test specimen number. Two specimens from each group were tested under axial compression and three specimens from each group were tested under axial tension. For example, specimen SCFT26.9-C10-1 refers to a SCFT specimen (with 26.9 mm outside diameter) tested under axial compression, with L/D ratio of 10, and the specimen is the first of the two tested specimens.

5.3 Instrumentation and Testing

A 500 kN universal testing machine in the High Bay laboratory at the University of Wollongong, Australia, was used to conduct the tests for all specimens. For tension tests, different wedge grips of the machine jaw were used based on the outside diameters of steel tube specimens. Tensile testing of steel tubes was conducted according to ASTM A370-14 (ASTM, 2014a). Full-size tubular sections were used to conduct the tensile test. To avoid the crushing at the ends of the tube due to gripping, two metal plugs fabricated from solid steel were inserted in both ends of the tube. The metal plugs were designed based on the inside diameters of the steel tubes to suit the 21.7 and 29.7 mm steel tubes. Figure 5.2 shows the schematic of the metal plugs for the steel tubes. Flat grips were used for the axial compression test. The SCFT specimens were tested with the axial load applied on the entire section. The ends of steel tube specimen were milled for a flat surface. The specimens were tested under displacement controlled load applications at 1 mm/min.

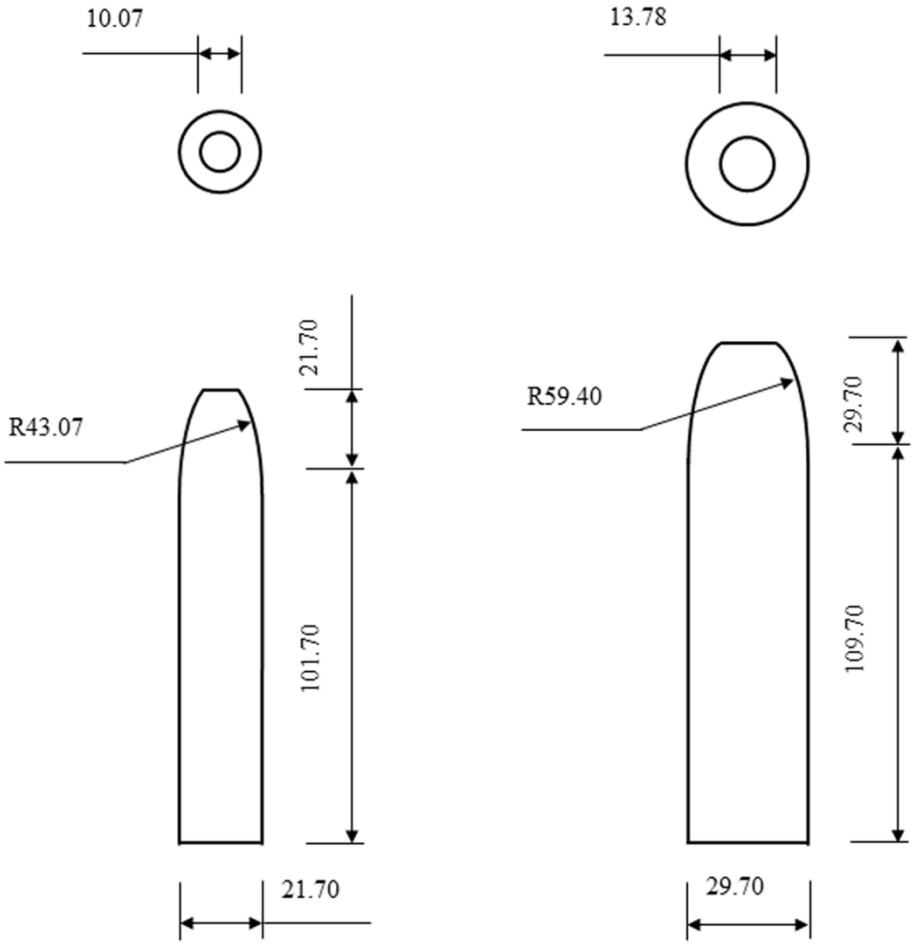

Figure 5.2: Metal plugs: (a) UT26.9 steel tube plug and (b) UT33.7 steel tube plug (all dimensions are in mm)

5.4 Test Results of UT Specimens

5.4.1 UTs under Axial Tension

Test results of cold-formed UT specimens under axial tension are reported in Table 5.2. Figure 5.3 shows the stress-strain behaviour of cold-formed UT specimens under axial tension. It was observed from the stress-strain behaviour of the tested specimens that the UT specimens did not show clearly defined yield points. Hence, yield stresses were calculated based on 0.2% proof stress (AISI, 1996). The average ultimate strength to yield stress ratio for UT specimens was greater than 1.08 (Table 5.2), which satisfies the ductility requirement specified in Specification for the Design of Cold-Formed Steel Structural Members (AISI 1996).

Table 5.2: Test results of UT specimens under axial tension

Group	Specimen	Yield[a] stress: MPa	Yield[a] strain: %	Ultimate strength: MPa	Corresponding strain: %	Young's modulus: GPa
UT26.9	UT26.9-T-1	360	0.55	399	2.53	193
	UT26.9-T-2	355	0.51	389	2.50	192
	UT26.9-T-3	350	0.52	385	2.57	191
	Ave UT26.9-T	355	0.53	391	2.53	192
UT33.7	UT33.7-T-1	455	0.53	491	4.47	195
	UT33.7-T-2	447	0.65	500	6.69	197
	UT33.7-T-3	448	0.57	495	4.52	196
	Ave UT33.7-T	450	0.58	495	5.23	196

[a] Yield stress and yield strain of specimens were calculated based on 0.2% proof stress.

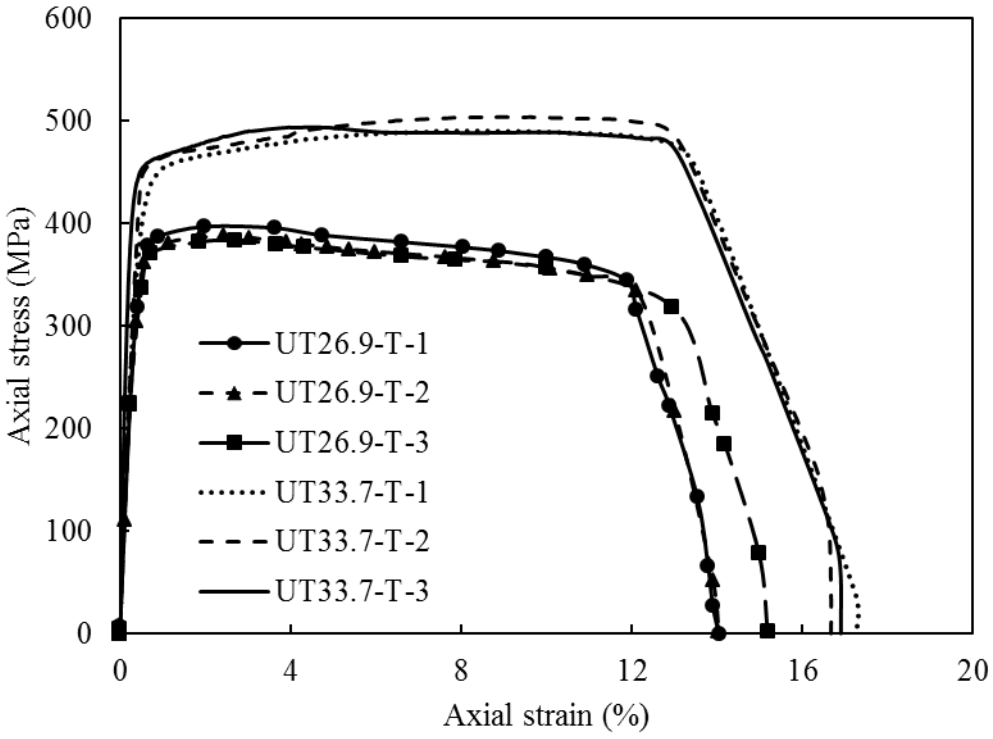

Figure 5.3: Stress-strain behaviour of cold-formed UT specimens under axial tension

5.4.2 UTs under Axial Compression

Test results of UT specimens under axial compression are reported in Table 5.3. The axial load-axial deformation behaviours of the specimens in the Group UT26.9 and Group UT33.7 under axial compression are shown in Figure 5.4. For each group of steel tubes, two specimens were tested for each L/D ratio. It was observed that the two tested specimens for each L/D ratio experienced similar axial load-axial deformation behaviour. Consequently, the axial load-axial deformation behaviour of one of the two tested specimens (the first specimen) for each L/D ratio is shown in Figure 5.4 for ease of comparison. The behaviour of UT specimens under axial compression is significantly influenced by the L/D ratio.

Table 5.3: Test results of UT specimens under axial compression

Group UT26.9			Group UT33.7		
Specimen	Ultimate load: kN	Corresponding deformation: mm	Specimen	Ultimate load: kN	Corresponding deformation: mm
UT26.9-C2-1	83.8	4.88	UT33.7-C2-1	102	3.67
UT26.9-C2-2	83.7	4.53	UT33.7-C2-2	101	3.61
Ave UT26.9-C2	83.8	4.71	Ave UT33.7-C2	101.5	3.64
UT26.9-C4-1	81.8	3.97	UT33.7-C4-1	100	5.86
UT26.9-C4-2	80.8	3.88	UT33.7-C4-2	100.4	5.83
Ave UT26.9-C4	81.3	3.93	Ave UT33.7-C4	100.2	5.85
UT26.9-C6-1	78.4	3.42	UT33.7-C6-1	94.2	5.97
UT26.9-C6-2	79.4	3.40	UT33.7-C6-2	93.4	5.84
Ave UT26.9-C6	78.9	3.41	Ave UT33.7-C6	93.8	5.91
UT26.9-C8-1	73.6	2.52	UT33.7-C8-1	88.3	4.61
UT26.9-C8-2	73.3	2.33	UT33.7-C8-2	88.9	5.00
Ave UT26.9-C8	73.5	2.4	Ave UT33.7-C8	88.6	4.81
UT26.9-C10-1	71.3	1.70	UT33.7-C10-1	83.7	3.82
UT26.9-C10-2	71.9	1.82	UT33.7-C10-2	83.8	4.00
Ave UT26.9-C10	71.6	1.76	Ave UT33.7-C10	83.8	3.91
UT26.9-C12-1	70.4	1.69	UT33.7-C12-1	81.4	3.53
UT26.9-C12-2	71.2	1.70	UT33.7-C12-2	81.6	3.65
Ave UT26.9-C12	70.8	1.70	Ave UT33.7-C12	81.5	3.59
UT26.9-C14-1	69.2	1.57	UT33.7-C14-1	78.7	3.36
UT26.9-C14-2	69.7	1.71	UT33.7-C14-2	78.5	3.13
Ave UT26.9-C14	69.5	1.64	Ave UT33.7-C14	78.6	3.25

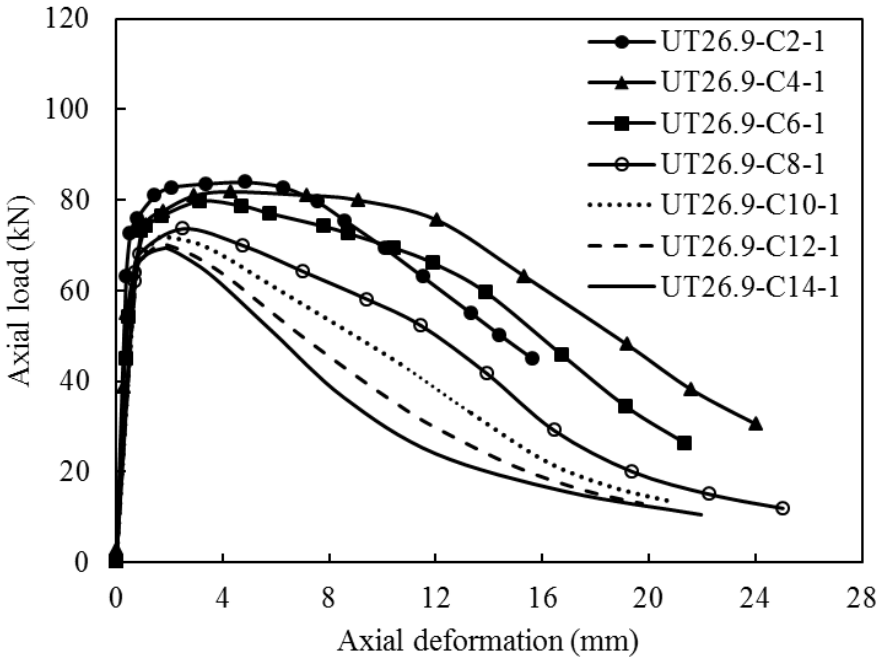

(a) Group UT26.9

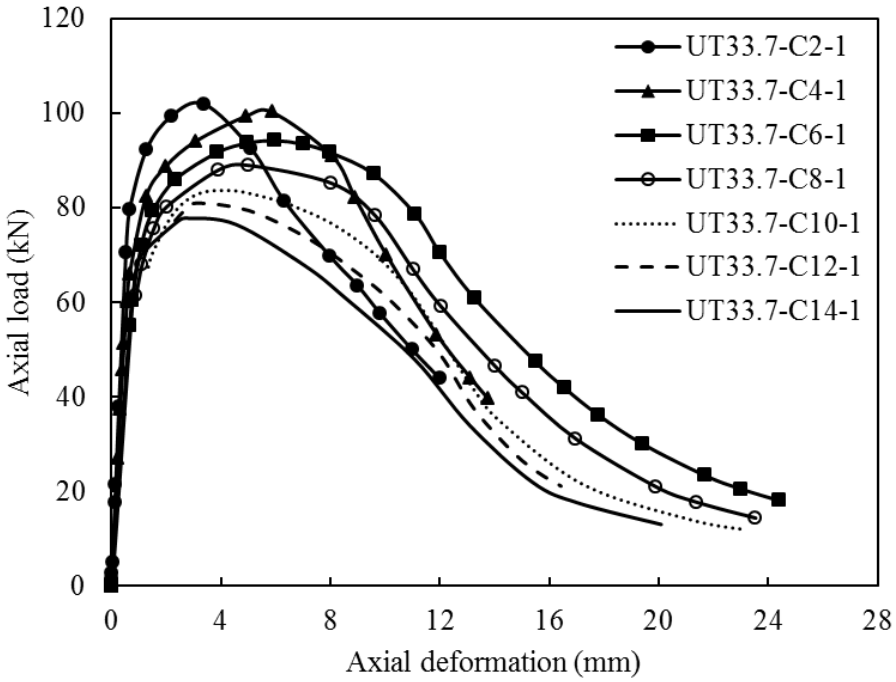

(b) Group UT33.7

Figure 5.4: Load-deformation behaviour of UT specimens under axial compression: (a) Group UT26.9 and (b) Group UT33.7

Two failure modes were observed for UT specimens depending on the L/D ratio of the specimens. The first type of failure mode was due to local buckling (elephant's foot buckling), which occurred in a ring shape at one end of the steel tube. The second type of failure mode was due to global buckling, which occurred along the entire length of the tube. Global buckling of the UT specimens occurred with insignificant local buckling at the ends of the UT specimen. After the ultimate load, global buckling failure was observed to occur as a bend in a sharp angle near the mid-height of the tube (inward buckling). For the L/D ratio of 2 and 4, the compressive failure in the UT specimens occurred due to local elephant's foot buckling. For the L/D ratio ≥ 6, the compressive failure modes of UT specimens changed from local elephant's foot buckling to global buckling. Figure 5.5 shows the typical failure modes of specimens in the Group UT26.9 and Group UT33.7.

Increasing the L/D ratio of specimens in the Group UT26.9 from 2 to 14 decreased the ultimate load and corresponding axial deformation by 17% and 65.2%, respectively. For specimens in the Group UT33.7, increasing the L/D ratio from 2 to 14 decreased the ultimate load by 22.6%. However, for specimens in the Group UT33.7 with L/D ratio of 2 and 4 the axial deformation corresponding to the ultimate axial load was less than that for specimens with L/D ratio of 6. The lower axial deformation of the specimens in the Group UT33.7 with L/D ratio of 2 and 4 may be attributed to the larger D/t ratio compared to the specimens in Group UT26.9. The formation of elephant's foot buckling in the one end of the specimen with the larger D/t ratio was faster than other specimens with smaller D/t ratios and hence the thinner tubes were less ductile (O'Shea and Bridge, 1997).

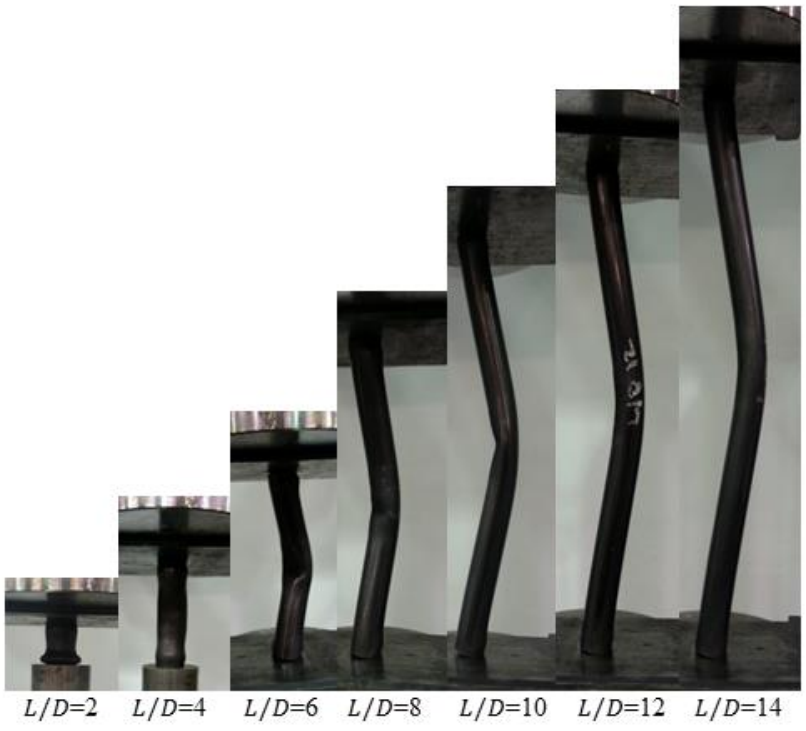

(a) Group UT26.9

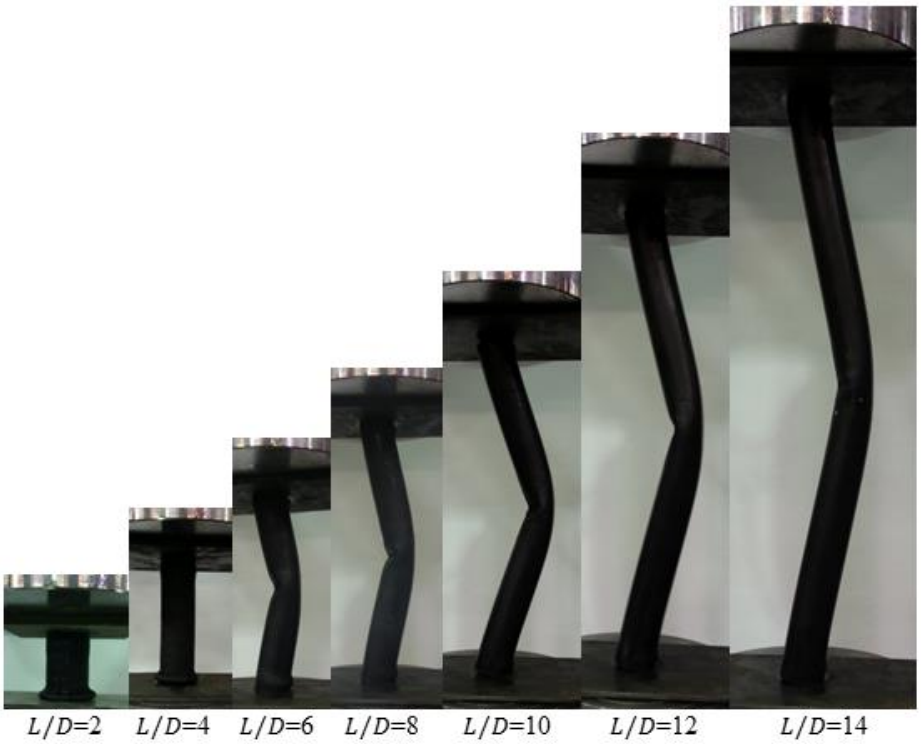

(b) Group UT33.7

Figure 5.5: Typical failure modes of UT specimens: (a) Group UT26.9 and (b) Group UT33.7

For specimens in Group UT33.7, the axial deformation corresponding to the ultimate load synchronized with elephant's foot buckling was less than the axial deformation corresponding to the ultimate axial load synchronized with global buckling. However, for specimens in Group UT33.7, increasing the L/D ratio from 6 to 14 decreased the axial deformation corresponding to the ultimate load by 45%. The D/t ratio of specimens in Group UT33.7 was 38.6% higher than the D/t ratio of specimens in Group UT26.9. For UT specimens with high D/t ratio, the influence of elephant's foot buckling on the axial deformation and ductility with L/D ratio of 2 and 4 was more significant than the influence of global buckling on the axial deformation and ductility of UT specimens with L/D ratio of 6.

5.5 Test Results of SCFTs

Test results of SCFT specimens under axial compression are reported in Table 5.4. The axial load-axial deformation behaviours of the specimens in the Group SCFT26.9 and Group SCFT33.7 that were tested under axial compression are shown in Figure 5.6. For each group of steel tubes, two specimens were tested for each L/D ratio. It was observed that the two tested specimens for each L/D ratio experienced similar axial load-axial deformation behaviour. Consequently, the axial load-axial deformation of one of the two tested specimens (the first specimen) for each L/D ratio is shown in Figure 5.6. It was also observed from axial load-axial deformation behaviour of the tested specimens with L/D ratio of 2 and 4 that the load capacity continued to increase after yielding of the steel. This increase of axial load after peak load occurred because the length of the specimen was short and hence the global buckling of the specimen did not occur.

Table 5.4: Test results of SCFT specimens under axial compression

Group SCFT26.9			Group SCFT33.7		
Specimen	Ultimate load[a]: kN	Corresponding deformation: mm	Specimen	Ultimate load[a]: kN	Corresponding deformation: mm
SCFT26.9-C2-1	117.6	3.67	SCFT33.7-C2-1	161.7	8.85
SCFT26.9-C2-2	116.4	3.41	SCFT33.7-C2-2	166.3	9.51
Ave SCFT26.9-C2	117	3.54	Ave SCFT33.7-C2	164	9.18
SCFT26.9-C4-1	104.6	3.36	SCFT33.7-C4-1	145.1	8.93
SCFT26.9-C4-2	103.8	3.12	SCFT33.7-C4-2	141.1	8.81
Ave SCFT26.9-C4	104.2	3.24	Ave SCFT33.7-C4	143.1	8.87
SCFT26.9-C6-1	104	3.27	SCFT33.7-C6-1	137.7	6.49
SCFT26.9-C6-2	102.7	2.98	SCFT33.7-C6-2	136.7	6.4
Ave SCFT26.9-C6	103.4	3.14	Ave SCFT33.7-C6	137.2	6.45
SCFT26.9-C8-1	97.9	3.16	SCFT33.7-C8-1	132	4.66
SCFT26.9-C8-2	97.8	2.96	SCFT26.9-C8-2	133.7	4.5
Ave SCFT26.9-C8	97.9	3.06	Ave SCFT33.7-C8	132.9	4.58
SCFT26.9-C10-1	92.7	2.31	SCFT33.7-C10-1	124.5	3.94
SCFT26.9-C10-2	93.3	2.35	SCFT33.7-C10-2	127.3	3.92
Ave SCFT26.9-C10	93	2.33	Ave SCFT33.7-C10	125.9	3.93
SCFT26.9-C12-1	90.7	2.14	SCFT33.7-C12-1	117.5	3.75
SCFT26.9-C12-2	91	1.93	SCFT33.7-C12-2	118	3.62
Ave SCFT26.9-C12	90.9	2.04	Ave SCFT33.7-C12	117.8	3.69
SCFT26.9-C14-1	83.7	1.94	SCFT33.7-C14-1	115.4	3.04
SCFT26.9-C14-2	87.9	2.24	SCFT33.7-C14-2	115.2	3.12
Ave SCFT26.9-C14	85.8	2.09	Ave SCFT33.7-C14	115.3	3.08

[a] The ultimate load of the SCFT specimens with L/D =2 and 4 represent the load at the first peak axial load.

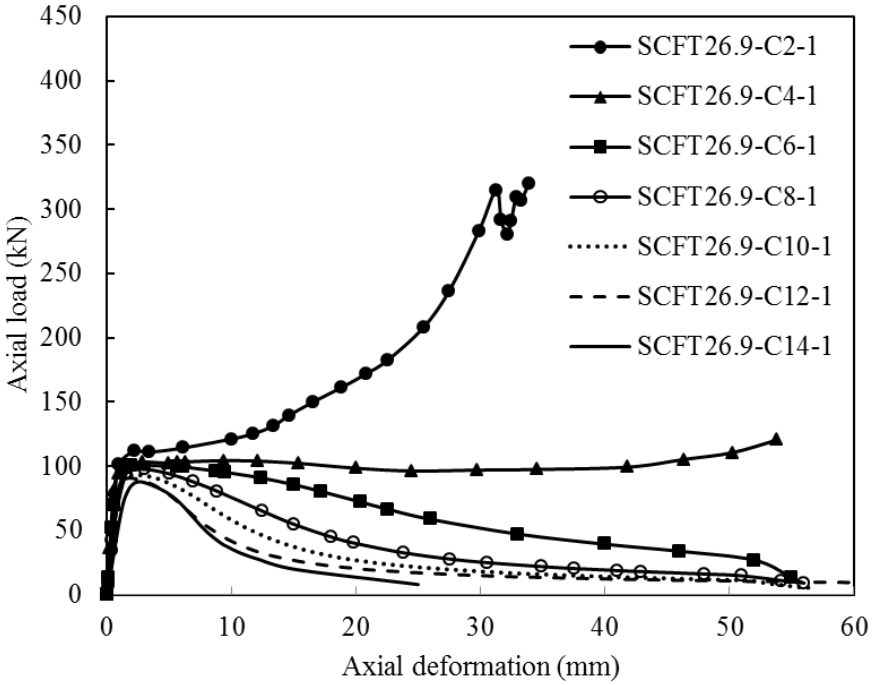

(a) Group SCFT26.9

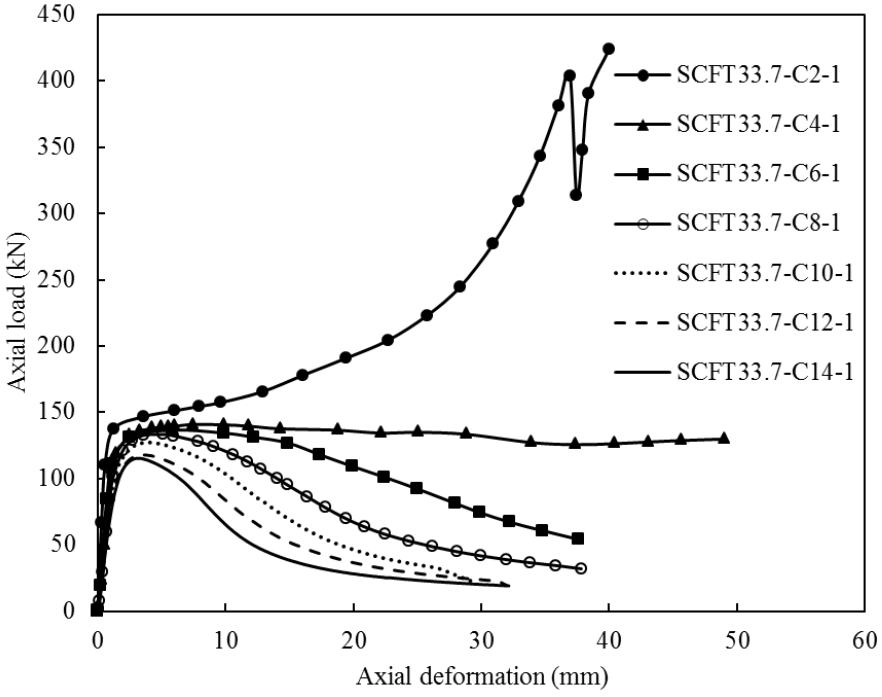

(a) Group SCFT33.7

Figure 5.6: Load-deformation behaviour of concrete-filled steel tube specimens under axial compression: (a) Group SCFT26.9 and (b) Group SCFT33.7

In the present study, however, the increasing axial load after the first peak of the specimens with L/D ratio of 2 and 4 was ignored and the first peak load was used for comparisons. For specimens with L/D ratio ≥ 6 there was no load increase after the first peak load. Increase in the L/D ratio of the SCFT specimens decreased the ultimate axial load and corresponding axial deformation. For specimens in Group SCFT26.9, increasing the L/D ratio from 2 to 14 decreased the ultimate axial load and the corresponding axial deformation by 26.7% and 41%, respectively. For specimens in Group SCFT33.7, increasing the L/D ratio from 2 to 14 decreased the ultimate axial load and the corresponding axial deformation by 29.7% and 66%, respectively. For specimens with L/D ratio of 2 and 4, the influence of the D/t ratio on specimens in Group SCFT33.7 was less than the influence of the D/t ratio on specimens in Group UT33.7. In the SCFT specimens with L/D ratio of 2 and 4, the elephant's foot buckling did not show any significant influence on the axial deformation and ductility because the infill concrete prevented the elephant's foot buckling.

The failure modes of the specimens in Group SCFT26.9 and Group SCFT33.7 were similar. The failure mode of the SCFT specimens was significantly influenced by the L/D ratio. For SCFT specimens with L/D ratio of 2 and 4, the first peak load occurred with small bulges along the steel tube specimen. The small bulges extended due to an expansion of the infill concrete after the yielding of the steel tube. Afterward, the specimens with L/D ratio of 2 showed a significant increase in the axial load capacity and the specimens with L/D ratio of 4 showed a slight increase in the axial load without any sudden loss of the axial load capacity and with significant ductility. The higher axial load capacity experienced by the SCFT specimens with L/D ratio of 2 and 4 was because the length of steel tubes was very short and the concrete inside the steel tubes

prevented the elephant's foot buckling. The axial strain of SCFT specimens with L/D ratio of 2 and 4 caused microcracking within the infill concrete of SCFT specimens and activated the confinement effect in the concrete. Finally, the specimens with L/D ratio of 2 and 4 failed due to crushing of the concrete core. The concrete crushing was caused by the increase in the outward local buckling of the steel tube. For specimens with L/D ratio $\geq$ 6, the failure occurred due to global buckling of the specimens. The global buckling occurred after the yielding of the steel tube. The specimens with L/D ratio ≥ 6 gradually lost the axial load capacity due to the formation of small bulges in the middle of the steel tube. The gradual loss of the axial load capacity experienced by the SCFT specimens with L/D ratio ≥ 6 was because the concrete inside the steel tubes prevented the inward buckling of the UT specimens. The small bulges prevented the occurrence of sudden failure owing to global buckling of the specimen. Figure 5.7 shows the typical failure modes of the SCFT specimens.

The SCFT specimens showed higher axial load capacities compared to the UT specimens owing to the influence of the infill concrete. The average axial load capacity of the specimens in Group SCFT26.9 was 30% higher than the average axial load capacity of the specimens in Group UT26.9. Also, the average axial load capacity of the specimens in the Group SCFT33.7 was 49% higher than the average axial load capacity of the specimen in Group UT33.7. In addition, unlike the UT specimens, the axial load of the SCFT specimens with L/D ratio of 2 and 4 showed higher axial load capacity after yielding of the steel tube. The higher axial load capacity of the SCFT specimens with L/D ratio of 2 and 4 was a result of the concrete inside the steel tubes preventing the elephant's foot buckling. This led to an increase in the axial deformation of SCFT specimens with L/D ratio of 2 and 4 owing to activation of the confinement effect in the

concrete. The concrete confinement significantly increased the axial load capacity of the SCFT specimens with L/D ratio of 2 and 4.

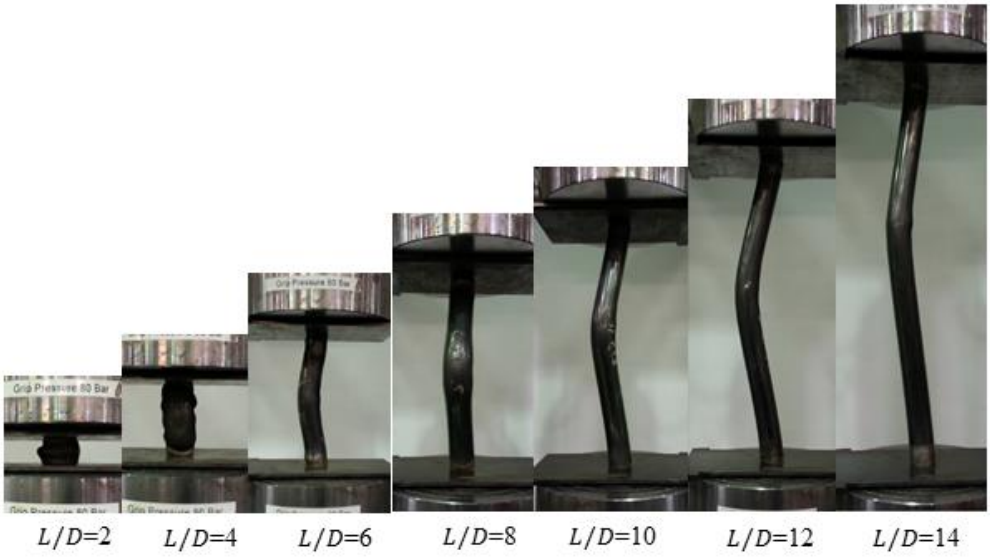

(a) Group SCFT26.9

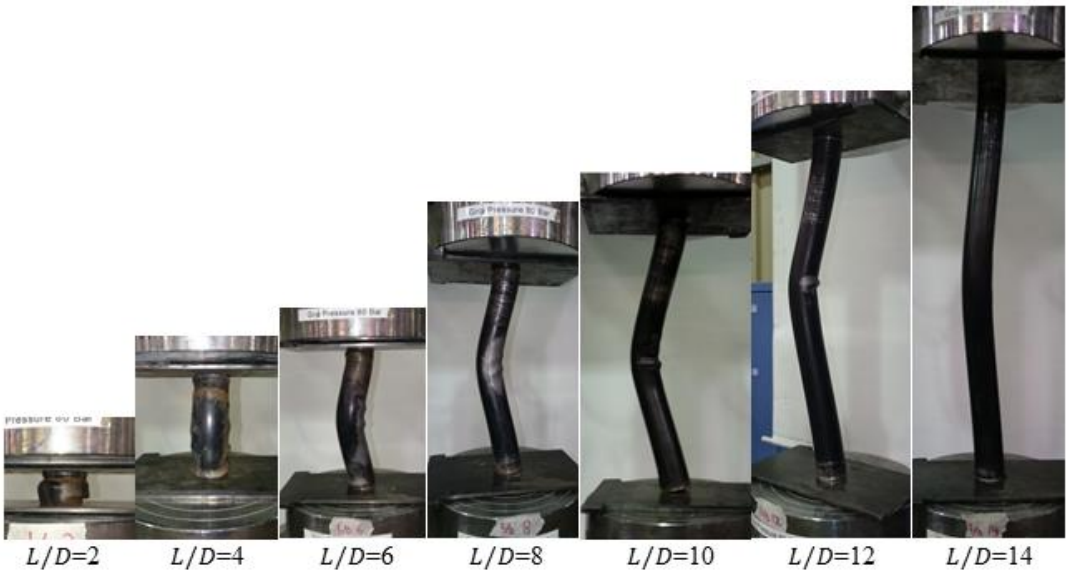

(b) Group SCFT33.7

Figure 5.7: Typical failure modes of concrete-filled steel tube specimens: (a) Group SCFT26.9, and (b) Group SCFT33.7

From the experimental results obtained for SCFT and UT specimens, the concrete enhancement factor (O'Shea and Bridge 1996) was calculated, given in Table 5.4. The experimental concrete enhancement factor was calculated by dividing the confined concrete strength with the unconfined compressive strength of the SCC. The confined concrete strength was calculated by subtracting the contribution of UT from the load carrying capacity of the SCFT and dividing the remainder by the area of concrete infill. The average experimental concrete enhancement factor of specimens in Group SCFT26.9 decreased from 1.577 to 1.015 when the L/D ratio increased from 2 to 10. The average experimental concrete enhancement factor of specimens in Group SCFT33.7 decreased from 1.583 to 1.067 when the L/D ratio increased from 2 to 10. However, for specimens with L/D ratio $\geq$ 12 the experimental concrete enhancement factor decreased to a value less than 1. The reduction of the experimental concrete enhancement factor to a value less than 1 was due to the effect of column slenderness (L/D). The SCFT specimens with L/D ratio $\geq$ 12 buckled before providing any confinement effect in the infill concrete. The global buckling of the SCFT specimens with L/D ratio $\geq$ 12 occurred at a strain in the infill concrete, which was lower than the strain necessary to induce microcracking in the infill concrete. Hence, the steel tube did not provide confinement effect in the concrete. Rather, the steel tube buckled before reaching the unconfined compressive strength of the concrete. Hence, the concrete enhancement factor of the SCFT specimens with L/D ratio $\geq$ 12 was less than 1.

5.6 Analytical Considerations

The American Standard ANSI/AISC 360-10 (AISC, 2010) was used to calculate the axial load capacity of the SCFT specimens under concentric axial load. The calculated results were compared with the experimental results. The ANSI/AISC 360-10 (AISC,

2010) covers three components in the composite columns: steel tube, concrete infill and reinforcing steel bars. The design standard was briefly reviewed for composite columns constructed with only two components: steel tube and concrete infill. The limits of the material parameters in ANSI/AISC 360-10 (AISC, 2010) for the design of CFT columns are: (a) the concrete compressive strength is ranged from 21 MPa to 70 MPa; (b) the yield tensile stress of the steel tube is less than 525 MPa; and (c) the amount of steel is more than 1% of the total cross section. The limits for the minimum diameter of steel tubes are not explicitly described in ANSI/AISC 360-10 (AISC, 2010). However, to classify the local buckling effect, ANSI/AISC 360-10 (AISC, 2010) specifies limits for compact, non-compact and slenderness composite members based on the maximum D/t ratio of the steel tube. In the present study, only the limits of compact sections were reviewed to evaluate the applicability of code recommendations for SCFT specimens.

In the American Standard ANSI/AISC 360-10 (AISC, 2010), design member capacity N_{cd} of a composite column is calculated by Equation 5.1.

$$N_{cd} = \emptyset_{co}\, N_c \tag{5.1}$$

where $\emptyset_{co}$ is the partial safety factor for a composite column capacity that is equal to 0.75, and the nominal member capacity N_c is calculated by Equations 5.2 and 5.3.

$$N_c = N_o \left[0.658^{\left(\frac{N_o}{N_e}\right)}\right], \quad \text{If } \frac{N_o}{N_e} \leq 2.25 \tag{5.2}$$

$$N_c = 0.877\, N_e, \qquad \text{If } \frac{N_o}{N_e} > 2.25 \tag{5.3}$$

$$N_o = f_y\, A_s + \alpha_1\, f_c'\, A_c \tag{5.4}$$

$$N_e = \frac{\pi^2\, EI_e}{(k_e\, L)^2} \tag{5.5}$$

where N_o is the squashing capacity of the cross-section, N_e is the Euler elastic buckling capacity, f_y is the steel yield stress, f_c' is the concrete compressive strength, A_s and A_c are the steel and concrete cross-section areas, respectively, α_1 is the reduction factor for the filling concrete which is equal to 0.95 for circular section, k_e is the member effective length factor and L is the column length. The effective flexural stiffness EI_e of a cross-section of a composite column is calculated by Equation 5.6.

$$EI_e = E_s\, I_s + \, C_3\, E_c\, I_c \tag{5.6}$$

$$C_3 = 0.6 + 2\left(\frac{A_s}{A_s + A_c}\right) \, \leq 0.9 \tag{5.7}$$

$$E_c = 4700\,\sqrt{f_c'} \qquad \text{(MPa)} \tag{5.8}$$

where E_s and E_c are the modulus of elasticity of the steel and concrete, respectively, I_s and I_c are the second moment of area of the steel and concrete, respectively, and C_3 is the coefficient of concrete effective stiffness.

In order to compare the experimental results with prediction results based on the recommendations in ANSI/AISC 360-10 (AISC, 2010), the partial safety factor ($\emptyset_{co}$) was taken as 1 in this study. The ratios of experimental results to the estimate from the design standard ($N_{exp}\,/N_c$) for SCFT specimens is reported in Table 5.5. The values of average nominal member capacity N_c predicted by the design standard were found to be conservative. The average $N_{exp}\,/N_c$ ratios for the specimens in Group SCFT26.9 and Group SCFT33.7 were 1.167 and 1.134, respectively, with standard deviations of 0.061 and 0.075, respectively. It is noted here that the above comment does not constitute a criticism to the recommendations in ANSI/AISC 360-10 (AISC, 2010), as the design recommendation in ANSI/AISC 360-10 (AISC, 2010) are not intended for SCFT specimens.

Table 5.5: Comparison of experimental results with design provision in code for SCFT specimens

Group	Specimen	N_{exp}: kN[a]	N_c: kN[b]	N_{exp}/N_c
SCFT26.9	SCFT26.9-C2	117	90.2	1.297
	SCFT26.9-C4	104.2	89.2	1.168
	SCFT26.9-C6	103.4	87.7	1.179
	SCFT26.9-C8	97.9	85.6	1.144
	SCFT26.9-C10	93	83	1.121
	SCFT26.9-C12	90.9	79.8	1.139
	SCFT26.9-C14	85.8	76.3	1.124
SCFT33.7	SCFT33.7-C2	164	126.6	1.295
	SCFT33.7-C4	143.1	125.1	1.144
	SCFT33.7-C6	137.2	122.7	1.119
	SCFT33.7-C8	132.9	119.3	1.114
	SCFT33.7-C10	125.9	115.1	1.094
	SCFT33.7-C12	117.8	110.1	1.070
	SCFT33.7-C14	115.3	104.6	1.103

[a] N_{exp} is the average ultimate load capacity of two SCFT specimens tested under axial compression.

[b] N_c is the nominal member capacity of SCFT specimens calculated from the design standard.

5.7 Conclusions

Based on the experimental investigation presented in the present study, the following conclusions can be drawn:

(a) The axial load capacity of SCFT specimens was found to be higher than the axial load capacity of corresponding UT specimens owing to the effect of the concrete infill. The average axial load capacity of the specimens in Groups SCFT26.9 and

SCFT33.7 were 30% and 49% higher than the average axial load capacity of the specimens in Groups UT26.9 and UT33.7, respectively. The greater effect of the infill concrete was observed for specimens tested with L/D ratio of 2 and 4.

(b) For L/D ratios of 2 and 4, the compressive failure in the UT specimens occurred as a result of local elephant's foot buckling. However, the compressive failure in the SCFT specimens was different to the compressive failure in the UT specimens. For SCFT specimens with L/D ratio of 2 and 4, the first peak axial load occurred with small bulges along the steel tube specimen. Then, the axial load continued to increase due to extension of small bulges during the compression test. The small bulges were extended as an expansion of the concrete core after the steel yielding. Finally, the specimens failed by crushing the concrete core owing to an increase in outward local buckling of the steel tube.

(c) For the L/D ratio ≥ 6, the compressive failure modes of UT specimens changed from local elephant's foot buckling to global buckling. Global buckling failure was observed to occur as a bend in a sharp angle near the mid-height of the tube (inward buckling). For SCFT specimens, the failure also occurred due to global buckling of the specimens. However, the SCFT specimens with L/D ratio ≥ 6 gradually lost the axial load capacity due to the formation of small bulges in the middle of the steel tube. The small bulges prevented the occurrence of sudden failure as a result of global buckling of the specimen.

(d) The design recommendations in the American standard ANSI/AISC 360-10 (AISC, 2010) for CFT columns conservatively predicted the experimental axial load capacity of the SCFT.

Acknowledgement

The authors thank the University of Wollongong, Australia, for the use of their research facilities. The first author thanks the Iraqi Government for the support of his PhD scholarship.

References

AISC. (2010). "Specification for structural steel buildings." *ANSI/AISC 360-10*, Chicago.

AISI. (1996). "Specification for the design of cold-formed steel structural members." Washington, DC, USA, American Iron and Steel Institute (AISI).

AS (Australian Standards). (2014). "Methods of testing concrete – Method 9: determination of the compressive strength of concrete specimens." *AS 1012.9-2014*, Sydney, NSW, Australia.

Aslani, F. (2015). "Nanoparticles in self-compacting concrete – a review." *Magazine of Concrete Research*, 67(20), 1084–1100.

ASTM. (2014a). "Standard test method and definition for mechanical testing of steel products." *ASTM A370-14*, West Conshohocken, PA.

ASTM. (2014b). "Standard test method for static segregation of self-consolidating concrete using column technique." *ASTM C1610/C1610M-14*, West Conshohocken, PA.

ASTM. (2014c). "Standard test method for slump flow of self-consolidating concrete." *ASTM C1611/C1611M-14*, West Conshohocken, PA.

ASTM. (2014d). "Standard test method for passing ability of self-consolidating concrete by J-ring." *ASTM C1621/C1621M-14*, West Conshohocken, PA.

Badry, F., Kulasegaram, S., and Karihaloo, B. L. (2016). "Effect of cone lift rate on the flow time of self-compacting concrete." *Magazine of Concrete Research*, 68(2), 80–86.

BSI (2005). "Design of composite steel and concrete structures. General rules and rules for buildings." Eurocode 4, EN 1994-1-1:2004, BSI, London, UK.

CSA (Canadian Standards Association). (2009). "Limit states design of steel structures." *CAN/CSA-S16-09*, Mississauga, Canada.

Chamani, M. R., Hosseinpour, M., Mostofinejad, D., and Esmaeilkhanian, B. (2014). "Evaluation of SCC yield stress from L-box test using the dam break model." *Magazine of Concrete Research*, 66(4), 175–185.

De Oliveira, W. L. A., De Nardin, S., El Debs, A. L. H. C., and El Debs, M. K. (2009). "Influence of concrete strength and length/diameter on the axial capacity of CFT columns." *Journal of Constructional Steel Research*, 65(12), 2103–2110.

EFNARC (European Federation of Specialist Construction Chemicals and Concrete Systems). (2002). "Specification and guidelines for self-compacting concrete." Norflolk, U.K., 1-32.

EFNARC (European Federation of Specialist Construction Chemicals and Concrete Systems). (2005). "The European guidelines for self-compacting concrete specification, production and use." Farnham, U.K., 1-63.

Elchalakani, M., Zhao, X. L., and Grzebieta, R. H. (2001). "Concrete-filled circular steel tubes subjected to pure bending." *Journal of Constructional Steel Research*, 57(11), 1141–1168.

Ellobody, E., Young, B., and Lam, D. (2006). "Behaviour of normal and high strength concrete-filled compact steel tube circular stub columns." *Journal of Constructional Steel Research*, 62(7), 706–715.

Fam, A., Qie, F. S., and Rizkalla, S. (2004). "Concrete-filled steel tubes subjected to axial compression and lateral cyclic loads." *Journal of Structural Engineering ASCE*, 130(4), 631-640.

Giakoumelis, G., and Lam, D. (2004). "Axial capacity of circular concrete-filled tube columns." *Journal of Constructional Steel Research*, 60(7), 1049-1068.

Gupta, P. K., Sarda, S. M., and Kumar, M. S. (2007). "Experimental and computational study of concrete filled steel tubular columns under axial loads." *Journal of Constructional Steel Research*, 63(2): 182-193.

Hadi, M. N. S., Alhussainy, F., and Sheikh, N. M. (2017). "Behavior of self-compacting concrete columns reinforced longitudinal with steel tubes." *Journal of Structural Engineering ASCE*, 143(6):1-14.

Han, L. H., and An, Y. F. (2014). "Performance of concrete-encased CFST stub columns under axial compression." *Journal of Constructional Steel Research*, 93: 62–76.

Han, L. H., He, S. H., and Liao, F. Y. (2011). "Performance and calculations of concrete filled steel tubes (CFST) under axial tension." *Journal of Constructional Steel Research*, 67(11): 1699-1709.

Han, L. H., Hou, C., and Wang, Q. L. (2012). "Square concrete filled steel tubular (CFST) members under loading and chloride corrosion: Experiments." *Journal of Constructional Steel Research*, 71, 11-25.

Huo, J., He, Y., and Chen, B. (2014). "Experimental study on impact behavior of concrete-filled steel tubes at elevated temperatures up to 800 ^{o}C." *Materials and Structures*, 47(1-2), 263-283.

Knowles, R. B., and Park, R. (1969). "Strength of concrete-filled steel tubular columns." *Journal of the Structural Division ASCE*, 95(12), 2565-2587.

Lai, M. H., and Ho, J. C. M. (2016) "Confining and hoop stresses in ring-confined thin-walled concrete-filled steel tube columns." *Magazine of Concrete Research*, 68(18), 916-935.

Lai, M. H., and Ho, J. C. M. (2015). "Optimal design of external rings for confined CFST columns." *Magazine of Concrete Research*, 67(19), 1017-1032.

Muciaccia, G., Giussani, F., Rosati, G., and Mola, F. (2011). "Response of self-compacting concrete filled tubes under eccentric compression." *Journal of Constructional Steel Research*, 67(5), 904-916.

O'Shea, M. D., and Bridge, R. Q. (1996). "Circular thin-walled tubes with high strength concrete infill." In *Composite Construction in Steel and Concrete III*, American Society of Civil Engineers: New York, NY, USA, 780-793.

O'Shea, M. D., and Bridge R. Q. (1997). "Local buckling of thin-walled circular steel sections with or without internal restraint." *Journal of Constructional Steel Research* 41(2-3): 137-157

Schneider, S. P. (1998). "Axially loaded concrete-filled steel tubes." *Journal of Structural Engineering ASCE*, 124(10), 1125-1138.

Shanmugam, N. E., and Lakshmi, B. (2001). "State of the art report on steel-concrete composite columns." *Journal of Constructional Steel Research*, 57(10), 1041-1080.

Zeghiche, J., and Chaoui, K. (2005). "An experimental behaviour of concrete-filled steel tubular columns." *Journal of Constructional Steel Research*, 61(1), 53-66.

CHAPTER 6: BEHAVIOUR OF SELF-COMPACTING CONCRETE COLUMNS REINFORCED LONGITUDINALLY WITH STEEL TUBES

Summary

This chapter experimentally investigates the behaviour of longitudinal steel tube reinforced SCC columns under different loading conditions. Two different sizes of small-diameter steel tubes are used in the study. The cross-sectional areas of the steel tubes are similar to the cross-sectional areas of reference steel bars. The main parameters investigated in the experimental programme included longitudinal reinforcement (deformed steel bars and steel tubes), size of the steel tube and the pitches of the steel helix. This study also revealed the challenges associated with using steel tubes as longitudinal reinforcement in SCC column specimens due to slip of steel tubes in concrete and explores remedial measures for the slip of steel tubes.

The next chapter (Chapter 7) presents the analytical model for the axial load-axial deformation behaviour of SCC columns reinforced with steel tubes. The developed analytical model has been validated with the experimental results of this chapter.

Citation

This chapter has been published in the Journal of Structural Engineering with the following citation:

Hadi MNS, Alhussainy F, Sheikh MN. (2017). "Behavior of self-compacting concrete columns reinforced longitudinally with steel tubes." *Journal of Structural Engineering ASCE*, 143(6), 1-14.

Abstract

This study investigates the behaviour of self-compacting concrete (SCC) specimens reinforced with small-diameter steel tubes in lieu of reinforcing bars. Twenty specimens were cast and tested. Four specimens were reinforced with normal steel bars (reference specimens) and the remaining 16 with steel tubes. All specimens contained steel helices with a pitch of either 50 mm or 75 mm. Deformed steel bars of 16-mm diameter were used in the four reference specimens as longitudinal reinforcement. Steel tubes of 33.7-mm outside diameter with 2-mm wall thickness (ST33.7) and steel tubes of 26.9-mm outside diameter with 2.6-mm wall thickness (ST26.9) were used as longitudinal reinforcement in the remaining 16 specimens. The specimens were divided into five groups with four specimens in each group. From each group, one specimen was tested under concentric load, one under 25-mm eccentric load, one under 50-mm eccentric load and one under flexural load. Although the nominal yield tensile strength of steel bar was 150 and 250 MPa greater than the nominal yield tensile strength of steel tubes ST33.7 and ST26.9, respectively, the results revealed that steel tube reinforced self-compacting concrete (STR SCC) specimens have ultimate load similar to reference specimens. Ductility of concentrically loaded STR SCC specimens was higher than that of the reference specimen. This study also reveals the challenges associated with using steel tubes as longitudinal reinforcement in STR SCC column specimens due to slip of steel tubes in concrete and explores remedial measures for the slip of steel tubes.

Keywords: Composite columns; self-compacting concrete; steel bars; steel tubes; stress-strain behaviour; debonding; concrete and masonry structures.

6.1 Introduction

Performance of concrete column has been widely improved by using composite material systems such as encased sections and concrete-filled tubes (Shanmugam and Lakshmi 2001). Different combinations of encased section and steel section were widely studied. The characteristics of the composite columns are governed by the geometric configuration and strength of materials. Steel sections and concrete have been used to construct composite columns with different cross sections. The synergies between steel and concrete in composite columns provide better performance in terms of high strength, stiffness, ductility, as well as fire and seismic resistance (Sakino et al. 2004; Giakoumelis and Lam 2004; Choi and Xiao 2010). Concrete-filled steel tube (CFT) columns consist of a steel tube and concrete infill. In some cases, internal steel reinforcement is used to provide proper connections between the concrete members (Moon et al. 2013). Another advantage of using internal steel reinforcement is that it enhances the strength of the concrete columns because the concrete core of these columns is confined by both steel-tube and internal-confinement reinforcement (Xiamuxi and Hasegawa 2012). Steel tube confines the concrete in a triaxial state. Therefore, a few stirrups can be used in the reinforced concrete column confined with thin-walled steel tube (Wang et al. 2015).

Composite columns offer considerable improvements over conventional columns reinforced with steel bars and are used in many structural applications. In traditional reinforced concrete columns, solid steel bars are used as longitudinal reinforcement. In this study, small-diameter steel tubes were used as longitudinal reinforcement for concrete columns. Steel tubes that have the same cross-sectional area as solid bars have

a higher second moment of area and radius of gyration than solid bars. Filling these steel tubes with concrete can further increase the yield and ultimate strength as well as the ductility of the concrete columns under axial compression load. This is because the concrete infill will contribute in delaying the local buckling and converts the failure mode of the steel tube wall from inward to outward (AISC 2010). For eccentric and flexural loading, using concrete-filled steel tubes in lieu of solid bars may increase the stiffness of the cracked concrete section of the specimens because the second moment of area of the cracked cross section for the steel tube reinforced specimen is slightly higher than that of the steel-bar-reinforced specimen. This is mostly due to the presence of the confined concrete inside the steel tubes. In addition, a circular tube section provides better confinement of concrete than other tube sections because the tube wall resists the concrete pressure by membrane-type hoop stresses instead of the plate bending (Sehneider 1998). Because the diameter of these steel tubes is quite small to be filled with the normal concrete, high-flowability concrete is needed to completely fill the tube without segregation, self-compacting concrete (SCC) is considered a suitable option.

SCC is an innovative material that can be used in complex forms and members that contain congestion of reinforcement, without needing vibration because it is able to compact under its own weight (Goodier 2003; De Schutter 2005; EFNARC 2005). Han and Yao (2004) showed that SCC is very suitable for CFT columns because the rheological properties of SCC. Roeder et al. (2010) indicated that the empty tube could be filled with concrete rapidly by using SCC, without requiring any vibration. Muciaccia et al. (2011) explained that the use of SCC in concrete-filled steel-tube columns provides ease in constructing difficult shapes and reduces cost because no

vibration is required. It was also found that the use of SCC in lieu of normal concrete did not affect the design requirements of the CFT columns. Use of SCC can help in investigating new types of composite concrete columns in order to gain better stiffness, ductility and strength of concrete columns.

The above review of literature shows that no study has yet been conducted on the behaviour of concrete columns reinforced with longitudinal small-diameter steel tubes. It is expected that the use steel tubes filled with SCC as reinforcement will decrease the overall buckling of longitudinal reinforcement and consequently increase the ductility of the column. Also, steel tubes will effectively confine the infill concrete, resulting in an increase of the axial compressive strength. Hence, significant investigative research is needed to explore the behaviour of columns reinforced with small-diameter steel tubes filled with SCC (STR SCC column). This study provides a basis for using steel tubes instead of the conventional steel reinforcing bars as a new method for reinforcing concrete columns. It also reveals the problems associated with the use of plain steel tubes as longitudinal reinforcement in STR SCC column specimens because of the slip of steel tubes in concrete. Remedial measures for the problem associated with the slip of steel tubes have also been investigated.

6.2 Experimental Program

A total of 20 circular SCC specimens reinforced longitudinally with steel bars and tubes were cast and tested at the High Bay Laboratory of the University of Wollongong, Australia. All specimens had the same dimensions: 240 mm in diameter, 800 mm in height, and a height-to-diameter (H/D) ratio of 3.3. The dimensions of the tested specimens were chosen to be suitable to the conditions and capacity of the available

testing facilities in the laboratory. A vertical-support member with a height-to-diameter ratio greater than or equal to 2.5 is considered as a column in Canadian Standards CAN/CSA S6-06 (CSA 2006). Moreover, ACI 318-11 (ACI 2011) defined a column as a member mainly used to support the axial compressive load with a height-to-least-lateral-dimension ratio greater than 3.

The SCC mix with a nominal compressive strength of 50 MPa was used in casting the specimens. The maximum aggregate size used in the SCC mix was 10 mm. The mix proportion of the SCC used in this study is shown in Table 6.1. All longitudinal steel tubes (33.7 and 26.9-mm outside diameters) were also filled with the SCC during the casting of the specimens. The specimens were divided into five groups with four specimens in each group. From each group, one specimen was tested under concentric load, two specimens were tested under 25 and 50-mm eccentric loads, and the last specimen was tested as a beam under flexural load (four-point load bending). The first group contained specimens reinforced with steel bars and considered as reference specimens, and the remaining specimens were reinforced with steel tubes.

Table 6.1: Mix proportion of the SCC used in this study

Material	Quantity
Cement	280 kg/m^3
Fly ash	120 kg/m^3
Slag	50 kg/m^3
Fine aggregate	950 kg/m^3
Coarse aggregate	780 kg/m^3
Water	182 kg/m^3
High-range water reducer (HRWR)	3.375 l/m^3
Water-to-Powder ratio	0.4

All specimens were reinforced transversally with plain R10 (10-mm-diameter plain steel bars) steel helices with a nominal tensile strength of 250 MPa. The specimens in the first group were reinforced longitudinally with six deformed steel bars of 16-mm diameter and nominal tensile strength of 500 MPa. The specimens in the second and third groups were reinforced longitudinally with six steel tubes of 33.7-mm outside diameter, 2 mm in thickness, and nominal tensile strength of 350 MPa (ST33.7). The remaining specimens in the fourth and fifth groups were reinforced longitudinally with six steel tubes of 26.9-mm outside diameter, 2.6 mm in thickness and nominal tensile strength of 250 MPa (ST26.9). Steel helices with 50-mm pitch were used in reinforcing the specimens transversally in the first, second, and the fourth groups. The pitch of the steel helix satisfies ACI 318-14 (ACI 2014) requirements. The specimens in the third and fifth groups were reinforced transversally with 75-mm-pitch steel helices. The specifications and reinforcement details of tested specimens are shown in Table 6.2 and Figure 6.1.

Table 6.2: Details of tested specimens

Group name	Specimen labels	Longitudinal reinforcement				Transverse reinforcement		Loading modes
		Number of bars or tubes	Outside diameter of bars or tubes (mm)	Thickness of tubes, (mm)	Reinforcement ratio, ρ_s (%)	Pitch (mm)	Reinforcement ratio, ρ_s (%)	
N16-H50	N16-H50-C	6	16 (N16)	—	2.67	50	3.3	Concentric
	N16-H50-E25	6	16 (N16)	—	2.67	50	3.3	e = 25 mm
	N16-H50-E50	6	16 (N16)	—	2.67	50	3.3	e = 50 mm
	N16-H50-F	6	16 (N16)	—	2.67	50	3.3	Flexural
ST33.7-H50	ST33.7-H50-C	6	33.7	2	2.64	50	3.3	Concentric
	ST33.7-H50-E25	6	33.7	2	2.64	50	3.3	e = 25 mm
	ST33.7-H50-E50	6	33.7	2	2.64	50	3.3	e = 50 mm
	ST33.7-H50-F	6	33.7	2	2.64	50	3.3	Flexural
ST33.7-H75	ST33.7-H75-C	6	33.7	2	2.64	75	2.2	Concentric
	ST33.7-H75-E25	6	33.7	2	2.64	75	2.2	e = 25 mm
	ST33.7-H75-E50	6	33.7	2	2.64	75	2.2	e = 50 mm
	ST33.7-H75-F	6	33.7	2	2.64	75	2.2	Flexural
ST26.9-H50	ST26.9-H50-C	6	26.9	2.6	2.63	50	3.3	Concentric
	ST26.9-H50-E25	6	26.9	2.6	2.63	50	3.3	e = 25 mm
	ST26.9-H50-E50	6	26.9	2.6	2.63	50	3.3	e = 50 mm
	ST26.9-H50-F	6	26.9	2.6	2.63	50	3.3	Flexural
ST26.9-H75	ST26.9-H75-C	6	26.9	2.6	2.63	75	2.2	Concentric
	ST26.9-H75-E25	6	26.9	2.6	2.63	75	2.2	e = 25 mm
	ST26.9-H75-E50	6	26.9	2.6	2.63	75	2.2	e = 50 mm
	ST26.9-H75-F	6	26.9	2.6	2.63	75	2.2	Flexural

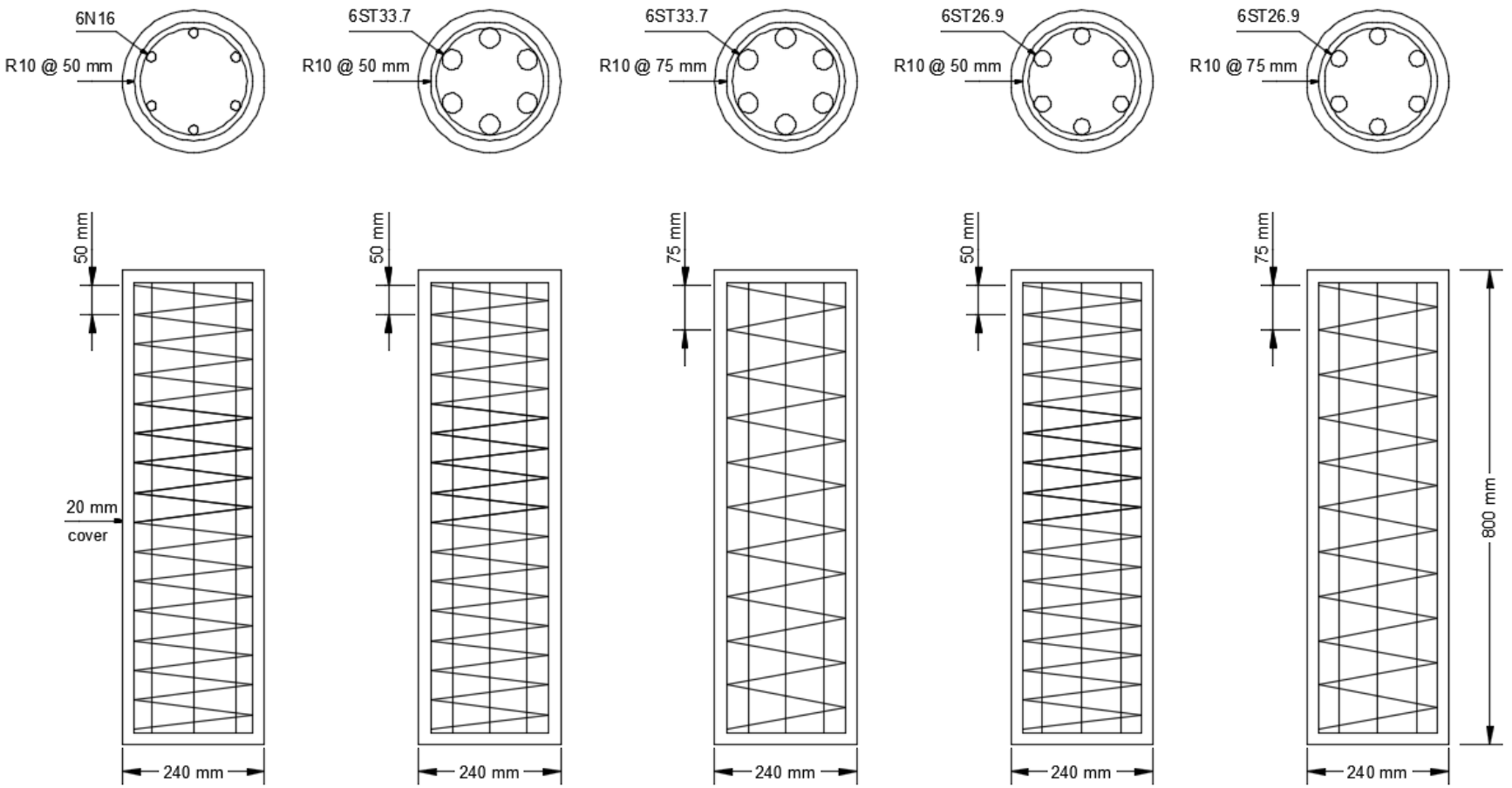

Group N16-H50 Group ST33.7-H50 Group ST33.7-H75 Group ST26.9-H50 Group ST26.9-H75

Figure 6.1: Reinforcement details of test specimens

Table 6.2 shows the group names and specimen labels. The groups are labelled in two parts, and the specimens are labelled in three parts. In the first part of the group names and specimen labels, the letters (N and ST) refer to the type of the longitudinal reinforcement in the specimen. The letter N refers to deformed steel bars, and the letters ST refer to the steel tubes. The number 16 refers to deformed steel bars of 16-mm diameter with a nominal tensile strength of 500 MPa. The number 33.7 refers to the steel tubes with 33.7-mm outside diameter and 2-mm wall thickness and with a nominal tensile strength of 350 MPa. The number 26.9 refers to the steel tubes with 26.9-mm outside diameter and 2.6-mm wall thickness and with a nominal tensile strength of 250 MPa. In the second part of the group names and specimen labels, the set of a letter and numbers refer to the helix pitch. H50 represents a 50-mm pitch and H75 represents a 75-mm pitch of the transverse reinforcement. In the third part of the specimen label refers to the type of the loading condition. The C refers to the concentric loading, E25 refers to the 25-mm eccentric loading, E50 refers to the 50-mm eccentric loading and F refers to the flexural loading (four-point load bending). For example, ST33.7-H50-E50 refers to the specimen that reinforced longitudinally with six ST33.7 steel tubes and transversally with a pitch of 50-mm helix and tested under 50-mm eccentric load.

6.3 Material Properties

Self-compacting concrete was prepared according to EFNARC (2002) method. A number of concrete mixes were investigated to achieve self-compacting concrete. The properties of fresh concrete were tested according to ASTM C1610-14 (ASTM 2014d); ASTM C1611-14 (ASTM 2014c) and ASTM C1621-14 (ASTM 2014b). For the water-to-powder ratio of 0.4, column segregation test according to ASTM C1610-14 (ASTM 2014d), slump flow test according to ASTM C1611-14 (ASTM 2014c) and J-ring test

according to ASTM C1621-14 (ASTM 2014b) were carried out. The test results were found to be satisfactory. All the specimens were cast using ready-mixed self-compacting concrete supplied by a local company. The average compressive strength of the SCC was 57 MPa at 28 days. Two different steel bars were used in this study, deformed steel N16 bars (16-mm-diameter deformed bars with 500-MPa nominal tensile strength) for longitudinal reinforcement in the first group (reference specimens) and plain mild steel R10 bars (10-mm-diameter plain bars with 250-MPa nominal tensile strength) for transverse reinforcement in all specimens. Three samples of N16 deformed bars and R10 plain bars were tested in accordance with Australian Standard AS 1391-2007 (AS 2007). Results of testing revealed that the N16 steel bar experienced strain hardening behaviour with an obvious yield stress; however, the yield stress of the R10 plain bar was not easily identified and was determined using the 0.2% proof stress. The average tensile strengths and elastic modulus of N16 bars were 556 MPa and 200 GPa, respectively. The average tensile strength and elastic modulus of R10 bars were 400 MPa and 195 GPa, respectively.

Two different steel tubes were used to reinforce remaining specimens in the longitudinal direction: steel tubes ST33.7 and ST26.9. Three samples of each ST33.7 and ST26.9 tubes were tested in accordance with ASTM A370-14 (ASTM 2014a). Steel plugs were designed based on the inner diameters of the steel tubes to suit the 29.7 and 21.7-mm steel tubes in tensile testing. Yield stresses of both steel tubes were not easily identified with a strain plateau and were instead determined using the 0.2% proof stress. The average tensile strength and elastic modulus of ST33.7 were 450 MPa and 196 GPa, respectively. The average tensile strength and elastic modulus of ST26.9 were 355 MPa and 192 GPa, respectively.

The bond stress between different longitudinal reinforcement and SCC was determined using pullout tests according to RILEM (1983). For each reinforcing type, three specimens were tested on the 28th day. The average bond stress of N16 steel bars was 19 MPa at failure. The specimens with N16 steel bar failed because of pullout. The average bond stress of ST33.7 and ST26.9 steel tubes filled with the SCC was 1.5 and 0.75 MPa, respectively, at failure. The specimens with SCC-filled ST33.7 and ST26.9 failed because of slip.

6.4 Specimen Preparation and Testing

6.4.1 Formwork

PVC pipes with a 240 mm inner diameter were used as formwork moulds for the concrete column specimens. The PVC pipe was cut for a length of 800 mm. Twenty pieces of PVC pipe moulds were prepared. These pipe moulds were then fixed to a non-absorbing plywood base plate. The formwork was constructed to keep both the top and bottom of the moulds in a fixed plumb position. The formwork was secured to a rigid pallet onto which the base plate was mounted as shown in Figure 6.2.

Figure 6.2: Construction of formwork

6.4.2 Longitudinal and Transverse Reinforcement

The internal longitudinal reinforcement bars and steel tubes were prepared and cut at 760 mm in order to provide 20 mm clear cover at the top and bottom of the reinforcement cage. In addition, the transverse steel helices were formed with a 200-mm outer diameter and pitches of 50 and 75 mm. In constructing the reinforcing cages, the longitudinal reinforcement was tied with equal spacing to the inside of the helices following the test matrix in Table 6.2 and Figure 6.1.

To construct the reinforcement cages, two 12-mm-thick circular plastic templates were made. The diameters of the holes in the templates were designed to suit various tube and bar sizes as well as to maintain the inner diameter of the helix as 180 mm. Circular Template 1 was designed to hold both ST26.9 and ST33.7 steel tubes, whereas Circular Template 2 was designed to hold the N16 bars. Figure 6.3 shows the circular template schematics. Each circular template contained six half-circle holes at the circumference to hold the longitudinal reinforcement. These holes were created at equal distances on the circumference of the circular template. The two identical circular templates were set up parallel to each other at the top and bottom by using a threaded steel rod. Hex steel nuts, washers, and lock washers were used to fix these two circular templates at the required distance to the threaded steel rod.

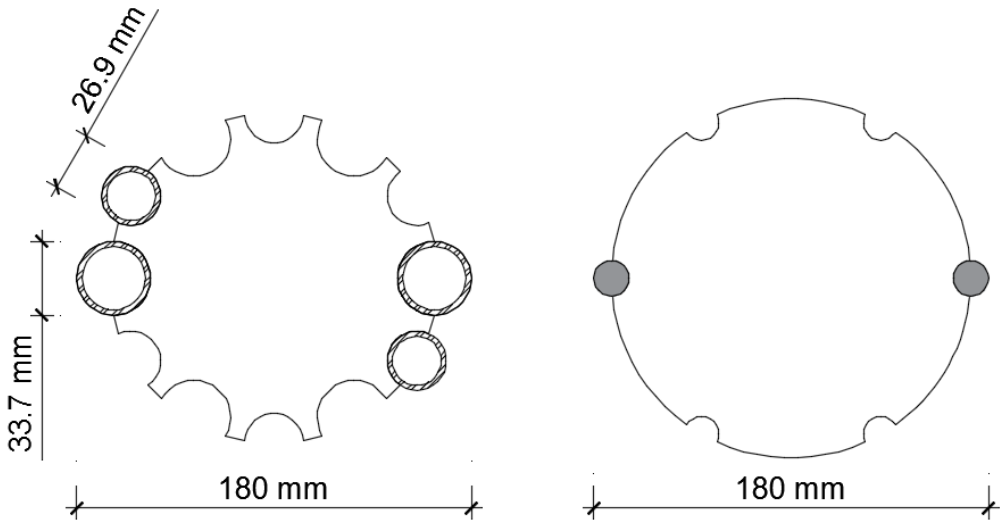

Circular template 1 Circular template 2

Figure 6.3: Circular templates

Figures 6.4(a & b) show the setup of circular templates for different longitudinal reinforcement. In addition, two aluminium forms were designed as a spacer for holding the helices at the desired pitch, as shown in Figure 6.4(c). The aluminium forms have grooves to adjust the spacing of helices at 50 and 75 mm. All longitudinal steel bars or steel tubes were tied together with the helix by using tie wire. Figure 6.5 shows 20 fabricated reinforcing cages.

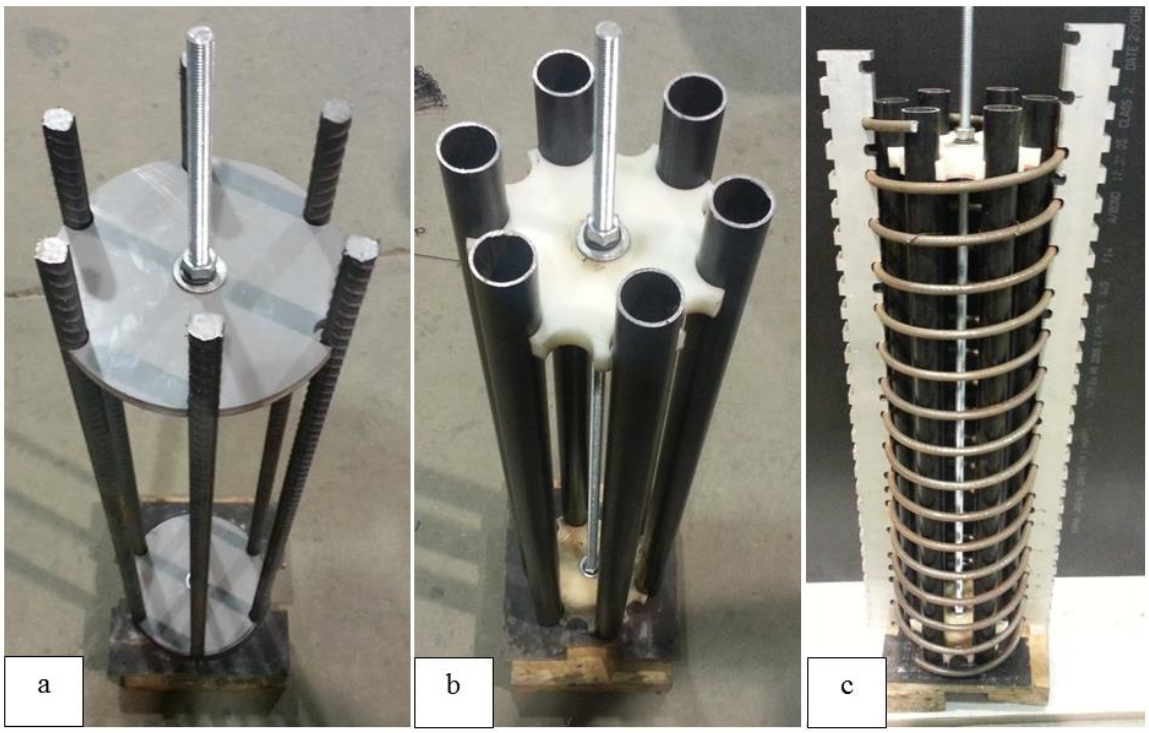

Figure 6.4: Fabrication of reinforcement cages: (a) longitudinal steel bars; (b) longitudinal steel tubes; (c) transverse reinforcement

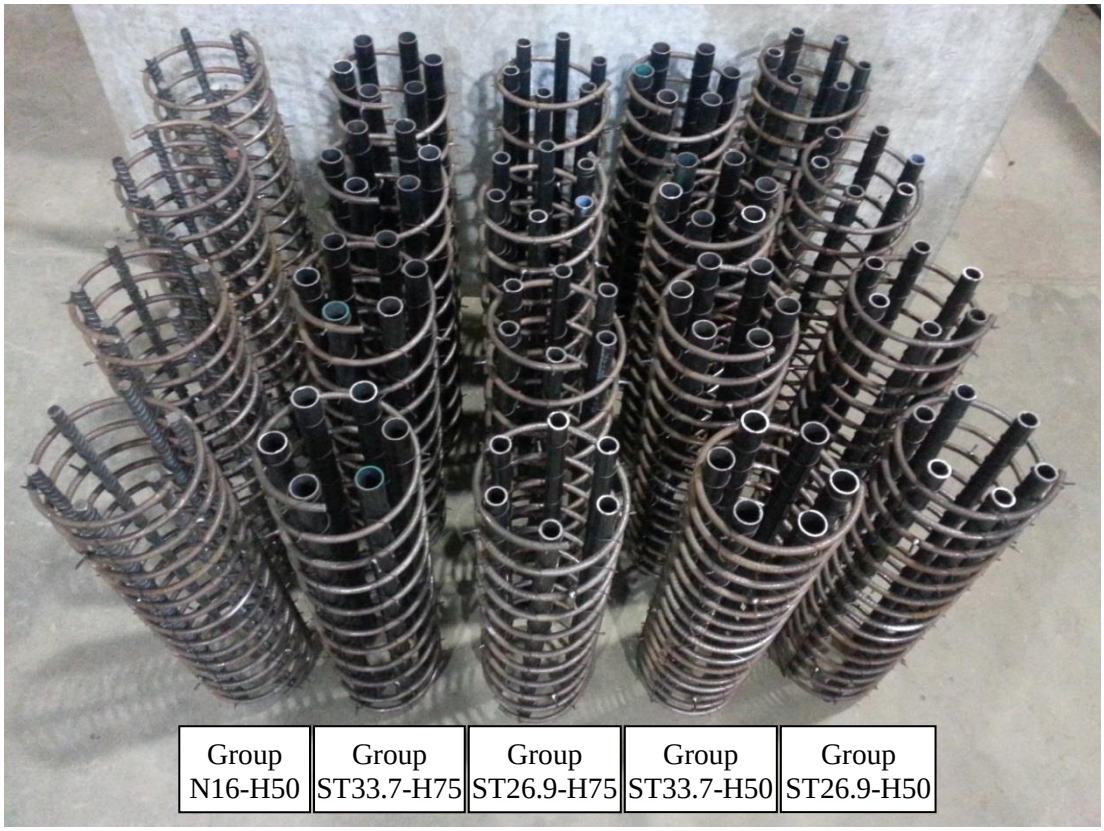

Figure 6.5: Fabricated reinforcing cages

6.4.3 Testing of the Specimens

The Denison 5,000-kN compression testing machine (London, U.K.) was used for the testing of all specimens. Of the 20 specimens, 15 were tested as columns in compression tests. The top and bottom of the column specimens were wrapped by two layers of carbon fibre-reinforced polymer (CFRP) sheets with 100-mm overlap to avoid premature failure of the concrete during axial compression tests. Also, the top and bottom end surfaces of the columns were capped with high-strength plaster to ensure a uniform distribution of the applied loads. The plaster was poured into the loading head moulds at the bottom end first and left to cure for 30 min before the column specimen was turned over, and similarly the plaster was poured into the top loading head mould in order to cap the top end.

For applying the eccentric loading on the column, steel loading heads manufactured at the University of Wollongong were used. The loading heads were used to transfer the load generated by the machine into the column specimen causing lateral deflection (δ). Steel loading heads consisted of two parts: a circular steel plate adapter and a steel plate with a ball joint, as shown in Figure 6.6(a). A steel ball joint was installed on a steel plate to induce eccentricities (e) of 25 and 50 mm to the top and bottom loading heads. Concentric loading, however, was applied directly through the circular steel plates attached at both ends of the column specimen without any steel ball joints. To measure the axial deformation of the column specimens, two linear variable differential transformers (LVDT) were used. The LVDTs were connected directly to the machine loading heads at opposite corners. A laser optical displacement sensor (LODS) was attached at the midheight of the test specimen to measure lateral displacement under eccentric loading. In addition, before casting, strain gauges were attached on the two opposite longitudinal reinforcements (bars and tubes) to measure axial strain. The LVDTs, LODS, and strain gauges were connected to the data logger, which recorded measurements and saved them on the control computer. Figure 6.6(b) shows the typical test setup of column specimens.

(a) Loading heads

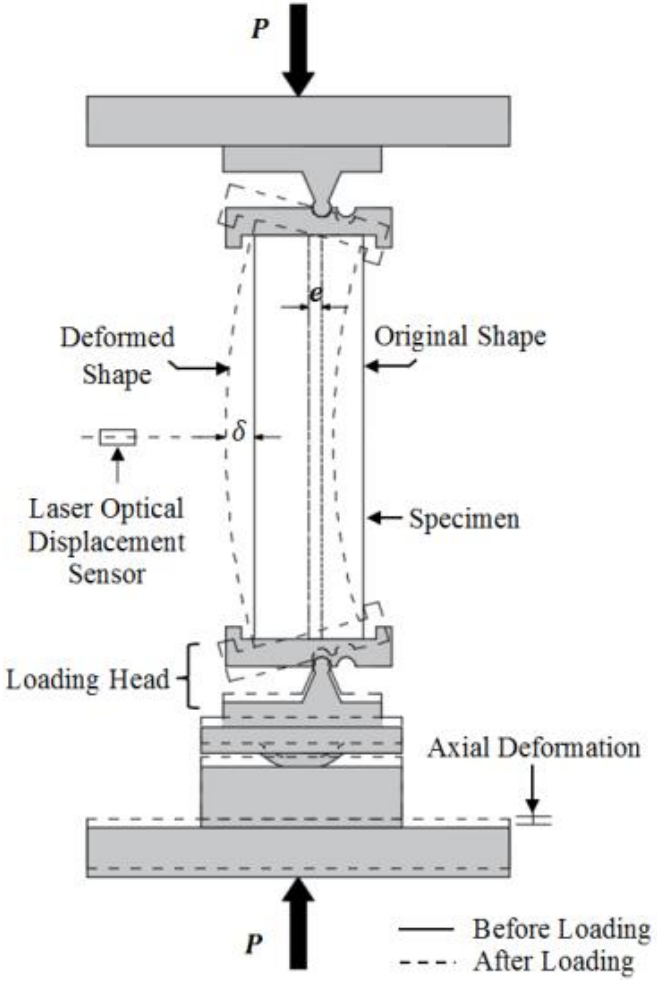

(b) Setup details of specimen

Figure 6.6: Typical test setup of column specimens: (a) loading heads; (b) setup details of specimens

Five specimens were tested as beams under flexural load (four-point load bending). The flexural loading system consisted of two circular steel loading rigs at the top and bottom of the beam specimens. These rigs were manufactured at the University of Wollongong to suit the Dension testing machine and 240-mm-round specimens. The specimens were tested by using a four-point load-bending arrangement with the loads applied at L/3 distance from the supports, where L is the span length. To measure the midspan deflection (δ) of the beam specimen, the same LODS was placed centrally underneath the rig. A slot at the bottom support of the rig allowed the LODS to optically measure the deflection. The LODS was connected to the data logger, which recorded the results. Figure 6.7 shows the schematic details of the four-point load-bending test arrangements. All tests were carried out at the displacement controlled loading rate of 0.3 mm/min, and the data was recorded at every 2 s.

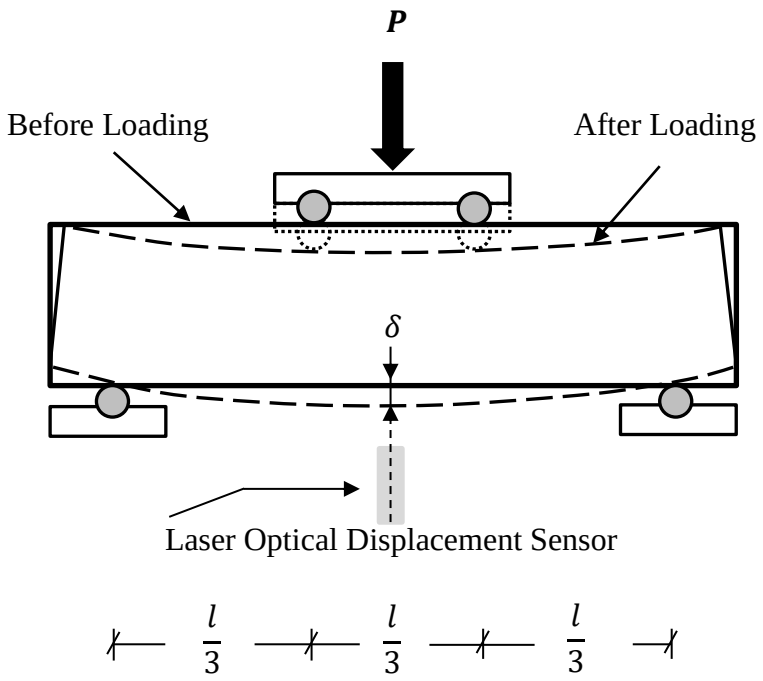

Figure 6.7: Four-point load-bending test arrangements

6.5 Experimental Results and Analysis

6.5.1 Column Specimens under Concentric Load

Five specimens were tested under concentric axial compression until failure. Table 6.3 reports the test results. Figure 6.8 shows the axial load-axial deformation diagrams of the five concentrically tested specimens. For all specimens, initial failure of the concrete cover started with cracks after the maximum load was reached. As the loading continued to increase, the buckling of longitudinal reinforcement occurred at the midheight of the column specimens. Finally, the specimens failed by fracture of the steel helices at the midheight. The failure modes of the specimens are shown in Figure 6.9. The average strains in the longitudinal steel bars and steel tubes indicated that steel bars and tubes yielded at the maximum axial load. The axial deformation corresponding to the first helix fracture in Specimen N16H50C was 20 mm, whereas in Specimens ST33.7H50C and ST26.9H50C, it was 33.5 and 36 mm, respectively. Specimen N16H50C had a lower axial deformation at the first fracture because the N16 steel deformed bar buckled earlier than the steel tubes. Consequently, more pressure was applied on the steel helix, causing the yielding and fracture of steel helices. Because of the different tensile strengths, the force contributions of steel tubes ST33.7 and ST26.9 in Specimens ST33.7H50C and ST26.9H50C were less than the N16 steel bars in Reference Specimen N16H50C by 19.9 and 37%, respectively. Nevertheless, Specimen ST33.7H50C had similar yield and maximum load as Reference Specimen N16H50C. Specimen ST26.9H50C had only 5% less maximum load than the reference specimen. Circular steel tubes provided confinement to the concrete and increased the compressive strength of concrete, which resulted in enhancing the capacity of the columns. Moreover, the ultimate axial deformation at failure for Specimens ST33.7H50C and ST26.9H50C were higher than for Reference Specimen N16H50C (Table 6.3).

Table 6.3: Results of specimens tested under concentric loading

Property	Specimen				
	N16H50C	ST33.7H50C	ST26.9H50C	ST33.7H75C	ST26.9H75C
Yield load (kN)	2505	2500	2375	2395	2275
Corresponding axial deformation (mm)	2.35	2.45	2.35	2.65	2.2
Maximum load (kN)	2734	2729	2598	2633	2443
Corresponding axial deformation (mm)	3.08	3.29	3.03	3.44	2.79
Ultimate axial deformation (mm)*	20	33.5	36	26.2	30.4
Ductility	16.96	22	22.84	13.91	18.91

***** Ultimate axial deformation was defined by the fracture of the steel helices.

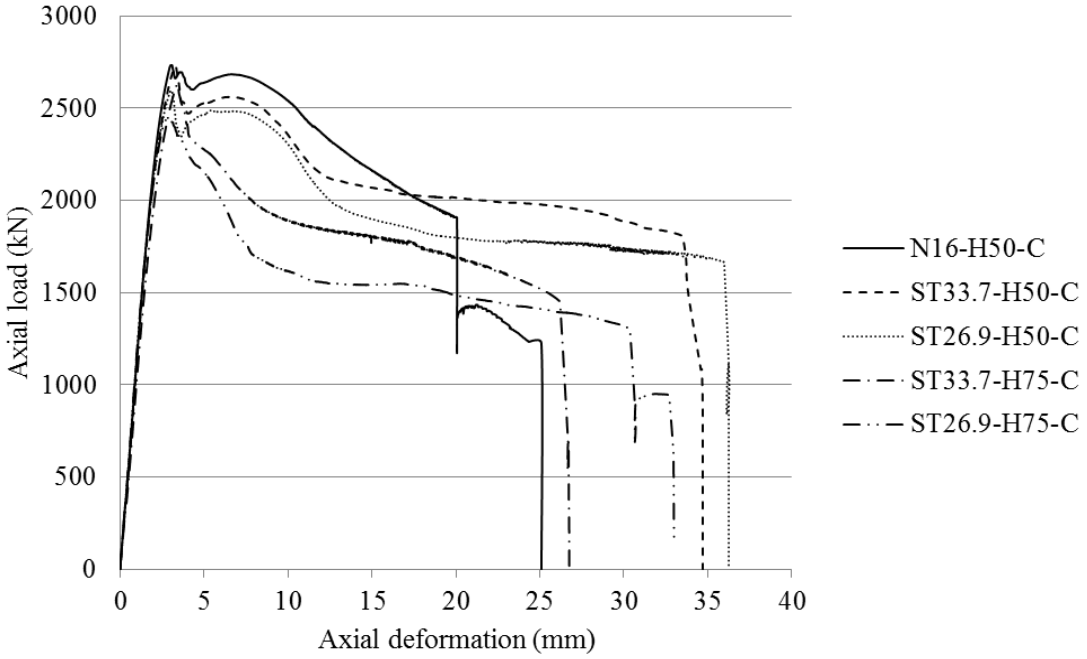

Figure 6.8: Axial load-axial deformation diagrams of specimens tested under concentric loading

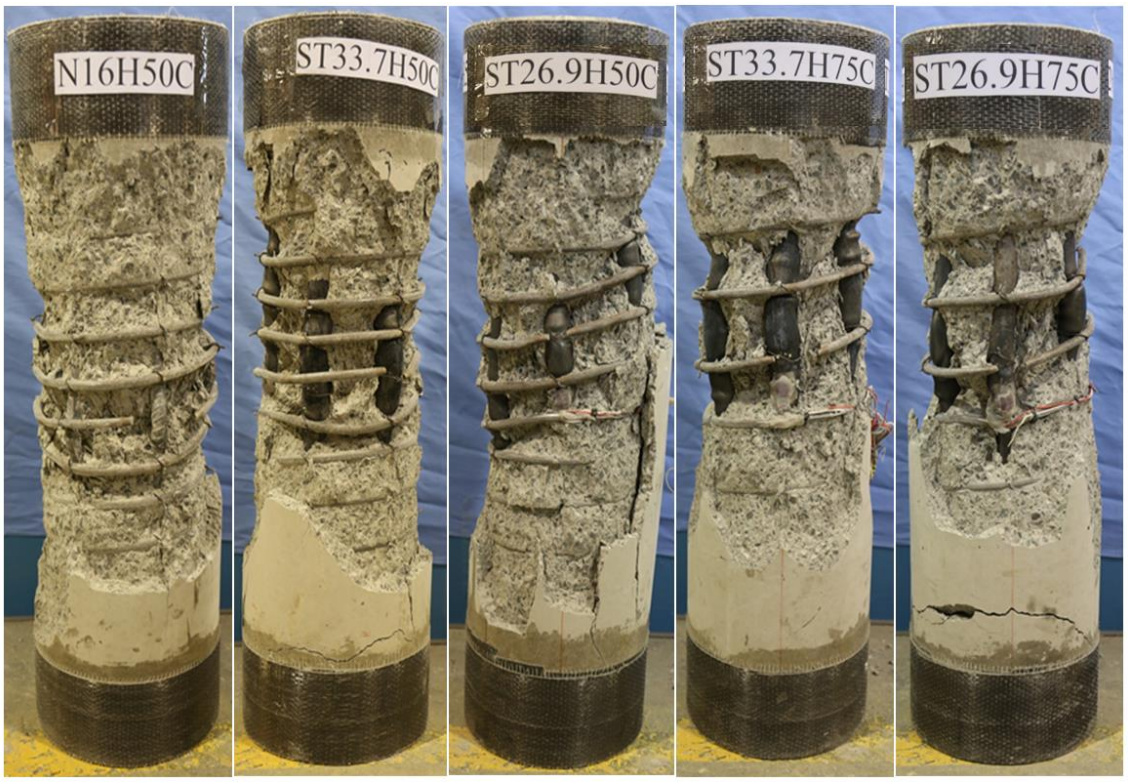

Figure 6.9: Failure modes of column specimens tested under concentric compression

For the increase of the pitch of helices from 50 to 75 mm in the specimens reinforced with steel tubes ST26.9, the maximum axial load reduced by 6%, whereas, increasing the pitch of helices from 50 to 75 mm in the specimens reinforced with steel tubes ST33.7 resulted in a maximum axial load decrease of only 3.5%. The reason for the differences in the reduction of maximum axial load is associated with the slenderness (L/D) ratio for steel tubes. The slenderness of steel tube ST26.9 is higher than that of steel tube ST33.7. From the test results, it was observed that specimens reinforced with ST33.7 steel tubes had a yield and maximum load capacity greater than specimens reinforced with ST26.9 steel tubes. This is because ST33.7 has higher nominal tensile strength than ST26.9. Moreover, the larger internal diameter of the ST33.7 tubes allowed for a large amount of concrete to be filled inside the tube, which contributed in increasing the capacity of the specimens, just as the confined concrete inside the tube positively contributed to the compressive strength of the specimens.

To study the behaviour of circular column specimens reinforced longitudinally with steel tubes, it is important to investigate the ductility of the specimens, which provides an indication of the post-peak axial load-axial deformation behaviour. In this paper, the ductility was calculated as the ratio of the area under the curve up to the ultimate deformation to the area under the curve up to the yield deformation (Hadi 2009). In order to specify yield deformation, the secant line was drawn from the origin to the point of 0.75 times of the first peak load. Then, the yield deformation was specified on the ascending load-deformation curve as corresponding to the intersection point of the extension secant line and a horizontal line from the first peak load (Foster and Attard 1997).

For concentric loads, the ductility of the column specimens reinforced with steel tubes was higher than that of the column specimens reinforced with steel bars for the same pitch of helix. The ductility of Specimens ST33.7H50C and ST26.9H50C was 30% higher than that of the reference specimen (Table 6.3). In spite of increasing the helix pitch from 50 to 75 mm in Specimen ST26.9H75C, the ductility of Specimen ST26.9H75C was 11% higher than that of the reference specimen; however, Specimen ST33.7H75C had a lower ductility than the reference specimen by 18%. This is mainly because Specimen ST33.7H75C has higher yield deformation than the reference specimen by about 13% (Table 6.3).

6.5.2 Column Specimens under Eccentric Load

Ten specimens were tested under eccentric loading: five under 25-mm eccentric load and five under 50-mm eccentric load. Test results of specimens under 25-mm eccentric loading are given in Table 6.4.

Table 6.4: Results of specimens tested under 25-mm eccentric loading

Property	Specimen				
	N16H50E25	**ST33.7H50E25**	**ST26.9H50E25**	**ST33.7H75E25**	**ST26.9H75E25**
Yield load (kN)	1690	1685	1650	1675	1545
Corresponding axial deformation (mm)	2.6	2.4	2.5	2.5	2.35
Maximum load (kN)	1824	1820	1780	1782	1631
Corresponding axial deformation (mm)	3.11	2.93	3.24	3.18	2.86
Corresponding lateral deformation (mm)	2.49	2.42	2.95	2.04	2.47
Ultimate axial deformation (mm)*	26.3	20.2	20.7	20	20.2
Ductility	13.1	8.56	8.3	7.23	7.37

***** Ultimate axial deformation was defined by 75% of the maximum load.

Figure 6.10 shows the axial load-axial deformation and axial load- lateral deformation diagrams of the specimens under 25-mm eccentric loading. For all specimens tested, the initial failure occurred as a result of cracks in the concrete cover once the specimens reached their maximum load. This was followed by a small drop in the maximum load due to spalling of concrete cover. After that, Reference Specimen N16H50E25 showed an increasing load. The load increased to a value less than the first maximum load. On the other hand, specimens reinforced with steel tubes showed a steady reduction in the load-deformation curve after spalling of the concrete cover. This is because debonding between steel tubes and concrete took place during the testing. For specimens reinforced with steel tubes, the failure occurred as results of a buckling of the longitudinal steel tubes in the compression region, whereas the failure of the reference column specimen

occurred because of a fracture in one of the longitudinal bars in the tension region combined with buckling in the longitudinal bars in the compression region, as shown in the Figure 6.11. After completion of the testing, by drilling holes in the specimens, the slip in both steel bars and steel tubes was measured using a measurement tape. It was found that the slip in steel tube was 20 mm, whereas no slip was observed in the N16 steel bars.

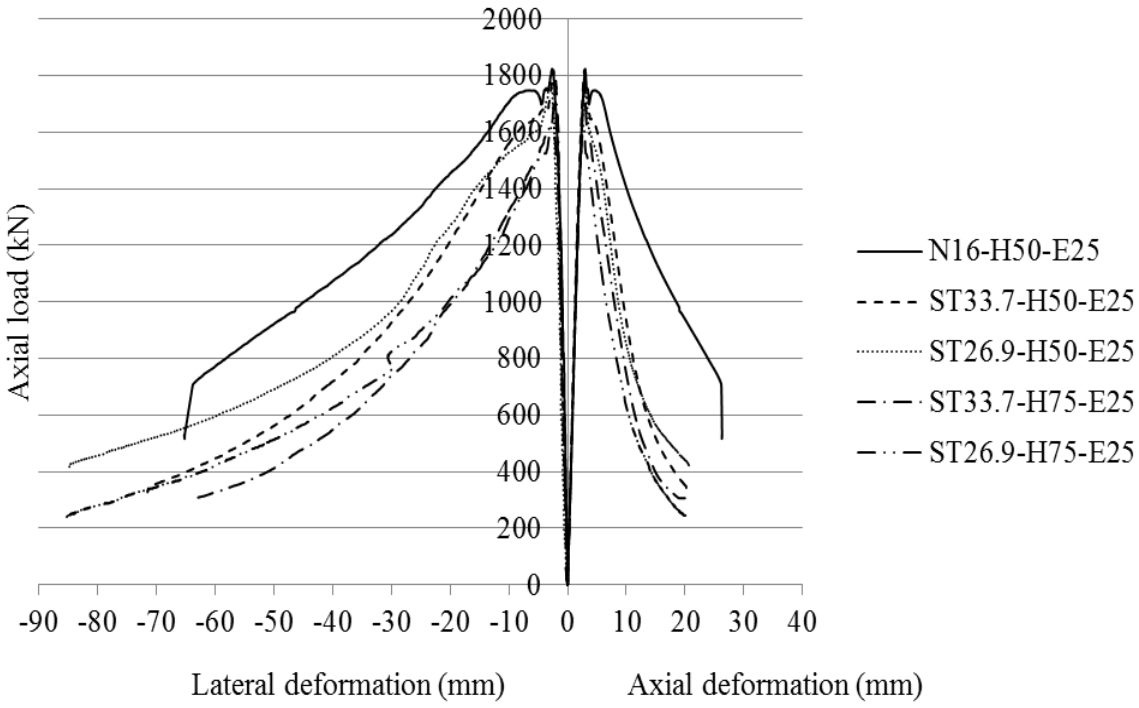

Figure 6.10: Axial load-axial deformation and axial load-lateral deformation diagrams of specimens tested under 25-mm eccentric loading

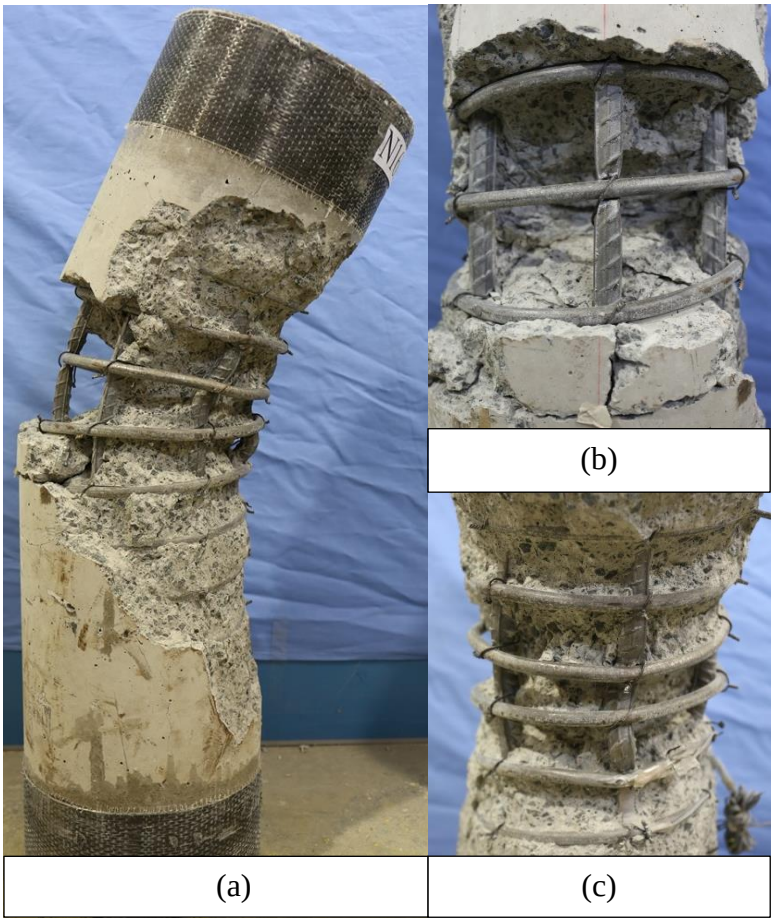

Figure 6.11: Failure mode of Reference Specimen N16H50E25: (a) specimen after failure; (b) tension region; (c) compression region

To overcome the slip of steel tubes for column specimens reinforced with steel tubes under eccentric loading, 4-mm-thick washers with inner diameters of 34 and 27 mm were welded to both ends of ST33.7 and ST26.9 steel tubes, respectively. The washers were cut to three-quarters of the shape. An initial attempt to prevent debonding was made on Specimens ST33.7H75E50 and ST26.9H75E50. First, the locations of the steel tubes were identified by mildly drilling the concrete cover at the top and bottom of the specimens. Second, a ring of the concrete cover was removed carefully by using a chisel and hummer in order to reveal the ends of the steel tubes. Third, the washers were fitted and properly welded around the ends of the tubes. Finally, high-strength plaster

(compressive strength of 70 MPa) was used to fill the concrete cover. Figure 6.12 shows the details of the remedial measure for the slip of the steel tubes.

Figure 6.12: Remedial measure for the slip of steel tubes: (a) specimen before repairing; (b) drilling of concrete cover; (c) specimen after removing concrete cover above tubes; (d) washers fitted on tubes; (e) welding of washers; (f) plaster infill.

Results of testing Specimens ST33.7H75E50 and ST26.9H75E50 indicated that slip still occurred even after the repair. This is because the concentrated stresses on the washers led to bending of the washers and tearing of the tubes near the welding area at both ends of the tube in the tension region. To solve this, for the remaining ST33.7H50E50 and ST26.9H50E50 specimens, two washers were welded at both ends of the longitudinal steel tubes in the tension region of each specimen (Figure 6.13). This was done in an attempt to distribute the tensile strain over four anchor points and prevent the first

washer from bending by supporting it by the second washer and to increase the resistant capacity of the steel tube wall before tearing at the ends and overall slip.

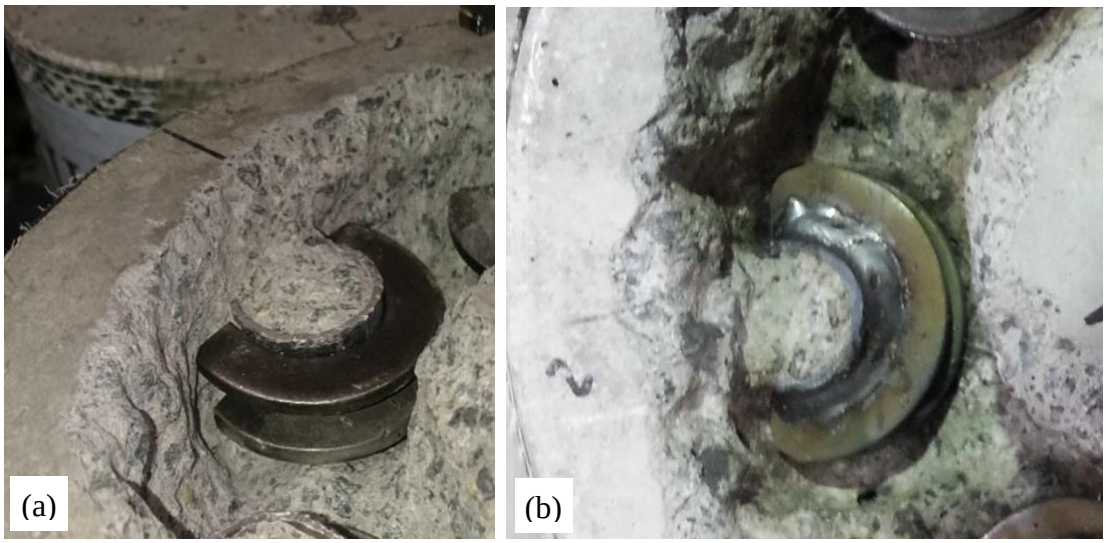

Figure 6.13: Configuration of two washers: (a) washers before welding; (b) washers after welding

Test results of specimens under 50-mm eccentric loading are reported in Table 6.5. Figure 6.14 shows the axial load-axial deformation and axial load-lateral deformation diagrams of the specimens tested under 50-mm eccentric loading. For all specimens tested, the initial failure occurred as a result of cracks within the concrete cover once the specimens reached their maximum load. This was followed by a small drop in the maximum load due to spalling of the concrete cover. After that, Reference Specimen N16H50E50 showed an increasing load. The load increased to a value less than the first maximum load. Axial load then steadily decreased until the failure occurred because of yielding of the longitudinal bars in the tension region combined with buckling of the longitudinal bars in the compression region. Specimen ST33.7H50E50 experienced a similar yield point to the reference specimen after initial spalling of the concrete cover, but the tube tearing and failure did not occur at the centre.

Table 6.5: Results of specimens tested under 50-mm eccentric loading

Property	Specimen				
	N16H50E50	**ST33.7H50E50**	**ST26.9H50E50**	**ST33.7H75E50**	**ST26.9H75E50**
Yield load (kN)	1200	1145	1185	1150	1100
Corresponding axial deformation (mm)	2.5	2.4	2.5	2.4	2.35
Maximum load (kN)	1300	1233	1267	1240	1175
Corresponding axial deformation (mm)	2.78	2.84	2.9	2.92	2.73
Corresponding lateral deformation (mm)	2.94	2.87	3	3.5	3.24
Ultimate axial deformation (mm)*	20.7	14.7	20.7	18.4	25.1
Ductility	11.54	8.7	8.63	7.56	9.78

***** Ultimate axial deformation was defined by 75% of the maximum load.

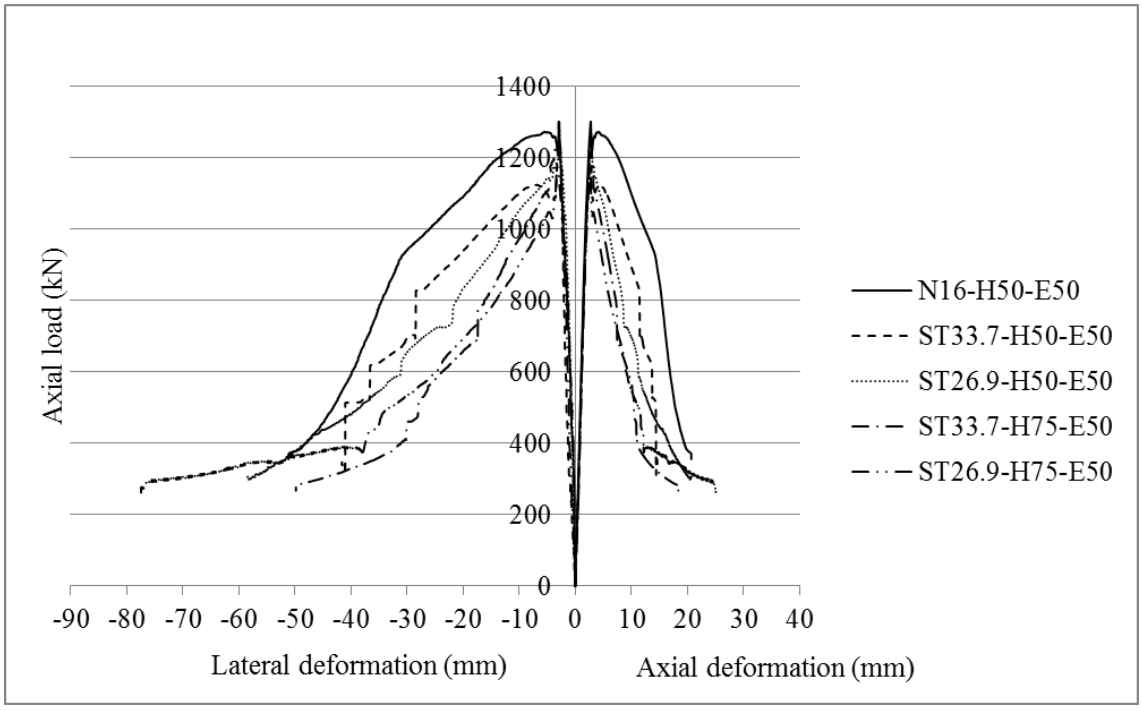

Figure 6.14: Axial load-axial deformation and axial load-lateral deformation diagrams of specimens tested under 50-mm eccentric loading

Similarly for Specimen ST26.9H50E50, two washers were welded at both ends of the longitudinal tubes that were supposed to be in the tension region during testing; however, during testing, the tubes with washer were placed inadvertently in the compression region rather than in the tension region, resulting in a steady reduction in the load-deformation curve after the spalling of the concrete cover. As in Specimens ST26.9H75E50 and ST33.7H75E50, the tubes tore around the single washers after reaching the maximum load, causing a slip with no signs of ductile behaviour; however, placing the tubes with double washers in the compression region resulted in a higher load-carrying capacity compared to Specimen ST33.7H50E50. This indicated that the slip may occur in tubes in compression loads as well as in tension under 50-mm eccentric loads. After the spalling of the concrete cover, the tube was compressed, and the double washers prevented slip in the compression region in this case.

For 25-mm eccentric loads, the ductility of the column specimens reinforced with steel tubes was lower than that of the column specimens reinforced with steel bars because of slip of the steel tubes. For 50-mm eccentric loads, the ductility of the column specimens reinforced with steel tubes was improved by the use of washers but was still lower than that of the column specimens reinforced with steel bars.

6.5.3 Flexural Specimens

The remaining five specimens were tested under four-point load bending as beams. Test results of specimens under flexural loading are reported in Table 6.6. Figure 6.15 shows the load-midspan deflection diagrams of the specimens tested under flexural loading.

Table 6.6: Results of specimens tested under flexural loading

Property	Specimen				
	N16H50F	ST33.7H50F	ST26.9H50F	ST33.7H75F	ST26.9H75F
Yield load (kN)	510	490	385	458	350
Corresponding midspan deflection (mm)	4.5	4.95	5.1	4.75	4.35
Maximum load (kN)	592	541	443	511	401
Corresponding midspan deflection (mm)	26.8	7.2	9.07	6.59	6.02
Ultimate midspan deflection (mm)*	44.1	47.5	39.8	37.9	23.9
Ductility	17.55	12.49	9.63	11.7	8.52

***** Ultimate midspan deflection was defined by the fracture of the bar/tube.

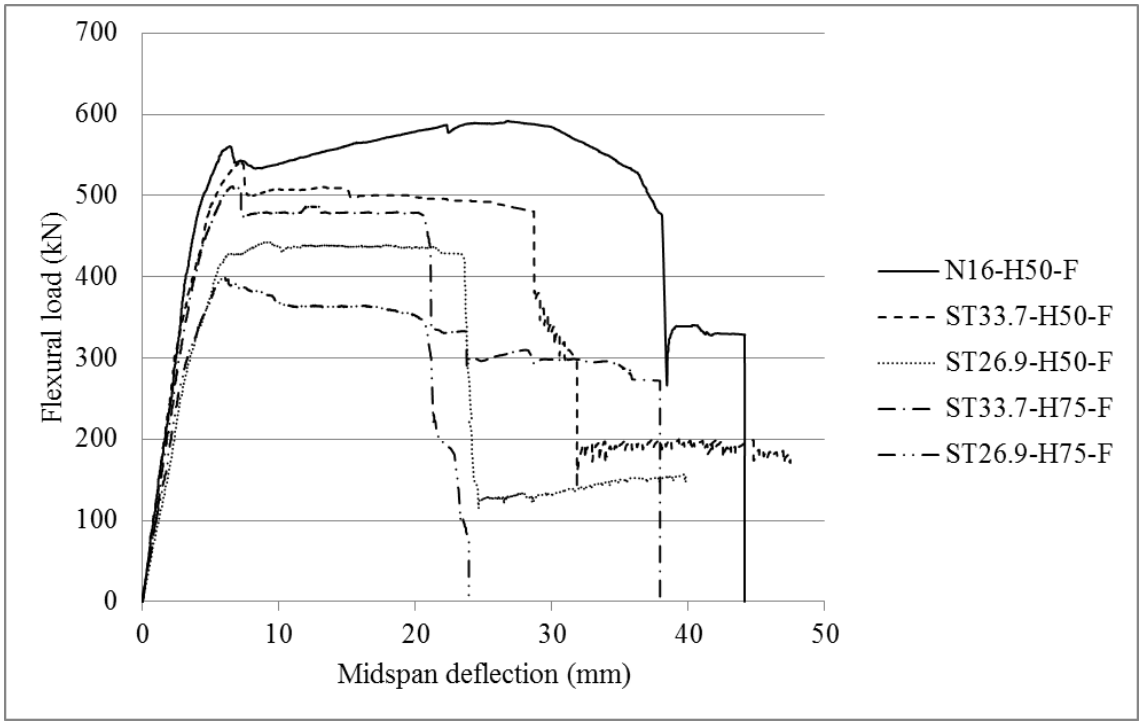

Figure 6.15: Load-midspan deflection of specimens tested under flexural loading

The span-to-depth ratio of the test specimen is relatively short, and hence the failure may not truly represent a pure bending condition; however, for uniformity and consistency, specimen dimensions were kept the same as other specimens tested under concentric and eccentric axial compression. It was expected that the steel tubes in the tension region for the specimens under flexural would be subjected to higher tensile stresses compared to the specimens under 25-mm and 50-mm eccentric loads, with a high possibility that slip would occur. To prevent slip of steel tubes inside these specimens, single washer and double washers were used in the compression and tension regions, respectively. Because of the relatively large cross-sectional area of the specimens, precautions were taken to avoid any bearing and shear failures. Bearing plate spacers of 50-mm width were used on the testing rigs, and CFRP sheets were used to wrap the specimen ends, leaving only one-third in the middle.

For all specimens, the failure mechanism was consistent. The initial failure occurred as a result of cracks within the concrete cover in the middle when maximum load was reached. This was followed by yielding and then fracture of the farthest bar or tube in the tension region. Afterword, the other bars or tubes in the tension region either fractured or kept yielding for a while and then fractured depending on the stresses distribution and corresponding generated cracks. The failure modes of specimens tested under flexural loading are shown in Figure 6.16. For specimens reinforced with steel tubes, the initial slope of load-midspan deflection diagrams in the specimens reinforced with tubes of a 350-MPa nominal tensile strength (ST33.7) was steeper than other specimens reinforced with tubes of a 250-MPa nominal tensile strength (ST26.9). It is clear that the large-diameter ST33.7 tube have a higher second moment of area, which provides a higher stiffness combined with the higher nominal tensile strength of steel in

the ST33.7 tubes. Also, the effect of tensile strength on the maximum load was higher than the effect of pitch. The lowest value of the maximum load was in Specimen ST26.9H75F, and followed by Specimen ST26.9H50F.

Figure 6.16: Failure modes of specimens tested under flexural loading

For flexural loads, the ductility of the specimens reinforced with steel tubes was lower than that of the specimens reinforced with steel bars. The ductility of Specimens ST33.7H50F and ST33.7H75F was less than the reference specimen by 29 and 33%, respectively (Table 6.6). The reason for this is that the tensile strength of steel tubes was lower than the tensile strength of the steel bars. In addition, the effect of tensile strength of the longitudinal reinforcing steel on the ductility of specimens was higher than the effect of the spacing of the pitch. The lowest value of the ductility was observed in Specimens ST26.9H75F and ST26.9H50F (Table 6.6).

6.5.4 Interaction Diagrams

The experimental axial load-bending moment (P-M) interaction of all specimen types is shown in Figure 6.17. Four points, one each for concentric, 25-mm eccentric, 50-mm eccentric, and flexural loading, were used to draw the P-M interaction diagrams. The first point consists of maximum axial load for specimens tested under concentric load. The second and the third points consist of the maximum axial load for specimens tested under 25 and 50-mm eccentric loads and the corresponding bending moments, respectively. The corresponding bending moments at the midheight of the columns under 25 and 50-mm eccentric loads were calculated as in Equation (6.1).

$$M = P_{Max}(e + \delta) \tag{6.1}$$

Where M and δ = moment and lateral deformation corresponding to the maximum axial load (P_{Max}), respectively, and e = the loading eccentricity. The fourth point consists of only pure bending moment for the specimen tested under four-point bending. The pure bending moments at midspan of the beams were calculated as in Equation (6.2).

$$M_p = (P_{Max}l)/6 \tag{6.2}$$

Where M_p = pure bending moment corresponding to the maximum load (P_{Max}) of the tested beam specimen; and the l = span length, or the distance between the supports.

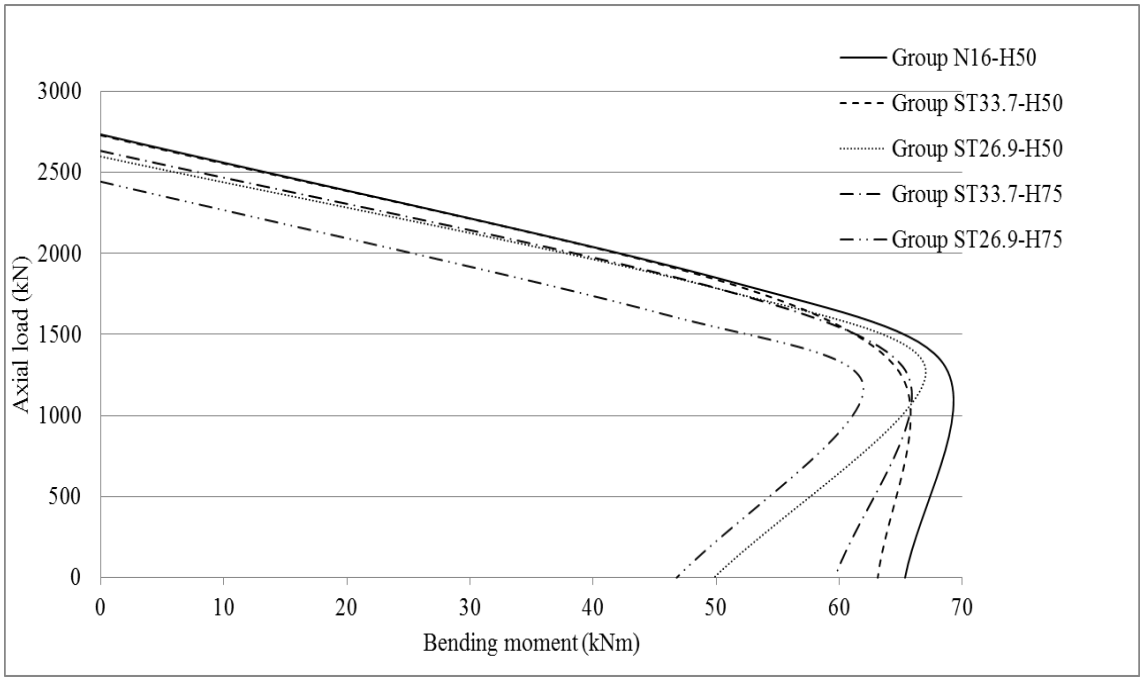

Figure 6.17: Experimental load-bending moment interactions for the tested specimens

Specimens of Group ST33.7H50 showed similar axial load-bending moment interaction behaviour to the reference specimens of Group N16H50. At the concentric load and 25-mm eccentric load, the axial load and bending moment capacities of specimens of Group ST33.7H50 were similar to the axial load and the bending moment capacities of the reference specimens of Group N16H50. At 50-mm eccentric load, the maximum axial load of Specimen ST33.7H50E50 was lower than the maximum axial load of reference specimen by 5%. This is because the use of a single washer for the longitudinal steel tubes was insufficient for preventing the slip of tubes in the compression region of the specimen. For flexural load, the bending moment of Specimen ST33.7H50F was 3.4% lower than the bending moment of N16H50F because of the lower tensile strength of longitudinal tube reinforcement compared to steel bars. Increasing the pitch of the helices in the specimen from 50 mm to 75 mm resulted in the

reduction of the axial load-carrying capacity and bending moments under concentric, eccentric, and flexural loads of Group ST33.7H75.

At the concentric load and 25-mm eccentric load, specimens of Group ST26.9H50 showed lower axial load-carrying capacity compared to the specimens of Group ST33.7H50 because of the lower tensile strength and small outside diameter steel tubes; however, at 50-mm eccentric load, placing the steel tubes with double washers in the compression region of Specimen ST26.9H50E50 resulted in a higher axial load-carrying capacity and corresponding bending moment compared to Specimen ST33.7H50E50. Under flexural loads, the bending moment of Specimen ST26.9H50F was 23.7% and 21% lower than the bending moment of Reference Specimen N16H50F and Specimen ST33.7H50F, respectively. Similar to the specimens of Group ST33.7H75, increasing the pitch of the helices in the specimen from 50 mm to 75 mm resulted in the reduction of the axial load-carrying capacity and bending moments under concentric, eccentric, and flexural loads of Group ST26.9H75. This indicates that the use of steel tubes with similar tensile strength as the steel bars may show a higher axial load-carrying capacity and corresponding bending moment in STR SCC specimens; however, the slip of steel tubes should be prevented. Adequate use of washers may be considered a viable solution.

Theoretical axial load-bending moment (P-M) interaction diagrams of all specimen types were determined by a layer-by-layer integration method. The cross section of concrete was assumed to consist of small parallel layers with a small thickness (t) and a variable width (b_n), as shown in Figure 6.18.

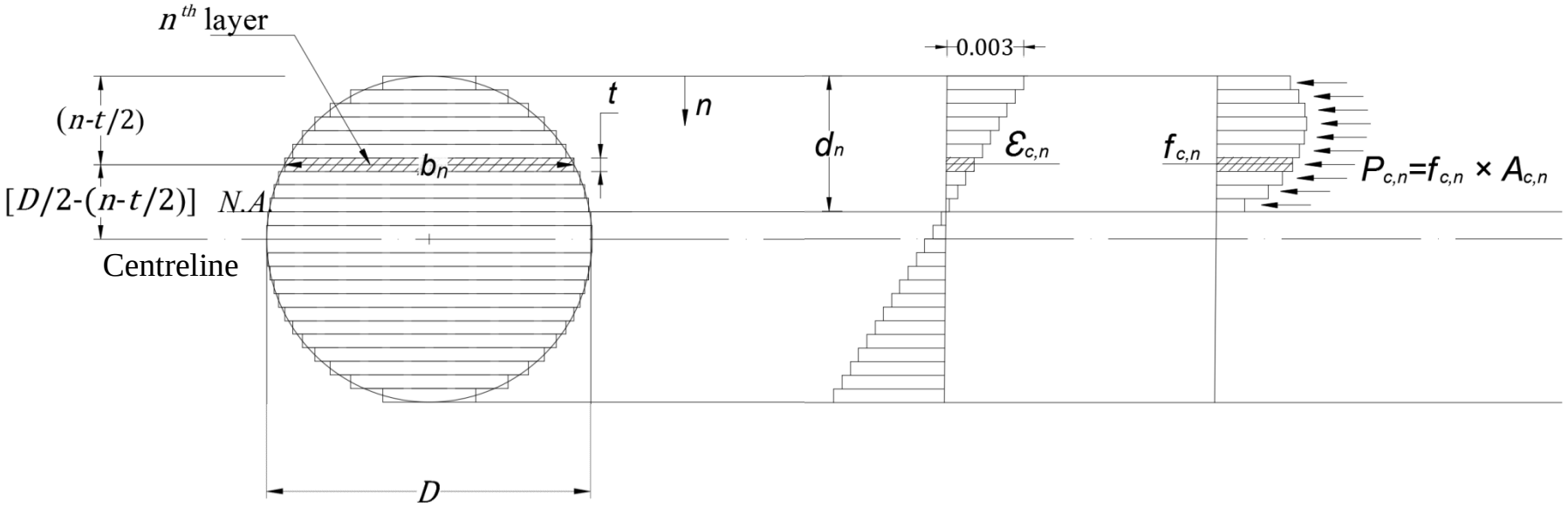

Cross-section divided into n number of layers Strain distribution Corresponding stress and force distribution

Figure 6.18: Layer-by-layer integration method

The number of layers (n) is calculated by dividing the diameter of the cross section (D) by the thickness of each layer. The cross section was divided into 240 small layers by assuming the thickness of each layer equal to 1 mm. Based on the assumptions that plane sections remain plane after bending, the strain ($\varepsilon_{c,n}$) in the centre of each layer can be calculated according to the linear distribution of strain, as a function of the depth of neutral axis (d_n) (Figure 6.18), which represents the distance from the extreme concrete compressive fibre to the neutral axis ($N.A$). After calculating the strain in each concrete layer, the corresponding stress value ($f_{c,n}$) on the centre of each layer was calculated according to the stress-strain model for unconfined concrete from Aslani and Nejadi (2012). The tensile strength of concrete was ignored in the calculations. The unconfined concrete strength was taken as 83% of 28-day cylinder compressive strength according to AS 3600-2009 (AS 2009). The ultimate strain in extreme concrete compressive fibre was considered as 0.003 according to AS 3600-2009 (AS 2009).

The force reaction in the centre of each concrete layer ($P_{c,n}$) was calculated by multiplying the stress in each layer by the corresponding area of concrete in each layer ($A_{c,n}$). The moment for each layer was calculated by multiplying the force in each layer by the distance from the centre of each layer to the centreline of the cross section. The total force of the concrete cross section was calculated as the summation of the forces acting on the strips. The tensile forces are considered negative, whereas the compressive forces are positive. In addition, the total moment of the concrete cross section was calculated as the summation of the moments with respect to the centreline of the cross section.

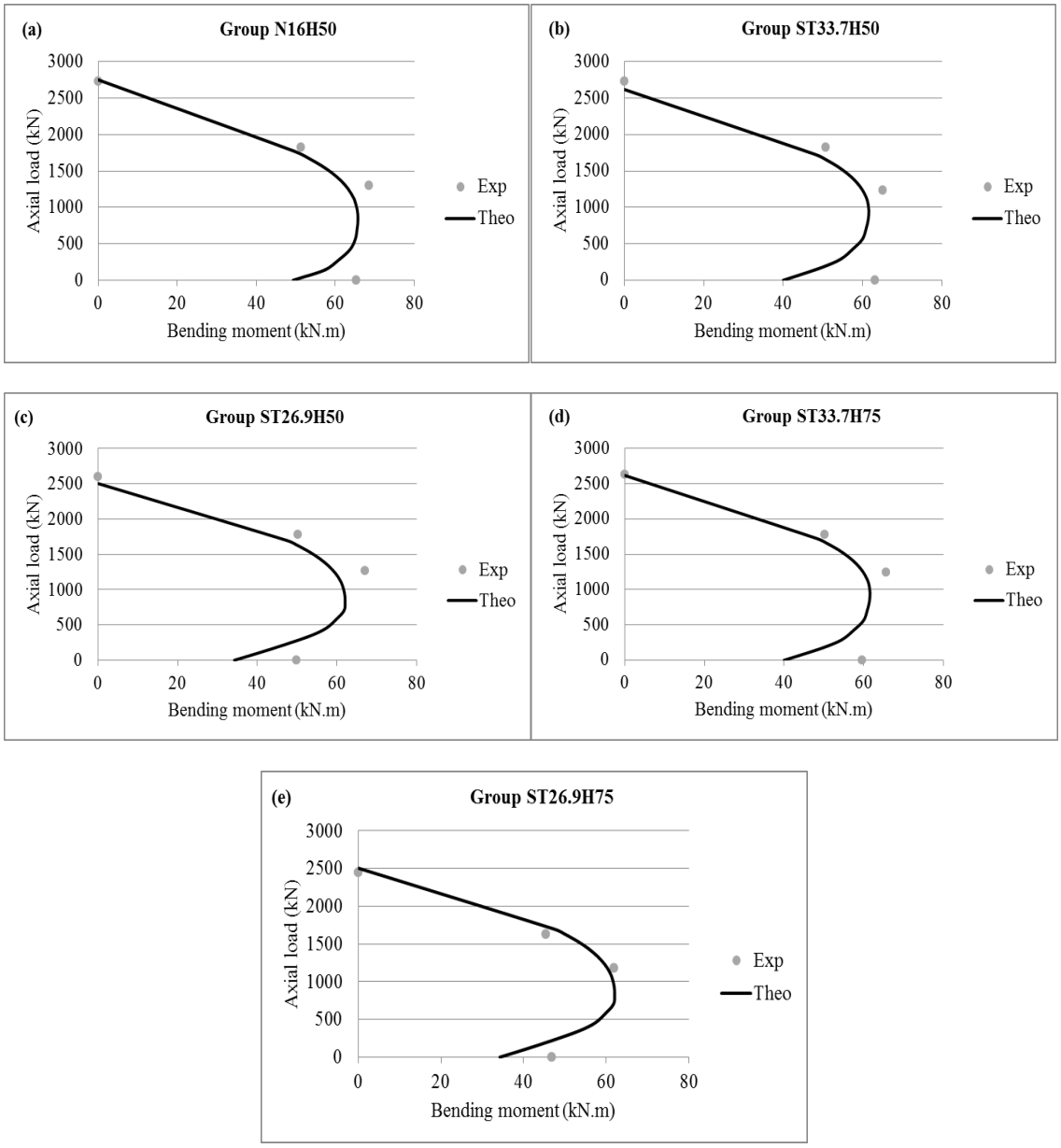

Figure 6.19: Comparison between theoretical and experimental P–M interactions for the tested specimens

Figure 6.19 compares the theoretical and the experimental P–M interactions for the specimens tested in this study. It was found that the theoretical results were in good agreement with the experimental results. The experimental bending moment of specimens reinforced with N16 steel bar, ST33.7 steel tube, and ST26.9 steel tube tested under four-point load bending was relatively greater than the calculated bending

moment. This might be because specimens tested as beam had shear spans shorter than twice the effective depth of the concrete cross section.

6.6 Conclusions

Use of small-diameter circular steel tubes filled with Self-Compacting Concrete (SCC) in lieu of conventional steel bars was investigated in reinforcing the concrete column. Hence, a new reinforcing method of the concrete column specimens was proposed in this paper. Problems associated with the use of steel tubes as longitudinal reinforcement in columns because of slip of steel tubes have been highlighted. The following conclusions can be drawn.

1. Because the tensile strength of steel bars and steel tubes are different, the force contribution of ST33.7 steel tubes in Specimen ST33.7H50 was found to be less than the force contribution of N16 steel bars in the Reference Specimen N16H50 by 19.9%. In spite of less force contribution of steel tubes, Column Specimen ST33.7H50 had similar yield and maximum load as Reference Specimen N16H50 under concentric and 25-mm eccentric axial compression. The yield loads of Specimens N16H50 and ST33.7H50 were 2505 and 2500 kN, respectively. The maximum loads of the Specimens N16H50 and ST33.7H50 were 2734 kN and 2729 kN, respectively. Hence, using steel tubes with similar tensile strength to steel bars might result in a higher maximum load capacity.
2. For concentric load and 25-mm eccentric load, specimens reinforced with ST33.7 steel tubes had a maximum load capacity greater than specimens reinforced with ST26.9 steel tubes. For 50-mm eccentric load, however, Specimen ST26.9H50E50 showed a maximum load higher than that of Specimen ST33.7H50E50 because of the slip of ST33.7 steel tubes.

3. Despite the fact that the cross-sectional areas of ST33.7 and ST26.9 steel tubes are the same, increasing the pitch of helices from 50 to 75 mm resulted in a higher reduction in the maximum axial load of specimens reinforced with ST26.9 tubes compared to specimens reinforced with ST33.7 tubes.
4. Under flexural loading, the maximum loads of Specimens ST33.7H50F and ST26.9H50F were 7 and 25% lower, respectively, than that of Reference Specimen N16H50F. In addition, the initial slope of load-midspan deflection diagrams in the specimens reinforced with ST33.7 tubes (nominal tensile strength=350 MPa) was steeper than that of the specimens reinforced with ST26.9 tubes (nominal tensile strength=250 MPa).
5. The ductility of STR SCC specimens was significantly influenced by the slip of steel tubes under eccentric loading; however, the STR SCC specimens showed a higher ductility than Reference Specimen N16H50C under concentric loading.
6. Welding a single washer at the ends of the steel tubes to prevent slip in concrete was insufficient and resulted in a tearing of the tubes near the welding area at both ends of the tube in the tension and compression regions. In contrast, welding double washers at the ends of the tubes prevented the slip of longitudinal steel tubes in concrete.

Acknowledgments

The authors thank the University of Wollongong and technical officers at the High Bay laboratory, especially Mr. Ritchie McLean, for their help in the experimental work of this study. The authors also thank the Orrcon steel company for supplying the steel tubes. Finally, the second author would like to acknowledge the Iraqi Government for the support of his Ph.D. scholarship.

References

ACI (American Concrete Institute). (2011). "Building code requirements for structural concrete." *ACI: 318M-11*, Farmington Hills, MI.

ACI (American Concrete Institute). (2014). "Building code requirements for structural concrete." *ACI: 318M-14*, Farmington Hills, MI.

AISC. (2010). "Specification for structural steel buildings." *ANSI/AISC 360-10*, Chicago.

AS (Australian Standard). (2007). "Metallic materials-tensile testing at ambient temperature." *AS 1391-2007*, Sydney, NSW, Australia.

AS (Australian Standard). (2009). "Concrete structure." *AS 3600-2009*, Sydney, NSW, Australia.

Aslani, F., and Nejadi, S. (2012). "Mechanical properties of conventional and self-compacting concrete: An analytical study." *Construction and Building Materials*, 36, 330-347.

ASTM. (2014a). "Standard test method and definition for mechanical testing of steel products." *ASTM A370-14*, West Conshohocken, PA.

ASTM. (2014b). "Standard test method for passing ability of self-consolidating concrete by J-ring." *ASTM C1621/C1621M-14*, West Conshohocken, PA.

ASTM. (2014c). "Standard test method for slump flow of self-consolidating concrete." *ASTM C1611/C1611M-14*, West Conshohocken, PA.

ASTM. (2014d). "Standard test method for static segregation of self-consolidating concrete using column technique." *ASTM C1610/C1610M-14*, West Conshohocken, PA.

Choi, K. K., and Xiao, Y. (2010). "Analytical model of circular CFRP confined concrete-filled steel tubular columns under axial compression." *Journal of Composites for Construction ASCE*, 14(1), 125-133.

CSA (Canadian Standards Association). (2006). "Canadian highway bridge design code." *CAN/CSA S6-6*, Rexdale, ON, Canada.

De Schutter, G. (2005). "Guidelines for testing fresh self-compacting concrete." Systematic pan-European inter-laboratory, Paisley, U.K., 1-23.

EFNARC (European Federation of Specialist Construction Chemicals and Concrete Systems). (2002). "Specification and guidelines for self-compacting concrete." Norflolk, U.K., 1-32.

EFNARC (European Federation of Specialist Construction Chemicals and Concrete Systems). (2005). "The European guidelines for self-compacting concrete specification, production and use." Farnham, U.K., 1-63.

Foster, S. J., and Attard, M. M. (1997). "Experimental tests on eccentrically loaded high-strength concrete columns." *ACI Structural Journal*, 94(3), 295-303.

Giakoumelis, G., and Lam, D. (2004). "Axial capacity of circular concrete-filled tube columns." *Journal of Constructional Steel Research*, 60(7), 1049-1068.

Goodier, C. I. (2003). "Development of self-compacting concrete." *Proceedings of the Institution of Civil Engineers-Structures and Buildings*, 156(4), 405-414.

Hadi, M. N. S. (2009). "Behaviour of eccentric loading of FRP confined fibre steel reinforced concrete columns." *Construction and Building Materials*, 23(2), 1102-1108.

Han, L.-H., and Yao, G.-H. (2004). "Experimental behaviour of thin-walled hollow structural steel (HSS) columns filled with self-consolidating concrete (SCC)." *Thin-Walled Structures*, 42(9), 1357-1377.

Moon, J., Lehman, D., Roeder, C., and Lee, H. (2013). "Strength of circular concrete-filled tubes with and without internal reinforcement under combined loading." *Journal of Structural Engineering ASCE*, 139(12), 04013012.

Muciaccia, G., Giussani, F., Rosati, G., and Mola, F. (2011). "Response of self-compacting concrete filled tubes under eccentric compression." *Journal of Constructional Steel Research*, 67(5), 904-916.

RILEM. (1983). "Bond test for reinforcing steel: 2. Pullout test." *Recommendation RC 6*, E & FN SPON, London, 218–220.

Roeder, C. W., Lehman, D. E., and Bishop, E. (2010). "Strength and stiffness of circular concrete-filled tubes." *Journal of Structural Engineering ASCE*, 136(12), 1545-1553.

Sakino, K., Nakahara, H., Morino, S., and Nishiyama, I. (2004). "Behavior of centrally loaded concrete-filled steel-tube short columns." *Journal of Structural Engineering ASCE*, 130(2), 180-188.

Schneider, S. P. (1998). "Axially loaded concrete-filled steel tubes." *Journal of Structural Engineering ASCE*, 124(10), 1125-1138.

Shanmugam, N. E., and Lakshmi, B. (2001). "State of the art report on steel-concrete composite columns." *Journal of Constructional Steel Research*, 57(10), 1041-1080.

Wang, X., Liu, J., and Zhang, S. (2015). "Behavior of short circular tubed-reinforced-concrete columns subjected to eccentric compression." *Engineering Structures*, 105, 77-86.

Xiamuxi, A., and Hasegawa, A. (2012). "A study on axial compressive behaviors of reinforced concrete filled tubular steel columns." *Journal of Constructional Steel Research*, 76, 144-154.

CHAPTER 7: AXIAL LOAD-AXIAL DEFORMATION BEHAVIOUR OF SCC COLUMNS REINFORCED WITH STEEL TUBES

Summary

This chapter presents a simplified analytical model for the axial load-axial deformation behaviour of SCC columns reinforced with steel tubes. The analytical model takes into account the contributions of the steel tubes, unconfined concrete cover, confined concrete core and confined concrete inside the steel tube. The results of the analytical model have been compared with experimental results of four SCC column specimens. The predictions of the developed analytical model have been found to be in good agreement with the experimental investigation results. The analytical observations, based on a detailed parametric study, reported in this study will contribute to good understanding on the axial load-axial deformation behaviour of SCC columns reinforced with steel tubes. A similar analytical modelling approach was also adopted in the next chapter (Chapter 8) for the axial load-bending moment interactions of self-compacting concrete columns reinforced with steel tubes. It is important to mention that the effect of the tensile strength of the SCC on the behaviour of SCC columns was not significant. Consequently, to avoid the complexities of the modelling in Chapters seven and eight, the tensile strength of SCC was assumed to be negligible.

Citation

This chapter has been submitted for possible publication to the ACI Structural Journal with the following citation:

Alhussainy F, Sheikh MN, Hadi MNS. (2017). "Axial load-axial deformation behavior of SCC columns reinforced with steel tubes." *ACI Structural Journal,* (Under review).

Abstract

A simplified analytical model has been developed for the axial load-axial deformation behaviour of self-compacting concrete (SCC) columns reinforced with steel tubes. The developed analytical model takes into account the contribution of the steel tubes, unconfined concrete cover, confined concrete core and confined concrete inside the steel tube. The results of the analytical model have been compared with experimental results of four SCC column specimens. The results of the analytical model are in good agreement with the experimental results. A parametric study has been conducted to investigate the influences of the compressive strength of SCC, tensile strength of steel tube, wall thickness of steel tube and pitch of steel helix on the axial load-axial deformation behaviour of SCC columns reinforced with steel tubes. The ductility of SCC columns has been found to be significantly influenced by the increase in the compressive strength of SCC and the pitch of steel helix.

Keywords: Composite columns; self-compacting concrete; steel tube; axial load-axial deformation; ductility.

7.1 Introduction

Steel sections and concrete are commonly used in the construction of composite columns. There are two main configurations of the composite columns: concrete-encased steel section columns and concrete-filled steel tube (CFT) columns (Wang 1999). The advantages of composite columns are high strength, stiffness, ductility, fire resistance and seismic resistance (Susantha et al. 2001; Hajjar 2002). Steel tubes with different cross-sections (rectangular, square, polygon and circular) are used to construct

CFT columns (Sakino et al. 2004; Han et al. 2014). Circular steel tube sections are usually preferred for the CFT columns because circular steel tubes provide better confinement to the infill concrete (Schneider 1998). In traditional CFT columns, steel tubes are usually filled with concrete without any internal steel reinforcement (De Oliveira et al 2009). In some cases, internal steel reinforcement is used for higher strengths and better connections between the concrete members (Moon et al. 2013).

Reinforced concrete (RC) columns are usually constructed of normal-vibrated concrete (NVC). However, the congestion of reinforcement in the construction of columns is a critical issue. Casting concrete in columns with a large amount of longitudinal and transverse reinforcements makes the placement of concrete difficult. For such columns, the self-compacting concrete (SCC) is considered a suitable option to overcome the difficulty of the placement of concrete because SCC possesses good workability with high flowability, passing ability and segregation resistances (EFNARC 2002). The SCC can be easily poured into complex or novel forms of construction without requiring vibration even in columns containing a large amount of reinforcement (Paultre et al. 2005; Khatab et al. 2017).

Lin et al. (2008) examined the behaviour of axially loaded RC columns constructed of NVC and SCC. Test results showed that the ductility, stiffness and crack control ability of the SCC columns were better than NVC columns. Lachemi et al. (2006) examined the performance of axially loaded CFT columns constructed of NVC and SCC. Two series of steel tube confined concrete columns with and without longitudinal and transverse reinforcement were tested. The test results showed that axial load carrying capacities of NVC columns and SCC columns were comparable. Also, the casting of

columns with SCC was easier than casting of columns with NVC, as SCC did not require any vibration.

Recently, the authors proposed a new method of reinforcing SCC columns with small diameter steel tubes as longitudinal reinforcement (Hadi et al. 2017). The behaviour of SCC columns reinforced with steel tubes is different from the behaviour of SCC columns reinforced with conventional steel bars. For the same cross-sectional area, the radius of gyration of the steel tube is higher than the radius of gyration of the solid steel bar. Steel tubes filled with SCC decreased the overall buckling of longitudinal reinforcement and consequently increased the ductility of the SCC columns. Also, steel tubes effectively confined the infill concrete resulting in an increase of the axial compressive strength. Using steel tubes with a tensile strength similar to that of steel bars in reinforcing SCC columns increased the maximum axial load of the column (Hadi et al. 2017). However, no analytical investigations have yet been carried out for the influence of different parameters (e.g., the compressive strength of SCC, tensile strength of steel tube, wall thickness of steel tube and pitch of steel helix) on the behaviour of SCC columns reinforced with steel tubes.

Detailed analytical investigations are required for the wide use of SCC columns reinforced with steel tubes. This paper develops an analytical model to predict the axial load-axial deformation behaviour of SCC columns reinforced with steel tubes. The results of the analytical model have been found well matching with the experimental investigation results. The influences of the compressive strength of SCC, tensile strength of steel tube, wall thickness of steel tube and pitch of steel helix on the axial

load-axial deformation behaviour of SCC columns reinforced with steel tubes have been investigated.

7.2 Research Significance

This study presents a simplified analytical model for the axial load-axial deformation behaviour of SCC columns reinforced with steel tubes. The analytical model takes into account the contributions of the steel tubes, unconfined concrete cover, confined concrete core and confined concrete inside the steel tube. The predictions of the developed analytical model have been found to be in good agreement with the experimental investigation results. The analytical observations, based on a detailed parametric study, reported in this study will contribute to good understanding on the axial load-axial deformation behaviour of SCC columns reinforced with steel tubes.

7.3 Analytical Modelling

The authors have recently proposed using small diameter steel tubes as longitudinal reinforcement for SCC columns. The innovative use of steel tubes for reinforcing SCC column was found to be highly effective, especially considering the maximum axial load and the ductility of the SCC columns (Hadi et al. 2017). The conventional SCC columns reinforced with steel bars usually consist of three main components: longitudinal steel bars, unconfined concrete cover and confined concrete core (Figure 7.1a). The SCC columns reinforced with steel tubes consist of four main components: longitudinal steel tubes, unconfined concrete cover, confined concrete core and confined concrete inside the steel tubes (Figure 7.1b).

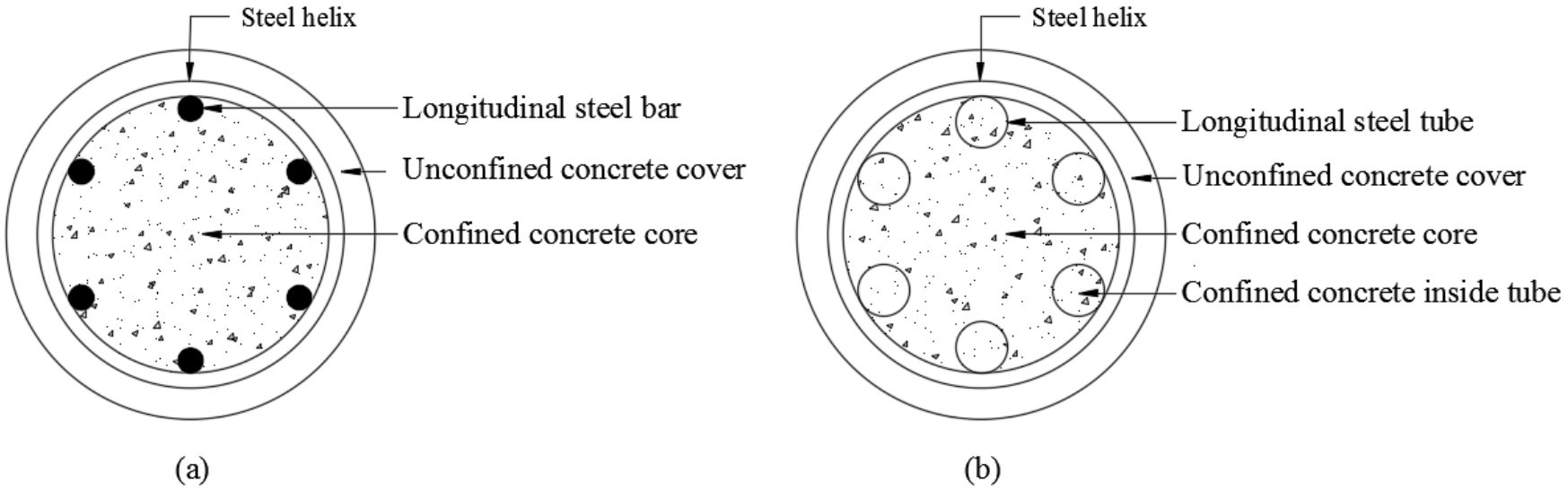

Figure 7.1: Cross-sections of the SCC columns: (a) column reinforced with steel bars; and (b) column reinforced with steel tubes

7.3.1 Modelling of Longitudinal Steel Tubes

A simplified stress-strain relationship is used in the analytical model of the longitudinal steel tubes. The stress-strain behaviour of the steel tubes under tension and compression is idealized as bilinear elasto-plastic (Equations 7.1a and 7.1b). The strain hardening response of the longitudinal steel tube was neglected for a simplified analytical model.

$$f_t = \varepsilon_t E_t \qquad \varepsilon_t \leq \varepsilon_{ty} \tag{7.1a}$$

$$f_t = f_{ty} \qquad \varepsilon_t > \varepsilon_{ty} \tag{7.1b}$$

where f_t is the stress of the steel tube, ε_t is the axial strain corresponding to the f_t, f_{ty} is the yield stress of the steel tube, ε_{ty} is the axial strain corresponding to the f_{ty} and E_t is the modulus of elasticity of the steel tube.

7.3.2 Modelling of Unconfined Concrete Cover

The stress-strain behaviour of self-compacting concrete (SCC) in Aslani and Nejadi (2012) is adopted to model the stress-strain behaviour of unconfined concrete cover in the SCC column. The stress-strain behaviour (Equation 7.2) of the SCC in Aslani and Nejadi (2012) is divided into two branches: ascending (Equation 7.3a) and descending (Equation 7.3b).

$$f_c = \frac{f_{co}\, n\, (\varepsilon_c/\varepsilon_{co})}{n-1+(\varepsilon_c/\varepsilon_{co})^n} \tag{7.2}$$

$$n = n_1 = \left[1.02 - 1.17(E_{sec,u}/E_c)\right]^{-0.74} \quad \text{if } \varepsilon_c \leq \varepsilon_{co} \tag{7.3a}$$

$$n = n_2 = n1 + (\varpi + 28 \times \xi) \qquad \text{if } \varepsilon_c > \varepsilon_{co} \tag{7.3b}$$

$$E_c = 3655 * (f_{co})^{0.548} \quad \text{(MPa)} \tag{7.4}$$

$$\varpi = (135.16 - 0.1744 \times f_{co})^{-0.46} \tag{7.5}$$

$$\xi = 0.83\exp(-911/f_{co}) \tag{7.6}$$

$$E_{sec,u} = \frac{f_{co}}{\varepsilon_{co}} \tag{7.7}$$

$$\varepsilon_{co} = \left(\frac{f_{co}}{E_c}\right)\left(\frac{\psi}{\psi-1}\right) \tag{7.8}$$

$$\psi = \left(\frac{f_{co}}{17}\right) + 0.8 \tag{7.9}$$

where ε_c is the axial strain at any unconfined concrete stress f_c; f_{co} is the unconfined concrete compressive strength; ε_{co} is the axial strain corresponding to f_{co}; E_c is the modulus of elasticity of SCC (with fly ash filler); $E_{sec,u}$ is the secant modulus of elasticity of unconfined concrete; n is the material parameter depending on the shape of the stress-strain curve; n_1 and n_2 are the modified material parameters at the ascending and descending branches, respectively; and ϖ and ξ are coefficients of linear equations expressed in term of f_{co}.

The unconfined concrete compressive strength f_{co} is considered equal to 28-day cylinder compressive strength (f_c') multiplied by a coefficient $\propto_1$ according to AS 3600 (2009). The coefficient $\propto_1$ is expressed as:

$$\propto_1 = 1.0 - 0.003 f_c' \quad (f_c' \text{ in MPa}) \qquad 0.72 \leq \propto_1 \leq 0.85 \tag{7.10}$$

7.3.3 Modelling of Confined Concrete

Two confined concrete models need to be used in the modelling SCC columns reinforced with longitudinal steel tubes for the stress-strain behaviour of confined concrete core and confined concrete inside the steel tubes. The concrete stress-strain model in Mander et al. (1988) is adopted to model the stress-strain behaviour of confined concrete core (Equation 7.11).

$$f_{cc} = \frac{f_{cc}' r_c \left(\varepsilon_{cc}/\varepsilon_{cc}'\right)}{r_c - 1 + \left(\varepsilon_{cc}/\varepsilon_{cc}'\right)^{r_c}} \tag{7.11}$$

$$r_c = \frac{E_c}{E_c - E_{sec,c}} \tag{7.12}$$

$$E_{sec,c} = \frac{f'_{cc}}{\varepsilon'_{cc}} \tag{7.13}$$

where ε_{cc} is the axial strain in concrete at any confined concrete stress f_{cc}, ε'_{cc} is the axial strain at the peak stress of confined concrete f'_{cc}, and $E_{sec,c}$ is the secant modulus of elasticity of the confined concrete. The f'_{cc} and ε'_{cc} are calculated using Equations (7.14) and (7.15), respectively.

$$f'_{cc} = f_{co}\left(2.254 \times \sqrt{1 + \frac{7.94 f_l}{f_{co}}} - \frac{2 f_l}{f_{co}} - 1.254\right) \tag{7.14}$$

$$\varepsilon'_{cc} = \varepsilon_{co}\left[1 + 5\left(\frac{f'_{cc}}{f_{co}} - 1\right)\right] \tag{7.15}$$

The ultimate confined concrete compressive strength in Mander et al. (1988) is usually used with normal strength concrete having a compressive strength ranging between 27 and 31 MPa (3.9 and 4.5 ksi). However, for concrete with the compressive strengths higher than 31 MPa (4.5 ksi), Bing et al. (2001) adjusted the peak stress of confined concrete f'_{cc} with a modification factor α_s (Equation (16)), which has been adopted herein.

$$f'_{cc} = f_{co}\left(2.254 \times \sqrt{1 + \frac{7.94 \alpha_s f_l}{f_{co}}} - \frac{2 \alpha_s f_l}{f_{co}} - 1.254\right) \tag{7.16}$$

$$\alpha_s = (21.2 - 0.35 f_{co})\frac{f_l}{f_{co}} \qquad when\ f_{co} \leq 52\ MPa \tag{7.17}$$

$$\alpha_s = 3.1\frac{f_l}{f_{co}} \qquad when\ f_{co} > 52\ MPa \tag{7.18}$$

where f_l is the effective confining pressure of the steel helix, which is calculated as:

$$f_l = \frac{1}{2}\, k_e\, \rho_{sh}\ f_{yh} \tag{7.19}$$

$$\rho_{sh} = \frac{4\, A_{sh}}{s\, D_c} \tag{7.20}$$

$$k_e = \frac{1 - \frac{s'}{2D_c}}{1 - \rho_{cc}} \tag{7.21}$$

where f_{yh} is the yield stress of steel helix, ρ_{sh} is the volumetric ratio of steel helix, A_{sh} is the area of steel helix, D_c is the centre-to-centre diameter of steel helix, k_e is the coefficient of the fully confined concrete core by steel helix, ρ_{cc} is the ratio of longitudinal steel area to the concrete core area, s is the centre-to-centre spacing of steel helix and s' is the clear spacing between the turns of steel helix.

The concrete stress-strain behaviour in Mander et al. (1988) is also adopted to model the stress-strain behaviour of confined SCC inside the steel tubes. However, the effective confining pressure provided by the steel tube is different from the effective confining pressure provided by the steel helix. The steel helix mainly provides confining pressure to the concrete core, whereas the steel tube resists axial stresses in addition to providing confinement to the concrete inside the steel tube. The common assumption adopted for the maximum confining pressure is that the steel helix will reach the yield stress (Mander et al. 1988). This assumption may not be applicable for the confining pressure provided by the steel tube. Thus, the effective confining pressure provided by the steel tube is calculated based on the equilibrium of forces using Equation (7.22).

$$f_{lt} = \frac{2\,\sigma_\theta t}{d_t - 2t} \tag{7.22}$$

where σ_θ is the hoop stress of the steel tube, d_t is the outside diameter of the steel tube, and t is the wall thickness of the steel tube. It is noted that a similar equation is also used for CFT columns (Wang et al. 2015). However, the hoop stress of the steel tube in SCC columns reinforced with steel tubes is different from the hoop stress of the CFT columns because steel tubes in SCC columns reinforced with steel tubes are subjected to the restraining effect provided by the concrete around the steel tube. The hoop stress of the steel tube in the SCC column reinforced with steel tubes is calculated as:

$$\sigma_\theta = \varepsilon_\theta\, E_t \tag{7.23}$$

where ε_θ is the hoop strain of the steel tube and E_t is the modulus of elasticity of the steel tube.

A hoop strain factor (α_θ) has been defined herein as:

$$\alpha_\theta = \sigma_\theta / f_{ty} \tag{7.24}$$

The α_θ of the CFT columns ranged 0.10 to 0.19 (Elremaily and Azizinamini 2002; Morino and Tasuda 2003). However, the α_θ of steel tube in SCC columns reinforced with steel tubes is higher than the α_θ of the CFT columns. This is because additional confining pressures are provided to the steel tube by the steel helix and the concrete around the steel tube in SCC columns reinforced with steel tubes.

7.4 Analytical Axial Load-Axial Deformation Behaviour

The axial load-axial deformation response of SCC columns reinforced with steel tubes is calculated based on the developed stress-strain responses of the SCC and steel tubes. For an axial strain, the stress in each component (longitudinal steel tubes, unconfined concrete cover, confined concrete core and confined concrete inside the steel tubes) is calculated. The axial deformation of the specimen is calculated by multiplying the considered axial strains with the total length of the specimen. The axial load contribution of each component is calculated by multiplying the stresses of each component with the respective cross-sectional area. The total axial load of the SCC columns reinforced with steel tubes is calculated as:

$$P_{axial} = f_t A_t + f_{c,cover} A_{cover} + f_{cc,core} A_{core} + f_{cc,tube} A_{tube} \tag{7.25}$$

where P_{axial} is the total axial load of specimens; f_t, $f_{c,cover}$, $f_{cc,core}$ and $f_{cc,tube}$ are the axial stresses in the longitudinal steel tubes, unconfined concrete cover, confined concrete core and confined concrete inside steel tubes, respectively; A_t, A_{cover}, A_{core}

and A_{tube} are the cross-sectional areas of longitudinal steel tubes, unconfined concrete cover, confined concrete core and confined concrete inside steel tubes, respectively.

7.5 Experimental Axial Load-Axial Deformation Behaviour

A total of four SCC column specimens reinforced with steel tubes were cast and tested under monotonic axial compression. All specimens were tested at the Structural Engineering Laboratories, School of Civil, Mining, and Environmental Engineering, University of Wollongong, Australia. The details of the experimental programme including the design of experiments, preparation and testing, failure modes and behaviour of the specimens under concentric, eccentric and flexural loads were presented in Hadi et al. (2017).

7.5.1 Details of the Column Specimens

All specimens were 240 mm (9.46 in.) in diameter and 800 mm (31.52 in.) in height. The SCC mix with a nominal compressive strength of 50 MPa (7.2 ksi) and a maximum aggregate size of 10 mm (0.394 in.) were used in casting the specimens. The first and second specimens were reinforced longitudinally with ST33.7 steel tubes. The ST33.7 steel tube had 33.7 mm (1.33 in.) outside diameter, 2 mm (0.079 in.) wall thickness and 350 MPa (50.7 ksi) nominal tensile strength. The first and second specimens were reinforced transversely with 50 mm and 75 mm (1.97 and 2.96 in.) pitch of the steel helices, respectively. The third and fourth specimens were reinforced longitudinally with ST26.9 steel tubes. The ST26.9 steel tube had 26.9 mm (1.06 in.) outside diameter, 2.6 mm (0.102 in.) wall thickness and 250 MPa (36.2 ksi) nominal tensile strength. The third and fourth specimens were also reinforced transversely with 50 mm and 75 mm (1.97 and 2.96 in.) pitch of the steel helices, respectively. Both ST33.7 and ST26.9 steel

tubes had approximately the same cross-sectional area. All specimens were reinforced transversely with R10 bar (10 mm (0.394 in.) diameter plain steel bar) with a nominal tensile strength of 250 MPa (36.2 ksi).

The SCC column specimens were labelled according to the type of longitudinal steel tubes and the pitch of the steel helix (Table 7.1). In the specimen label, ST33.7 and ST26.9 refer to the type of the steel tubes. Afterwards, H50 and H75 represent 50 mm and 75 mm (1.97 and 2.96 in.) pitch of the steel helices, respectively. The letter C at the end of the specimen label represents that the specimen was tested under concentric axial load. For example, ST26.9H50C refers to the column specimen reinforced longitudinally with ST26.9 steel tubes and transversely with 50 mm (1.97 in.) pitch of the steel helix and tested under concentric axial load. Table 7.1 provides details of the column specimens included in this study.

7.5.2 Materials Properties

The properties of fresh self-compacting concrete (SCC) were tested according to ASTM C1621/C1621M (ASTM 2014b), ASTM C1611/C1611M (ASTM 2014c) and ASTM C1610/C1610M (ASTM 2014d). The compressive strength of the SCC was determined by testing three cylinders of 100 mm (3.94 in.) diameter and 200 mm (7.88 in.) height according to ASTM C39/C39M (ASTM 2016). The average 28-day compressive strength of the SCC was 57 MPa (8.3 ksi). Two different steel tubes were used for steel tube reinforced SCC specimens: ST33.7 and ST26.9. Three samples from each of ST33.7 and ST26.9 tubes were tested according to ASTM A370 (ASTM 2014a). Yield stresses of both steel tubes were determined using the 0.2% offset method, as clearly defined yield stress was not observed.

Table 7.1: Details and experimental results of four column specimens tested under concentric load

No.	Specimen Designation	Longitudinal Reinforcement			Transverse Reinforcement		Experimental Results				
		Outside Diameter of Steel Tubes mm (in.)	Thickness of Tubes mm (in.)	Reinf. Ratio ρ_s (%)	Pitch mm (in.)	Reinf. Ratio ρ_{sh} (%)	Yield axial load kN (kip)	Corresponding axial deformation mm (in.)	Maximum axial load kN (kip)	Corresponding axial deformation mm (in.)	Ultimate axial deformation* mm (in.)
1	ST33.7H50C	33.7 (1.33)	2 (0.079)	2.64	50 (1.97)	3.3	2500 (563)	2.45 (0.097)	2729 (614)	3.29 (0.130)	33.5 (1.32)
2	ST33.7H75C	33.7 (1.33)	2 (0.079)	2.64	75 (2.96)	2.2	2395 (539)	2.65 (0.104)	2633 (592)	3.44 (0.136)	26.2 (1.03)
3	ST26.9H50C	26.9 (1.06)	2.6 (0.102)	2.63	50 (1.97)	3.3	2375 (534)	2.35 (0.093)	2598 (585)	3.03 (0.119)	36 (1.42)
4	ST26.9H75C	26.9 (1.06)	2.6 (0.102)	2.63	75 (2.96)	2.2	2275 (512)	2.2 (0.087)	2443 (550)	2.79 (0.110)	30.4 (1.20)

* Ultimate axial deformation was defined by the fracture of the steel helices.

The average yield stress (f_{ty}), yield strain (ε_{ty}) and modulus of elasticity (E_t) of ST33.7 steel tube were found as 450 MPa (65.2 ksi), 0.23% and 196 GPa (28420 ksi), respectively. The average yield stress, yield strain and modulus of elasticity of ST26.9 steel tube were found as 355 MPa (51.5 ksi), 0.187% and 192 GPa (27840 ksi), respectively.

Rounded steel R10 helices were used as transverse reinforcement in all of the specimens. Three samples of R10 rounded steel bars (gauge length 340 mm (13.40 in.)) were tested according to Australian Standard AS 1391 (2007). The yield stress of rounded steel bar was determined using the 0.2% offset method, as clearly defined yield stress was not observed. The average yield stress (f_{yh}), yield strain (ε_{yh}) and modulus of elasticity (E_{sh}) of R10 bars were found as 400 MPa (58.0 ksi), 0.22% and 195 GPa (28275 ksi), respectively.

7.5.3 Instrumentation

The test specimens were instrumented internally and externally to measure the strains of reinforcements (steel tubes and steel helices) and axial deformations of specimens. In order to observe the axial strains of longitudinal steel tubes, strain gauges were attached on the two opposite longitudinal steel tubes. Also, to observe the lateral strains of transverse reinforcement, two strain gauges were attached to the two opposite sides of the steel helices. All strain gauges were attached to the external faces of the longitudinal and transverse reinforcements at the midheight of the specimens. Two types of strain gauges were used in this study: single element strain gauges used for steel helices and biaxial two element strain gauges used for steel tubes. Biaxial two element strain gauges were used to measure both the axial and the lateral strains of the longitudinal steel tube.

The biaxial two element strain gauges were placed at the mid-height of the steel tubes ensuring that they were centrally placed between two turns of the helix.

The test specimens were instrumented with two linear variable differential transducers (LVDTs) fixed diagonally at opposite corners in the testing machine to measure the axial deformations. All specimens were tested in a 5000 kN (1125 kip) compression testing machine. Testing was carried out at a displacement controlled loading rate of 0.3 mm/min (0.012 in./min) until the failure of the specimen.

7.5.4 Experimental Results of the SCC Column Specimens

Experimental results of four SCC column specimens tested under concentric axial load in terms of yield axial load and corresponding axial deformation, maximum axial load and corresponding axial deformation and ultimate axial deformation are presented in Table 7.1. The ultimate axial deformation corresponds to the deformation at the fracture of steel helices. Although the cross-sectional areas of the ST33.7 and ST26.9 steel tubes are similar, the yield axial load of Specimen ST33.7H50C was 5% greater than the yield axial load of Specimen ST26.9H50C and the maximum axial load of Specimen ST33.7H50C was 4.8% greater than the maximum axial load of Specimen ST26.9H50C. The greater yield and maximum axial load of specimen reinforced with ST33.7 steel tubes were because ST33.7 steel tube had higher tensile strength than ST26.9 steel tube. Besides, ST33.7 steel tube had large inside and outside diameters compared to ST26.9 steel tube. The large inside diameter of ST33.7 steel tube allowed a large amount of concrete to be filled inside the tube which contributed in increasing the compressive strength of the column specimens. The large outside diameter of ST33.7

steel tube had a lower slenderness (s/d_t) ratio which positively contributed to the maximum axial load of Specimen ST33.7H50C.

Table 7.2 reports the strains in the longitudinal and transverse reinforcements for all tested specimens. In Column 1 of Table 7.2, the letters SA, SL and SH refer to the strain gauges that were placed on the steel tubes in the longitudinal direction, on the steel tubes in the lateral direction and on the steel helix in the lateral direction, respectively. The numbers 1 and 2 afterwards refer to the first and second strain gauges, respectively. The averages of the recorded strains are also reported in Table 7.2.

Table 7.2: The strains of the longitudinal and transverse reinforcements for the column specimens tested under concentric load

Labels of strain gauges	Strain gauge reading corresponding to the maximum load (%)			
	ST33.7H50C	ST26.9H50C	ST33.7H75C	ST26.9H75C
SA-1 (compression)	0.318	0.3	0.294	0.244
SA-2 (compression)	0.378	0.4	0.327	0.280
Average SA (compression)	0.348	0.35	0.311	0.262
SL-1 (tension)	0.092	0.059	0.070	0.045
SL-2 (tension)	0.088	0.093	0.078	0.043
Average SL (tension)	0.090	0.076	0.074	0.044
SH-1 (tension)	0.080	0.054	0.071	0.060
SH-2 (tension)	0.064	0.082	0.088	0.076
Average SH (tension)	0.072	0.068	0.080	0.068

The average axial strains in the longitudinal steel tubes indicated that steel tubes yielded at the maximum axial load. Also, it was found that the contribution of ST33.7 steel tubes was 29.8% of the maximum axial load of Specimen ST33.7H50C, whereas the contribution of ST33.7 steel tubes was 27.6% of the maximum axial load of Specimen ST33.7H75C. The contribution of ST26.9 steel tubes was 30.7% of the maximum axial load of Specimen ST26.9H50C, whereas the contribution of ST26.9 steel tubes was 24.5% of the maximum axial load of Specimen ST26.9H75C. The maximum axial load of steel tubes filled with concrete decreased with the increase in the s/d_t ratio of steel tubes (De Oliveira et al. 2010). Thus, increasing s/d_t ratio of the steel tubes resulted in the lower contributions of steel tubes in the maximum axial load of the tested column specimen.

The compressive strength of the confined concrete core and the compressive strength of the confined concrete inside the steel tube have been compared. It has been observed that steel tubes effectively confined the concrete inside the tube and resulted in higher axial compressive strengths of the SCC columns. To compare the compressive strength of the confined concrete core ($f_{cc,core}$) and confined concrete inside the steel tube ($f_{cc,tube}$), the enhancement factor of the confined concrete core ($f_{cc,core}/f_{co}$) and the confined concrete inside the steel tube ($f_{cc,tube}/f_{co}$) were calculated based on the developed stress-strain behaviours of the SCC and steel tubes (Table 7.3). The unconfined concrete strength (f_{co}) is taken as 0.95 times the 28-day cylinder compressive strength for concrete inside the steel tubes (ANSI 2010). For the concrete core confined by steel helix, the enhancement factors were 1.32 and 1.13 for the pitch of steel helices of 50 and 75 mm (1.97 and 2.96 in.), respectively. However, for the confined concrete inside ST33.7 steel tube, the enhancement factors were 2.6 and 2.25

for the pitch of steel helices of 50 and 75 mm (1.97 and 2.96 in.), respectively. Also, for confined concrete inside the ST26.9 steel tube, the enhancement factors were 3.41 and 2.34 for the pitch of steel helices of 50 and 75 mm (1.97 and 2.96 in.), respectively. It can be observed that the enhancement factors of the confined concrete inside steel tubes were higher than the enhancement factors of the confined concrete core for the same pitch of steel helices. The enhancement factor is higher inside the steel tube, which is because the concrete inside the steel tube was effectively confined by the wall of steel tube as well as the steel helix and the concrete around the steel tube.

Table 7.3: The concrete enhancement factor for the types of confined concrete in the SCC columns

Types of confined concrete in the specimens	Confined concrete [($f_{cc,core}$) or ($f_{cc,tube}$)] MPa (ksi)	Unconfined concrete (f_{co}) MPa (ksi)	concrete enhancement factor [($f_{cc,core}/f_{co}$) or ($f_{cc,tube}/f_{co}$)]
Confined concrete core [pitch =50 mm (1.97 in.)]	62.7 (9.1)	47.3 (6.9)	1.33
Confined concrete core [pitch =75 mm (2.96 in.)]	53.6 (7.8)	47.3 (6.9)	1.13
Confined concrete inside steel tube ST33.7 [pitch =50 mm (1.97 in.)]	141 (20.4)	54.2 (7.9)	2.60
Confined concrete inside steel tube ST33.7 [pitch =75 mm (2.96 in.)]	122 (17.7)	54.2 (7.9)	2.25
Confined concrete inside steel tube ST26.9 [pitch =50 mm (1.97 in.)]	185 (26.8)	54.2 (7.9)	3.41
Confined concrete inside steel tube ST26.9 [pitch =75 mm (2.96 in.)]	127 (18.4)	54.2 (7.9)	2.34

Note:
f_{co} represents the unconfined concrete strength.
$f_{cc,core}$ represents the compressive strength of the confined concrete core.
$f_{cc,tube}$ represents the compressive strength of the confined concrete inside the steel tube.

The enhancement factor of confined concrete inside the ST26.9 steel tube was 31% more than the enhancement factor of confined concrete inside the ST33.7 steel tube, when the pitch of steel helix was 50 mm (1.97 in.). The enhancement factor of the concrete inside the steel tube was larger for smaller diameter steel tube, as the strength of confined concrete inside the steel tube increased with decreasing the diameter of the steel tube (Sakino et al. 2004). Also, outside diameter to thickness (d_t/t) ratio of the ST26.9 steel tube was 10.35, whereas the d_t/t ratio of the ST33.7 steel tube was 16.85. The lower d_t/t ratio of steel tube provided higher confinement to the concrete inside the steel tube (Abed et al 2013). The steel helix also provided confinement to the steel tubes in the SCC column. This additional confinement by steel helix resulted in restricting the lateral dilation of the steel tube due to axial compression at the connecting area between the steel helix and steel tubes. Thus, the confinement of concrete inside steel tubes also decreases with the increase in the spacing of the steel helix.

7.6 Analytical versus Experimental Results

The analytical and experimental axial load-axial deformation behaviours of the SCC column specimens reinforced with steel tubes are compared (Figure 7.2). For all the column specimens, for the ascending part of the curve up to the maximum axial load, the analytical axial load-axial deformation curve correlated well with the experimental axial load-axial deformation curve. This good correlation is particularly because the stress-strain response of the different components of the specimens up to the maximum axial load was relatively linear. It can also be observed that, after the maximum axial load, the descending parts of the analytical axial load-axial deformation curves show good agreements with the experimental axial load-axial deformation curves.

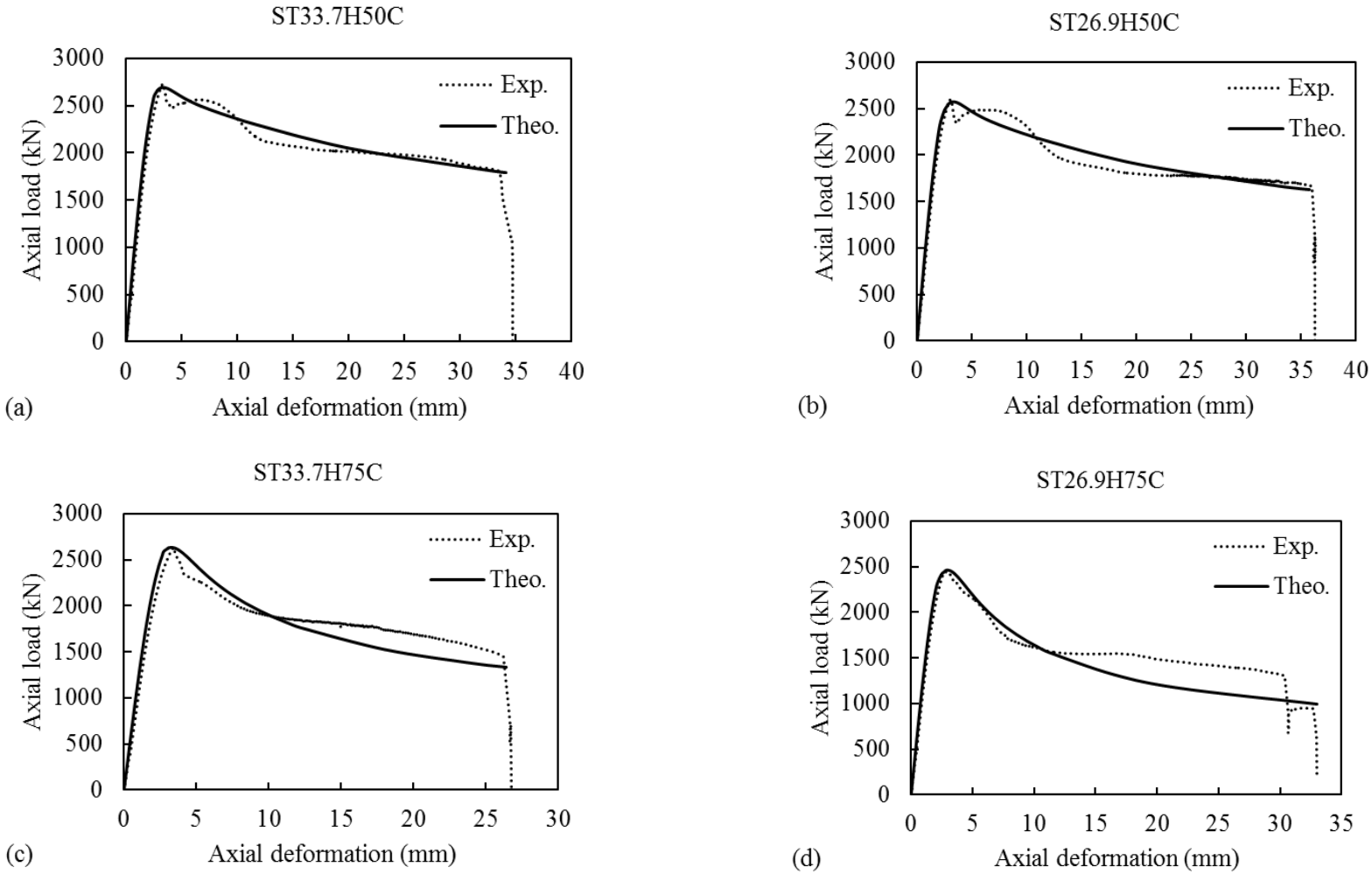

Figure 7.2: Comparison between analytical and experimental axial load-axial deformation behaviour of the tested specimens: (a) ST33.7H50C; (b) ST26.9H50C; (c) ST33.7H75C; and (d) ST26.9H75C . (Note: 1 mm = 0.0394 in.; 1 kN = 0.225 kip)

The experimental axial load-axial deformation curve shows a small drop and a rise in the descending part of the curve. However, the analytical axial load-axial deformation curve shows a gradual decrease in the descending part of the curve. The small drop in the experimental axial load-axial deformation curve has not been captured by the analytical curve, as the drop occurred instantaneously due to the spalling of concrete cover and then the axial load increased to a value less than the maximum axial load due to the confinement provided by the steel helices.

7.7 Parametric Study

The developed analytical model was used to study the influences of different parameters on the axial load-axial deformation behaviours of SCC columns reinforced with steel tubes. The parameters studied were the compressive strength of SCC, tensile strength of steel tube, wall thickness of steel tube and pitch of steel helix.

7.7.1 Effect of Concrete Compressive Strength

Four different concrete compressive strengths (30, 40, 50 and 57 MPa (4.3, 5.8, 7.2, 8.3 ksi)) were considered. The SCC columns were reinforced longitudinally with either ST33.7 steel tube or ST26.9 steel tube and transversely with 50 mm (1.97 in.) pitch of steel helix. The tensile strengths of ST33.7 and ST26.9 steel tubes were 450 MPa and 355 MPa (65.2 and 51.5 ksi), respectively, which were similar to the yield strength of the steel tubes used in reinforcing the tested column specimens.

The influence of concrete strength on the axial load-axial deformation behaviours of the SCC columns is shown in Figure 7.3. As expected, the maximum axial load of the SCC columns reinforced with steel tubes increased with the increase in the compressive

strength of concrete. It was observed that as the concrete compressive strength increased from 30 MPa to 57 MPa (4.3 ksi to 8.3 ksi), the maximum axial load of the columns reinforced with ST33.7 and ST26.9 steel tubes increased by about 22% and 24.6%, respectively (Figure 7.3). This is particularly because increasing the strength of concrete increased the contribution of the concrete to the maximum axial load of the column. Also, the maximum axial load of the steel tubes filled with concrete increased with increasing concrete strength (De Oliveira et al. 2009). For the descending part of the axial load-axial deformation response, the slope of the axial load-axial deformation curve after the maximum axial load increased with the increase in the concrete strength. Ozbakkaloglu and Saatcioglu (2004) reported that the reduction in the axial load capacity after the peak load was a function of the concrete strength and the rate of drop in the axial load carrying capacity increased with increasing concrete strength.

The ductility of columns was significantly influenced by the increase in the compressive strength of concrete. The ductility is an indication of the post-peak axial load-axial deformation behaviour. In this study, the ductility was calculated as a ratio of the axial deformation at the first helix fracture (δ_u) to the axial yield deformation (δ_y) (Pessiki and Pieroni 1997), as in Equation (26). The δ_y represents the deformation corresponding to the intersection point of a horizontal line from the maximum axial load and an extension secant line from the original point and the point at 0.75 times the maximum axial load (Foster, S. J., and Attard 1997).

$$Ductility = \delta_u/\delta_y \tag{7.26}$$

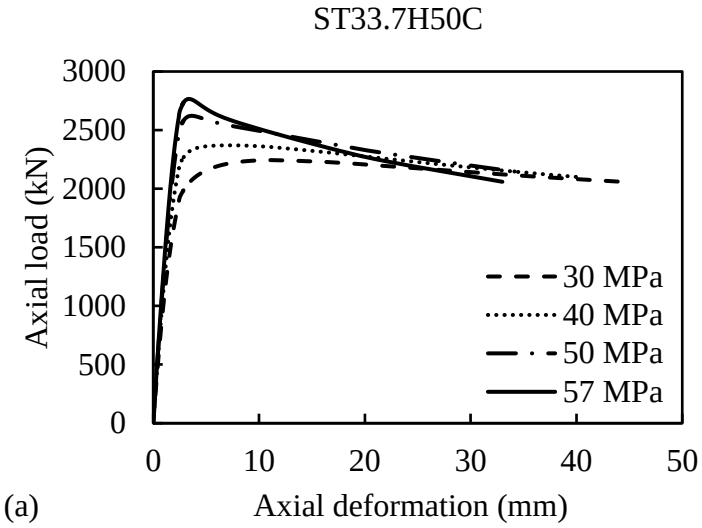

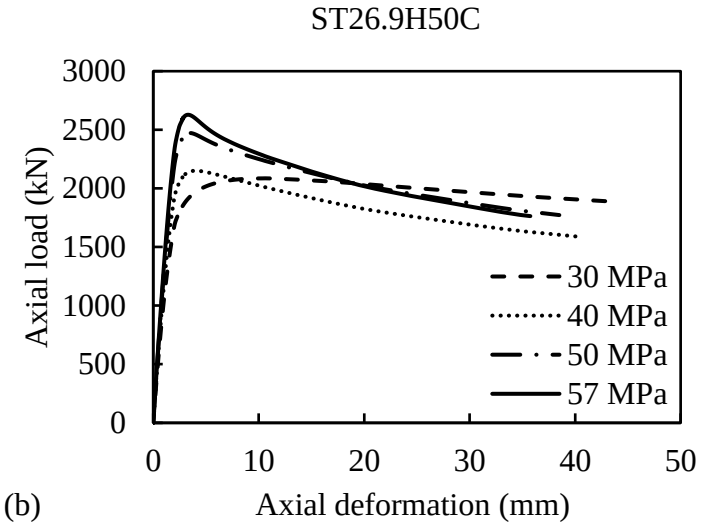

Figure 7.3: Influence of concrete strength on axial load-axial deformation behaviours for the SCC columns: (a) ST33.7H50C; and (b) ST26.9H50C

It was observed that as the compressive strength of concrete increased from 30 MPa to 57 MPa (4.3 ksi to 8.3 ksi), the ductility of Specimen ST33.7H50C decreased by about 14.4%, whereas the ductility of Specimen ST26.9H50C decreased by about 17.3% (Figure 7.3). For the increase in the compressive strength of concrete from 30 MPa to 57 MPa (4.3 ksi to 8.3 ksi), columns reinforced with ST26.9 steel tubes showed a rapid

descending axial load-axial deformation curve than columns reinforced with ST33.7 steel tubes. The s/d_t ratio of Specimen ST26.9H50C was 20% higher than the s/d_t ratio of Specimen ST33.7H50C, as the outside diameter of the ST26.9 steel tube was smaller than the outside diameter of the ST33.7 steel tube. Increasing s/d_t ratio of columns caused an increase in the slope of the post peak axial load-axial deformation of the column (Figure 7.3).

7.7.2 Effect of Tensile Strength and Wall Thickness of the Steel Tube

Steel tubes with four different tensile strengths (250, 355, 450 and 550 MPa (36.2, 51.5, 65.2 and 79.7 ksi)) and with four different wall thicknesses (1.5, 2.0, 2.6 and 3.0 mm (0.059, 0.079, 0.102 and 0.118 in.)) were considered. The SCC columns were reinforced longitudinally with either ST33.7 steel tube or ST26.9 steel tube and transversely with 50 mm pitch (1.97 in.) of steel helix. The compressive strength of the SCC was considered 57 MPa (8.3 ksi) which was similar to the compressive strength of the SCC used in casting the tested column specimens. The influence of tensile strength of steel tubes on axial load-axial deformation behaviours for the SCC columns is shown in Figure 7.4. It was observed that the tensile strength of the steel tubes did not influence the overall trend of the axial load-axial deformation behaviour of the SCC columns. However, it was observed that as the tensile strength of longitudinal steel tubes increased from 250 MPa to 550 MPa (36.2 ksi to 79.7 ksi), the maximum axial load of Specimens ST33.7H50C and ST26.9H50C increased by about 16.6% and 15%, respectively (Figure 7.4). The higher strength of longitudinal steel tubes increased the contribution of steel tube in carrying the axial load of the column.

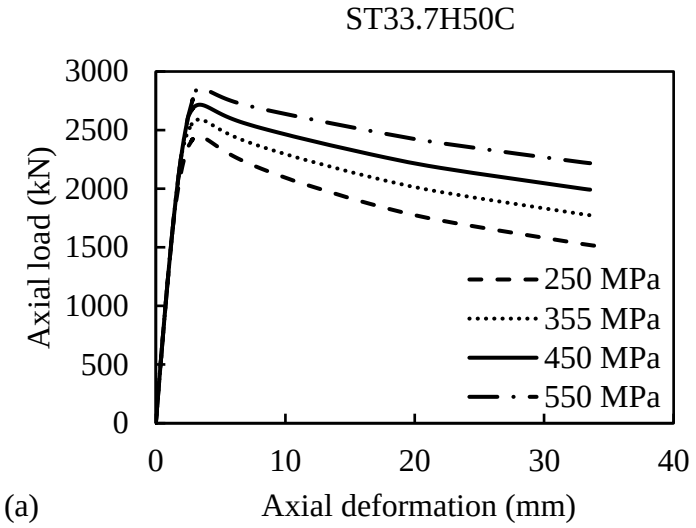

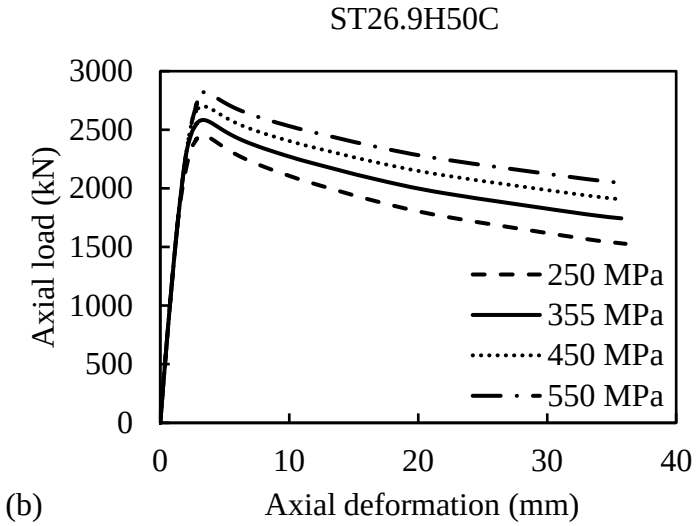

Figure 7.4: Influence of tensile strength of steel tubes on axial load-axial deformation behaviours for the SCC columns: (a) ST33.7H50C; and (b) ST26.9H50C

The influence of wall thicknesses of steel tubes on axial load-axial deformation behaviours for the SCC columns is shown in Figure 7.5. The thicknesses of steel tubes did not significantly influence the overall trend of the axial load-axial deformation behaviour of the columns. However, the maximum axial load of the SCC columns was increased with the increase in the wall thickness of steel tubes. It was observed that as

the wall thickness of steel tubes increased from 1.5 mm to 3.0 mm (0.059 in. to 0.118 in.), the maximum axial load of the columns reinforced with ST33.7 steel tubes increased by about 13.8%, whereas the maximum axial load of the columns reinforced with ST26.9 steel tubes increased by about 8.4% (Figure 7.5). The reason for the differences in the maximum axial load is associated with the cross-sectional area of the steel tube. The cross-sectional area of the ST33.7 steel tube was 28.4% larger than the cross-sectional area of the ST26.9 steel tube, when the wall thickness of the both steel tubes was considered 3 mm (0.118 in.). The higher wall thickness of steel tube increased the cross-sectional area of the steel tube and increased the contribution of steel tube in carrying the axial load of the column. Also, increasing wall thickness of steel tube increased the compressive strength of the concrete inside the steel tube and increased the compressive strength of the SCC column. The confinement of concrete inside the steel tube increased with decreasing d_t/t ratio of the steel tube.

In spite of the maximum axial load of the columns increased by the increase in the tensile strength and wall thickness of steel tube, the ductility of the SCC columns was not significantly influenced. For the increase of the wall thickness of steel tubes in the SCC columns from 1.5 mm to 3.0 mm (0.059 in. to 0.118 in.), the ductility of the SCC columns reinforced with steel tubes increased by only 6% (Figure 7.5). Although increasing the wall thickness of steel tube resulted in an increase in the strength and ductility of concrete inside the steel tubes, the concrete inside the steel tubes was a small proportion of the total cross-sectional area of the column.

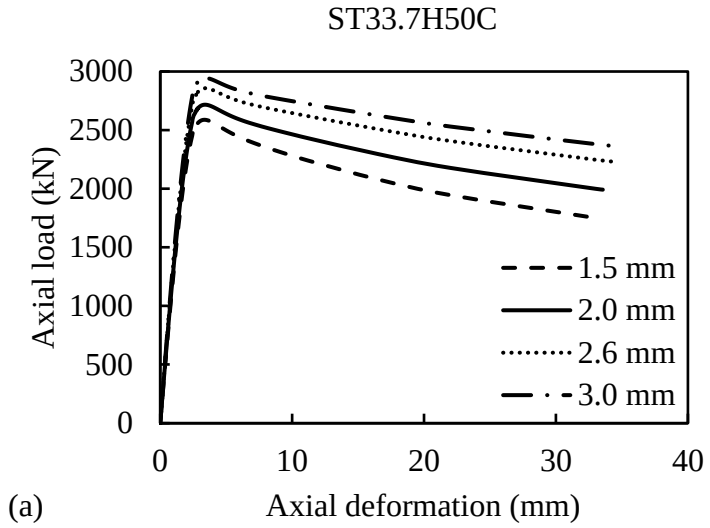

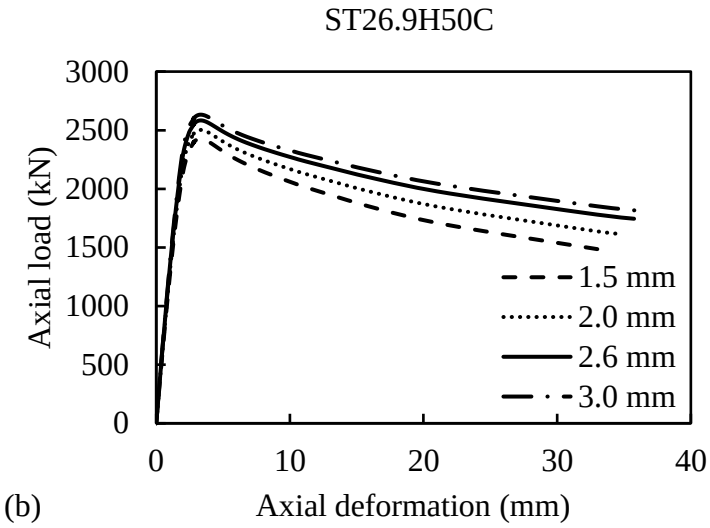

Figure 7.5: Influence of wall thicknesses of steel tubes on axial load-axial deformation behaviours for the SCC columns: (a) ST33.7H50C; and (b) ST26.9H50C

7.7.3 Effect of Pitch of Steel Helices

Four different pitches of steel helices (30, 50, 70 and 90 mm (1.18, 1.97, 2.76 and 3.55 in.)) were considered. The SCC columns were reinforced longitudinally with either ST33.7 steel tube or ST26.9 steel tube. The tensile strengths of ST33.7 and ST26.9 steel

tubes were 450 MPa and 355 MPa (65.2 ksi and 51.5 ksi), respectively. The compressive strength of the SCC was 57 MPa (8.3 ksi).

The influence of different pitch of steel helices on axial load-axial deformation behaviours of the SCC columns is shown in Figure 7.6. For SCC columns reinforced longitudinally with steel tubes and transversely with 30 mm (1.18 in.) pitch of steel helices, there are two peak axial loads in the axial load-axial deformation curves of the SCC columns. For SCC column reinforced with ST33.7 steel tubes, the first and second peak axial loads were 2840 and 3088 kN (639 and 695 kip), respectively. For SCC column reinforced with ST26.9 steel tubes, the first and second peak axial loads were 2695 and 2950 kN (606 and 664 kip), respectively. It is noted that the first peak axial load was sustained by the columns prior to the spalling of concrete cover and the second peak axial load was sustained by the confined concrete core. The second peak axial load was higher than the first peak axial load due to the confinement pressure provided by the closely spaced steel helix. The SCC columns reinforced transversely with steel helices having a pitch of 50 mm (1.97 in.) or larger did not show a second peak axial load. All columns showed the same initial behaviour up to the first peak axial load. However, for the increase of the pitch of steel helices from 30 to 90 mm (1.18 to 3.55 in.) in the SCC columns reinforced with ST26.9 steel tubes, the first peak axial load decreased by 10.6% (Figure 7.6). Whereas increasing the pitch of steel helices from 30 to 90 mm (1.18 to 3.55 in.) in the SCC columns reinforced with ST33.7 steel tubes, the first peak axial load decreased by 8.4% (Figure 7.6). The reason for the differences in the first peak axial loads is associated with the s/d_t ratio of steel tubes. The s/d_t ratio of the ST26.9 steel tube was 25% higher than the s/d_t ratio of the ST33.7 steel tube when the pitch of steel helix was 90 mm (3.55 in.).

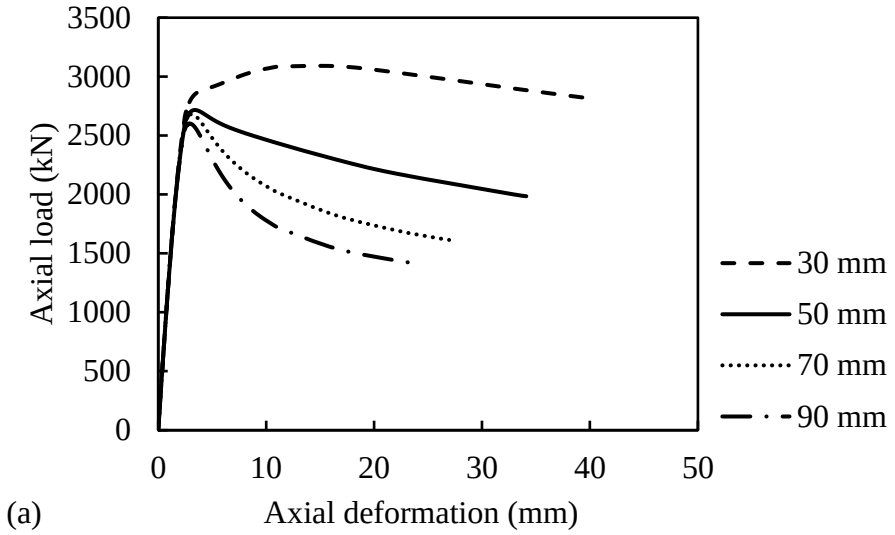

(a)

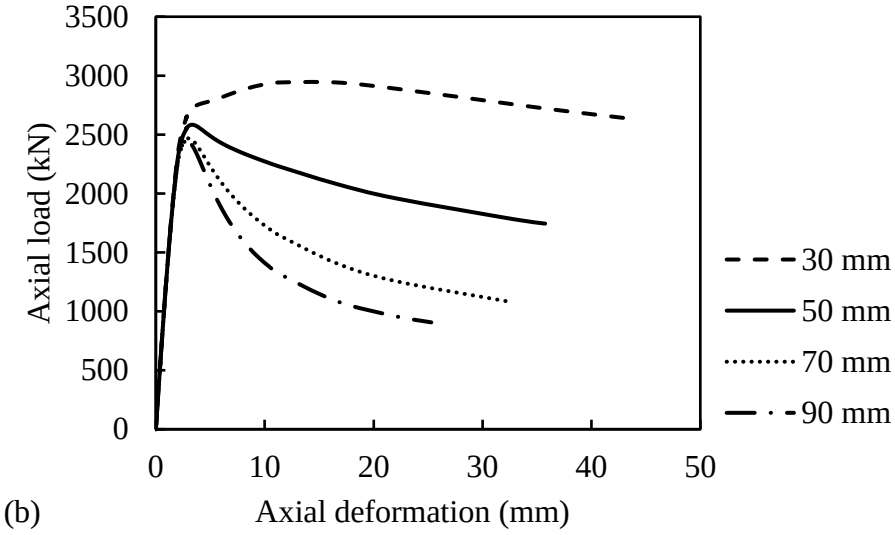

(b)

Figure 7.6: Influence of pitch of steel helices on axial load-axial deformation behaviours for the SCC columns: (a) columns reinforced with ST33.7 steel tubes; and (b) columns reinforced with ST26.9 steel tubes

It was observed that for increasing the pitch of steel helices from 30 to 90 mm (1.18 to 3.55 in.) in the SCC columns reinforced with ST26.9 steel tubes, the ductility decreased

by 40% (Figure 7.6). Whereas increasing the pitch of steel helices from 30 to 90 mm (1.18 to 3.55 in.) in the SCC columns reinforced with ST33.7 steel tubes, the ductility decreased by 37% (Figure 7.6). The higher ductility of the column transversely reinforced with a shorter spacing of steel helix is mainly attributed to the delay in the first helix fracture compared to the early first helix fracture of the column transversely reinforced with a larger spacing of steel helix. Increasing the pitch of steel helices from 30 to 90 mm (1.18 to 3.55 in.) in the SCC columns resulted in the increase of the s/d_t ratio of steel tubes. The ability of the column transversely reinforced with closely spaced steel helix in sustaining the lateral pressure provided by the longitudinal steel tubes under axial compression was higher than the ability of the column transversely reinforced with largely spaced steel helix. The lateral pressure exerted by the longitudinal steel tubes in the largely spaced steel helix resulted in the early yielding and fracturing of steel helix. Also, increasing the pitch of steel helices from 30 to 90 mm (1.18 to 3.55 in.) significantly influenced the descending part of the axial load-axial deformation behaviour of the SCC column and resulted in an increase of the slope of the post-peak axial load-axial deformation curve (Figure 7.6).

7.8 Conclusions

This study presents analytical investigations on the axial load-axial deformation behaviour of self-compacting concrete (SCC) columns reinforced with steel tubes. Two types of steel tubes were used in the SCC columns as longitudinal reinforcement. The influences of different parameters including the compressive strength of SCC, tensile strength of steel tube, wall thickness of steel tube and pitch of steel helix were investigated. Based on the analytical results of this study, the following conclusions are drawn:

1. The analytical axial load-axial deformation response of the SCC columns reinforced with steel tubes was calculated based on the stress-strain responses of the longitudinal steel tubes, unconfined concrete cover, confined concrete core and confined concrete inside the steel tube. The analytical and experimental axial load-axial deformation curves of columns showed good agreements.

2. The compressive strength of the confined concrete core and the compressive strength of the confined concrete inside the steel tube were compared. For the SCC columns reinforced transversely with steel helices having a pitch of 50 mm (1.97 in.), the enhancement factor of the confined concrete core was 1.32, whereas the enhancement factors of the confined concrete inside the ST33.7 and ST26.9 steel tubes were 2.6 and 3.41, respectively. The enhancement factors of the confined concrete inside the steel tubes were higher than the enhancement factors of the confined concrete core for the same pitch of steel helices. Thus, steel tubes effectively confined the concrete inside the tube and resulted in higher axial compressive strengths of the SCC columns.

3. As the concrete compressive strength increased from 30 MPa to 57 MPa (4.3 ksi to 8.3 ksi), the maximum axial load of the SCC columns reinforced with ST33.7 and ST26.9 steel tubes increased by about 23% and 24.6%, respectively. With the increase in the compressive strength of concrete from 30 MPa to 57 MPa (4.3 ksi to 8.3 ksi), the ductility of Specimen ST33.7H50C decreased by about 14.4%, whereas the ductility of Specimen ST26.9H50C decreased by about 17.3%.

4. As the tensile strength of longitudinal steel tubes increased from 250 MPa to 550 MPa (36.2 ksi to 79.7 ksi), the maximum axial load of Specimens ST33.7H50C and ST26.9H50C increased by about 16.6% and 15%, respectively. Also, as the wall thickness of longitudinal steel tubes increased from 1.5 mm to 3.0 mm (0.059 in. to

0.118 in.), the maximum axial load of the SCC columns reinforced with ST33.7 steel tubes increased by about 13.8%, whereas the maximum axial load of the SCC columns reinforced with ST26.9 steel tubes increased by about 8.4%. However, the ductility of SCC columns reinforced with steel tubes was not significantly influenced by the increase in the tensile strength and wall thickness of steel tube.

5. For SCC columns reinforced longitudinally with steel tubes and transversely with 30 mm pitch of steel helices, there are two peak axial loads in the axial load-axial deformation curves of the SCC columns. However, the SCC columns reinforced transversely with steel helices having a pitch of 50 mm (1.97 in.) or larger did not show a second peak axial load. For the increase of the pitch of steel helices from 30 to 90 mm (1.18 to 3.55 in.) in the SCC columns reinforced with ST26.9 steel tubes, the first peak axial load decreased by 10.6%. Whereas increasing the pitch of steel helices from 30 to 90 mm (1.18 to 3.55 in.) in the SCC columns reinforced with ST33.7 steel tubes, the first peak axial load decreased by 8.4%. The s/d_t ratio of the ST26.9 steel tube was 25% higher than the s/d_t ratio of the ST33.7 steel tube when the pitch of steel helix was 90 mm (3.55 in.).

6. For the increase of the pitch of steel helices from 30 to 90 mm (1.18 to 3.55 in.) in the SCC columns reinforced with ST26.9 steel tubes, the ductility decreased by 40%. Whereas increasing the pitch of steel helices from 30 to 90 mm (1.18 to 3.55 in.) in the SCC columns reinforced with ST33.7 steel tubes, the ductility decreased by 37%.

Notation

A_{core} = area of the concrete core confined by steel helix

A_{cover} = area of unconfined concrete cover

A_{sh} = cross-sectional area of the steel helix

A_t = cross-sectional area of the steel tube

A_{tube} = area of the confined concrete inside steel tubes

D_c = centre-to-centre diameter of the steel helix

d_t = outside diameter of the steel tube

E_c = modulus of elasticity of the concrete

E_{sh} = modulus of elasticity of the steel helix

$E_{sec,c}$ = confined secant modulus of elasticity of the concrete

$E_{sec,u}$ = unconfined secant modulus of elasticity of the concrete

E_t = modulus of elasticity of the steel tube

P_{axial} = total axial load of specimens

f_c = unconfined concrete stress

f_c' = 28-day cylinder concrete compressive strength

$f_{cc,core}$ = axial stress in the confined concrete core

$f_{cc,tube}$ = axial stress in the longitudinal steel tubes

f_{cc} = confined concrete stress

f_{cc}' = peak stress of confined concrete

f_{co} = unconfined concrete compressive strength which is equal to $\propto_1$ multiplied by f_c'

f_l = effective confining pressure of steel helix

f_{lt} = effective confining pressure of the steel tube

f_t = stress of the steel tube in the linear elastic portion

f_{ty} = yield stress of the steel tube

f_{yh} = yield stress of the steel helix

k_e = coefficient of the fully confined concrete core by steel helix

n_1 = modified material parameter at the ascending part

n_2 = modified material parameters at the descending part

s' = clear spacing of the steel helix

n = material parameter depending on the shape of stress-strain curve

s = pitch (centre-to-centre spacing) of the steel helix

t = wall thickness of the steel tube

$\propto_1$ = coefficient of concrete compressive strength, as given in AS 3600[20]

α_s = modification factor for the peak stress of confined concrete

α_θ = hoop strain factor

δ_u = axial deformation of the column at the first helix fracture

δ_y = axial yield deformation of the column

ε_c = axial strain corresponding to f_c

ε_{cc} = axial strain corresponding to f_{cc}

ε'_{cc} = axial strain corresponding to f'_{cc}

ε_{co} = axial strain corresponding to f_{co}

ε_t = axial strain corresponding to f_t

ε_{ty} = axial strain corresponding to f_{ty}

ε_{yh} = axial strain corresponding to f_{yh}

ε_θ = hoop strain of the steel tube

ρ_{cc} = ratio of longitudinal steel area to core area

ρ_s = longitudinal reinforcement ratio

ρ_{sh} = volumetric ratio of steel helix

σ_θ = hoop stress of the steel tube

ϖ, ξ = coefficients of linear equations for model Aslani and Nejadi[19]

Acknowledgment

The authors thank the University of Wollongong, Australia and technical officers at the High Bay Laboratory, especially Mr. Ritchie McLean, for their help in the experimental work of this study. Finally, the first author would like to acknowledge the Iraqi Government for the support of his PhD scholarship.

Reference

Abed, F., AlHamaydeh, M., and Abdalla, S. (2013). "Experimental and numerical investigations of the compressive behavior of concrete filled steel tubes (CFSTs)." *Journal of Constructional Steel Research*, 809, 429-439.

AISC. (2010). "Specification for structural steel buildings." *ANSI/AISC 360-10*, Chicago.

AS (Australian Standard). (2007). "Metallic materials-tensile testing at ambient temperature." *AS 1391-2007*, Sydney, NSW, Australia.

AS (Australian Standard). (2009). "Concrete structure." *AS 3600-2009*, Sydney, NSW, Australia.

Aslani, F., and Nejadi, S. (2012). "Mechanical properties of conventional and self-compacting concrete: An analytical study." *Construction and Building Materials*, 36, 330-347.

ASTM. (2014a). "Standard test method and definition for mechanical testing of steel products." *ASTM A370-14*, West Conshohocken, PA.

ASTM. (2014b). "Standard test method for passing ability of self-consolidating concrete by J-ring." *ASTM C1621/C1621M-14*, West Conshohocken, PA.

ASTM. (2014c). "Standard test method for slump flow of self-consolidating concrete." *ASTM C1611/C1611M-14*, West Conshohocken, PA.

ASTM. (2014d). "Standard test method for static segregation of self-consolidating concrete using column technique." *ASTM C1610/C1610M-14*, West Conshohocken, PA.

ASTM. (2016). "Standard test method for compressive strength of cylindrical concrete specimens." *ASTM C39/C39M-16*, West Conshohocken, PA.

Bing, L., Park, R., and Tanaka, H. (2001). "Stress-strain behavior of high-strength concrete confined by ultra-high- and normal-strength transverse reinforcements." *ACI Structural Journal*, 98(3), 395-406.

De Oliveira, W. L. A., De Nardin, S., El Debs, A. L. H. C., and El Debs, M. K. (2009). "Influence of concrete strength and length/diameter on the axial capacity of CFT columns." *Journal of Constructional Steel Research*, 65(12), 2103–2110.

De Oliveira, W. L. A., De Nardin, S., El Debs, A. L. H. C., and El Debs, M. K. (2010). "Evaluation of passive confinement in CFT columns." *Journal of Constructional Steel Research*, 66(4), 487-495.

EFNARC (European Federation of Specialist Construction Chemicals and Concrete Systems). (2002). "Specification and guidelines for self-compacting concrete." Norflolk, U.K., 1-32.

Elremaily, A., and Azizinamini, A. (2002). "Behavior and strength of circular concrete-filled tube columns." *Journal of Constructional Steel Research*, 58(12), 1567-1591.

Foster, S. J., and Attard, M. M. (1997). "Experimental tests on eccentrically loaded high-strength concrete columns." *ACI Structural Journal*, 94(3), 295-303.

Hadi, M. N. S., Alhussainy, F., and Sheikh, N. M. (2017). "Behavior of self-compacting concrete columns reinforced longitudinal with steel tubes." *Journal of Structural Engineering ASCE*, 143(6):1-14.

Hajjar, J. F. (2002). "Composite steel and concrete structural systems for seismic engineering." *Journal of Constructional Steel Research*, 58(5-8), 703-723.

Han, L.-H., Li, W., and Bjorhovde, R. (2014). "Developments and advanced applications of concrete-filled steel tubular (CFST) structures: members." *Journal of Constructional Steel Research*, 100, 211-228.

Khatab, M. A. T., Ashour, A. F., Sheehan, T., and Lam, D. (2017). "Experimental investigation on continuous reinforced SCC deep beams and comparisons with code provisions and models." *Engineering Structures*, 131, 264-274.

Lachemi, M., Hossain, K. M. A., and Lambros, V. B. (2006). "Axial load behavior of self-consolidating concrete-filled steel tube columns in construction and service stages." *ACI Structural Journal*, 103(1), 38-47.

Lin, C.-H., Hwang, C.-L., Lin, S.-P., and Liu, C.-H. (2008). "Self-consolidating concrete columns under concentric compression." *ACI Structural Journal*, 105(4), 425-432.

Mander, J. B., Priestley, M. J. N., and Park, R. (1988). "Theoretical stress-strain model for confined concrete." *Journal of Structural Engineering, ASCE*, 114(8), 1804-1826.

Moon, J., Lehman, D., Roeder, C., and Lee, H. (2013). "Strength of circular concrete-filled tubes with and without internal reinforcement under combined loading." *Journal of Structural Engineering ASCE*, 139(12), 04013012.

Morino, S., and Tasuda, K. (2002). "Design and construction of concrete-filled steel tube column system in Japan." *Earthquake Engineering and Engineering Seismology*, 4(1), 51-73.

Ozbakkaloglu, T., and Saatcioglu, M. (2004). "Rectangular stress block for high-strength concrete." *ACI Structural Journal*, 101(4), 475-483.

Paultre, P., Khayat, K. H., Cusson, D., and Tremblay, S. (2005). "Structural performance of self- consolidating concrete used in confined concrete columns." *ACI Structural Journal*, 102(4), 560-568.

Pessiki, S., and Pieroni, A. (1997). "Axial load behavior of large scale spirally reinforced high strength concrete columns." *ACI Structural Journal*, 94(3), 304-313.

Sakino, K., Nakahara, H., Morino, S., and Nishiyama, I. (2004). "Behavior of centrally loaded concrete-filled steel-tube short columns." *Journal of Structural Engineering, ASCE*, 130(2), 180-188.

Schneider, S. P. (1998). "Axially loaded concrete-filled steel tubes." *Journal of Structural Engineering ASCE*, 124(10), 1125-1138.

Susantha, K. A. S., Ge, H., and Usami, T. (2001). "Uniaxial stress–strain relationship of concrete confined by various shaped steel tubes." *Engineering Structures*, 23(10), 1331-1347.

Wang, X., Liu, J., and Zhang, S. (2015). "Behavior of short circular tubed-reinforced-concrete columns subjected to eccentric compression." *Engineering Structures*, 105, 77-86.

Wang, Y. C. (1999). "Tests on slender composite columns." *Journal of Constructional Steel Research*, 49(1), 25-41.

CHAPTER 8: AXIAL LOAD-BENDING MOMENT INTERACTIONS OF SELF-COMPACTING CONCRETE COLUMNS REINFORCED WITH STEEL TUBES

Summary

Chapter seven presented a simplified analytical model of SCC columns reinforced with steel tubes under concentric axial load. This chapter presents an analytical model for the axial load-bending moment interactions of SCC columns reinforced with steel tubes under different loading conditions including concentric axial load, 25 mm eccentric and 50 mm eccentric axial loads and flexural load. Results of the analytical model have been compared with experimental results of sixteen SCC column specimens. The predictions of the developed analytical model have been found to be in good agreement with the experimental investigation results. A parametric study was conducted to investigate the influences of the compressive strength of the SCC, tensile strength of the steel tube, wall thickness of the steel tube and pitch of the steel helix on the axial load-bending moment interactions of SCC columns reinforced with steel tubes. It was found that the compressive strength of concrete significantly influenced the maximum axial load capacity of the SCC columns under concentric, 25 mm eccentric and 50 mm eccentric axial loads, while the tensile strength of longitudinal steel tubes significantly influenced the maximum bending moment of SCC columns under flexural load.

It is important to mention that no slip of steel tubes occurred in the SCC columns under concentric axial loads. Under eccentric axial loads, the slip of steel tubes in the SCC columns occurred after the maximum axial load of the SCC was reached. The maximum axial loads of SCC columns under eccentric loads were used in determining the axial

load-bending moment interaction of SCC columns. In addition, under flexural loads, the problem of slip of steel tubes was adequately prevented in the SCC columns.

Citation

This chapter has been submitted for possible publication to the Journal of Engineering Structures with the following citation:

Alhussainy F, Sheikh MN, Hadi MNS. (2018). "Axial load-bending moment interactions of self-compacting concrete columns reinforced with steel tubes." *Engineering Structures*, (Under review).

Highlights

- Behaviour of SCC columns reinforced with steel tubes is analytically investigated.
- An analytical model for load-moment interactions of SCC columns is developed.
- Results of the analytical model are in good agreement with the experimental results.
- Compressive strength of concrete significantly influences the axial load of SCC columns.
- Tensile strength of steel tubes significantly influences the pure moment of SCC columns.

Abstract

In this study, an analytical model has been developed for the axial load-bending moment interactions of self-compacting concrete (SCC) columns reinforced with steel tubes. The developed analytical model takes into account the contributions of the steel tubes, unconfined concrete cover, confined concrete core and confined concrete inside the steel tube. Results of the analytical model were compared with experimental investigation results of sixteen SCC column specimens of 240 mm diameter and 800 mm height. The results of the analytical model have been found to be in good agreement

with the experimental results. A parametric study was conducted to investigate the influences of the compressive strength of the SCC, tensile strength of the steel tube, wall thickness of the steel tube and pitch of the steel helix on the axial load-bending moment interactions of SCC columns reinforced with steel tubes. It was found that the compressive strength of concrete significantly influenced the maximum axial load capacity of the SCC columns under concentric, 25 mm eccentric and 50 mm eccentric axial loads, while the tensile strength of longitudinal steel tubes significantly influenced the maximum bending moment of SCC columns under flexural load.

Keywords: Composite columns; self-compacting concrete; steel tube; axial load; eccentricity; stress-strain.

8.1 Introduction

Steel sections are usually used in the construction of composite columns in two forms: steel section encased in concrete (commonly known as encased steel section columns) and steel section infilled with concrete (commonly known as concrete filled steel tube columns) (Shanmugam and Lakshmi 2001). The composite columns constructed with steel sections and concrete are generally used in high-rise buildings due to their high axial load capacity, ductility as well as fire and seismic resistance (Johansson and Gylltof 2002; Patel et al. 2015; Ouyang et al. 2017; Li et al. 2017; Liu et al. 2017). In concrete filled steel tube (CFT) columns, steel tubes act as longitudinal and also as transverse reinforcement (Yu et al. 2007). The infill concrete prevents the local buckling of the steel tube. The traditional CFT column is usually constructed by filling the steel tube with concrete without using any internal reinforcement (Han 2002; Du et al. 2016; Lai and Varma 2016). Longitudinal and transverse steel reinforcement can also be used

in the CFT columns to increase the strengths of CFT columns and to provide better connections between the CFT columns and other structural elements (Xiamuxi and Hasegawa 2012; Moon et al. 2013). Also, the addition of steel reinforcement in the CFT columns reduces the problem of local buckling of large-diameter steel tubes (Chen et al. 2017). Circular steel tube sections are usually preferred in the construction of the CFT columns because the wall of the circular steel tube resists the lateral concrete pressure by membrane-type hoop stresses compared to the steel plate bending of the square or rectangular steel tubes (Sehneider 1998).

The CFT columns are usually constructed of normal vibrated concrete (NVC). Recently, the self-compacting concrete (SCC) is also used in the construction of CFT columns (Li et al. 2017; Han and Yao 2004). The SCC possesses excellent engineering properties including high flowability, passing ability, and segregation resistances (EFNARC 2002; Ahari et al. 2015; Ghafoori et al. 2016). The SCC can flow and consolidate under its own weight (Heirman et al. 2008). Hence, no vibration is required for compaction (Barluenga et al. 2017).

Han et al. (2005) examined the behaviour of square and circular CFT columns constructed of SCC under axial load. The test results showed that the failure mode of CFT columns constructed of SCC was similar to the failure mode of CFT columns constructed of NVC. It was also found that the resistance of the local buckling by circular CFT columns was more than the resistance of the local buckling by square CFT columns. Zhu et al. (2010) examined the performance of axially loaded composite columns constructed of high strength SCC with steel tubes and steel sections. Square steel tubes with cruciform steel and I-shaped steel sections were used in the construction

of composite columns. The test results indicated that the failure modes of the composite columns (steel tubes with encased steel sections) were quite different from the failure modes of the traditional CFT columns without encased steel sections because the encased steel sections delayed the formation of shear sliding cracks.

Recently, the behaviour of a new type of composite column constructed with SCC and reinforced with small diameter circular steel tubes was investigated by Hadi et al. (2017). The use of steel tubes in reinforcing SCC columns showed several advantages including high maximum axial load and high ductility. For the same cross-sectional area, the radius of gyration of a circular steel tube is higher than the radius of gyration of a solid steel bar. Hence, the bending stiffness of the steel tube is higher than the bending stiffness of the steel bar. It was found that the steel tube sections effectively confined the infill concrete (Hadi et al. 2017). Also, the infill concrete prevented local buckling of the steel tube by changing the failure mode from inward to outward buckling (Alhussainy et al. 2017). Hence, for the similar tensile strength and cross-sectional area of steel tubes and steel bars, the maximum axial load and ductility of the SCC columns reinforced with steel tubes are higher than the SCC columns reinforced with steel bars (Hadi et al. 2017). However, no analytical study, encompassing the influences of different parameters, has yet been conducted to investigate the behaviour of SCC columns reinforced with small diameter steel tubes.

This paper develops an analytical model to predict the axial load-bending moment interactions of SCC columns reinforced with small diameter steel tubes. The analytical model has been validated with the experimental results of Hadi et al. (2017). The analytical model takes into account the contributions of the steel tubes, unconfined

concrete cover, confined concrete core and confined concrete inside the steel tube. The results of the analytical model have been found to be well matching with the experimental investigation results. The influences of the compressive strength of the SCC, tensile strength of the steel tube, wall thickness of the steel tube and pitch of the steel helix on the axial load-bending moment interactions of SCC columns reinforced with steel tubes have been investigated.

8.2 Development of an Analytical Model

The SCC columns reinforced with steel tubes can be broadly divided into four main components: (1) longitudinal steel tubes, (2) unconfined concrete cover, (3) confined concrete core and (4) confined concrete inside the steel tubes (Figure 1). Each component of the SCC column reinforced with small diameter steel tubes contributes to sustaining the axial load. The stress-strain relationships of the components of SCC columns reinforced with small diameter steel tubes are presented below.

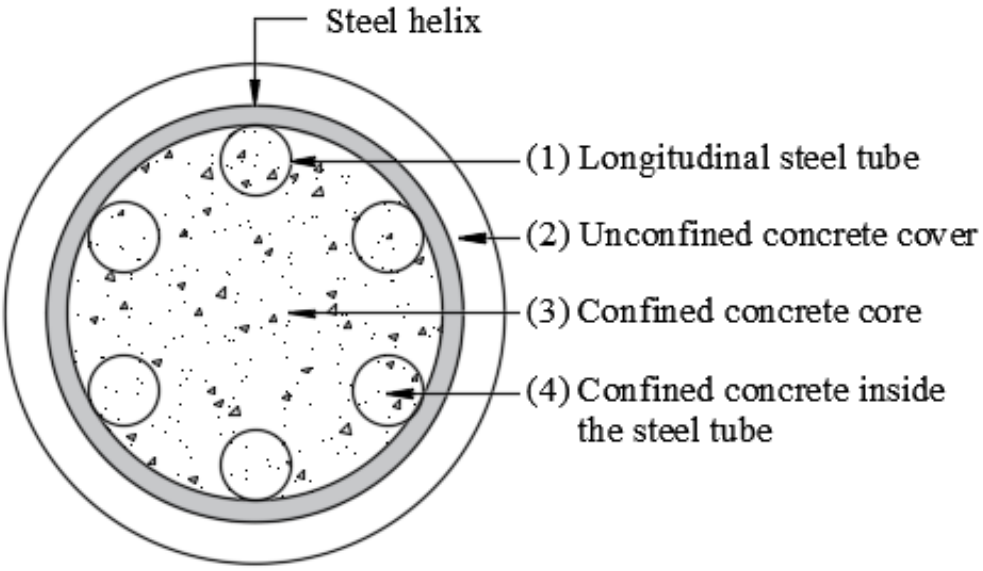

Figure 8.1: Components in the SCC column reinforced with steel tubes

8.2.1 Longitudinal Steel Tubes

A simplified stress-strain relationship of the longitudinal steel tubes is used in the analytical model. The stress-strain relationship of the steel tubes under tension and compression is idealized as bilinear elasto-plastic (Equations 8.1a and 8.1b). The strain hardening response of the longitudinal steel tube was neglected for the simplified analytical model.

$$f_t = \varepsilon_t E_t \qquad \varepsilon_t \leq \varepsilon_{ty} \tag{8.1a}$$

$$f_t = f_{ty} \qquad \varepsilon_t > \varepsilon_{ty} \tag{8.1b}$$

where f_t is the axial stress of the steel tube; f_{ty} is the yield stress of the steel tube; ε_t is the axial strain corresponding to the f_t; ε_{ty} is the axial strain corresponding to the f_{ty}; and E_t is the modulus of elasticity of the steel tube.

8.2.2 Unconfined Concrete Cover

The stress-strain relationship of self-compacting concrete (SCC) in Aslani and Nejadi (2012) is adopted to model the stress-strain relationship of unconfined concrete cover in the SCC column specimens (Equation 8.2).

$$f_c = \frac{f_{co}\, n'\, (\varepsilon_c/\varepsilon_{co})}{n' - 1 + (\varepsilon_c/\varepsilon_{co})^{n'}} \tag{8.2}$$

$$n' = n'_1 = \left[1.02 - 1.17(E_{sec,u}/E_c)\right]^{-0.74} \quad \text{If } \varepsilon_c \leq \varepsilon_{co} \tag{8.3a}$$

$$n' = n'_2 = n'_1 + (\varpi + 28 \times \xi) \qquad \text{If } \varepsilon_c > \varepsilon_{co} \tag{8.3b}$$

$$E_c = 3655 \times (f_{co})^{0.548} \quad \text{(MPa)} \tag{8.4}$$

$$\varpi = (135.16 - 0.1744 \times f_{co})^{-0.46} \tag{8.5}$$

$$\xi = 0.83\exp(-911/f_{co}) \tag{8.6}$$

$$E_{sec,u} = \frac{f_{co}}{\varepsilon_{co}} \tag{8.7}$$

$$\varepsilon_{co} = \left(\frac{f_{co}}{E_c}\right)\left(\frac{\psi}{\psi - 1}\right) \tag{8.8}$$

$$\psi = \left(\frac{f_{co}}{17}\right) + 0.8 \tag{8.9}$$

where f_c is the unconfined concrete stress; f_{co} is the unconfined concrete compressive strength; ε_c is the axial strain corresponding to f_c; ε_{co} is the axial strain corresponding to f_{co}; E_c is the modulus of elasticity of the SCC; $E_{sec,u}$ is the secant modulus of elasticity of the unconfined concrete; n' is a material parameter depending on the shape of stress-strain curve; n_1' and n_2' are the modified material parameters for the ascending branch (Equation 8.3a) and descending branch (Equation 8.3b), respectively; and ϖ, ξ and ψ are coefficients expressed in terms of f_{co}.

The unconfined concrete compressive strength f_{co} is assumed to equal to 28-day cylinder compressive strength (f_c') multiplied by the coefficient $\propto_1$ according to AS 3600 (2009). The coefficient $\propto_1$ is expressed as:

$$\propto_1 = 1.0 - 0.003 f_c' \quad (f_c' \text{ in MPa}) \qquad 0.72 \leq \propto_1 \leq 0.85 \tag{8.10}$$

8.2.3 Confined Concrete Core

Two confined concrete stress-strain relationships are needed for the SCC columns reinforced with small diameter longitudinal steel tubes: stress-strain relationship of confined concrete core and the stress-strain relationship of confined concrete inside the steel tubes. The concrete stress-strain relationship in Mander et al. (1988) is used to model the stress-strain relationship of the confined concrete core (Equation 8.11).

$$f_{cc} = \frac{f_{cc}' r_c \left(\varepsilon_{cc}/\varepsilon_{cc}'\right)}{r_c - 1 + \left(\varepsilon_{cc}/\varepsilon_{cc}'\right)^{r_c}} \tag{8.11}$$

$$r_c = \frac{E_c}{E_c - E_{sec,c}} \tag{8.12}$$

$$E_{sec,c} = \frac{f_{cc}'}{\varepsilon_{cc}'} \tag{8.13}$$

where f_{cc} is the confined concrete stress; f'_{cc} is the peak stress of confined concrete; ε_{cc} is the axial strain corresponding to f_{cc}; ε'_{cc} is the axial strain corresponding to f'_{cc}; and $E_{sec,c}$ is the secant modulus of elasticity of the confined concrete. The f'_{cc} and ε'_{cc} are calculated using Equations (8.14) and (8.15), respectively.

$$f'_{cc} = f_{co}\left(2.254 \times \sqrt{1 + \frac{7.94 f_l}{f_{co}}} - \frac{2 f_l}{f_{co}} - 1.254\right) \tag{8.14}$$

$$\varepsilon'_{cc} = \varepsilon_{co}\left[1 + 5\left(\frac{f'_{cc}}{f_{co}} - 1\right)\right] \tag{8.15}$$

where f_l is the effective confining pressure of the steel helix, which is calculated as:

$$f_l = \frac{1}{2}\, k_e\, \rho_{sh}\; f_{yh} \tag{8.16}$$

$$\rho_{sh} = \frac{4\, A_{sh}}{s\, D_c} \tag{8.17}$$

$$k_e = \frac{1 - \frac{s'}{2D_c}}{1 - \rho_{cc}} \tag{8.18}$$

where k_e is the coefficient of the confined concrete core by the steel helix; ρ_{sh} is the volumetric ratio of the steel helix; f_{yh} is the yield tensile stress of the steel helix; A_{sh} is the area of the steel helix; D_c is the centre-to-centre diameter of the steel helix; ρ_{cc} is the ratio of area of longitudinal steel reinforcement to the area of the concrete core of the column; s is the centre-to-centre spacing of the steel helix; and s' is the clear spacing between the turns of the steel helix.

The peak stress of confined concrete (f'_{cc}) in Mander et al. (1988) is usually used with normal strength concrete having the compressive strength of 31 MPa. However, for concrete with the compressive strength higher than 31 MPa, Bing et al. (2001) adjusted the peak stress of confined concrete f'_{cc} with a modification factor α_s (Equations 8.19-8.21), which has been adopted in this study.

$$f'_{cc} = f_{co}\left(2.254 \times \sqrt{1 + \frac{7.94\alpha_s f_l}{f_{co}}} - \frac{2\alpha_s f_l}{f_{co}} - 1.254\right) \quad (8.19)$$

$$\alpha_s = (21.2 - 0.35 f_{co})\frac{f_l}{f_{co}} \qquad when\ f_{co} \leq 52\ MPa \quad (8.20)$$

$$\alpha_s = 3.1\frac{f_l}{f_{co}} \qquad when\ f_{co} > 52\ MPa \quad (8.21)$$

8.2.4 Confined Concrete inside the Steel Tubes

To model the stress-strain relationship of confined SCC inside the steel tubes, the concrete stress-strain relationship in Mander et al. (1988) is also adopted (Equation 8.11). However, for the SCC inside the steel tubes, the unconfined concrete compressive strength f_{co} of the SCC is assumed to be equal to 28-day cylinder compressive strength (f'_c) multiplied by the coefficient of compressive strength of concrete ($\propto_1$). The $\propto_1$ is taken equal to 0.95 in this study, according to the AISC (2010). In addition, the effective confining pressure provided by the steel tube is different from the effective confining pressure provided by the steel helix. The steel helix mainly provides confining pressure to the concrete core, whereas steel tube resists axial stresses in addition to providing confinement to the concrete inside the steel tube. The common assumption adopted for the maximum confining pressure was that the steel helix would reach its yield stress (Mander et al. 1988). This assumption may not be applicable to the confining pressure provided by the steel tube. Thus, the effective confining pressure provided by the steel tube is calculated based on the equilibrium of forces (Figure 8.2) using Equation (8.22).

$$f_{lt} = \frac{2\,t\,\sigma_\theta}{d_t - 2t} \quad (8.22)$$

where t is the wall thickness of the steel tube; d_t is the outside diameter of the steel tube; and σ_θ is the hoop stress of the steel tube. It is noted that a similar equation is used to calculate the effective confining stress for circular CFT columns (Liu et al. 2017). However, the hoop stress of the small diameter steel tube in SCC columns is different

from the hoop stress of the CFT columns because the small diameter steel tubes used in reinforcing SCC columns have restraining effect by the concrete around the steel tube. The hoop stress of the steel tube in the SCC column is calculated as:

$$\sigma_\theta = \varepsilon_\theta \, E_t \tag{8.23}$$

where ε_θ is the hoop strain of the steel tube and E_t is the modulus of elasticity of the steel tube.

At the maximum axial load, the experimental hoop stress of the longitudinal steel tube in the SCC columns can be used to calculate the coefficient hoop factors (α_θ) as:

$$\alpha_\theta = \sigma_\theta / f_{ty} \tag{8.24}$$

The α_θ of the CFT columns ranges between 0.10 and 0.19 (Elremaily and Azizinamini 2002; Morino and Tasuda 2002). However, the α_θ of steel tubes used in reinforcing SCC columns is higher than the α_θ of the CFT columns, because of the additional confinement provided by the steel helix and the concrete around the steel tube.

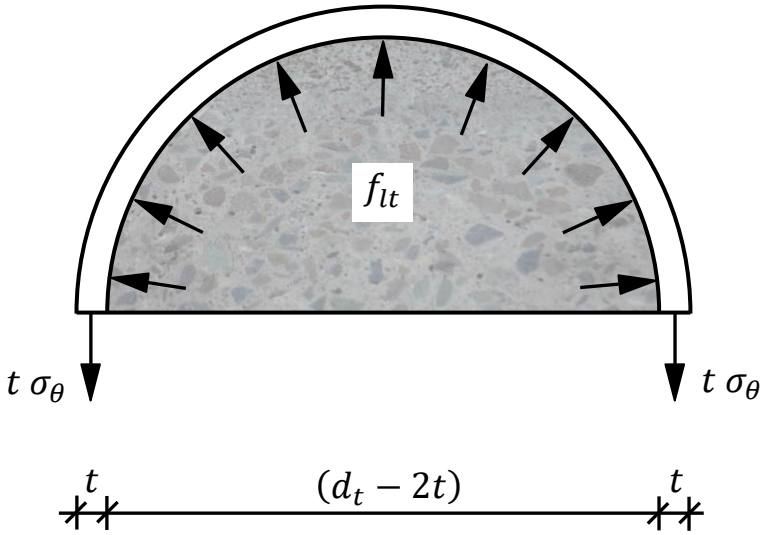

Figure 8.2: The effective confining pressure of the steel tube filled with SCC

8.3 Analytical Axial Load-Bending Moment Interactions

The analytical axial load-bending moment (P-M) interactions of SCC columns reinforced with steel tubes are constructed based on the stress-strain relationships for the longitudinal steel tubes, unconfined concrete cover, confined concrete core and confined concrete inside steel tubes.

For SCC columns under concentric axial load, the axial load contribution of each component of the column was calculated by multiplying the stresses of each component with the respective cross-sectional area. For an axial strain, the stress in each component (longitudinal steel tubes, unconfined concrete cover, confined concrete core and confined concrete inside the steel tubes) is calculated. The total axial load of the SCC columns reinforced with steel tubes is calculated as:

$$P_{axial} = f_t A_t + f_{c,cover} A_{cover} + f_{cc,core} A_{core} + f_{cc,tube} A_{tube} \qquad (8.25)$$

where P_{axial} is the total axial load of columns under concentric axial load; f_t, $f_{c,cover}$, $f_{cc,core}$ and $f_{cc,tube}$ are the axial stress in the longitudinal steel tubes, axial stress in the unconfined concrete cover, axial stress in the confined concrete core and axial stress in the confined concrete inside steel tubes, respectively; and A_t, A_{cover}, A_{core} and A_{tube} are the cross-sectional areas of longitudinal steel tubes, unconfined concrete cover, confined concrete core and confined concrete inside steel tubes, respectively.

For SCC columns under 25 and 50 mm eccentric axial loads and flexural loads, the compressive force of the concrete was determined by using the layer-by-layer integration method. The cross-section of the column was divided into n number of small parallel layers, as shown in Figure 8.3.

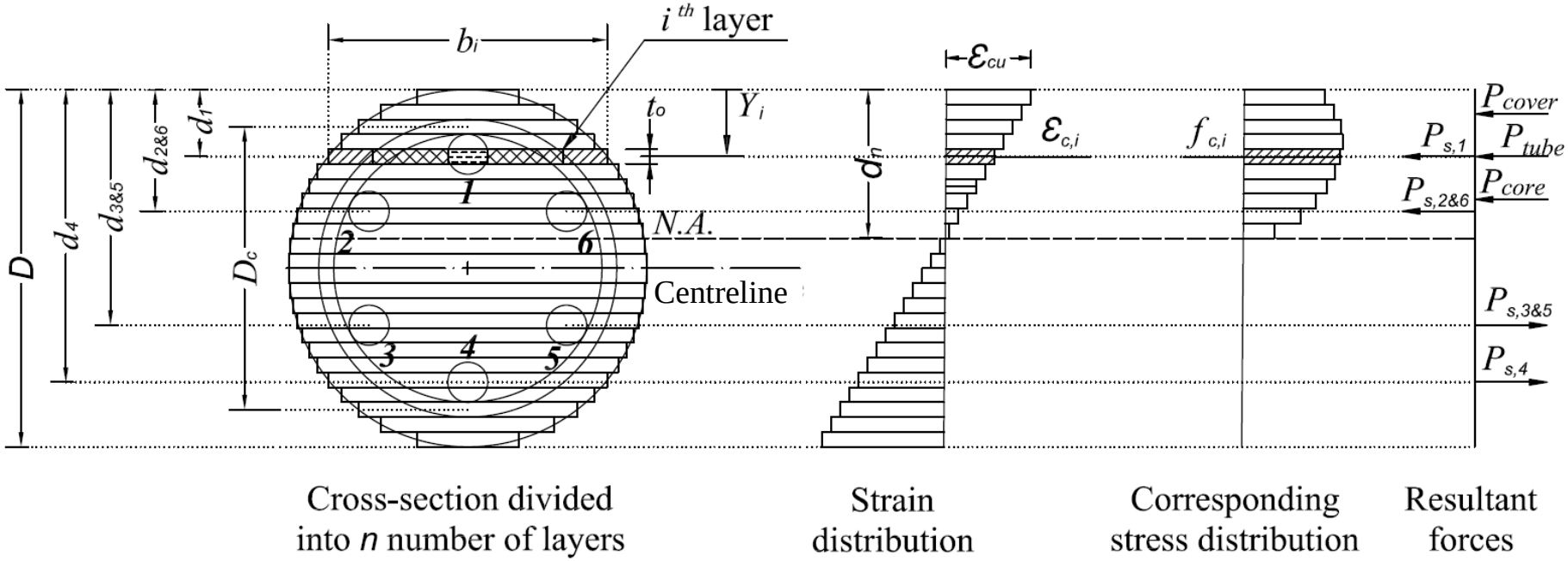

Figure 8.3: Layer-by-layer integration method

The thickness of each layer (t_o) is calculated by dividing the diameter of the column (D) by n. In this study, the n is taken equal to the diameter of the column. Hence, t_o is equal to 1 mm. The distance from the extreme concrete compressive fibre to the mid-height of each layer (Y_i) can be calculated as:

$$Y_i = \left(i - \frac{1}{2}\right) t_o \tag{8.26}$$

where, i = 1, 2, 3,….., n, starting from the top of the section. Based on the location of the concrete layer, the average width of each component of the layer ($b_{cover,i}$, $b_{core,i}$ and $b_{tube,i}$) can be calculated using Equation (8.27) to Equation (8.31).

$$b_{(inside\ helix),i} = 0 \qquad \text{for} \quad \left(\frac{D}{2} + \frac{D_c}{2}\right) \leq Y_i \leq \left(\frac{D}{2} - \frac{D_c}{2}\right) \tag{8.27a}$$

$$b_{(inside\ helix),i} = 2 \times \sqrt{\left(\frac{D_c}{2}\right)^2 - \left(\frac{D}{2} - Y_i\right)^2} \quad \text{for} \quad \left(\frac{D}{2} - \frac{D_c}{2}\right) < Y_i < \left(\frac{D}{2} + \frac{D_c}{2}\right) \tag{8.27b}$$

$$b_{cover,i} = 2 \times \sqrt{\left(\frac{D}{2}\right)^2 - \left(\frac{D}{2} - Y_i\right)^2} - b_{(inside\ helix),i} \tag{8.28}$$

For the layers within the concrete core that do not cross the tubes:

$$b_{core,i} = b_{(inside\ helix),i} \tag{8.29}$$

For the layers within the concrete core that crosses the tubes:

$$b_{core,i} = b_{(inside\ helix),i} - b_{tube,i} \tag{8.30}$$

For the steel tubes:

$$b_{j,i} = 0 \qquad \text{for} \quad \left(d_j + \frac{d_t}{2}\right) \leq Y_i \leq \left(d_j - \frac{d_t}{2}\right) \tag{8.31a}$$

$$b_{j,i} = 2 \times \sqrt{\left(\frac{d_t}{2}\right)^2 - \left(d_j - Y_i\right)^2} \quad \text{for} \quad \left(d_j - \frac{d_t}{2}\right) < Y_i < \left(d_j + \frac{d_t}{2}\right) \tag{8.31b}$$

where, j = 1, 2, 3,…., m; m is number of longitudinal steel tubes in the column and d_j is the distance from the extreme concrete compressive fibre to the centreline of the steel tube.

The strain distribution within the circular column cross-section is considered linear by assuming plane sections remain plane after bending. The strain ($\varepsilon_{c,i}$) at the centre of each layer can be calculated as:

$$\varepsilon_{c,i} = \varepsilon_{cu} \times \frac{d_n - Y_i}{d_n} \tag{8.32}$$

where ε_{cu} is the ultimate strain of concrete and d_n is the depth of neutral axis ($N.A.$), as shown in Figure 8.3.

After calculating the strain in each layer, the corresponding stresses at the centre of each layer are calculated according to the stress-strain relationships of unconfined concrete, confined concrete core and confined concrete inside the steel tubes. It is noted that the tensile strength of concrete is ignored in the calculations.

The compressive forces at the centre of each concrete layer can be calculated using Equation (8.33) to Equation (8.35).

$$P_{cover,i} = f_{cover,i} \times b_{cover,i} \times t_o \tag{8.33}$$

$$P_{core,i} = f_{core,i} \times b_{core,i} \times t_o \tag{8.34}$$

$$P_{tube,i} = f_{tube,i} \times b_{tube,i} \times t_o \tag{8.35}$$

where $P_{cover,i}$, $f_{cover,i}$ and $b_{cover,i}$ are the compressive force, compressive stress and width, respectively, of the concrete cover in the i^{th} layer; $P_{core,i}$, $f_{core,i}$ and $b_{core,i}$ are the compressive force, compressive stress and width, respectively, of the concrete core

in the i^{th} layer; and $P_{tube,i}$, $f_{tube,i}$ and $b_{tube,i}$ are the compressive force, compressive stress and width, respectively, of the concrete inside the steel tube in the i^{th} layer.

The bending moment for each layer is calculated by multiplying the force in each layer by the distance from the centre of each layer to the centreline of the circular column cross-section. The total force of the concrete cross-section is calculated as the summation of the forces acting on the layers. The tensile forces are considered negative while the compressive forces are considered positive. Therefore, the axial load carrying capacity of the column (P_T) is equal to the summation of the forces acting on the concrete and forces acting on the steel tubes (Equation 8.36). Similarly, the moment carrying capacity is equal to the sum of the moments with respect to the plastic centroid of the specimen cross-section under a given axial load eccentricity (Equation 8.37).

$$P_T = \sum_{i=1}^{n}\left(P_{cover,i} + P_{core,i} + P_{tube,i}\right) + \sum_{j=1}^{m} P_{s,j} \quad (8.36)$$

$$M_T = \sum_{i=1}^{n}\left(P_{cover,i} + P_{core,i} + P_{tube,i}\right)\left(\frac{D}{2} - Y_i\right) + \sum_{j=1}^{m} P_{s,j}\left(\frac{D}{2} - d_j\right) \quad (8.37)$$

where, $P_{s,j}$ is the force of the steel tube.

8.4 Experimental Program

The details of the experimental program including the design of experiments, specimen preparation and testing, failure modes and behaviour of the specimens under concentric axial load, eccentric axial load and flexural load were presented in Hadi et al. (2017). All specimens were tested at the Structural Engineering Laboratories, School of Civil, Mining, and Environmental Engineering, University of Wollongong, Australia. For clarity, the SCC specimens reinforced with steel tubes under different loading conditions are briefly reviewed in this paper.

A total of 16 self-compacting concrete (SCC) specimens reinforced with steel tubes were cast and tested under different loading conditions. All specimens were 240 mm in diameter and 800 mm in height. The specimens were divided into four groups with four specimens in each group. For each group, the first specimen was tested under concentric axial load, the second and third specimens were tested under 25 and 50 mm eccentric axial loads, respectively, and the last specimen was tested under flexural load. The specimens in the first and second groups were reinforced longitudinally with ST33.7 steel tubes. The ST33.7 steel tube had 33.7 mm outside diameter, 2 mm wall thickness and 350 MPa nominal tensile strength. The specimens in the first and second groups were reinforced transversely with steel helices at 50 mm and 75 mm pitch, respectively. The specimens in the third and fourth groups were reinforced longitudinally with ST26.9 steel tubes. The ST26.9 steel tube had 26.9 mm outside diameter, 2.6 mm wall thickness and 250 MPa nominal tensile strength. The specimens in the third and fourth groups were also reinforced transversely with steel helices at 50 mm and 75 mm pitch, respectively. All specimens were reinforced transversely with 10 mm diameter round steel bar (R10). The nominal tensile strength of the R10 bar was 250 MPa. Table 8.1 provides details of the SCC specimens reinforced with small diameter steel tubes.

Table 8.1: Details of SCC specimens reinforced with steel tubes included in this study (Hadi et al. 2017)

Group Name	Specimen Labels	Longitudinal Reinforcement				Transverse Reinforcement		Loading Conditions
		Number of Steel Tubes	Outside Diameter of Steel Tubes (mm)	Thickness of Tubes (mm)	Reinforcement Ratio, ρ_s (%)	Pitch (mm)	Reinforcement Ratio, ρ_{sh} (%)	
ST33.7-H50	ST33.7-H50-C	6	33.7	2	2.64	50	3.3	Concentric
	ST33.7-H50-E25	6	33.7	2	2.64	50	3.3	e = 25 mm
	ST33.7-H50-E50	6	33.7	2	2.64	50	3.3	e = 50 mm
	ST33.7-H50-F	6	33.7	2	2.64	50	3.3	Flexural
ST33.7-H75	ST33.7-H75-C	6	33.7	2	2.64	75	2.2	Concentric
	ST33.7-H75-E25	6	33.7	2	2.64	75	2.2	e = 25 mm
	ST33.7-H75-E50	6	33.7	2	2.64	75	2.2	e = 50 mm
	ST33.7-H75-F	6	33.7	2	2.64	75	2.2	Flexural
ST26.9-H50	ST26.9-H50-C	6	26.9	2.6	2.63	50	3.3	Concentric
	ST26.9-H50-E25	6	26.9	2.6	2.63	50	3.3	e = 25 mm
	ST26.9-H50-E50	6	26.9	2.6	2.63	50	3.3	e = 50 mm
	ST26.9-H50-F	6	26.9	2.6	2.63	50	3.3	Flexural
ST26.9-H75	ST26.9-H75-C	6	26.9	2.6	2.63	75	2.2	Concentric
	ST26.9-H75-E25	6	26.9	2.6	2.63	75	2.2	e = 25 mm
	ST26.9-H75-E50	6	26.9	2.6	2.63	75	2.2	e = 50 mm
	ST26.9-H75-F	6	26.9	2.6	2.63	75	2.2	Flexural

8.5 Analytical versus Experimental Results

The analytical and experimental axial load-bending moment (P-M) interactions of the SCC specimens reinforced with small diameter steel tubes are compared (Figure 8.4). Experimental P-M interactions of SCC specimens were constructed based on four points: concentric axial load, 25 and 50 mm eccentric axial loads, and flexural load (Hadi et al. 2017). It was found that the analytical P-M interactions were in good agreement with the experimental P-M interactions. Under concentric axial load, the analytical and experimental maximum axial loads were similar. Hence, the maximum axial load of the SCC columns under concentric axial load calculated by the superposition of the load-deformation behaviour of the different components (longitudinal steel tubes, unconfined concrete cover, confined concrete core and confined concrete inside the steel tubes) represented the maximum axial load of the column reasonably accurately.

Under 25 mm eccentric axial load, the analytical maximum axial load and bending moment calculated for SCC columns longitudinally reinforced with ST33.7 steel tubes and transversely reinforced with either 50 mm or 75 mm pitch of the steel helix were about 4% smaller than the experimental maximum axial load and bending moment. The analytical maximum axial load and bending moment calculated for SCC columns longitudinally reinforced with ST26.9 steel tubes and transversely reinforced with 50 mm pitch of the steel helix were about 5% smaller than the experimental maximum axial load and bending moment. However, the analytical maximum axial load and bending moment calculated for SCC columns longitudinally reinforced with ST26.9 steel tubes and transversely reinforced with 75 mm pitch of the steel helix were about 2% higher than the experimental maximum axial load and bending moment. The lower

experimental maximum axial load and bending moment of the column might be because the slip of ST26.9 steel tube in the concrete, which occurred due to the higher slenderness (s/d_t) ratio of ST26.9 compared to the slenderness ratio of ST33.7.

Under 50 mm eccentric axial load, the analytical maximum axial load and bending moment calculated for SCC columns longitudinally reinforced with ST33.7 steel tubes and transversely reinforced with either 50 mm or 75 mm pitch of the steel helix were about 7% smaller than the experimental maximum axial load and bending moment. The analytical maximum axial load and bending moment calculated for SCC columns longitudinally reinforced with ST26.9 steel tubes and transversely reinforced with 50 mm pitch of the steel helix were about 9% smaller than the experimental maximum axial load and bending moment. The analytical maximum axial load and bending moment calculated for SCC columns longitudinally reinforced with ST26.9 steel tubes and transversely reinforced with 75 mm pitch of the steel helix were about 4% smaller than the experimental maximum axial load and bending moment. It is evident that the results of the analytical model match very well with the experimental investigation results of SCC column specimens under concentric and eccentric axial loads.

Under flexural load, the experimental bending moments of specimens reinforced with ST33.7 and ST26.9 steel tubes were about 45-55% higher than the analytical bending moments. The higher experimental bending moments was because the specimens tested under flexural load had a shear span to depth ratio less than twice the effective depth of the concrete cross-section. Hence, the failure of the specimens might not be due to the pure bending. None-the less, the analytical model provides satisfactory estimates of the maximum axial load and bending moment of the SCC columns reinforced with small diameter steel tubes (Figure 8.4).

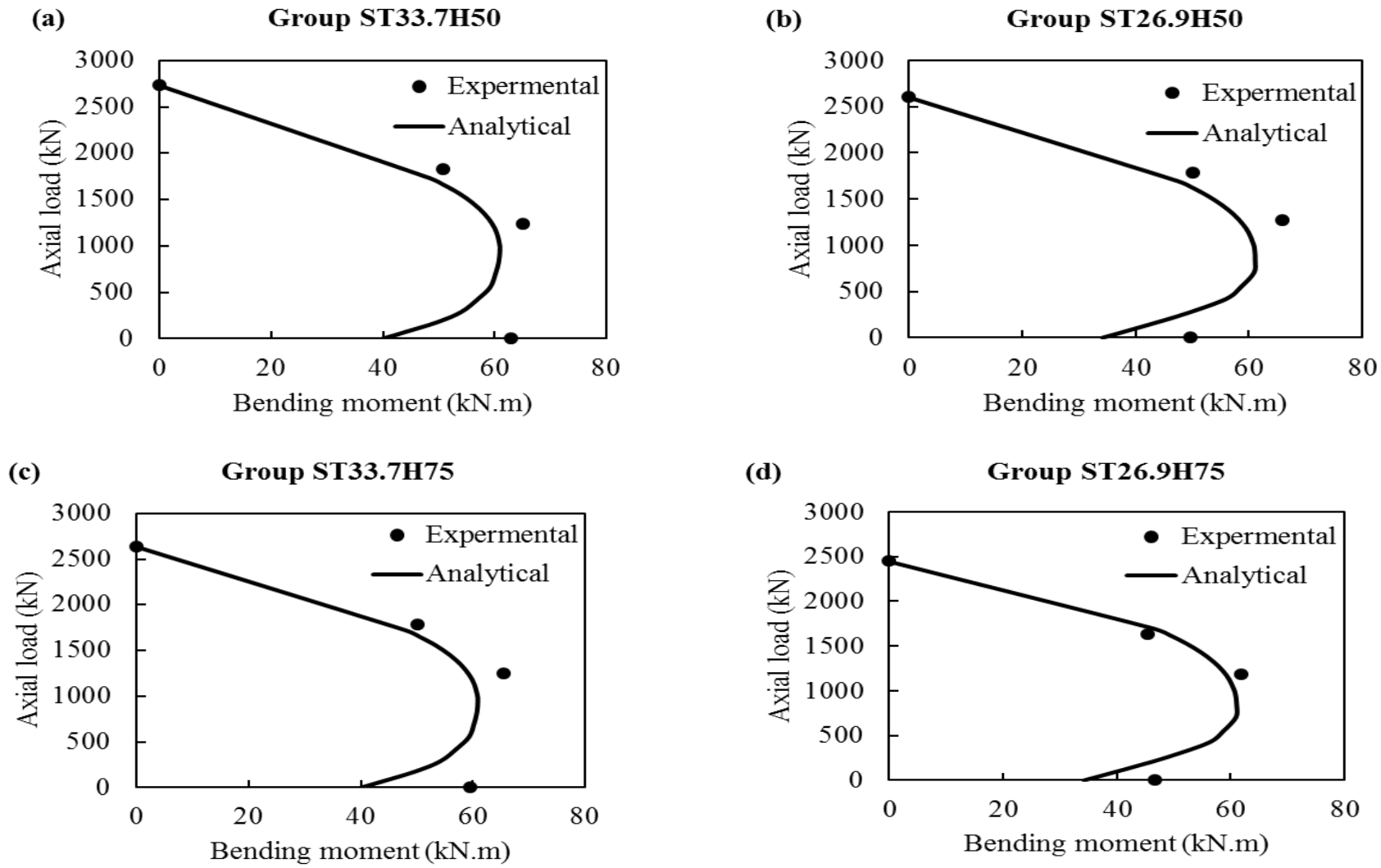

Figure 8.4: Comparison between analytical and experimental axial load-bending moment interactions of the tested specimens in Hadi et al. (2017): (a) Group ST33.7H50; (b) Group ST26.9H50; (c) Group ST33.7H75; and (d) Group ST26.9H75

8.6 Parametric Study

The developed analytical model was used to study the influences of different parameters on the axial load-bending moment (P-M) interactions of SCC columns reinforced with steel tubes. The parameters studied were the compressive strength of the SCC, tensile strength of the steel tube, wall thickness of the steel tube and pitch of the steel helix.

8.6.1 Influence of Compressive Strength of Concrete

Four different compressive strengths of concrete (30 MPa, 40 MPa, 50 MPa and 57 MPa) were considered. The SCC columns were reinforced longitudinally with either six ST33.7 or six ST26.9 steel tubes and transversely with 50 mm pitch of the steel helix of 10 mm diameter. The tensile strengths of ST33.7 and ST26.9 steel tubes were 450 MPa and 355 MPa, respectively, which were similar to the yield strength of the steel tubes used in reinforcing the tested specimens in Hadi et al. (2017). The influence of compressive strength of concrete on the P-M interactions of the SCC columns reinforced with small diameter steel tubes is shown in Figure 8.5. It was observed that the maximum axial load and bending moment capacities of the columns increased with the increase in the compressive strength of concrete.

For the increase of the compressive strength of concrete from 30 MPa to 57 MPa, under concentric axial load, the maximum axial load of the SCC columns reinforced with ST33.7 steel tubes increased from 2236 kN to 2729 kN. The maximum axial load of the SCC columns reinforced with ST26.9 steel tubes increased from 2085 kN to 2598 kN. For the increase of the compressive strength of concrete from 30 MPa to 57 MPa, the maximum axial load of the SCC columns reinforced with ST33.7 and ST26.9 steel tubes increased by about 22% and 24.6%, respectively (Table 8.2). Increase in the

compressive strength of concrete increased the contribution of the concrete to the axial load carrying capacity of the column. Also, the axial load capacity of the steel tubes filled with concrete increased with increasing compressive strength of concrete (Oliveira et al. 2009). The confinement of the concrete inside the ST26.9 steel tubes was higher than the confinement of the concrete inside the ST33.7 steel tubes because the outside diameter to thickness (d_t/t) ratio of ST26.9 steel tube was 39% lower than the d_t/t ratio of ST33.7 steel tube. The lower d_t/t ratio of steel tube provided higher confinement to the concrete inside the steel tube (Uy et al. 2011).

For the increase of the compressive strength of concrete from 30 MPa to 57 MPa, under concentric, 25 mm eccentric and 50 mm eccentric axial load, the maximum axial load capacities of the SCC columns increased by 493 kN, 469 kN and 316 kN, respectively (Table 8.2). Under concentric, 25 mm eccentric and 50 mm eccentric axial load, the contributions of the concrete were 70%, 67% and 60%, respectively, in the maximum axial load capacity of the SCC column. For the increase of the compressive strength of concrete from 30 MPa to 57 MPa, under 25 and 50 mm eccentric axial loads and flexural load, the bending moment capacities of the SCC columns reinforced with ST33.7 steel tubes increased by about 37.1%, 38.5 and 12.1%, respectively. The bending moment capacities of the SCC columns reinforced with ST26.9 steel tubes increased by about 36.6%, 37.9 and 12.5%, respectively (Table 8.2). The increase in the bending moment capacity of SCC columns under flexural load was less than the increase in the bending moment capacities of SCC columns under eccentric axial loads. This is particularly because the contribution of the concrete, including the concrete inside the steel tubes, was 30% in the maximum load capacity of the columns under flexural load, as the majority of the load was carried by the steel tubes.

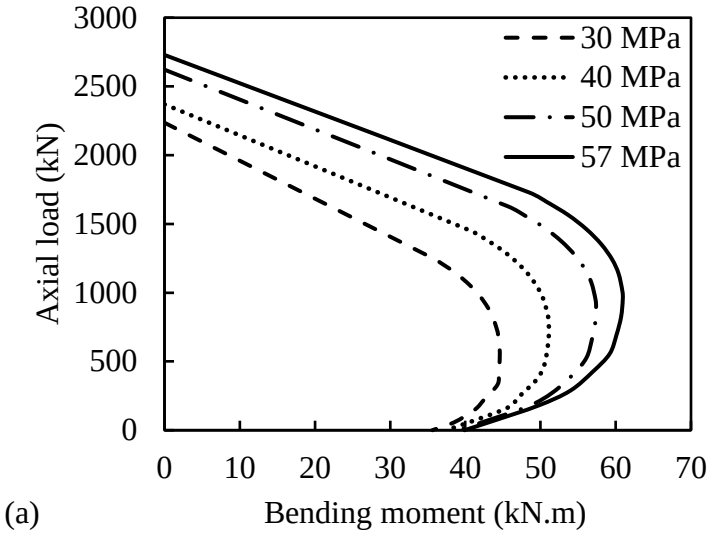

(a)

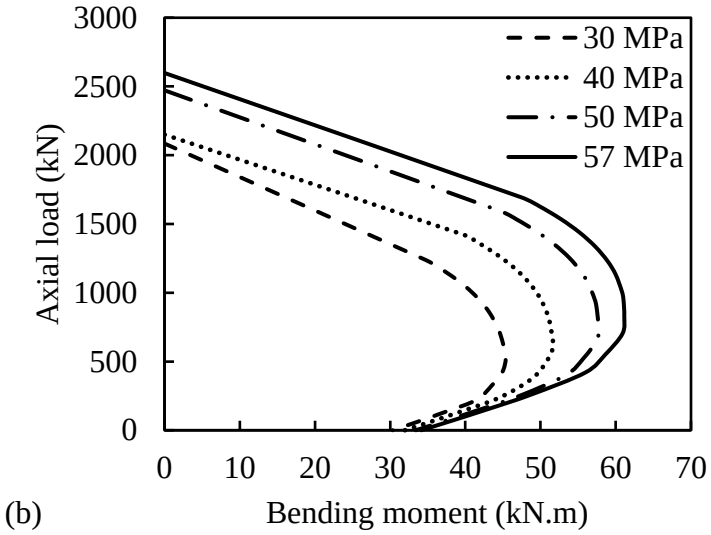

(b)

Figure 8.5: The influence of compressive strength of concrete on the axial load-bending moment interactions of the SCC columns: (a) columns reinforced with ST33.7 steel tubes; and (b) columns reinforced with ST26.9 steel tubes

Table 8.2: Influence of the compressive strength of concrete on the P-M interactions of SCC columns

Compressive Strength of Concrete (MPa)	Loading Conditions	Specimens Reinforced with ST33.7		Specimens Reinforced with ST26.9	
		P (kN)	M (kN.m)	P (kN)	M (kN.m)
30	Concentric	2236	0	2085	0
	e = 25 mm	1261	35.3	1239	34.7
	e = 50 mm	823	43.6	822	43.5
	Flexural	0	35.6	0	30.3
40	Concentric	2370	0	2150	0
	e = 25 mm	1452	40.7	1421	39.8
	e = 50 mm	951	50.4	945	50.1
	Flexural	0	37.4	0	32.0
50	Concentric	2622	0	2472	0
	e = 25 mm	1629	45.6	1594	44.6
	e = 50 mm	1071	56.8	1064	56.4
	Flexural	0	39.1	0	33.4
57	Concentric	2729	0	2598	0
	e = 25 mm	1730	48.4	1694	47.4
	e = 50 mm	1139	60.4	1132	60.0
	Flexural	0	39.9	0	34.1

8.6.2 Influence of Tensile Strength and Wall Thickness of the Steel Tube

Steel tubes with four different tensile strengths (250 MPa, 355 MPa, 450 MPa and 550 MPa) and with four different wall thicknesses (1.5 mm, 2.0 mm, 2.6 mm and 3.0 mm) were considered. The SCC columns were reinforced longitudinally with either six ST33.7 or six ST26.9 steel tubes and transversely with 50 mm pitch of the steel helix of 10 mm diameter. The compressive strength of the SCC was considered 57 MPa, which was similar to the compressive strength of the SCC of the tested specimens in Hadi et al. (2017). The influence of tensile strength of steel tubes on the P-M interactions of the SCC columns is shown in Figure 8.6. As expected, for the increase in the tensile

strength of steel tubes, the rate of increase of the bending moment capacities of the SCC columns under flexural load was higher than the rate of increase of the maximum axial load capacities of the SCC columns under concentric axial load.

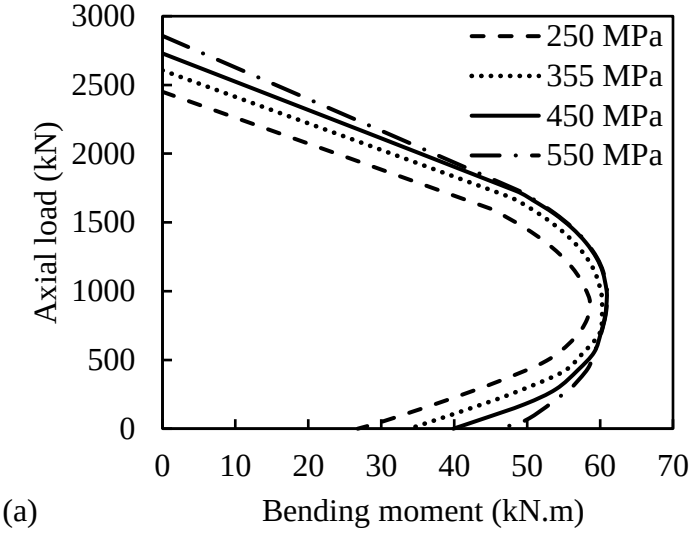

(a)

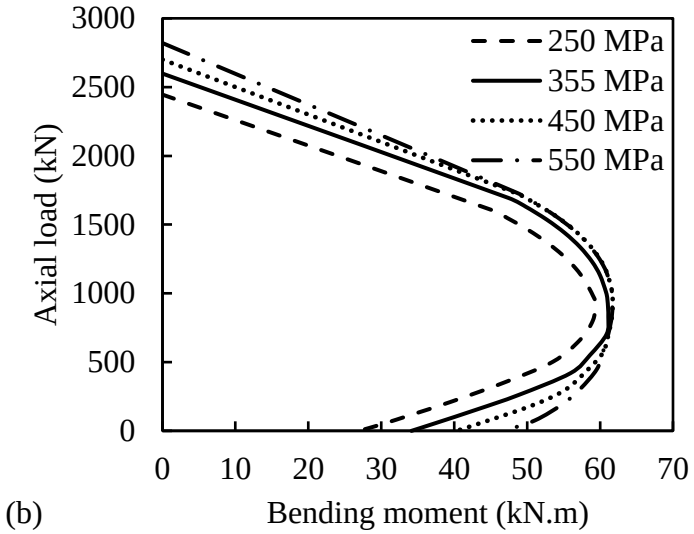

(b)

Figure 8.6: The influence of tensile strength of steel tubes on the axial load-bending moment interactions of the SCC columns: (a) columns reinforced with ST33.7 steel tubes; and (b) columns reinforced with ST26.9 steel tubes

For the increase of the tensile strength of longitudinal steel tubes from 250 MPa to 550 MPa, under concentric axial load, the maximum axial load of the SCC columns reinforced with ST33.7 and ST26.9 steel tubes increased by about 16.6% and 15.3%, respectively (Table 8.3). For the increase of the tensile strength of longitudinal steel tubes from 250 MPa to 550 MPa, under 25 mm eccentric axial load, the maximum axial load and bending moment capacities of the SCC columns reinforced with ST33.7 steel tubes increased by about 8.4% and 8.2%, respectively. The maximum axial load and bending moment capacities of the SCC columns reinforced with ST26.9 steel tubes increased by about 7.7% and 7.8%, respectively (Table 8.3). For the increase of the tensile strength of longitudinal steel tubes from 250 MPa to 550 MPa, under 50 mm eccentric axial load, the maximum axial load and bending moment capacities of the SCC columns reinforced with ST33.7 steel tubes increased by about 5.5% and 5.2%, respectively. The maximum axial load and bending moment capacities of the SCC columns reinforced with ST26.9 steel tubes increased by about 5.2% and 5.1%, respectively (Table 8.3). Under 50 mm eccentric axial load, the compression region was about 67% of the cross-sectional area of the column. In the compression region, the longitudinal steel tubes filled with concrete are influenced by slenderness (s/d_t) ratio and outside diameter to thickness (d_t/t) ratio of the steel tube more than the tensile strength of the steel tubes. For the increase of the tensile strength of longitudinal steel tubes from 250 MPa to 550 MPa, under flexural load, the bending moment capacities of the SCC columns reinforced with ST33.7 and ST26.9 steel tubes increased by about 72.4% and 73.9%, respectively (Table 8.3). It can be seen that the effect of tensile strength of steel tubes on the pure bending moment capacity of SCC columns is higher than the effect of tensile strength of steel tubes on the maximum axial load capacity of SCC columns. Under flexural load, the contribution of steel tubes was 70% in the

maximum load capacity of the column. The capacity of the SCC column under flexural load is based on the tensile strength of steel tubes and the effective depth of the cross-section of the SCC column. Therefore, especially after the initial crack of the concrete cover, the maximum load capacity of SCC columns under flexural load is mainly dependent on the steel tubes.

Table 8.3: Influence of the tensile strength of steel tube on the P-M interactions of SCC columns

Tensile Strength of Steel Tube (MPa)	Loading Conditions	Specimens Reinforced with ST33.7		Specimens Reinforced with ST26.9	
		P (kN)	M (kN.m)	P (kN)	M (kN.m)
250	Concentric	2450	0	2445	0
	e = 25 mm	1602	44.9	1608	45.0
	e = 50 mm	1082	57.4	1092	57.9
	Flexural	0	26.8	0	26.9
355	Concentric	2606	0	2598	0
	e = 25 mm	1691	47.3	1694	47.4
	e = 50 mm	1121	59.4	1132	60.0
	Flexural	0	33.9	0	34.1
450	Concentric	2729	0	2700	0
	e = 25 mm	1730	48.4	1729	48.4
	e = 50 mm	1139	60.4	1149	60.9
	Flexural	0	39.9	0	40.3
550	Concentric	2857	0	2820	0
	e = 25 mm	1737	48.6	1732	48.5
	e = 50 mm	1141	60.4	1149	60.9
	Flexural	0	46.2	0	46.8

The influence of wall thicknesses of steel tubes on the P-M interactions of the SCC columns is shown in Figure 8.7. The thicknesses of steel tubes did not significantly influence the overall trend of the P-M interactions of the SCC columns. However, the

maximum axial load and bending moment capacities of the SCC columns were increased with the increase in the wall thickness of the steel tubes.

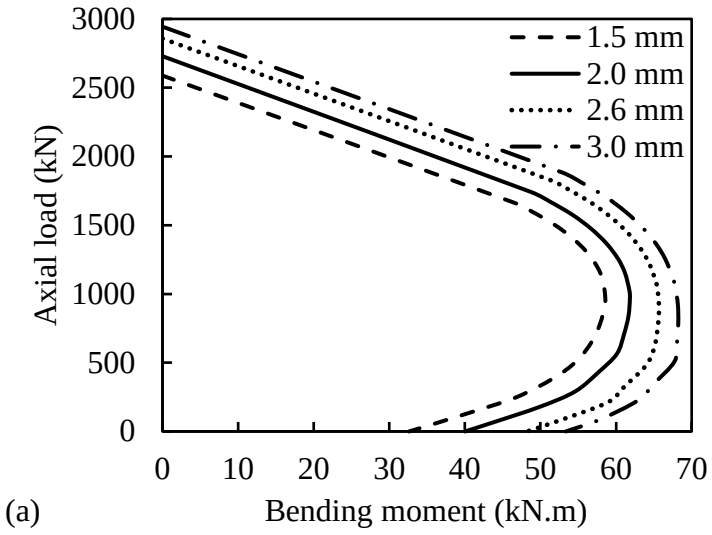

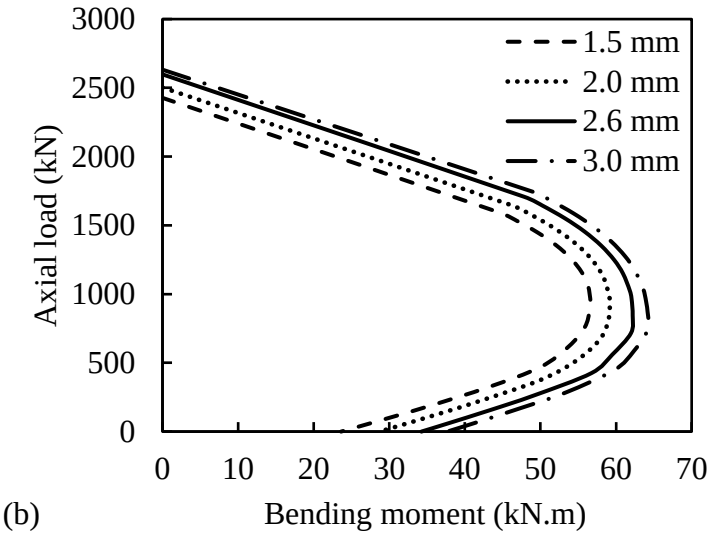

Figure 8.7: The influence of wall thicknesses of steel tubes on the axial load-bending moment interactions of the SCC columns: (a) columns reinforced with ST33.7 steel tubes; and (b) columns reinforced with ST26.9 steel tubes

For the increase of the wall thickness of longitudinal steel tubes from 1.5 mm to 3.0 mm, under concentric axial load, the maximum axial load of the SCC columns reinforced with ST33.7 and ST26.9 steel tubes increased by about 13.8% and 8.4%, respectively (Table 8.4). For the increase of the wall thickness of longitudinal steel tubes from 1.5 mm to 3.0 mm, under 25 mm eccentric axial load, the maximum axial load and bending moment capacities of the SCC column reinforced with ST33.7 steel tubes increased by about 13.4% and 13.3%, respectively. The maximum axial load and bending moment capacities of the SCC column reinforced with ST26.9 steel tubes increased by about 9.6% and 9.7%, respectively (Table 8.4). The higher cross-sectional area of the steel tubes increased the contribution of steel tubes in the maximum axial load and bending moment capacities of SCC columns under eccentric load. For the increase of the wall thickness of longitudinal steel tubes from 1.5 mm to 3.0 mm, under 50 mm eccentric axial load, the maximum axial load and bending moment capacities of the SCC column reinforced with ST33.7 steel tubes increased by about 14.2% and 14.1%, respectively. The maximum axial load and bending moment capacities of the SCC column reinforced with ST26.9 steel tubes increased by about 10.9% and 10.8%, respectively (Table 8.4). For the increase of the wall thickness of longitudinal steel tubes from 1.5 mm to 3.0 mm, under flexural load, the bending moment capacities of the SCC columns reinforced with ST33.7 and ST26.9 increased by about 63.8% and 59.7%, respectively (Table 8.4). The higher wall thickness of steel tube increased the cross-sectional area of the steel tube and increased the contribution of steel tube in the maximum axial load of the SCC column. Also, increasing wall thickness of the steel tube increased the compressive strength of the concrete inside the steel tube and increased the compressive strength of the SCC column. Increase in the wall thickness of

the steel tube decreased the d_t/t ratio of the steel tube and the confinement of concrete inside steel tubes increased with decreasing the d_t/t ratio of the steel tubes.

Table 8.4: Influence of the wall thickness of steel tube on the P-M interactions of SCC columns

Wall thickness of Steel Tube (mm)	Loading Conditions	Specimens Reinforced with ST33.7		Specimens Reinforced with ST26.9	
		P (kN)	M (kN.m)	P (kN)	M (kN.m)
1.5	Concentric	2588	0	2427	0
	e = 25 mm	1663	46.6	1593	44.6
	e = 50 mm	1099	58.3	1062	56.3
	Flexural	0	32.6	0	23.6
2.0	Concentric	2729	0	2502	0
	e = 25 mm	1730	48.4	1647	46.1
	e = 50 mm	1139	60.4	1103	58.5
	Flexural	0	39.9	0	28.7
2.6	Concentric	2857	0	2598	0
	e = 25 mm	1830	51.2	1694	47.4
	e = 50 mm	1216	64.4	1132	60.0
	Flexural	0	48.2	0	34.1
3.0	Concentric	2944	0	2632	0
	e = 25 mm	1885	52.8	1746	48.9
	e = 50 mm	1255	66.5	1178	62.4
	Flexural	0	53.4	0	37.7

The maximum axial load and bending moment capacities of the SCC columns reinforced with ST33.7 steel tubes were higher than the maximum axial load and bending moment capacities of the SCC columns reinforced with ST26.9 steel tubes. The differences in the maximum axial load and bending moment capacities are associated with the differences between cross-sectional areas of the ST33.7 and ST26.9 steel tubes when the wall thickness of both steel tubes was considered the same. For the wall thickness of the steel tubes (ST33.7 and ST26.9) of 1.5 mm, the cross-sectional area of

the ST33.7 steel tube was about 26.8% larger than the cross-sectional area of the ST26.9 steel tube. For the wall thickness of the steel tubes (ST33.7 and ST26.9) of 3 mm, the cross-sectional area of the ST33.7 steel tube was about 28.4% larger than the cross-sectional area of the ST26.9 steel tube.

8.6.3. Influence of the Pitches of Steel Helices

Steel helices of 10 mm diameter with four different pitches (30 mm, 50 mm, 70 mm and 90 mm) were considered. The SCC columns were reinforced longitudinally with either six ST33.7 or six ST26.9 steel tubes. The tensile strengths of ST33.7 and ST26.9 steel tubes were 450 MPa and 355 MPa, respectively. The compressive strength of the SCC was 57 MPa.

The influence of different pitches of steel helices on P-M interactions of the SCC columns is shown in Figure 8.8. For SCC columns reinforced longitudinally with steel tubes and transversely with 30 mm pitch of the steel helix, there are two peak loads in the axial load-axial deformation curves of the SCC columns. For SCC column reinforced with steel tubes ST33.7, the first and second peak loads were 2840 and 3088 kN, respectively. For SCC column reinforced with steel tubes ST26.9, the first and second peak loads were 2695 and 2950 kN, respectively. It is noted that SCC columns sustained the first peak load prior to the spalling of concrete cover and the second peak load after the spalling of concrete cover. The second peak load was higher than the first peak load due to the effective confinement provided by the closely spaced steel helices. The confinement efficiency of the steel helix increases with a decrease in the spacing of the steel helix (Paultre and Légeron 2008). The SCC columns with equal or more than 50 mm pitch of steel helices did not show a second peak load. It is worth mentioning

that the first peak load was taken into account in the maximum axial load capacity of the P-M interactions of the SCC columns reinforced longitudinally with ST33.7 and ST26.9 steel tubes and transversely with 30 mm pitch of steel helix.

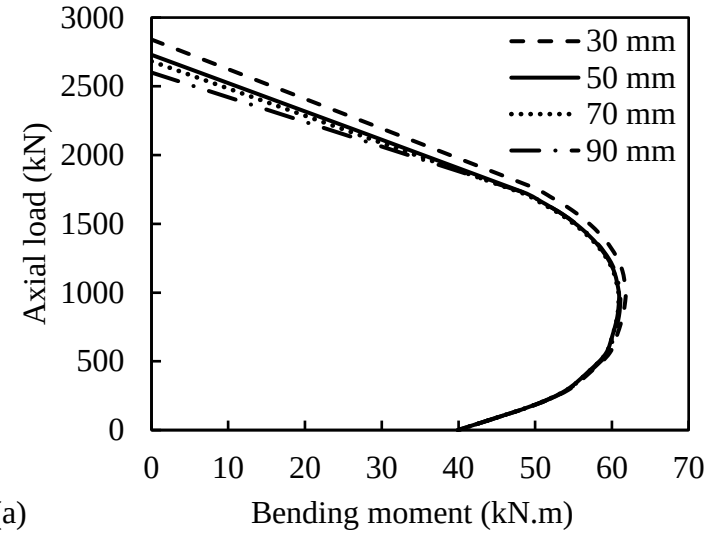

(a)

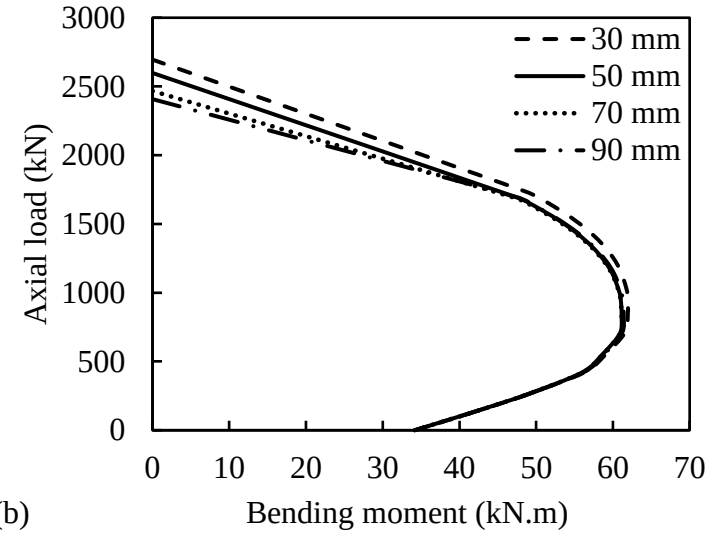

(b)

Figure 8.8: The influence of the pitches of steel helices on axial the load-bending moment interactions of the SCC columns: (a) columns reinforced with ST33.7 steel tubes; and (b) columns reinforced with ST26.9 steel tubes

For the increase of the pitch of steel helices from 30 to 90 mm, under concentric axial load, the maximum axial load capacities of the SCC columns reinforced with ST33.7 and ST26.9 steel tubes decreased by about 8.4% and 10.6%, respectively (Table 5). The differences in the maximum axial load capacities of the SCC columns reinforced with ST33.7 and ST26.9 steel tubes is due to the differences in the s/d_t ratio of steel tubes. When the pitch of steel helix was 90 mm, the s/d_t ratio of the ST26.9 steel tube was 25% higher than the s/d_t ratio of the ST33.7 steel tube because of the differences in the outside diameter of steel tubes. Increase in the s/d_t ratio of the steel tubes resulted in the lower contributions of steel tubes to the maximum axial load capacity of the SCC columns.

Table 8.5: Influence of the pitch of steel helices on the P-M interactions of SCC columns

Spacing of Steel Helices (mm)	Loading Conditions	Specimens Reinforced with ST33.7		Specimens Reinforced with ST26.9	
		P (kN)	M (kN.m)	P (kN)	M (kN.m)
30	Concentric	2840*	0	2695*	0
	e = 25 mm	1769	49.6	1736	48.6
	e = 50 mm	1158	61.4	1151	61.0
	Flexural	0	40.0	0	34.2
50	Concentric	2729	0	2598	0
	e = 25 mm	1730	48.4	1694	47.4
	e = 50 mm	1139	60.4	1132	60.0
	Flexural	0	39.9	0	34.1
70	Concentric	2682	0	2467	0
	e = 25 mm	1724	48.3	1688	47.3
	e = 50 mm	1138	60.3	1130	59.9
	Flexural	0	39.9	0	34.1
90	Concentric	2600	0	2408	0
	e = 25 mm	1729	48.4	1695	47.4
	e = 50 mm	1142	60.5	1135	60.2
	Flexural	0	39.9	0	34.1

* First peak axial load of specimens

For the increase of the pitch of steel helices from 30 to 90 mm, under 25 mm eccentric axial load, the maximum axial load and bending moment capacities of the SCC columns reinforced with ST33.7 and ST26.9 steel tubes decreased by about 2.4% (Table 8.5). For the increase of the pitch of steel helices from 30 to 90 mm, under 50 mm eccentric axial load, the maximum axial load and bending moment capacities of the SCC columns reinforced with ST33.7 and ST26.9 steel tubes decreased by only 1.4% (Table 8.5). The confinement effect by steel helices on the maximum axial loads of the SCC columns under eccentric axial load was significantly less than the confinement effect by steel helices on the maximum axial loads of the SCC columns under concentric axial load. Under flexural load, no significant differences were observed in the bending moment capacities of the SCC columns reinforced with steel tubes (Table 8.5).

8.7 Conclusions

This study develops an analytical model to investigate the axial load-bending moment interactions of self-compacting concrete (SCC) columns reinforced with steel tubes. The developed analytical model takes into account the contribution of the steel tubes, unconfined concrete cover, confined concrete core and confined concrete inside the steel tube. The influences of different parameters (e.g., the compressive strength of the SCC, tensile strength of the steel tube, wall thickness of the steel tube and pitch of the steel helix) on the behaviour of SCC columns reinforced with steel tubes have been investigated. Based on analytical results of this study, the following conclusions are drawn:

1. The results of the analytical model match very well with the experimental investigation results of SCC columns under concentric and eccentric axial loads. However, for the SCC columns under flexural load, the experimental bending moments

of SCC column specimens were higher than the analytical bending moments. The higher experimental bending moments was because the specimens tested under flexural load had a shear span to depth ratio less than twice the effective depth of the concrete cross-section. Hence, the failure of the specimens might not be due to the pure bending.

2. Increasing compressive strength of concrete led to a substantial increase in the maximum axial load and bending moment capacities of the SCC columns. However, for the increase of the compressive strength of concrete from 30 to 57 MPa, the rate of increase of the maximum axial load and bending moment capacities of SCC columns under concentric, 25 and 50 mm eccentric axil loads was higher than the rate of increase of the maximum bending moment capacities of SCC columns under flexural load.

3. The influence of tensile strength of steel tubes on the maximum bending capacity was more than the influence of tensile strength of steel tubes on the maximum axial load capacity of the SCC columns. For columns under concentric axial load, as the tensile strength of steel tubes increased from 250 MPa to 550 MPa, the maximum axial load of SCC columns reinforced with ST33.7 and ST26.9 increased by about 16.6% and 15.3%, respectively. For SCC columns under flexural load, the bending moment capacities of SCC columns reinforced with ST33.7 and ST26.9 steel tubes increased by about 72.4% and 73.9%, respectively.

4. The thicknesses of steel tubes did not significantly influence the overall trend of the P-M interactions of the SCC columns. However, the maximum axial load and bending moment capacities of the SCC columns were increased with the increase of the wall thickness of the steel tubes.

5. For the increase of the pitch of steel helices from 30 to 90 mm in the SCC columns reinforced with ST26.9 steel tubes, the first peak axial load decreased by 10.6%. For the

increase of the pitch of steel helices from 30 to 90 mm in the SCC columns reinforced with ST33.7 steel tubes, the first peak axial load decreased by 8.4%. The slenderness (s/d_t) ratio of the ST26.9 steel tube was 25% higher than the slenderness ratio of the ST33.7 steel tube when the pitch of steel helix was 90 mm. The increase in the slenderness ratio of the steel tubes reduces the contributions of the steel tubes to the maximum axial load capacity of the columns.

6. Increasing the pitch of steel helices from 30 to 90 mm, under 25 mm eccentric axial load, the maximum axial load and bending moment capacities of the SCC columns reinforced with ST33.7 and ST26.9 steel tubes decreased by about 2.4%. Under 50 mm eccentric axial load, the maximum axial load and bending moment capacities of the SCC columns reinforced with ST33.7 and ST26.9 steel tubes decreased by only 1.4%. However, under flexural load, no significant differences were observed in the bending moment capacities of the SCC columns reinforced with steel tubes.

Notation

The following symbols are used in this paper:

A_{core} = area of the concrete core confined by steel helix

A_{cover} = area of unconfined concrete cover

A_{sh} = area of the steel helix

A_t = cross-sectional area of the longitudinal steel tube

A_{tube} = area of the concrete inside steel tubes

$b_{cover,i}$ = width of the concrete cover in the i^{th} layer

$b_{core,i}$ = width of the concrete core in the i^{th} layer

$b_{tube,i}$ = width of the concrete inside the steel tube in the i^{th} layer

D = diameter of the column

D_c = centre-to-centre diameter of the steel helix

d_j = distance from the extreme concrete compressive fibre to the centre line of the steel tube

d_n = depth of neutral axis ($N.A.$)

d_t = outside diameter of the steel tube

E_c = modulus of elasticity of the concrete

E_{sh} = modulus of elasticity of the steel helix

$E_{sec,c}$ = secant modulus of elasticity of the confined concrete

$E_{sec,u}$ = secant modulus of elasticity of the unconfined concrete

E_t = modulus of elasticity of the steel tube

f_c = unconfined concrete stress

f_{cc} = confined concrete stress

f_c' = 28-day cylinder concrete compressive strength

f_{cc}' = peak stress of confined concrete

$f_{cc,core}$ = axial stress in the confined concrete core

$f_{cc,tube}$ = axial stress in the longitudinal steel tubes

f_{co} = unconfined concrete compressive strength which is equal to $\propto_1$ multiplied by f_c'

$f_{cover,i}$ = compressive stress of the concrete cover in the i^{th} layer

$f_{core,i}$ = compressive stress of the concrete core in the i^{th} layer

$f_{tube,i}$ = compressive stress of the concrete inside the steel tube in the i^{th} layer

f_l = effective confining pressure of the steel helix

f_{lt} = effective confining pressure of the steel tube

f_t = stress of the steel tube in the linear elastic portion

f_{ty} = yield stress of the steel tube

f_{yh} = yield stress of the steel helix

k_e = coefficient of the confined concrete core by steel helix

M_T = moment carrying capacity of the column

m = number of longitudinal steel tubes

n = number of small parallel layers

n' = material parameter depending on the shape of stress-strain curve

n_1' = modified material parameter at the ascending part

n_2' = modified material parameters at the descending part

P_{axial} = total axial load of columns under concentric axial load

$P_{cover,i}$ = compressive force of the concrete cover in the i^{th} layer

$P_{core,i}$ = compressive force of the concrete core in the i^{th} layer

$P_{tube,i}$ = compressive force of the concrete inside the steel tube in the i^{th} layer

$P_{s,j}$ = force of the steel tube

P_T = axial load carrying capacity of the column under 25 mm, 50 mm eccentric and flexural loads

s = pitch (centre-to-centre spacing) of the steel helix

s' = clear spacing of the steel helix

t = wall thickness of the steel tube

t_o = thickness of each layer

Y_i = distance from the extreme concrete compressive fibre to the mid-height of each layer

$\propto_1$ = coefficient of compressive strength of concrete

α_s = modification factor for the peak stress of confined concrete

α_θ = hoop strain factor

ε_c = axial strain corresponding to f_c

ε_{cc} = axial strain corresponding to f_{cc}

ε_{cc}' = axial strain corresponding to f_{cc}'

$\varepsilon_{c,i}$ = strain in the centre of each layer

ε_{co} = axial strain corresponding to f_{co}

ε_{cu} = ultimate strain of concrete

ε_{t} = axial strain corresponding to f_{t}

ε_{ty} = axial strain corresponding to f_{ty}

ε_{yh} = axial strain corresponding to f_{yh}

ε_{θ} = hoop strain of the steel tube

ρ_{cc} = ratio of area of longitudinal steel reinforcement to the area of the concrete core of the column

ρ_{s} = longitudinal reinforcement ratio

ρ_{sh} = volumetric ratio of steel helix

σ_{θ} = hoop stress of the steel tube

ϖ, ξ, ψ = coefficients of equations for model Aslani and Nejadi (2012)

Acknowledgements

The authors thank the University of Wollongong, Australia and technical officers at the High Bay laboratory for their help in the experimental work of this study. The first author would like to acknowledge the Iraqi Government for the support of his PhD scholarship.

References

Ahari, R. S., Erdem, T. K., and Ramyar, K. (2015). "Permeability properties of self-consolidating concrete containing various supplementary cementitious materials." *Construction and Building Materials*, 79, 326-336.

AISC. (2010). "Specification for structural steel buildings." *ANSI/AISC 360-10*, Chicago.

Alhussainy, F., Sheikh, M. N., and Hadi, M. N. S. (2017). "Behaviour of small-diameter self-compacting concrete-filled steel tubes." *Magazine of Concrete Research*, http://dx.doi.org/10.1680/jmacr.16.00531

AS (Australian Standard). (2009). "Concrete structure." *AS 3600-2009*, Sydney, NSW, Australia.

Aslani, F., and Nejadi, S. (2012). "Mechanical properties of conventional and self-compacting concrete: An analytical study." *Construction and Building Materials*, 36, 330-347.

Barluenga, G., Giménez, M., Rodríguez, A., and Rio, O. (2017). "Quality Control Parameters for on-site evaluation of pumped Self-Compacting Concrete." *Construction and Building Materials*, 154, 1112-1120.

Bing, L., Park, R., and Tanaka, H. (2001). "Stress-strain behavior of high-strength concrete confined by ultra-high- and normal-strength transverse reinforcements," *ACI Structural Journal*, 98(3), 395-406.

Chen, J., Wang, J., and Jin, W.-L. (2017). "Concrete-filled steel tubes with reinforcing bars or angles under axial tension." *Journal of Constructional Steel Research*, 133, 374-382.

De Oliveira, W. L. A., De Nardin, S., El Debs, A. L. H. C., and El Debs, M. K. (2009). "Influence of concrete strength and length/diameter on the axial capacity of CFT columns." *Journal of Constructional Steel Research*, 65(12), 2103-2110.

Du, Y., Chen, Z., and Xiong, M.-X. (2016). "Experimental behavior and design method of rectangular concrete-filled tubular columns using Q460 high-strength steel." *Construction and Building Materials*, 125, 856-872.

EFNARC (European Federation of Specialist Construction Chemicals and Concrete Systems). (2002). "Specification and guidelines for self-compacting concrete." Norflolk, U.K., 1-32.

Elremaily, A., and Azizinamini, A. (2002). "Behavior and strength of circular concrete-filled tube columns," *Journal of Constructional Steel Research*, 58(12), 1567-1591.

Ghafoori, N., Spitek, R., and Najimi, M. (2016). "Influence of limestone size and content on transport properties of self-consolidating concrete." *Construction and Building Materials*, 127, 588-595.

Hadi, M. N. S., Alhussainy, F., and Sheikh, N. M. (2017). "Behavior of self-compacting concrete columns reinforced longitudinal with steel tubes." *Journal of Structural Engineering ASCE*, 143(6), 1-14.

Han, L.-H. (2002). "Tests on stub columns of concrete-filled RHS sections." *Journal of Constructional Steel Research*, 58(3), 353-372.

Han, L.-H., and Yao, G.-H. (2004). "Experimental behaviour of thin-walled hollow structural steel (HSS) columns filled with self-consolidating concrete (SCC)." *Thin-Walled Structures*, 42(9), 1357-1377.

Han, L.-H., Yao, G.-H., and Zhao, X.-L. (2005). "Tests and calculations for hollow structural steel (HSS) stub columns filled with self-consolidating concrete (SCC)." *Journal of Constructional Steel Research*, 61(9), 1241-1269.

Heirman, G., Vandewalle, L., Van Gemert, D., Boel, V., Audenaert, K., De Schutter, G., Desmet, B., and Vantomme, J. (2008). "Time-dependent deformations of limestone powder type self-compacting concrete." *Engineering Structures*, 30(10), 2945-2956.

Johansson, M., and Gylltof, K. (2002). "Mechanical behavior of circular steel-concrete composite stub columns." *Journal of Structural Engineering ASCE*, 128(8), 1073-1081.

Lai, Z., and Varma, A. H. (2016). "Effective stress-strain relationships for analysis of noncompact and slender filled composite (CFT) members." *Engineering Structures*, 124, 457-472.

Li, S., Liu, Z., Lu, Y., and Zhu, T. (2017). "Shear performance of steel fibers reinforced self-confinement and self-compacting concrete-filled steel tube stub columns." *Construction and Building Materials*, 147, 758-775.

Liu, S.-W., Chan, T.-M., Chan, S.-L., and So, D. K.-L. (2017). "Direct analysis of high-strength concrete-filled-tubular columns with circular & octagonal sections." *Journal of Constructional Steel Research*, 129, 301-314.

Mander, J. B., Priestley, M. J. N., and Park, R. (1988). "Theoretical stress-strain model for confined concrete." *Journal of Structural Engineering, ASCE*, 114(8), 1804-1826.

Moon, J., Lehman, D., Roeder, C., and Lee, H. (2013). "Strength of circular concrete-filled tubes with and without internal reinforcement under combined loading." *Journal of Structural Engineering ASCE*, 139(12), 04013012.

Morino, S., and Tasuda, K. (2002). "Design and construction of concrete-filled steel tube column system in Japan." *Earthquake Engineering and Engineering Seismology*, 4(1), 51-73.

Ouyang, Y., Kwan, A. K. H., Lo, S. H., and Ho, J. C. M. (2017). "Finite element analysis of concrete-filled steel tube (CFST) columns with circular sections under eccentric load." *Engineering Structure*, 148, 387-398.

Patel, V. I., Liang, Q. Q., and Hadi, M. N. S. "Nonlinear Analysis of Concrete-Filled Steel Tubular Columns, first ed.", Scholars' Press, Germany, 2015.

Paultre, P., and Légeron, F. (2008). "Confinement reinforcement design for reinforced concrete columns." *Journal of Structural Engineering ASCE*, 134(5), 738-749.

Schneider, S. P. (1998). "Axially loaded concrete-filled steel tubes." *Journal of Structural Engineering ASCE*, 124(10), 1125-1138.

Shanmugam, N. E., and Lakshmi, B. (2001). "State of the art report on steel-concrete composite columns." *Journal of Constructional Steel Research*, 57(10), 1041-1080.

Uy, B., Tao, Z., and Han, L.-H. (2011). "Behaviour of short and slender concrete-filled stainless steel tubular columns." *Journal of Constructional Steel Research*, 67(3), 360–378.

Xiamuxi, A., and Hasegawa, A. (2012). "A study on axial compressive behaviors of reinforced concrete filled tubular steel columns." *Journal of Constructional Steel Research*, 76, 144-154.

Yu, Z.-W., Ding, F.-X., and Cai, C.S. (2007). "Experimental behavior of circular concrete-filled steel tube stub columns." *Journal of Constructional Steel Research*, 63(2) 165-174.

Zhu, M., Liu, J., Wang, Q., and Feng, X. (2010). "Experimental research on square steel tubular columns filled with steel-reinforced self-consolidating high-strength concrete under axial load." *Engineering Structures*, 32, 2278-2286.

CHAPTER 9: CONCLUSIONS AND RECOMMENDATIONS

9.1 Introduction

The main objective of this study is to investigate the behaviour of columns reinforced with small-diameter steel tubes filled with SCC (STR SCC column) under different loading conditions. From the results of the theoretical and experimental studies, some key conclusions are drawn in the sections below.

9.2 Mechanical Properties of Self-Compacting Concrete

A number of concrete mixes were investigated to achieve self-compacting concrete (SCC). The properties of fresh concrete were tested according to ASTM methods. The standard mechanical properties including compressive strength, splitting tensile strength, flexural strength and the modulus of elasticity under compression as well as the uniaxial direct tensile strength of the SCC were determined. Based on the results of the experimental program carried out on the properties of the SCC, the following conclusions can be drawn:

1. A new method of testing SCC under uniaxial tension was proposed. The method was developed to overcome the difficulties associated with testing methods adopted in the previous research studies. Also, the direct tensile testing method developed in this study provides rational and reliable results for the direct tensile strength of the normal strength concrete (NSC), high-strength concrete (HSC) and steel fibre reinforced high-strength concrete (SFHSC) using a simple and effective testing technique.

2. The average direct tensile strengths of the tested specimens were found to be less than the average flexural strength and splitting tensile strength.
3. The direct tensile strength of the SCC specimens tested based on the designed and developed test setup was approximately equal to 90 percent of the splitting tensile strength.
4. The average modulus of elasticity in direct tension was found to be 20 GPa, which was equal to the two-thirds of the modulus of elasticity in compression.

9.3 Behaviour of Small Diameter Steel Tubes under Axial Compression

Steel tubes are widely used in different structural applications and are subjected to different types of loading. Small diameter steel tubes in lieu of solid steel bars were used as the main reinforcement in circular reinforced concrete columns. Based on the experimental investigations carried out on the behaviour of small-diameter steel tubes under axial compression, the following conclusions can be drawn:

1. The behaviour of galvanized and cold-formed small diameter steel tubes under axial compression is significantly influenced by the L/D ratio. For the L/D ratio of 2 and 4, the compressive failure in the steel tube specimens occurred due to local elephant's foot buckling. For the L/D ratio ≥ 6, the compressive failure modes of galvanized and cold-formed steel tube specimens changed from local elephant's foot buckling to global buckling. In structural applications, steel tubes with $L/D < 6$ should be used to prevent global buckling and to increase the ductility.
2. The stress-strain behaviour of galvanized steel tube specimens with L/D ratio ≤ 6 exhibited strain hardening after the yield stress. It is noted that the cold-formed steel tube specimens exhibited no clear yield point under axial tension and also under axial compression. However, the ultimate compressive strength of cold-formed steel tube

specimen was higher than the yield compressive stress for specimens with L/D ratio of 10 and below.

3. The average ultimate compressive strength to yield compressive stress ratios of galvanized tube specimens were greater than 1.08 for the specimens with L/D ratio ≤ 4. The average ultimate compressive strength to yield compressive stress ratios of cold-formed tube specimens were greater than 1.08 for the specimens with L/D ratio ≤ 8.

4. The yield compressive stress was slightly larger than the yield tensile stress for galvanized steel tube specimens with L/D ratio ≤ 6. The yield compressive stress was slightly larger than the yield tensile stress for cold-formed steel tube specimens with L/D ratio of 2. The ultimate compressive strength of galvanized and cold-formed steel tube was found to be less than the ultimate tensile strength for specimens with L/D ratio ≥ 6.

9.4 Behaviour of Small-Diameter Self-Compacting Concrete-Filled Steel Tubes

Based on the experimental and analytical investigations carried out on the behaviour of small-diameter SCC-filled steel tubes under axial compression, the following conclusions can be drawn:

1. The axial load capacity of self-compacting concrete-filled steel tubes (SCFT) specimens was found to be higher than the axial load capacity of corresponding unfilled steel tube (UT) specimens due to the effect of the concrete infill. The average axial load capacity of the specimens in Group SCFT26.9 and Group SCFT33.7 were 30% and 49% higher than the average axial load capacity of the

specimens in Group UT26.9 and Group UT33.7, respectively. The greater effect of the infill concrete was observed for specimens tested with L/D ratio of 2 and 4.

2. For L/D ratio of 2 and 4, the compressive failure in the UT specimens occurred as a result of local elephant's foot buckling. However, the compressive failure in the SCFT specimens was different to the compressive failure in the UT specimens. For SCFT specimens with L/D ratio of 2 and 4, the first peak axial load occurred with small bulges along the steel tube specimen. Then, the axial load continued to increase due to extension of small bulges during the compression test. The small bulges were extended as an expansion of the concrete core after the steel yielding. Finally, the specimens failed by crushing the concrete core due to an increase in outward local buckling of the steel tube.

3. For the L/D ratio ≥ 6, the compressive failure modes of UT specimens changed from local elephant's foot buckling to global buckling. Global buckling failure was observed to occur as a bend in a sharp angle near the mid-height of the tube (inward buckling). For SCFT specimens, the failure also occurred due to global buckling of the specimens. However, the SCFT specimens with L/D ratio ≥ 6 gradually lost the axial load capacity due to the formation of small bulges in the middle of the steel tube. The small bulges prevented the occurrence of sudden failure as a result of global buckling of the specimen.

4. The design recommendations in the American standard ANSI/AISC 360-10 (2010) for CFT columns conservatively predicted the experimental axial load capacity of the SCFT.

9.5 Behaviour of Self-Compacting Concrete Columns Reinforced Longitudinally with Steel Tubes

Use of small-diameter circular steel tubes filled with the SCC in lieu of conventional steel bars was investigated in reinforcing the concrete column. Hence, a new reinforcing method of the concrete column specimens was proposed. Problems associated with the use of steel tubes as longitudinal reinforcement in columns because of slip of steel tubes have been highlighted. The following conclusions can be drawn.

1. Because the tensile strength of steel bars and steel tubes are different, the force contribution of ST33.7 steel tubes in Specimen ST33.7H50 was found to be less than the force contribution of N16 steel bars in the Reference Specimen N16H50 by 19.9%. In spite of less force contribution of steel tubes, Column Specimen ST33.7H50 had similar yield and maximum load as Reference Specimen N16H50 under concentric and 25-mm eccentric axial compression. The yield loads of Specimens N16H50 and ST33.7H50 were 2505 and 2500 kN, respectively. The maximum loads of the Specimens N16H50 and ST33.7H50 were 2734 kN and 2729 kN, respectively. Hence, using steel tubes with similar tensile strength to steel bars might result in a higher maximum load capacity.
2. For concentric load and 25-mm eccentric load, specimens reinforced with ST33.7 steel tubes had a maximum load capacity greater than specimens reinforced with ST26.9 steel tubes. For 50-mm eccentric load, however, Specimen ST26.9H50E50 showed a maximum load higher than that of Specimen ST33.7H50E50 because of the slip of ST33.7 steel tubes.
3. Despite the fact that the cross-sectional areas of ST33.7 and ST26.9 steel tubes are the same, increasing the pitch of helices from 50 to 75 mm resulted in a higher

reduction in the maximum axial load of specimens reinforced with ST26.9 tubes compared to specimens reinforced with ST33.7 tubes.

4. Under flexural loading, the maximum loads of Specimens ST33.7H50F and ST26.9H50F were 7 and 25% lower, respectively, than that of Reference Specimen N16H50F. In addition, the initial slope of load-midspan deflection diagrams in the specimens reinforced with ST33.7 tubes (nominal tensile strength=350 MPa) was steeper than that of the specimens reinforced with ST26.9 tubes (nominal tensile strength=250 MPa).
5. The ductility of STR SCC specimens was significantly influenced by the slip of steel tubes under eccentric loading; however, the STR SCC specimens showed a higher ductility than Reference Specimen N16H50C under concentric loading.
6. Welding a single washer at the ends of the steel tubes to prevent slip in concrete was insufficient and resulted in a tearing of the tubes near the welding area at both ends of the tube in the tension and compression regions. In contrast, welding double washers at the ends of the tubes prevented the slip of longitudinal steel tubes in concrete.

9.6 Analytical Investigations of SCC Columns Reinforced with Steel Tubes

Analytical investigations on the axial load-axial deformation behaviour of self-compacting concrete (SCC) columns reinforced with steel tubes were carried out. Two types of steel tubes were used in the SCC columns as longitudinal reinforcement. The influences of different parameters including the compressive strength of SCC, tensile strength of steel tube, wall thickness of steel tube and pitch of steel helix were investigated. Based on the analytical results, the following conclusions are drawn:

1. The analytical axial load-axial deformation response of the SCC columns reinforced with steel tubes was calculated based on the stress-strain responses of the longitudinal steel tubes, unconfined concrete cover, confined concrete core and confined concrete inside the steel tube. The analytical and experimental axial load-axial deformation curves of columns showed good agreements.

2. The compressive strength of the confined concrete core and the compressive strength of the confined concrete inside the steel tube were compared. For the SCC columns reinforced transversely with steel helices having a pitch of 50 mm, the enhancement factor of the confined concrete core was 1.32, whereas the enhancement factors of the confined concrete inside the ST33.7 and ST26.9 steel tubes were 2.6 and 3.41, respectively. The enhancement factors of the confined concrete inside the steel tubes were higher than the enhancement factors of the confined concrete core for the same pitch of steel helices. Thus, steel tubes effectively confined the concrete inside the tube and resulted in higher axial compressive strengths of the SCC columns.

3. As the concrete compressive strength increased from 30 MPa to 57 MPa, the maximum axial load of the SCC columns reinforced with ST33.7 and ST26.9 steel tubes increased by about 23% and 24.6%, respectively. With the increase in the compressive strength of concrete from 30 MPa to 57 MPa, the ductility of Specimen ST33.7H50C decreased by about 14.4%, whereas the ductility of Specimen ST26.9H50C decreased by about 17.3%.

4. As the tensile strength of longitudinal steel tubes increased from 250 MPa to 550 MPa, the maximum axial load of Specimens ST33.7H50C and ST26.9H50C increased by about 16.6% and 15%, respectively. Also, as the wall thickness of longitudinal steel tubes increased from 1.5 mm to 3.0 mm, the maximum axial load of the SCC columns

reinforced with ST33.7 steel tubes increased by about 13.8%, whereas the maximum axial load of the SCC columns reinforced with ST26.9 steel tubes increased by about 8.4%. However, the ductility of SCC columns reinforced with steel tubes was not significantly influenced by the increase in the tensile strength and wall thickness of steel tube.

5. For SCC columns reinforced longitudinally with steel tubes and transversely with 30 mm pitch of steel helices, there are two peak axial loads in the axial load-axial deformation curves of the SCC columns. However, the SCC columns reinforced transversely with steel helices having a pitch of 50 mm or larger did not show a second peak axial load. For the increase of the pitch of steel helices from 30 to 90 mm in the SCC columns reinforced with ST26.9 steel tubes, the first peak axial load decreased by 10.6%. Whereas increasing the pitch of steel helices from 30 to 90 mm in the SCC columns reinforced with ST33.7 steel tubes, the first peak axial load decreased by 8.4%. The s/d_t ratio of the ST26.9 steel tube was 25% higher than the s/d_t ratio of the ST33.7 steel tube when the pitch of steel helix was 90 mm.

6. For the increase of the pitch of steel helices from 30 to 90 mm in the SCC columns reinforced with ST26.9 steel tubes, the ductility decreased by 40%. Whereas increasing the pitch of steel helices from 30 to 90 mm in the SCC columns reinforced with ST33.7 steel tubes, the ductility decreased by 37%.

9.7 Recommendations for Future Studies

Based on the experimental and analytical investigations carried out on the behaviour of columns reinforced with small-diameter steel tubes filled with SCC (STR SCC column), the following topics are recommended for future studies:

1. To prevent premature failures due to the slip of steel tubes within the concrete, the surface of the steel tubes can be coated to increase the roughness. Future research investigations on the bond stress between the coated steel tubes and concrete need to be carried out for the efficient design and construction of STR SCC columns.
2. The STR SCC columns with a wide range of concrete compressive strengths, steel tubes and cross-sections (rectangular and square) need to be investigated experimentally and analytically to better understand the behaviour of STR SCC columns.
3. Effects of high tensile strength of steel tubes on the behaviour and performance of STR SCC columns need to be investigated.
4. Full-scale testing of the STR SCC column specimens is recommended. In addition, the slenderness effect of STR SCC column specimens is recommended to be investigated.
5. Experimental investigations are needed for very small and very large pitches of steel helices to verify the results of the analytical modelling.
6. Finite element modelling of the STR SCC columns needs to be carried out to simulate the behaviour of full-size STR SCC column specimens under different loading condition. The slip model of steel tubes in STR SCC columns is also recommended to be investigated.